Development of Covalent and Noncovalent E3 Ubiquitin Ligase Ligands for Degrading Cancer-associated Proteins

By

Yunxiang Wu

A dissertation submitted in partial fulfillment of the requirements for the degree of

Doctor of Philosophy

(Pharmaceutical Sciences)

at the

UNIVERSITY OF WISCONSIN–MADISON

2024

Date of final oral examination: 08/26/2024

The dissertation is approved by the following members of the Final Oral Committee:

Weiping Tang, Professor, Pharmaceutical Sciences

Jennifer Golden, Associate Professor, Pharmaceutical Sciences

Lingjun Li, Professor, Pharmaceutical Sciences

Bo Liu, Professor, Cell and Regenerative Biology

Abstract

This dissertation focuses on the development of both covalent and non-covalent E3 ubiquitin ligase ligands for the targeted degradation of cancer-associated proteins. Targeted protein degradation (TPD) has emerged as a transformative therapeutic strategy, and Proteolysis Targeting Chimeras (PROTACs) have played a pivotal role in advancing this approach. PROTACs exploit the ubiquitin-proteasome system to selectively degrade proteins of interest, offering a novel means to target previously undruggable proteins. Chapter 1 presents my efforts in the development of a novel platform, CLIPTAC (Click-PROTAC), which employs covalent E3 ligase ligands integrated through bioorthogonal chemistry to potentially enhance specificity, efficacy, and pharmacokinetic properties. Our proof-of-concept study successfully demonstrated the degradation of ERα and BRD4 using specific combinations of covalent ligands. Utilizing in-cell tetrazine and trans-cyclooctene coupling chemistry, we created a platform that can potentially enhance cell permeability of the PROTACs by forming the final PROTAC molecule inside the cell. Chapter 2 details the design, synthesis, and evaluation of these ligands, aiming to overcome the limitations of traditional CRBN ligands. Various analogues were synthesized and assessed for their binding affinities with the CRBN-DDB1 complex. Additionally, new BTK degraders were developed by conjugating these ligands with ibrutinib, demonstrating potent degradation activity in BTK-HiBiT cells and efficient downstream signaling inhibition. Furthermore, this last two chapter presents the design and synthesis of PROTACs targeting receptor-interacting protein kinases (RIPKs) and MDM2. Biological evaluation of these PROTACs revealed significant protein degradation and downstream effects, showcasing their potential as effective therapeutic agents.

Acknowledgments

As I near the completion of my Ph.D. journey, I find myself reflecting on the many individuals who have contributed to my growth and success over the past five years. This dissertation would not have been possible without the support, guidance, and encouragement of many people, and I would like to take this opportunity to express my deepest gratitude.

First and foremost, I wish to express my sincere appreciation to my advisor, Weiping Tang. Your profound knowledge, unwavering support, and insightful guidance have been invaluable throughout my doctoral studies. You have always been there to provide constructive criticism, while also allowing me the freedom to explore my own ideas. Your commitment to my development as a researcher and a person is something I will always be grateful for.

I am also deeply thankful to the members of my dissertation committee, Bo Liu, Lingjun Li, and Jennifer Golden. Your expert advice and thoughtful feedback have greatly enhanced the quality of my research. I have learned a tremendous amount from our discussions, and your encouragement has kept me motivated throughout this challenging process.

A heartfelt thank you goes to my colleagues in the Tang group. Working alongside such talented and passionate individuals has been a true pleasure. Special thanks to Dr.Zhongrui Zhang, Ira Tandon, Dr. Chunrong Li, Yaxian Liao, Hong Ju and all other members in Tang lab for your collaboration, friendship, and for making the lab a place of both hard work and laughter.

Lastly, I want to express my deepest gratitude to my family. Although we have been separated by distance, your unwavering love and support have been my greatest source of strength. To my parents, thank you for your sacrifices and for always believing in me.

As I conclude this chapter and look toward the future, I will carry with me the lessons, friendships, and memories that have shaped my Ph.D. journey. Thank you all for being part of this incredible experience.

Abbreviations and Acronyms

4Å MS = 4 Å molecular sieves

Ac = Acetyl

Ar = Aryl

Bn = Benzyl

Boc = tert-butyloxycarbonyl

BTM = Benzotetramisole

Bu or n-Bu = n-Butyl

tBu = tert-Butyl

Bz = Benzoyl

Cp = Cyclopentadienyl

Cym = Cymene

DBU = 1,8-Diazabyciclo[5.4.0]undec-7-ene

DCC = 1,3-Dicyclohexylcarbodiimide

DCE = 1,2-Dichloroethene

DCM = Dichloromethane

DIBAL = Diisobutylaluminium hydride

DIC = N,N′-Diisopropylcarbodiimide

DIPEA = N,N-Diisopropylethylamine

DMAP = 4-Dimethylaminopyridine

DMF = N,N-Dimethylformamide

DMSO = Dimethylsulphoxide

EDCI = 1-Ethyl-3-(3-dimethylaminopropyl)carbodiimide

Et = Ethyl

Et2O = Diethyl ether

Fmoc = Fluorenylmethyloxycarbonyl

FG = Functional group

HOBt = Hydroxybenzotriazole

LAH = Lithium aluminium hydride

LG = Leaving group

LDA = Lithium diisopropylamide

Me = Methyl

Ms = Mesylate

Nu = Nucleophile

OAc = Acetate

OMe = Methoxy

OTf = Trifluoromethanesulfonate

PG = Protecting group

Ph = Phenyl

iPr = iso-Propyl

Py = Pyridine

TBAF = Tetrabutylammonium fluoride

TBPS = tert-Butyldiphenylsilyl

TBS = tert-Butyldimethylsilyl

TES = Triethylsilyl

Tf_2O = Triflic anhydride

THF = Tetrahydrofurane

TIPS = Triisopropylsilyl

TMS = Trimethylsilyl

Ts = para-Toluenesulphonyl

Contents

Chapter 1

In-cell Self-assembly of Proteolysis Targeting Chimeras (PROTAC) with Covalent E3 Ligase Ligands

1.1. Introduction

PROTACs (PROteolysis TArgeting Chimeras) have emerged as a promising strategy to degrade proteins of interest that cannot be easily drugged using other strategies[1]. As hetero bifunctional small molecules, PROTACs recruit an E3 ligase to the target protein, forming a ternary complex that facilitates ubiquitination and subsequent degradation of the target protein (**Scheme 1.1)**. PROTACs offer several advantages over traditional inhibitors. Unlike inhibitors that typically function by blocking the activity of target proteins, PROTACs work by inducing the degradation of these proteins. This leads to a more thorough and lasting reduction of the target protein within cells. By leveraging the cell's natural protein degradation machinery, PROTACs do not rely on maintaining high occupancy of the target site, which is a common necessity for inhibitors to be effective. Because the activity of PROTACs does not solely rely on binding affinity, cancer cells that are resistant to inhibitors due to lower binding affinity caused by mutations may still be sensitive to PROTACs. Furthermore, PROTACs have the capability to target proteins with scaffolding functions, which are difficult to drug with small molecule inhibitors. In essence, PROTACs offer the benefits of complete degradation of target proteins, overcoming drug resistance, and broadening the scope of targetable proteins, thus representing a significant advancement in therapeutic strategies.

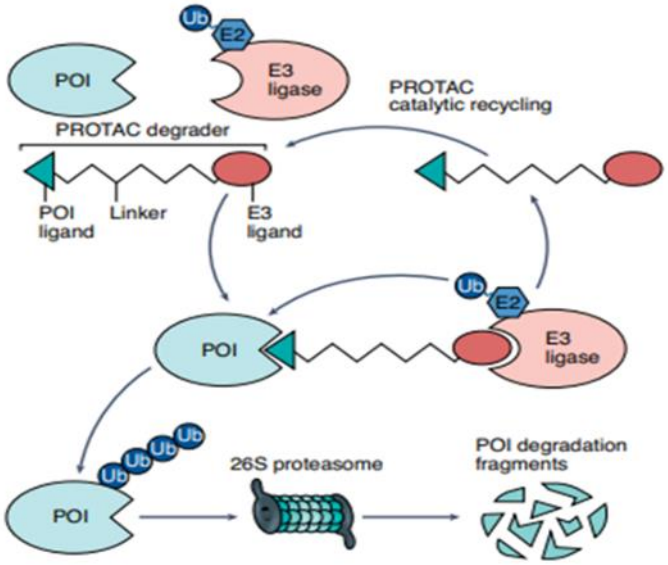

Scheme 1.1. PROTAC strategy mechanism[2]

Among PROTACs developed in recent years, most of them utilize CRBN or VHL ligands as E3 ligase ligands[3] (**Scheme 1.2**). Despite the significant success achieved with CRBN and VHL in PROTAC development, it is necessary to develop more E3 ligase ligands because the existing ligands often lack tissue specificity or desirable pharmacokinetic properties[4]. Novel E3 ligase ligands can enhance the efficiency and selectivity of PROTACs by engaging different ligases that may offer improved tissue distribution, reduced off-target effects, and the ability to degrade a broader range of disease-relevant proteins. Additionally, new ligands can address resistance mechanisms that emerge with current E3 ligase ligands, ultimately broadening therapeutic applications of PROTAC technology.

Company	Degrader	Target	Indications	E3 ligase	ROA	Highest phase	Clinical trial no. (if applicable)
Arvinas	ARV-110	AR	Prostate cancer	CRBN	Oral	Phase II	NCT03888612
Arvinas/Pfizer	ARV-471	ER	Breast cancer	CRBN	Oral	Phase II	NCT04072952
Accutar Biotech	AC682	ER	Breast cancer	CRBN	Oral	Phase I	NCT05080842
Arvinas	ARV-766	AR	Prostate cancer	Undisclosed	Oral	Phase I	NCT05067140
Bristol Myers Squibb	CC-94676	AR	Prostate cancer	CRBN	Oral	Phase I	NCT04428788
Dialectic Therapeutics	DT2216	BCL-x_L	Liquid and solid tumours	VHL	I.v.	Phase I	NCT04886622
Foghorn Therapeutics	FHD-609	BRD9	Synovial sarcoma	Undisclosed	I.v.	Phase I	NCT04965753
Kymera/Sanofi	KT-474	IRAK4	Autoimmune diseases (e.g., AD, HS, RA)	Undisclosed	Oral	Phase I	NCT04772885
Kymera	KT-413	IRAK4	Diffuse large B cell lymphoma (MYD88-mutant)	CRBN	I.v.	Phase I	
Kymera	KT-333	STAT3	Liquid and solid tumours	Undisclosed	Undisclosed	Phase I	
Nurix Therapeutics	NX-2127	BTK	B cell malignancies	CRBN	Oral	Phase I	NCT04830137
Nurix Therapeutics	NX-5948	BTK	B cell malignancies and autoimmune diseases	CRBN	Oral	Phase I	NCT05131022
C4 Therapeutics	CFT8634	BRD9	Synovial sarcoma	CRBN	Oral	IND-e	
C4 Therapeutics	CFT8919	EGFR-L858R	Non-small-cell lung cancer	CRBN	Oral	IND-e	
Cullgen	CG001419	TRK	Cancer and other indications	CRBN	Oral	IND-e	

Scheme 1.2. PROTACs in Clinical Development[3]

To expand the toolbox available for PROTACs, many research groups have developed new covalent E3 ligase ligands[5] (**Scheme 1.3**). Covalent E3 ligase ligands can be potentially advantageous over non-covalent ligands, because only binary complex is involved. Additionally, covalent ligands can provide a prolonged duration of action, allowing for less frequent dosing and improved patient compliance.

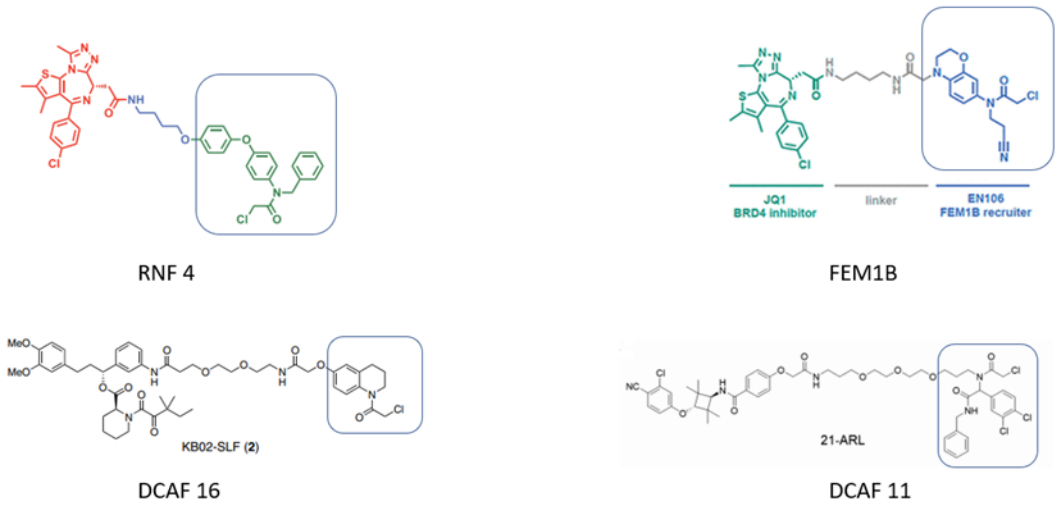

Scheme 1.3. Electrophilic PROTACs[5]

Selecting the most suitable E3 ligase ligand and linker for PROTACs can be challenging. To address this issue, we developed a platform called "Rapid-TAC"[6]. We split a complete PROTAC into two parts: one part is the E3 ligase ligand, various linkers, and a reactive group A, and the other part is the target protein ligand and a reactive group B. Group A, and Group B can spontaneously react to form a complete PROTAC (**Scheme 1.4**). The Rapid-TAC platform offers significant advantages for developing PROTACs, including high-throughput screening capabilities that enable quick assessment of numerous E3 ligase ligands. Its automated and miniaturized processes streamline synthesis and testing, saving time and resources. One of the limitations is that our platform can only support the screening of non-covalent E3 ligase ligands, as reactive group A usually contains an amino group. The amino group, being a nucleophilic group, can react with the Michael acceptor in covalent ligands. For this project, we aim to identify a suitable conjugation reaction and apply it to our new platform, which is capable of screening covalent E3 ligase ligands and linkers.

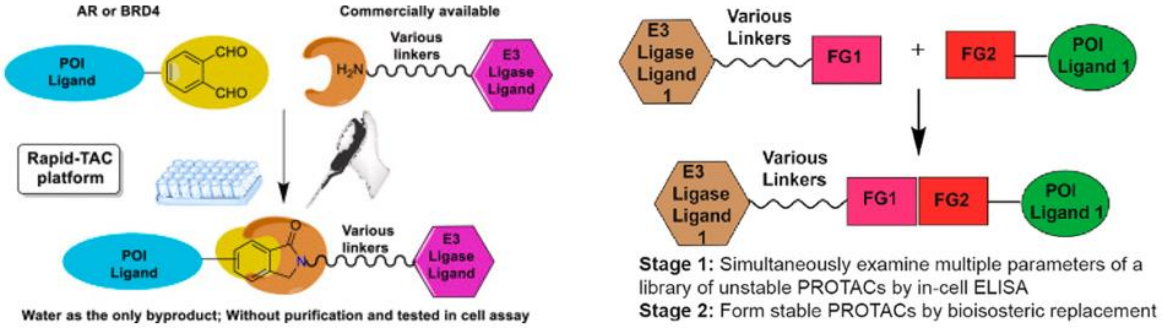

Scheme 1.4. Graphical abstract of Rapid-TAC[6]

Bioorthogonal chemistry refers to a class of high-yield chemical reactions that can occur rapidly and selectively in biological environments[7]. We plan to utilize tetrazine and trans-cyclooctene as the two coupling partners for two main reasons. First, the second-order rate constant of this combination is the highest among known bioorthogonal reactions. Given the low concentrations of the coupling partners in our system, a high reaction rate is essential to ensure that our PROTAC can self-assemble within cells. Second, the two reactants, tetrazine and trans-cyclooctene, have very limited interaction with target proteins in cells, which helps reduce nonspecific binding by the coupling partners. Additionally, in 2016, the Heightman group successfully developed in-cell self-assembling PROTACs using these two coupling partners[8], demonstrating that this bioorthogonal reaction is suitable for the in-situ formation of PROTACs in cells (**Scheme 1.5)**.

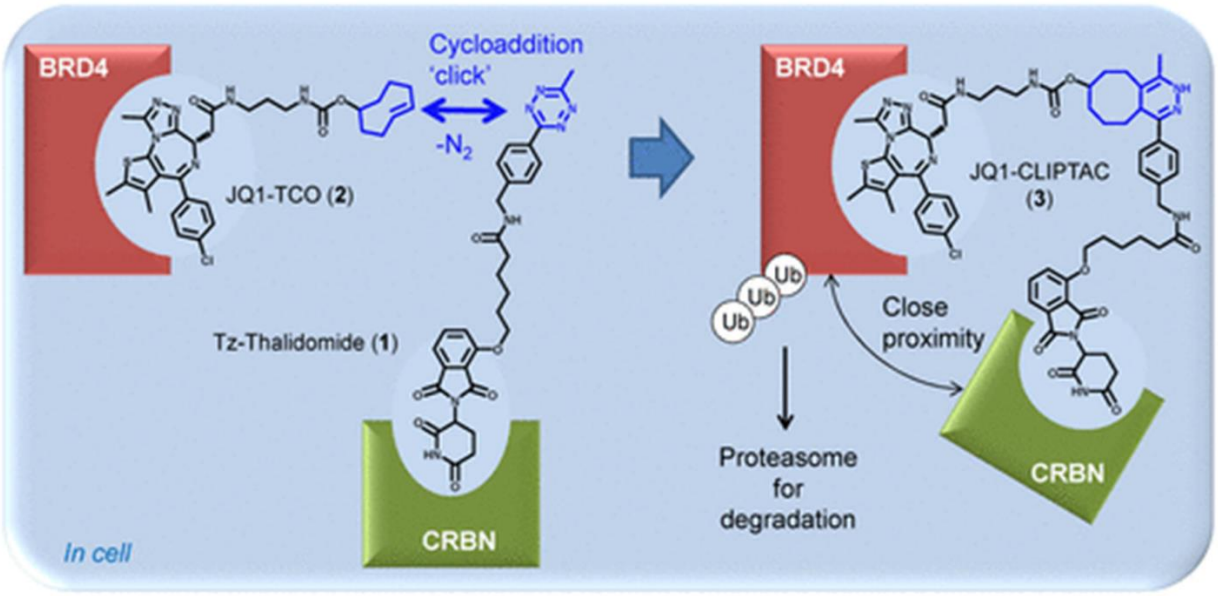

Scheme 1.5. Graphical abstract of Rapid-TAC[8]

Based on this tetrazine and trans-cyclooctene chemistry, we designed our new platform as shown in **Scheme 1.6**. We split the electrophilic PROTACs into two parts: one part is a tetrazine-tagged covalent E3 ligase ligand, and the other part is a cyclooctene-tagged target protein ligand. These two partners can spontaneously react within cells to form a complete PROTAC (**Scheme 1.6**). We also call it CLIPTAC (Click-PROTAC)

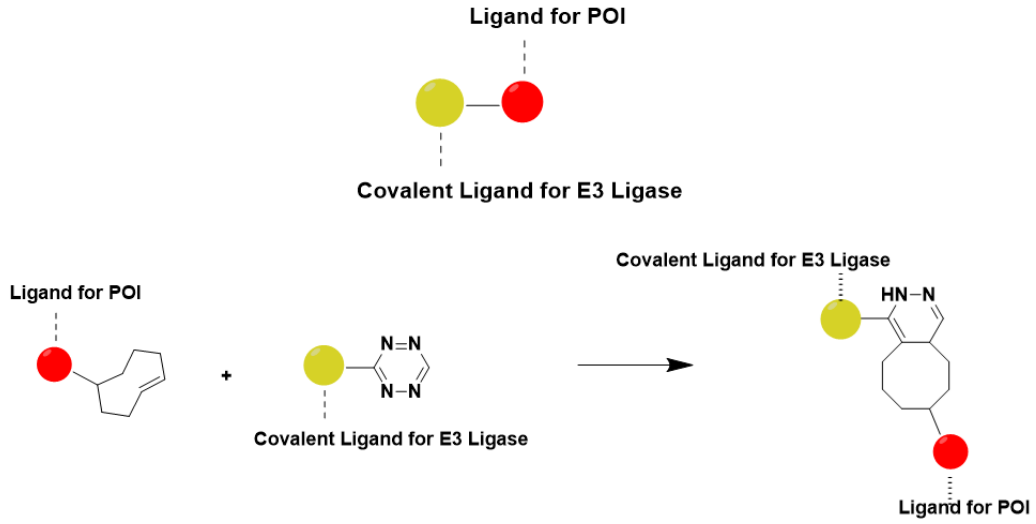

Scheme 1.6. Schematic illustration of electrophilic CLIPTAC

The mechanism of our proposal is illustrated in (**Scheme 1.7**)**.** First, the tetrazine-tagged covalent E3 ligase ligand forms a covalent bond with the E3 ligase. Subsequently, the modified E3 ligase reacts with the trans-cyclooctene-tagged ligand to form the electrophilic CLIPTAC.

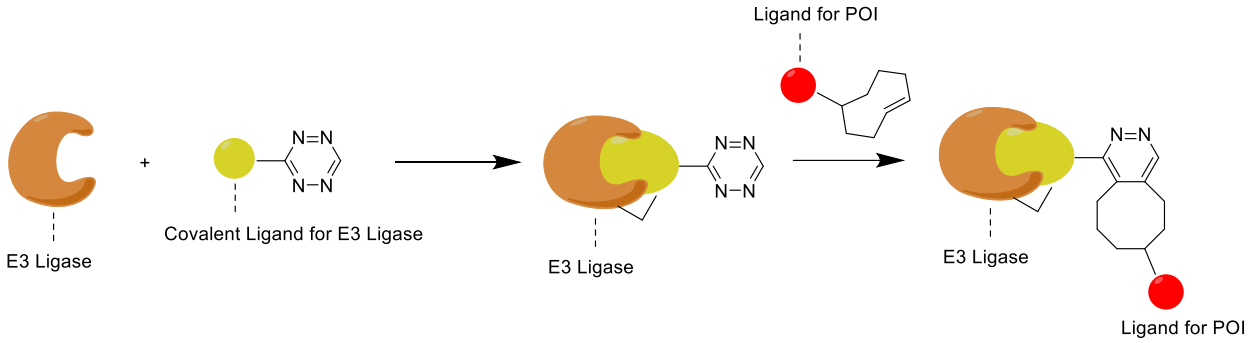

Scheme 1.7. Schematic illustration of electrophilic CLIPTAC

1.2. Design of Chemical Probes

To verify whether our proposal can be used in discovering new E3 ligases, we conducted a proof-of-concept (POC) study. AM-A3, an ERα degrader developed by our group, was divided into two chemical entities. Probe A consists of a known ligand for Keap1 and a tetrazine group capable of conducting an inverse Diels-Alder reaction with a trans-cyclooctene group, while Probe B consists of a ligand for ERα and a trans-cyclooctene group that can react with a tetrazine group. To increase the chance of success (**Scheme 1.8)**, I also synthesized a tetrazine-RNF26 compound (Probe A') and a JQ1-TCO compound (Probe B'). With these chemical probes, we can test four combinations: (1) JQ1-TCO with tetrazine-RNF126; (2) JQ1-TCO with tetrazine-Keap1; (3) ERα-TCO with tetrazine-RNF126; (4) ERα-TCO with tetrazine-Keap1 (**Scheme 1.9)**.

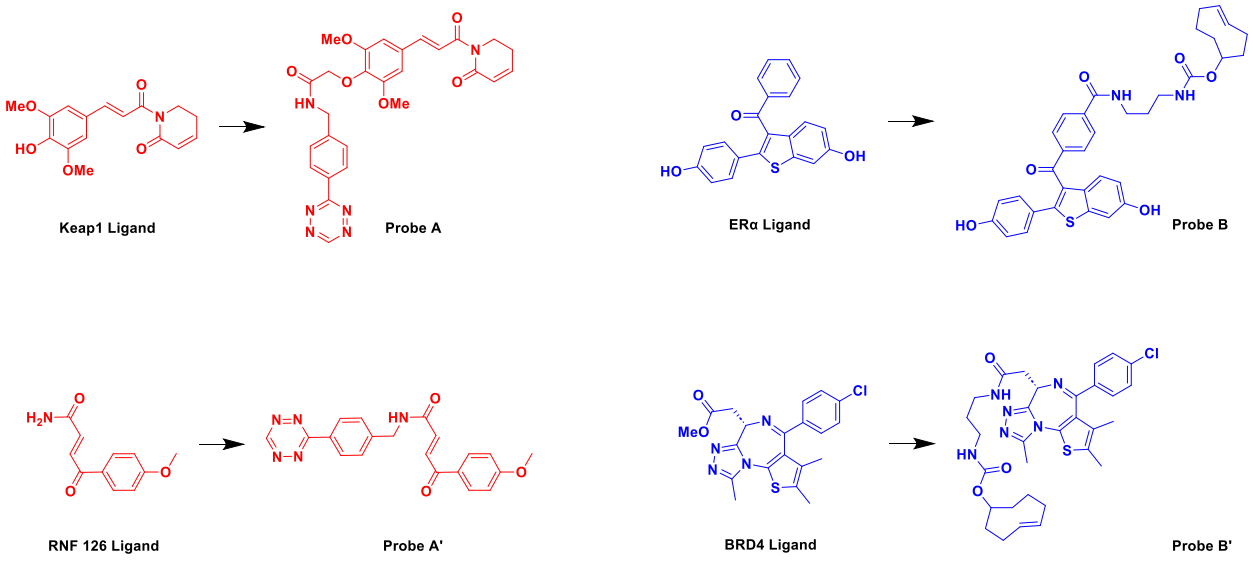

Scheme 1.8. Design of chemical probes

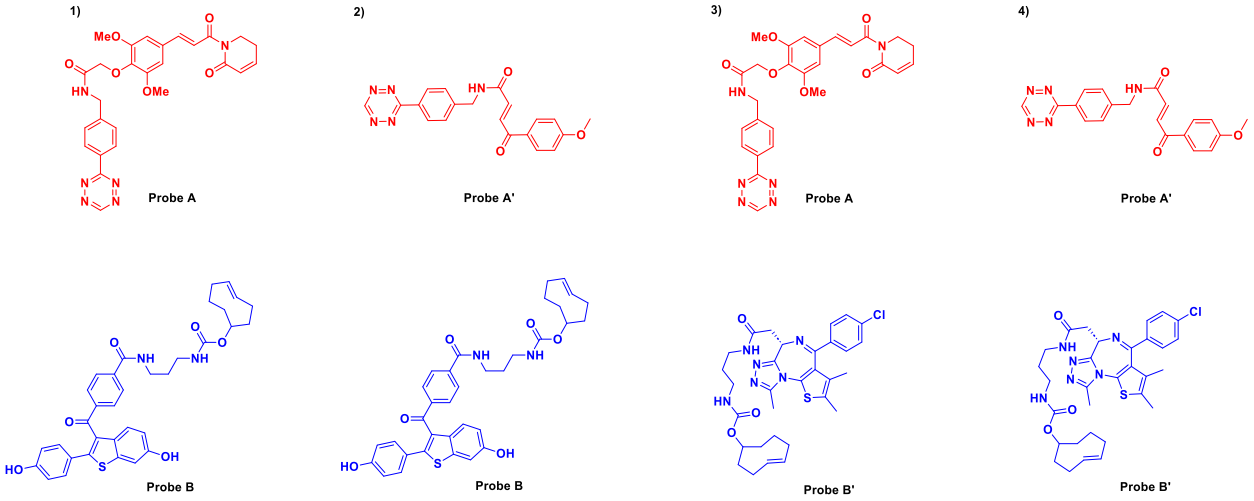

Scheme 1.9. Four combinations

1.3. Synthesis of Chemical Probes

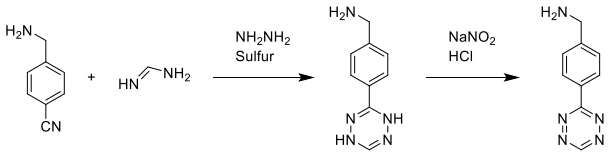

231 mg

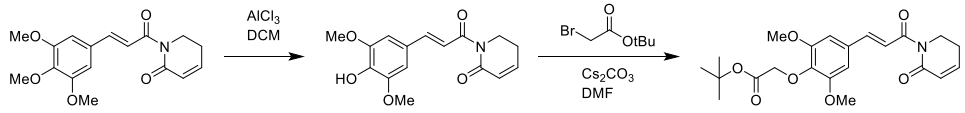

343 mg, 77 %

375 mg, 85 %

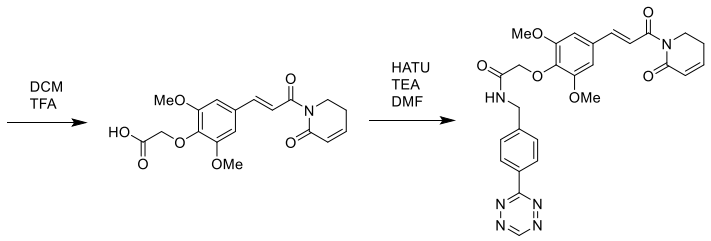

7 mg, 27 %

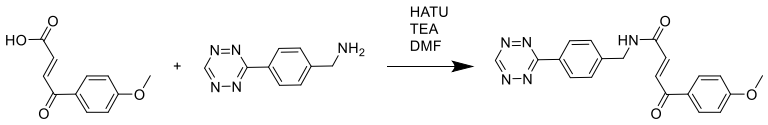

8 mg, 32 %

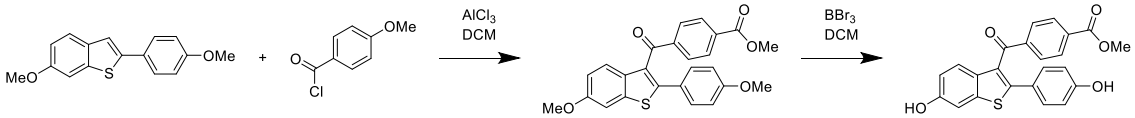

74 %, 400 mg

34 %, 40 mg

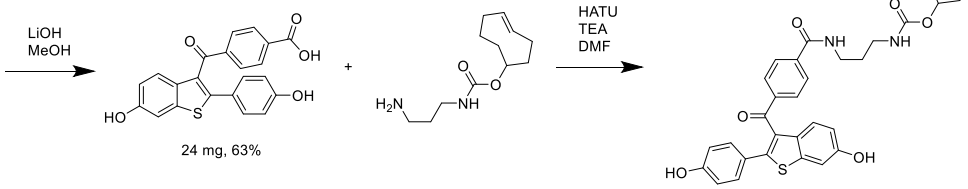

24 mg, 63%

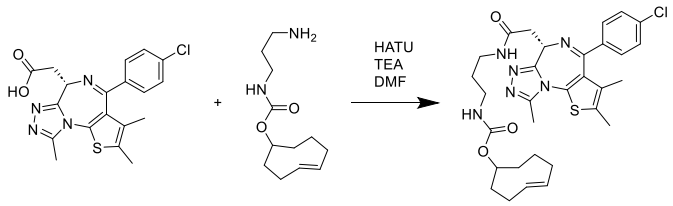

1.4. General Procedure of Biological Experiments

Next, we tested whether these four combinations could achieve the degradation of the protein of interest (POI). First, we incubated cells with probe A for 30 minutes. With the aid of an electrophilic E3 ligase ligand, probe A can form a covalent bond with the E3 ligase. After washing off probe A, we treated the cells with probe B for 6 hours. Following this, we prepared cell lysates and evaluated the protein levels by western blotting. To demonstrate the degradation of the POI via hijacking of the ubiquitin-proteasome system, we also pretreated the cells with a proteasome inhibitor or a Neddylation inhibitor. If these inhibitors can attenuate the degradation of the POI, it indicates that the degradation is due to the ubiquitin-proteasome system (**Scheme 1.10**).

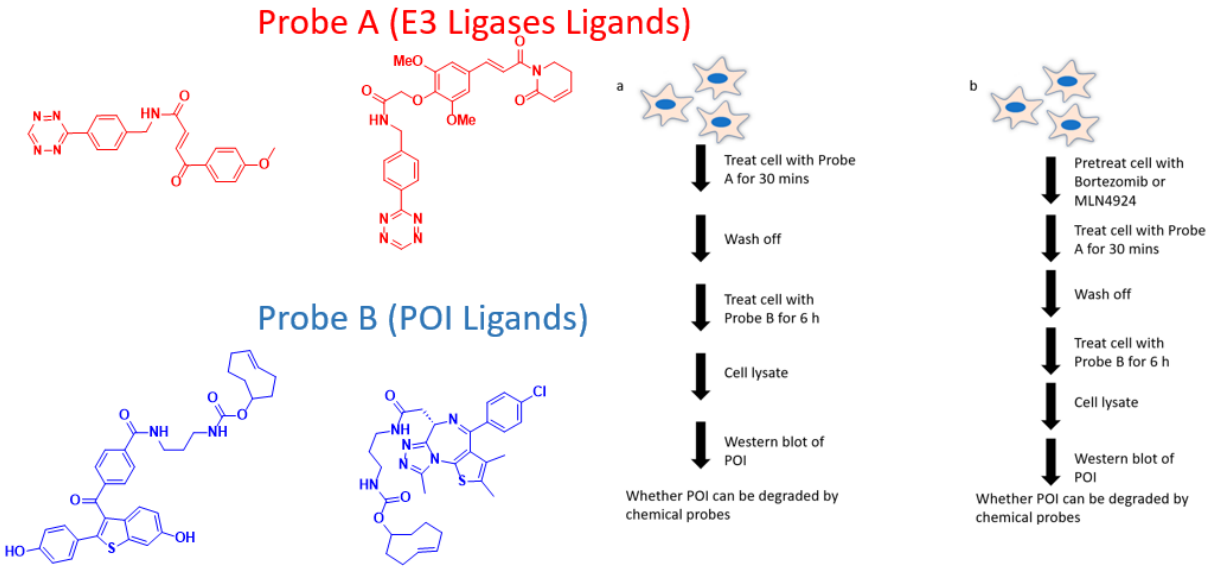

Scheme 1.10. General procedure of biological experiments

1.5. Biological Activities of Chemical Probes

Dr. Zhongrui Zhang and Ira Tandon tested the biological activities of these chemical probes in several cell lines (**Scheme 1.11**). Using combo 2 (RNF126 ligand + ERα), we successfully degraded ERα. However, when treating cells with combo 1 (Keap1 ligand + ERα), no degradation of ERα was observed. These results indicate that the RNF126 ligand is a better option for preparing ERα PROTACs. Conversely, for the degradation of BRD4, we achieved degradation only with Keap1-recruiting CLIPTAC and did not observe any degradation of BRD4 with RNF126-recruiting CLIPTAC.

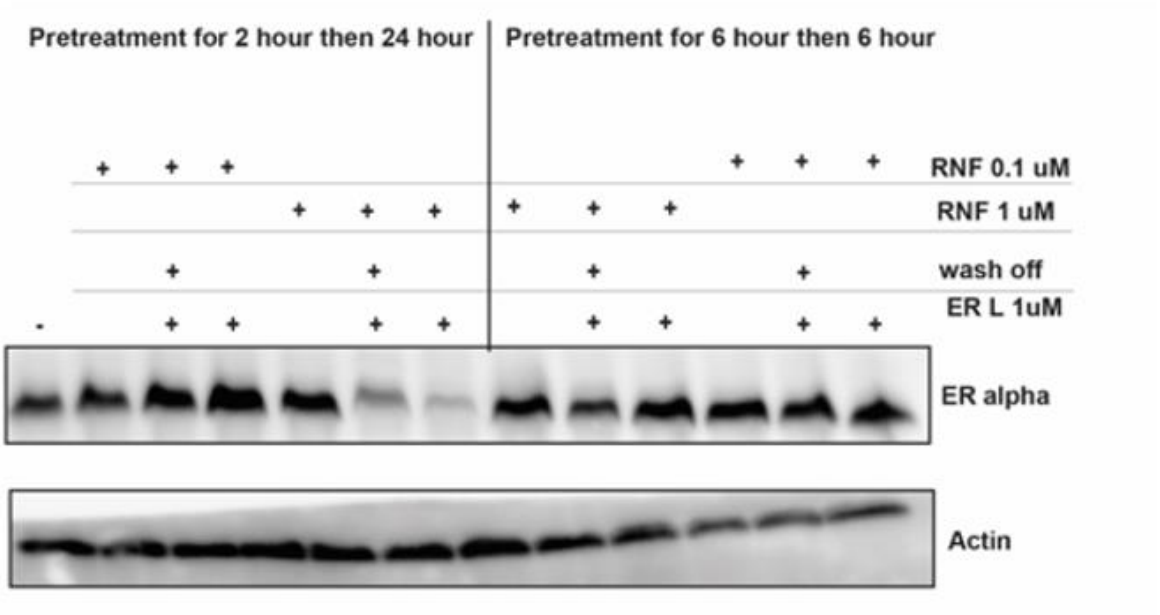
Pretreatment for 2 hour then 24 hour
Pretreatment for 6 hour then 6 hour
RNF 0.1 uM
RNF 1 uM
wash off
ER L 1uM
-
ER alpha
Actin

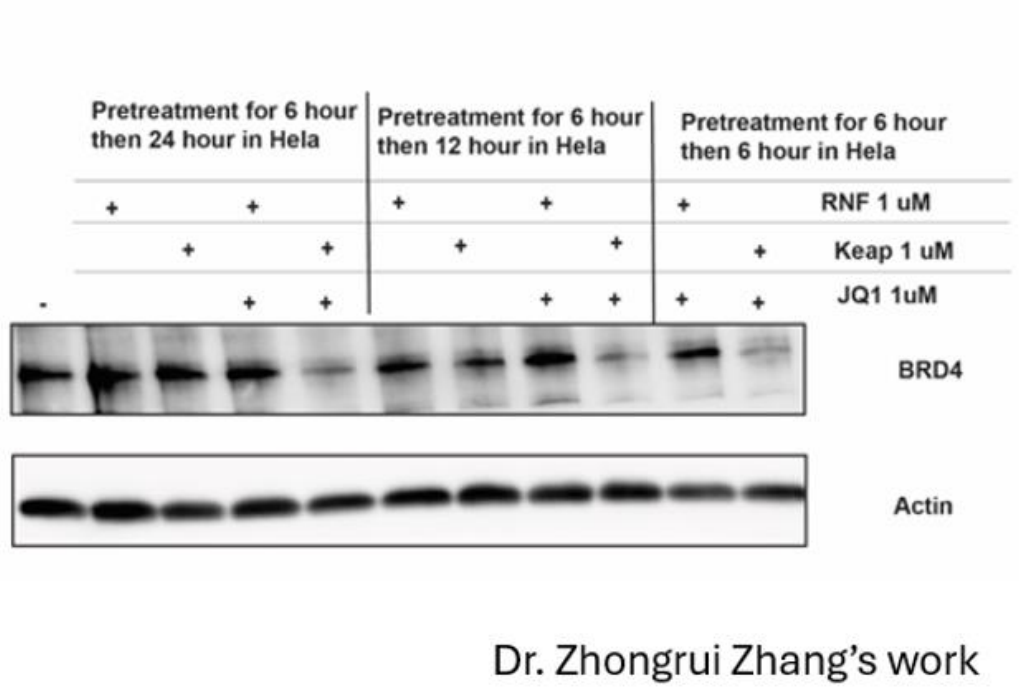

Scheme 1.11. CLIPTACs were tested by western blot in MCF-7 cells

In a subsequent experiment, we focused on the investigation of potential benefits of electrophilic CLIPTAC: enhanced cell permeability due to its lower molecular weight and reduced polar surface area compared to traditional PROTACs (**Scheme 1.12**). Our main objective was to compare the effectiveness of a pre-assembled PROTAC mixture (PRE-MIX) with our CLIPTAC system in degrading BRD4 in HeLa cells. Western blot analysis revealed a clear difference between the two conditions. Under the CLIPTAC treatment with 5 μM PL-Tz and 1 μM JQ1-TCO, most BRD4 proteins were degraded. In contrast, the PRE-MIX treatment, despite using the same concentration of 5 μM, resulted in less degradation of BRD4.

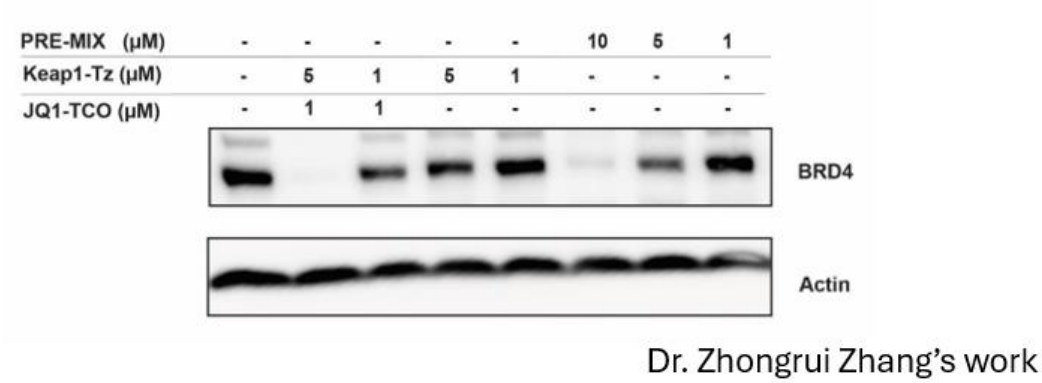

Scheme 1.12. Comparative Analysis of Sequential CLIPTAC and Pre-Assembled

To verify the mechanism behind the CLIPTAC strategy, we examined the ubiquitin-proteasome pathway (**Scheme 1.13**). which plays a vital role in PROTAC-induced protein degradation. Consequently, we designed a series of experiments utilizing competitive inhibitors that interfere with various stages of this pathway. The loss of BRD4 was attenuated by proteasome and NEDDylation inhibitors, consistent with a proteasome- and Cullin E3 ligase-dependent mechanism of BRD4 degradation.

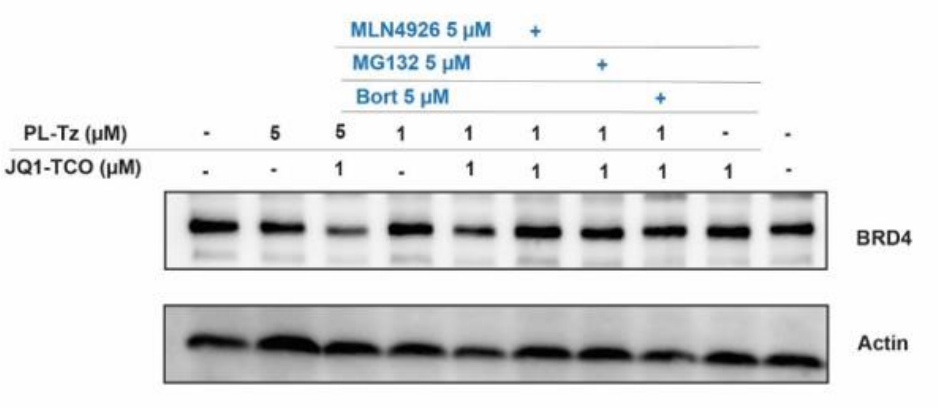

Dr. Zhongrui Zhang's work

Scheme 1.13. Validation of the Ubiquitin-Proteasome Pathway Mechanism

In conclusion, our findings demonstrate that CLIPTAC offers several advantages over traditional PROTACs. First, CLIPTAC enhances cell permeability and effective protein degradation by leveraging its smaller molecular weight and reduced polar surface area. Second, CLIPTAC facilitates the selection of appropriate E3 ligase ligands for different target proteins. These results highlight the potential of CLIPTAC to expand the scope of therapeutic applications and improve the efficacy of protein degradation technologies.

1.6. Potential Applications of Electrophilic CLIPTAC

The success of our proof-of-concept study motivates us to further explore the application of electrophilic CLIPTAC. Fragment-based ligand discovery (FBLD) is an effective strategy for identifying small molecules that elucidate protein functions and serve as leads for new drugs.

However, traditional FBLD methods are limited to proteins that can be produced in large quantities, leaving many human proteins unexplored. To address this limitation, the research groups of Benjamin Cravatt and Steven Gygi developed a proteome-wide covalent ligand discovery technique[9] using cysteine-reactive small-molecule fragments in native biological systems (**Scheme 1.14**). Their work significantly broadens the scope of the ligandable proteome and establishes covalent FBLD as a versatile method for investigating protein functions in complex biological environments. This research has identified many covalent E3 ligase ligands. However, the potential of these E3 ligase ligands for use in PROTACs remains uncertain. In this project, we aim to identify covalent E3 ligase ligands that can be utilized in the development of PROTACs.

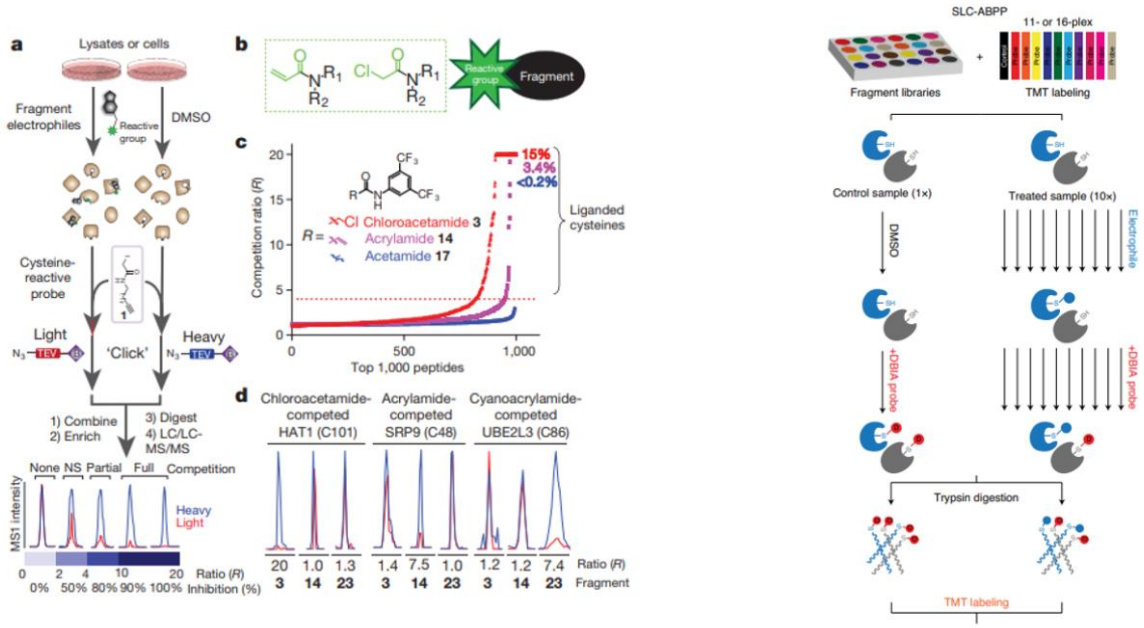

Scheme 1.14. Proteome-wide covalent ligand discovery in native biological systems[9]

1.7. Design of New Chemical Probes for Different E3 Ligase

After reviewing the study conducted by Gygi's group, we selected compound AC 36 for further investigation (**Scheme 1.15**). In our selection process, we considered not only the binding affinity

but also the selectivity of each compound. We hope this strategy will help us narrow down the potential E3 ligases that these compounds can recruit.

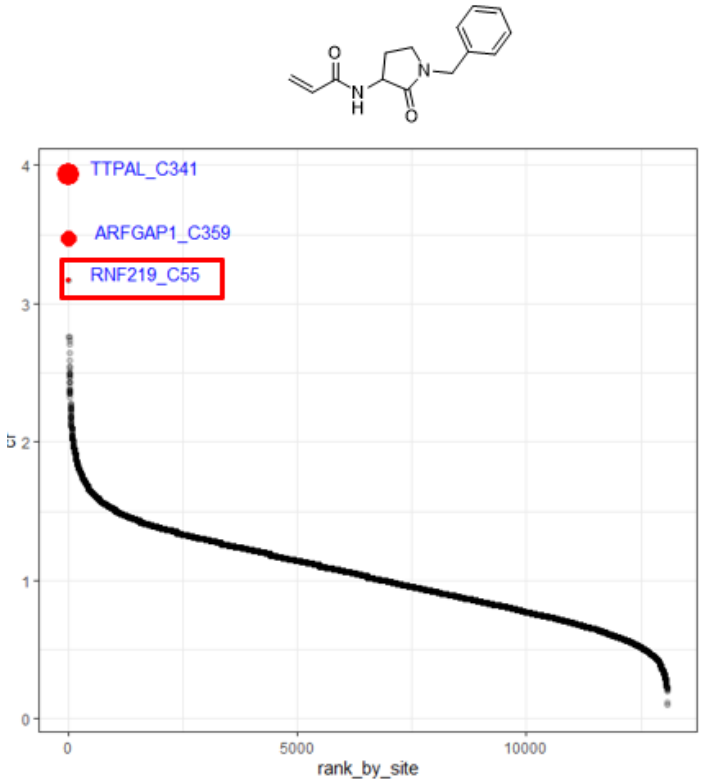

Scheme 1.15. Proteome-wide covalent ligand discovery in native biological systems[9]

Upon analyzing the structure of AC 36, we identified two potential sites for attaching a linker. Consequently, we designed two analogues, AC 36-1 and AC 36-2, for further biological study. Although we successfully obtained the desired products, unfortunately, unlike previous tetrazine-based chemical probes, these two probes are not stable in DMSO solution. To address this limitation, we attempted to use methyl tetrazine to replace tetrazine, resulting in a more stable analogue, AC 36-3. We then proceeded to use AC 36-3 for further biological studies (**Scheme 1.16**).

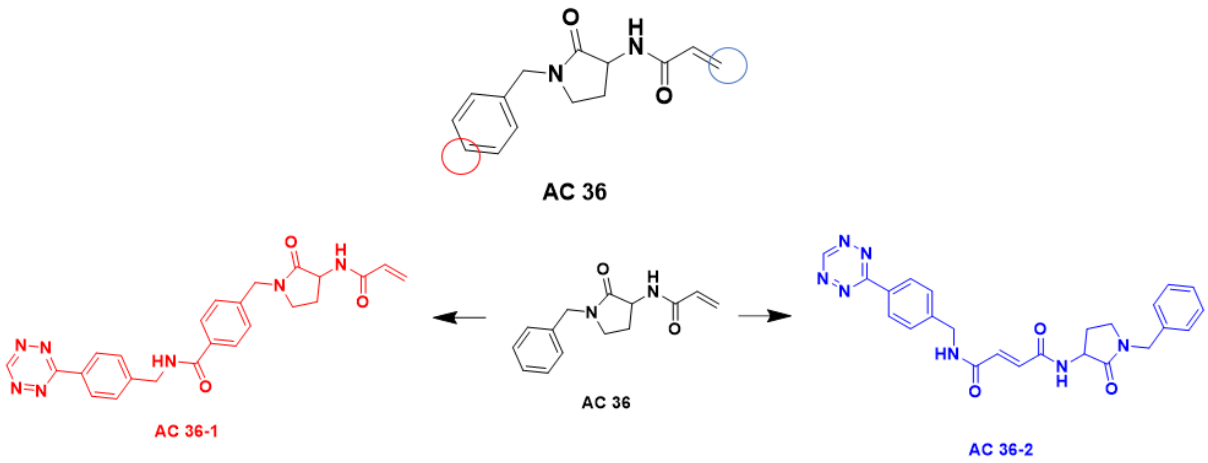
AC 36
AC 36-1
AC 36
AC 36-2

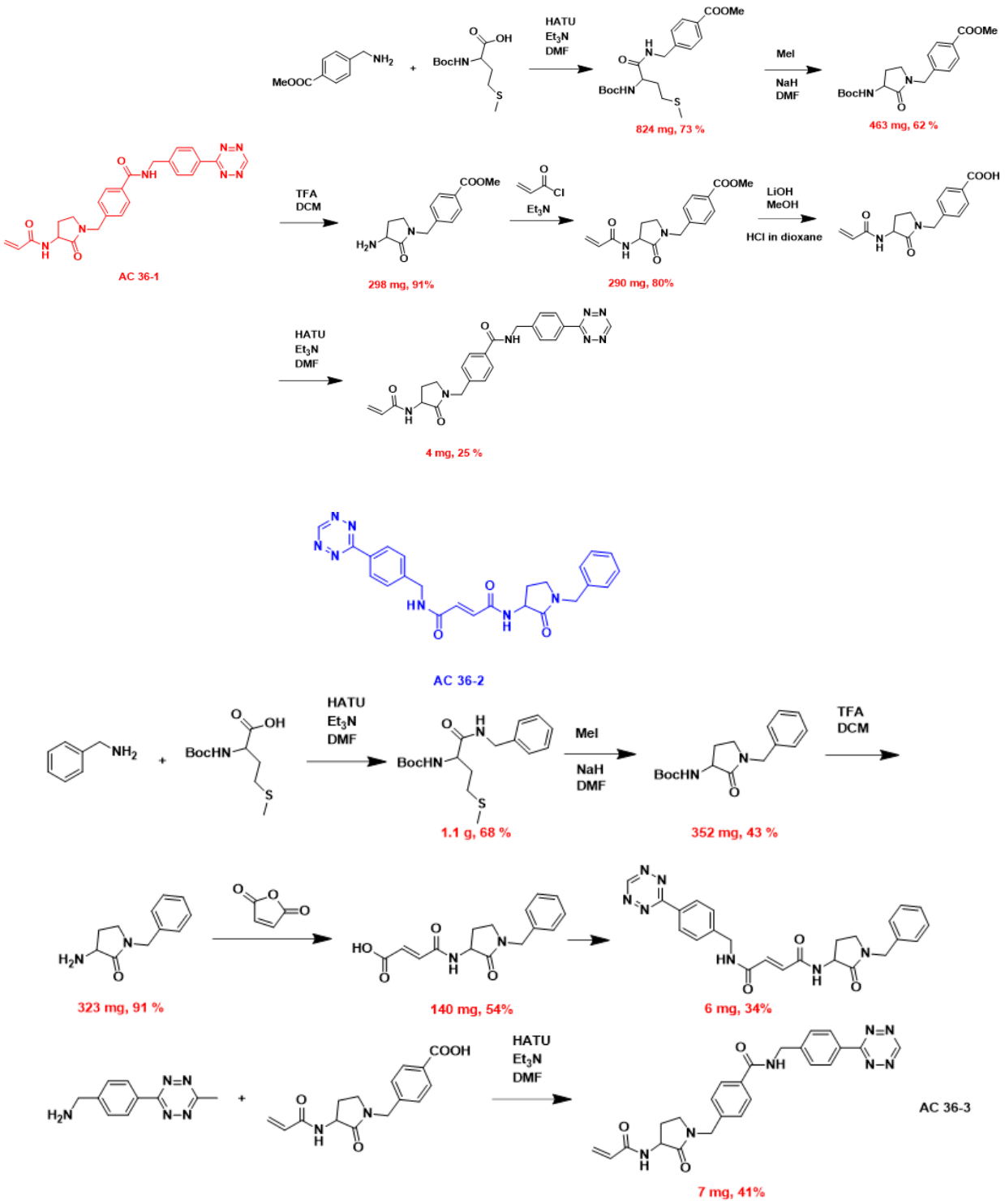

Scheme 1.16. Synthesis of AC 36 analogues

1.8. Biological Study of RNF219 Ligand Based Chemical probes

We attempted to degrade BRD4 using two probes: JQ-1-TCO and AC 36-3. However, Western blot analysis did not show any degradation of BRD4 (**Scheme 1.17**). Our electrophilic CLIPTAC may fail to degrade a target protein due to inefficient recruitment of the E3 ligase, which can be caused by poor binding affinity or steric hindrance, preventing the formation of a stable ternary complex. Additionally, even if ubiquitination occurs, the target protein might not be effectively recognized or processed by the proteasome, possibly due to suboptimal ubiquitin chain formation or proteasomal processing inefficiencies.

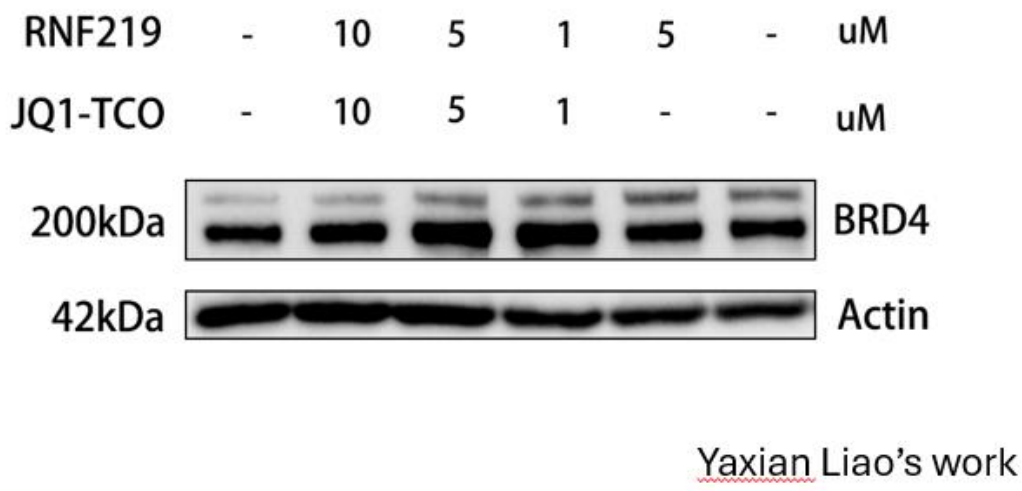

Scheme 1.17. Biological study of new CLIPTACs

1.9. Discussion and Perspectives

This research successfully demonstrates the potential of CLIPTACs (Click-PROTACs) as an innovative strategy for targeted protein degradation. Our proof-of-concept study validates the feasibility of using covalent E3 ligase ligands, integrated through bioorthogonal chemistry, to achieve efficient and specific degradation of target proteins. By leveraging the unique properties of tetrazine and trans-cyclooctene coupling partners, the CLIPTAC platform may offer enhanced cell permeability and improved pharmacokinetic properties compared to traditional PROTACs.

The development and testing of our Rapid-TAC platform facilitated the high-throughput screening of various E3 ligase ligands and linkers, proving its utility in quickly identifying suitable candidates for PROTAC development. Our findings revealed that RNF126 and Keap1 ligands effectively degrade ERα and BRD4, respectively, showcasing the versatility of our approach.

Moreover, the electrophilic CLIPTAC strategy has the potential to expand the scope of targetable proteins and addresses limitations associated with current PROTAC technologies. The platform's capability to integrate covalent ligands broadens the range of E3 ligase ligands and enhances the therapeutic potential of PROTACs.

Future studies will aim to further optimize this platform and explore its applications in fragment-based ligand discovery, ultimately contributing to the broader field of drug discovery.

1.10. Experimental Sections

General Information

Unless otherwise stated, all commercial reagents were used as received. Reactions were conducted in dry glassware using anhydrous solvents (pass through activated alumina columns). Unless stated otherwise, reactions were performed at room temperature (rt). Thin-layer chromatography (TLC) was conducted on plates (EMD Chemical Inc. 60, F254) and visualized using a combination of UV, sulfuric acid, and ceric ammonium molybdate staining. Flash column chromatography was performed with silica gel (Silicycle, 40-63 μm). Infrared spectra (IR) were obtained on a Bruker Equinox 55 Spectrophotometer. Optical rotations were recorded on Perkin-Elmer 241 polarimeter. ^{1}H and ^{13}C nuclear magnetic resonance spectra (NMR) were obtained on a Brooker 400 MHz. Chemical shifts were reported in parts per million (ppm), and the residual solvent peak was used as an internal reference: proton (chloroform δ 7.26), carbon (chloroform δ 77.16) or tetramethylsilane (TMS δ 0.00) was used as a reference. Multiplicity was indicated as follows: s (singlet), d (doublet), t (triplet), m (multiplet), dd (doublet of doublet), td (triplet of doublet), bs (broad singlet). Coupling constants (*J*) were reported in Hertz (Hz). All high-resolution mass spectra were performed by Analytical Instrument Center at the School of Pharmacy (UW-Madison) on an Electron Spray Injection (ESI) mass spectrometer.

Experimental Procedures

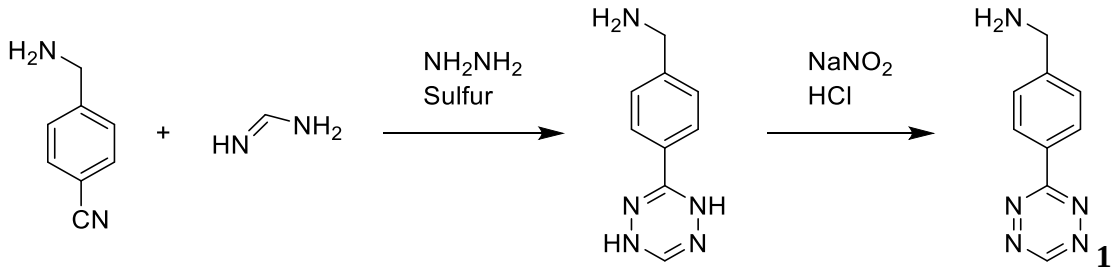

To a mixture of 4-(aminomethyl) benzonitrile hydrochloride (0.42 g, 2.5 mmol), formamidine acetate (1.04 g, 10.0 mmol), and elemental sulfur (80 mg, 2.5 mmol) in a round-bottom flask, was carefully added anhydrous hydrazine (1.0 mL). The mixture was stirred at room temperature for 20 h. Subsequently, 1% aqueous HCl (25 mL) was slowly added, and the mixture was stirred for an additional 10 min. The precipitate formed in this process was removed by filtration. The resulting red-orange solution was cooled to 0°C. $NaNO_2$ (0.85 g, 12 mmol in 7.5 mL water) was then carefully added to the solution, followed by the addition of acetic acid (25 mL). After stirring the mixture at room temperature for 3 h, the solution was concentrated in vacuo. The residue was purified by silica gel column chromatography. ^{1}H NMR (400 MHz, d_6-DMSO) 10.62 (1H, s), 8.57 (2H, d, J 8.4), 7.76 (2H, d, J 8.4), 4.18 (2H, d, J 5.5); ^{13}C NMR (101 MHz, d_6-DMSO) 165.3, 138.6, 131.8, 129.7, 127.4, 41.7; LCMS: m/z 188.1

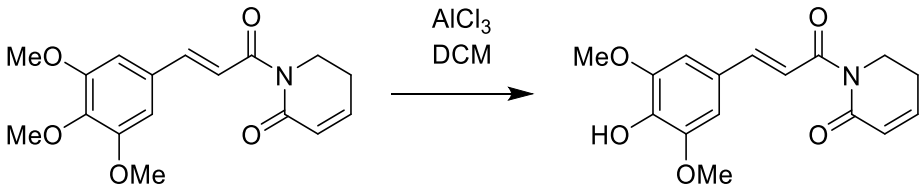

To a stirred solution of piperlongumine (5.60 g, 17.6 mmol) in anhydrous dichloromethane (DCM) was added $AlCl_3$ (23.3 g, 174 mmol) at 28°C. The $AlCl_3$ cannot be completely dissolved, and the red suspension turned into a yellow suspension after stirring at 28°C for 15 minutes. Saturated $NaHCO_3$ was then added, and the mixture was extracted with dichloromethane (2 × 150 mL). The combined organic layers were washed with brine (3 × 50 mL), dried over anhydrous Na_2SO_4, concentrated in vacuo, and washed with a dichloromethane/petroleum ether mixture (v/v = 2:3) to yield the desired product. ^{1}H NMR (400 MHz, $CDCl_3$) δ 7.64 (d, J = 15.4 Hz, 1H), 7.42 (d, J= 15.4 Hz, 1H), 6.92 (dt, J= 9.7, 4.2 Hz, 1H), 6.83 (s, 2H), 6.08 (dt, J = 9.7, 1.9 Hz, 1H), 5.74 (s, 1H), 4.03 (t, J = 6.5 Hz, 2H), 3.92 (s, 6H), 2.51-2.44 (m, 2H). LCMS: 304.2

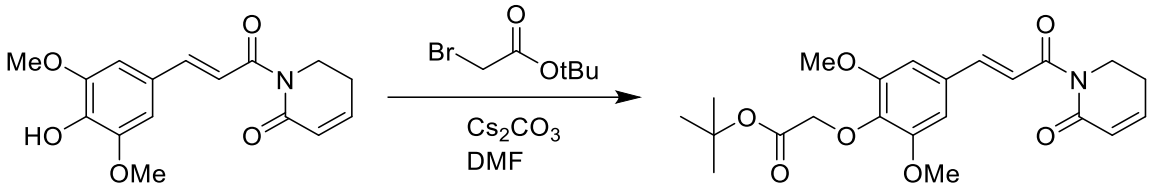

To a solution of piperlongumine (304 mg, 1 mmol) in anhydrous DMF was added tert-butyl bromoacetate (220 mg, 1.2 mmol, 1.2 eq) and cesium carbonate (646 mg, 2 mmol, 2.0 eq). The mixture was then stirred at 55°C for 4 h. Upon completion of the reaction, 10 mL of water was slowly added, followed by extraction with ethyl acetate (3 × 20 mL). The combined organic layers were concentrated in vacuo. The residue was purified by flash column chromatography on silica gel to afford the desired product. ^{1}H NMR (400 MHz, $CDCl_3$) δ 7.64 (d, J = 15.5 Hz, 1H), 7.39 (d, J= 15.5 Hz, 1H), 6.92 (d, J= 9.7 Hz, 1H), 6.76 (s, 2H), 6.02 (dd, J= 9.7, 1.9 Hz, 1H), 4.57 (s, 2H), 4.02 (t, J= 6.5 Hz, 2H), 3.82 (s, 6H), 2.50 - 2.43 (m, 2H), 1.45 (s, 9H).

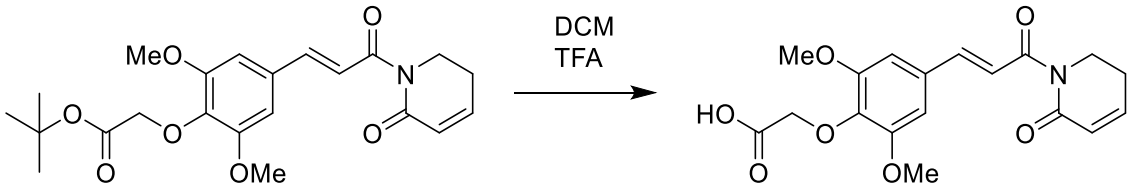

To a solution of t-butyl protected piperlongumine in anhydrous DCM (2 mL) was added TFA (1 mL) slowly. The mixture was stirred at room temperature for 2 h. The solvent was then removed in vacuo, and the residue was directly used in the next step.

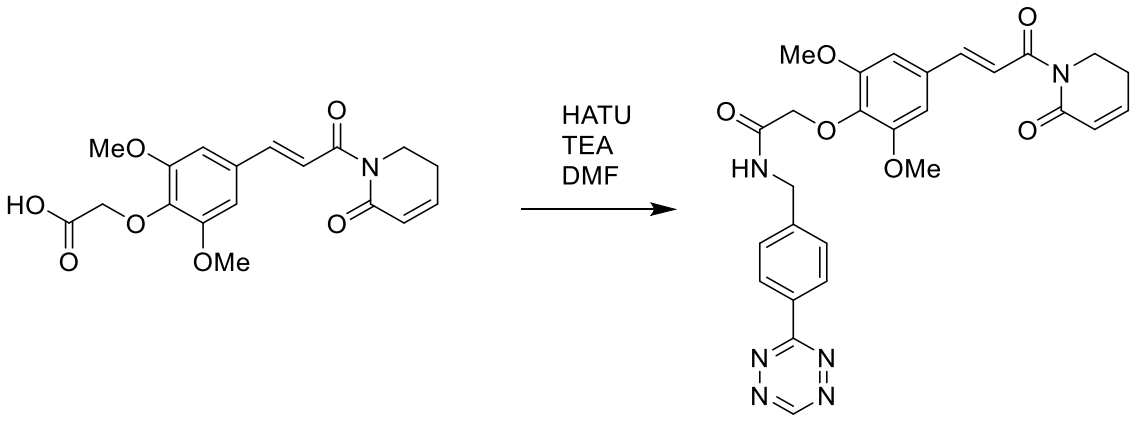

To a solution of tetrazine amine (19 mg, 0.1 mmol) in DMF was added HATU (40 mg, 0.12 mmol), piperlongumine (41 mg, 0.1 mmol), and DIPEA (21 mg, 0.2 mmol). The reaction mixture was stirred at room temperature overnight. The mixture was then extracted and concentrated in vacuo. The residue was purified by flash column chromatography on silica gel to afford the desired product. ^{1}H NMR (400 MHz, DMSO) δ 10.59 (s, 1H), 8.60 (t, *J* = 6.1 Hz, 1H), 8.49 (d, *J* = 8.2 Hz, 2H), 7.59 – 7.54 (m, 3H), 7.29 (d, *J* = 15.5 Hz, 1H), 7.14 – 7.07 (m, 1H), 6.99 (s, 1H), 5.97 (d, *J* = 9.7 Hz, 1H), 4.54 (d, *J* = 6.1 Hz, 1H), 4.46 (s, 2H), 3.96 – 3.83 (m, 2H), 3.80 (s, 6H), 3.76 – 3.70 (m, 1H), 3.69 (s, 2H).

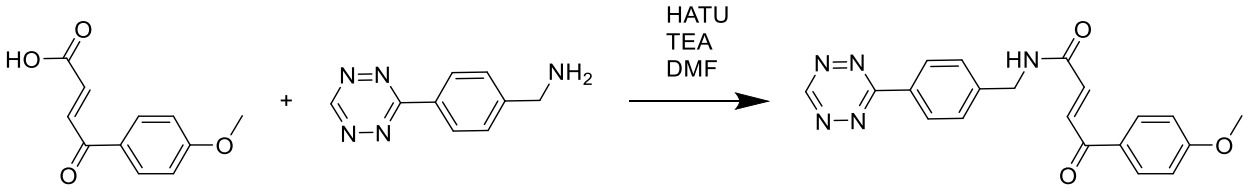

To a solution of tetrazine amine (19 mg, 0.1 mmol) in DMF was added HATU (40 mg, 0.12 mmol), piperlongumine (41 mg, 0.1 mmol), and DIPEA (21 mg, 0.2 mmol). The reaction mixture was stirred at room temperature overnight. The mixture was then extracted and concentrated in vacuo.

The residue was purified by flash column chromatography on silica gel to afford the desired product.

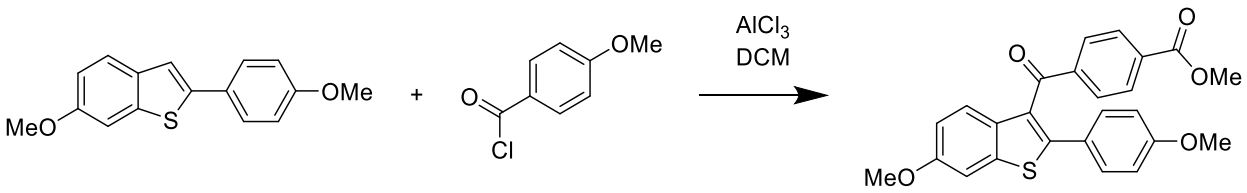

To a mixture of 6-methoxy-2-(4-methoxyphenyl) benzo[b]thiophene (270 mg, 1 mmol) and methyl 4-(chlorocarbonyl) benzoate (187 mg, 1.1 mmol, 1.1 eq.) was added $AlCl_3$ (120 mg, 3 mmol, 3.0 eq.) slowly. The mixture was stirred at room temperature for 6 h. The reaction was then quenched with aqueous HCl and extracted with ethyl acetate. The residue was concentrated and purified by flash column chromatography on silica gel to afford the desired product.

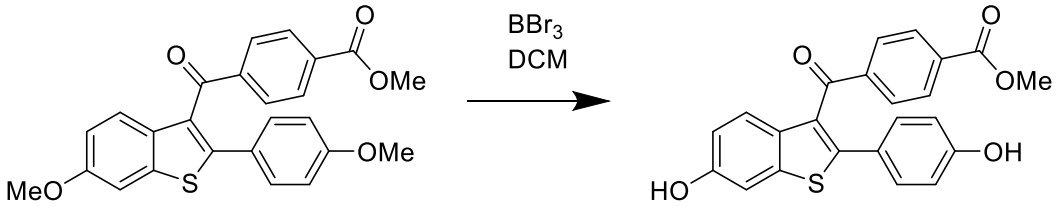

To a solution of methyl 4-[[6-methoxy-2-(4-methoxyphenyl)benzo[b]thien-3-yl]carbonyl]benzoate (432 mg, 1 mmol) was slowly added BBr_3 (550 mg, 2.2 mmol, 2.2 eq.). The mixture was stirred for 4 h at room temperature. The reaction was then quenched with aqueous NH_4Cl and extracted with ethyl acetate. The solvent was removed under reduced pressure. The residue was purified by flash column chromatography on silica gel to afford the desired product.

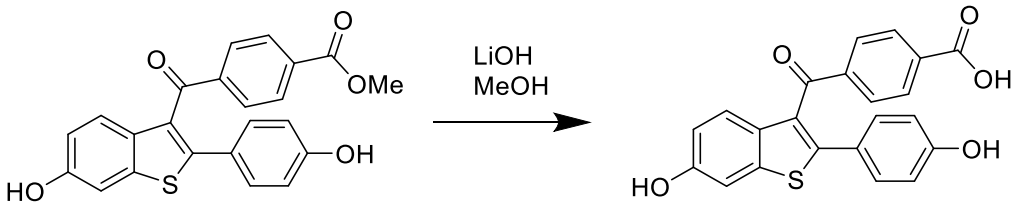

To a solution of methyl 4-[[6-methoxy-2-(4-methoxyphenyl)benzo[b]thien-3-yl]carbonyl]benzoic acid in MeOH was added LiOH (80 mg, 2 mmol). The mixture was stirred at 60°C for 6 h. The mixture was then acidified with aqueous HCl and washed with water. The aqueous layer was extracted with ethyl acetate, and the solvent was removed in vacuo. The residue was directly used in the next step.

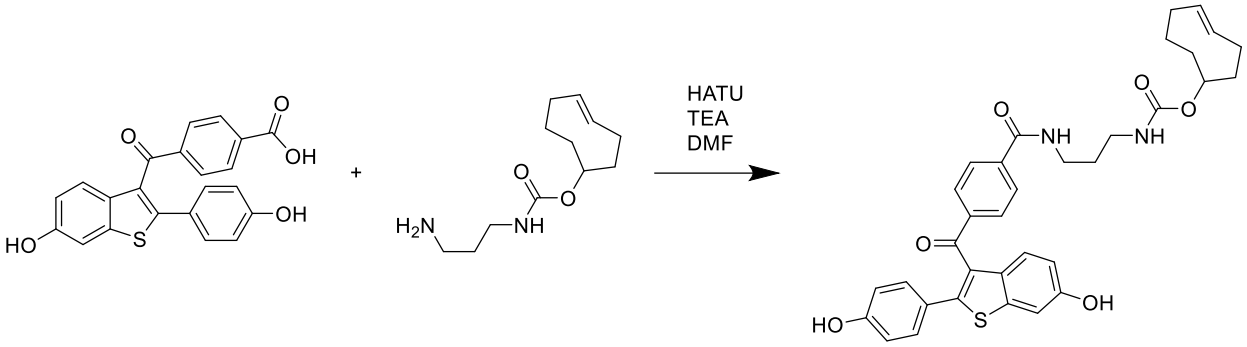

To a solution of trans-cyclooctene amine (19 mg, 0.1 mmol) in DMF was added HATU (40 mg, 0.12 mmol), ERα ligand (41 mg, 0.1 mmol), and DIPEA (21 mg, 0.2 mmol). The reaction mixture was stirred at room temperature overnight. The mixture was then extracted and concentrated in vacuo. The residue was purified by flash column chromatography on silica gel to afford the desired product.

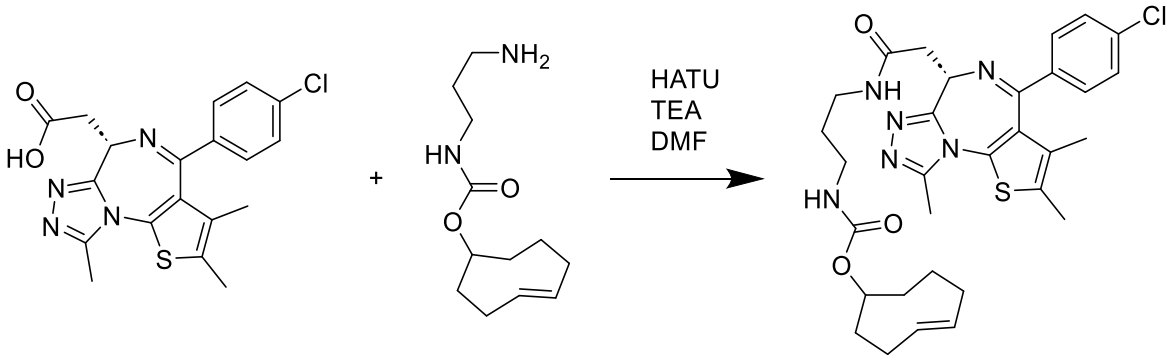

To a solution of trans-cyclooctene amine (19 mg, 0.1 mmol) in DMF was added HATU (40 mg, 0.12 mmol), JQ-1 (41 mg, 0.1 mmol), and DIPEA (21 mg, 0.2 mmol). The reaction mixture was

stirred at room temperature overnight. The mixture was then extracted and concentrated in vacuo. The residue was purified by flash column chromatography on silica gel to afford the desired product.

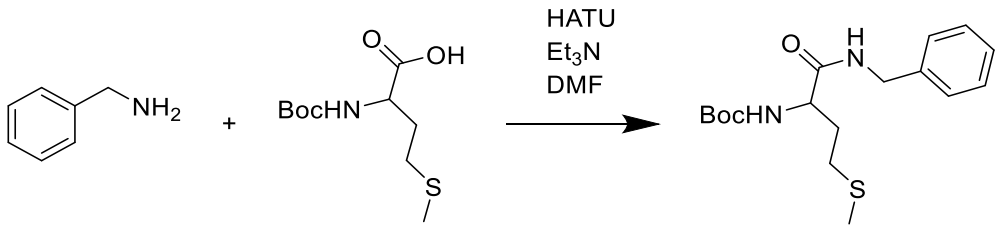

N-methylmorpholine (2.2 mL, 1.2 equivalents) is added to a solution of N-Boc-methionine (4.2 g) in dry THF (100 mL) under an argon atmosphere at -78 °C, followed by the addition of isobutylchloroformate (1.95 mL, 1.2 equivalents). The mixture is stirred for 10 minutes before adding the amine (1.1 eq.). After an additional 10 minutes, the reaction mixture is slowly warmed to room temperature and stirred until the reaction is complete. The solvent is then removed under reduced pressure, and the desired product is isolated by column chromatography on silica gel using 30% ethyl acetate in hexane as the eluent. ^{1}H NMR (400 MHz, $CDCl_3$) δ 7.34 - 7.24 (m, 5H), 6.65 (brs, 1H), 5.23 (brs, 1H), 4.44 (d, *J* = 5.4 Hz, 2H), 4.28 (m, 1H), 2.56 (m, 1H), 2.50 (m, 1H), 2.12 (m, 1H), 2.07 (s, 3H), 1.92 (m, 1H), 1.41 (s, 9H).

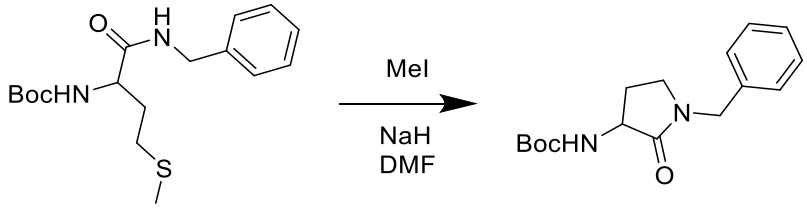

To a solution of N-Boc-amide (5 mmol) and tert-butyl 1-(benzylamino)-4-(methylthio)-1-oxobutan-2-ylcarbamate was added methyl iodide (10 mL/g) at room temperature under an argon

atmosphere and stirred for 24 h. During the reaction, a thick solid of the corresponding sulfonium salt is formed. After the reaction is complete, the excess methyl iodide was removed by rotary evaporation. The sulfonium salt is dissolved in DMF (10 mL/g) and stirred at 0°C for 15 min. NaH (880 mg, 1.1 equivalents) is then added in one portion, and the reaction mixture is stirred at this temperature for 30 min. The mixture is then warmed to room temperature and stirred until the reaction is complete as confirmed by TLC (about 2 h). The reaction is then quenched with methanol and water. The aqueous layer is extracted with EtOAc three times (3 × 50 mL), and the organic layers are combined and washed with water (3 × 25 mL) and brine. The organic layer is dried over anhydrous $MgSO_4$, filtered, and concentrated. Finally, the residue is purified by column chromatography on silica gel using 20-30% ethyl acetate in hexane as the eluent. ^1H NMR (400 MHz, $CDCl_3$) δ 7.31 (dd, J = 6.6, 7.8 Hz, 2H), 7.26 (m, 1H), 7.19 (d, J = 7.8 Hz, 2H), 5.17 (brs, 1H), 4.56-4.44 (m, 2H), 4.23 (m, 1H), 3.22 (dd, J = 4.2, 9.6 Hz, 2H), 2.63 (m, 1H), 1.85 (m, 1H), 1.43 (s, 9H).

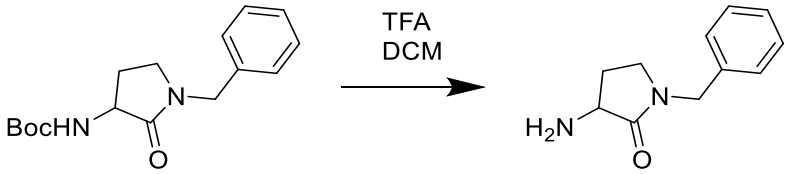

To a solution of t-butyl protected intermediate in anhydrous DCM (2 mL) was slowly added TFA (1 mL). The mixture was stirred at room temperature for 2 h. The solvent was then removed in vacuo, and the residue was directly used in the next step.

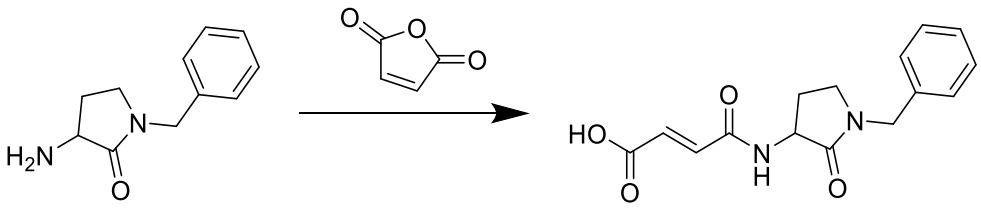

To a solution of the above intermediate (190 mg) in anhydrous THF (2 mL) was added maleic anhydride (110 mg, 1.1 equivalents) and Et_3N (200 mg, 2.0 equivalents). The mixture was heated at 60 °C. After completion, the solvent was removed under reduced pressure, and the residue was directly used in the next step.

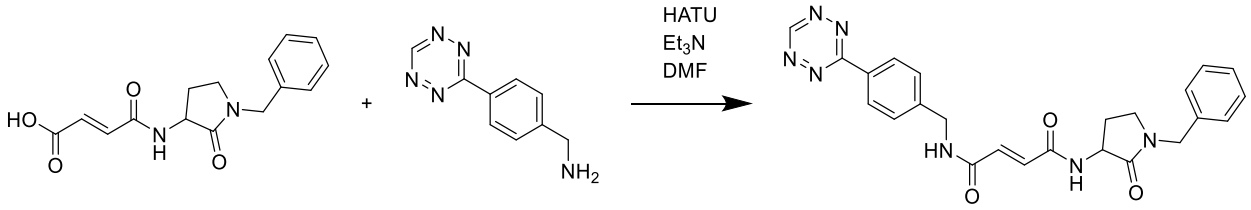

To a solution of tetrazine amine (19 mg, 0.1 mmol) in DMF was added HATU (40 mg, 0.12 mmol), RNF 219 ligand (29 mg, 0.1 mmol), and DIPEA (21 mg, 0.2 mmol). The reaction mixture was stirred at room temperature overnight. The mixture was then extracted and concentrated in vacuo. The residue was purified by flash column chromatography on silica gel to afford the desired product.

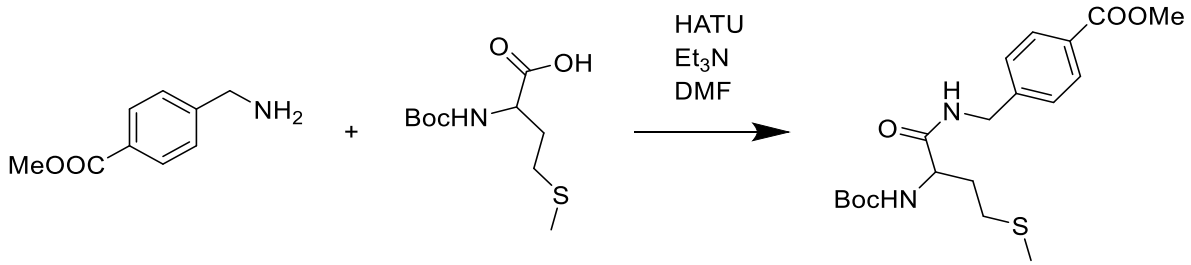

N-methylmorpholine (2.2 mL, 1.2 equivalents) is added to a solution of N-Boc-methionine (4.2 g) in dry THF (100 mL) under an argon atmosphere at -78 °C, followed by the addition of isobutylchloroformate (1.95 mL, 1.2 equivalents). The mixture is stirred for 10 min before adding the amine (1.1 eq.). After an additional 10 min, the reaction mixture is slowly warmed to room temperature and stirred until the reaction is complete. The solvent is then removed under reduced

pressure, and the desired product is isolated by column chromatography on silica gel using 30% ethyl acetate in hexane as the eluent.

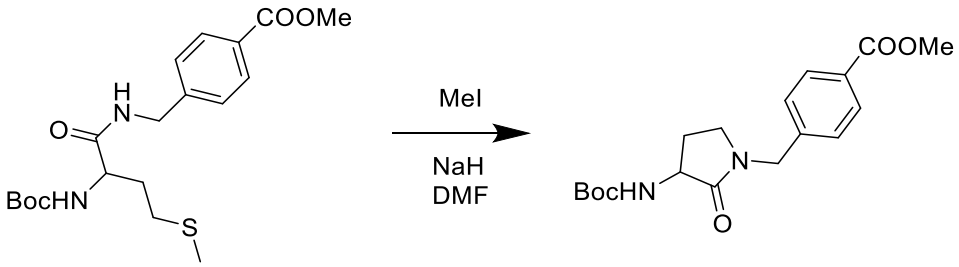

To a solution of N-Boc-amide (5 mmol) and tert-butyl 1-(benzylamino)-4-(methylthio)-1-oxobutan-2-ylcarbamate was added methyl iodide (10 mL/g) at room temperature under an argon atmosphere. The resulting solution was stirred for 24 h. During the reaction, a thick solid of the corresponding sulfonium salt is formed. After the reaction is complete, the excess methyl iodide was removed by rotary evaporation. The sulfonium salt is dissolved in DMF (10 mL/g) and stirred at 0°C for 15 min. NaH (880 mg, 1.1 equivalents) is then added in one portion, and the reaction mixture is stirred at this temperature for 30 min. The mixture is then warmed to room temperature and stirred until the reaction is complete as confirmed by TLC (about 2 h). The reaction is quenched by methanol and water. The aqueous layer is extracted with EtOAc three times (3 × 50 mL), and the organic layers are combined and washed with water (3 × 25 mL) and brine. The organic layer is dried over anhydrous $MgSO_4$, filtered, and concentrated. Finally, the residue is purified by column chromatography on silica gel using 20-30% ethyl acetate in hexane as the eluent.

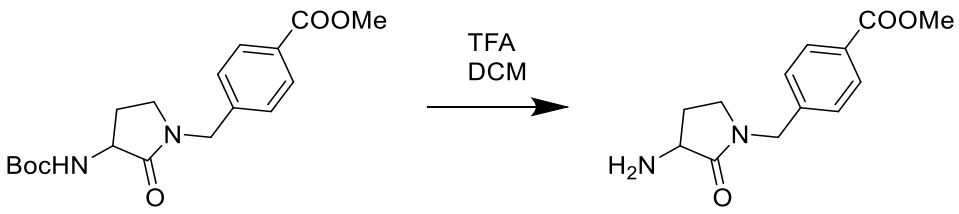

To a solution of t-butyl protected intermediate in anhydrous DCM (2 mL) was added TFA (1 mL). The mixture was stirred at room temperature for 2 h. The solvent was then removed in vacuo, and the residue was directly used in the next step.

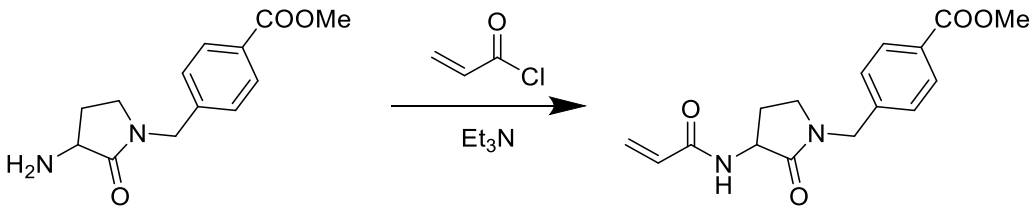

To a solution of the intermediate (248 mg) in anhydrous DMF (2 mL) was added acryl chloride (110 mg, 1.1 equivalents) and Et_3N (200 mg, 2.0 equivalents). The mixture was stirred at room temperature. After completion, the solvent was removed under reduced pressure, and the residue is purified by column chromatography on silica gel using 20-70% ethyl acetate in hexane as the eluent.

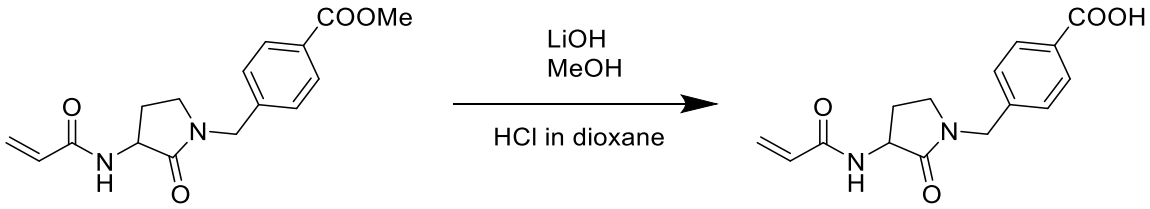

To a solution of intermediate (302 mg) in MeOH was added LiOH (80 mg, 2 mmol). The mixture was stirred at room temperature for 6 h. The mixture was then acidified with aqueous HCl and washed with water. The aqueous layer was extracted with ethyl acetate, and the solvent was removed in vacuo. The residue was directly used in the next step.

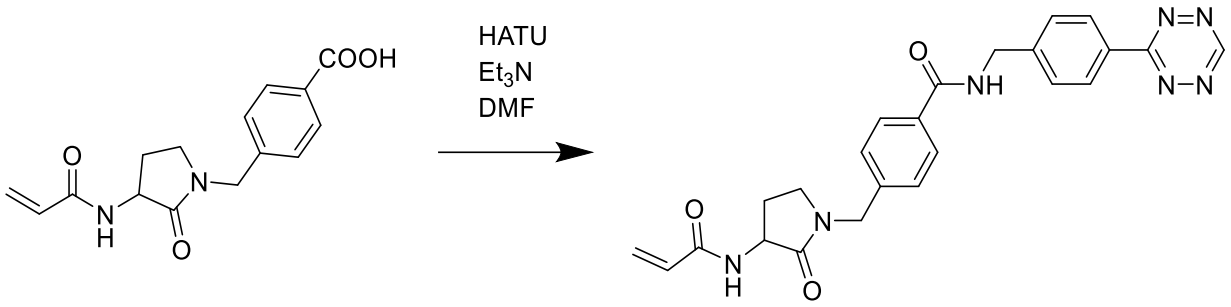

To a solution of tetrazine amine (19 mg, 0.1 mmol) in DMF was added HATU (40 mg, 0.12 mmol), RNF 219 ligand (29 mg, 0.1 mmol), and DIPEA (21 mg, 0.2 mmol). The reaction mixture was stirred at room temperature overnight. The mixture was then extracted and concentrated in vacuo. The residue was purified by flash column chromatography on silica gel to afford the desired product.

1.11. References

1. (a) Lai, A. C.; Crews, C. M. Induced protein degradation: an emerging drug discovery paradigm. *Nat. Rev. Drug Discov.* **2017**, 16, 101−114. (b) Crews, C. M.; Georg, G.; Wang, S. Inducing protein degradation as a therapeutic strategy. *J. Med. Chem.* **2016**, 59, 5129−5130. (c) Neklesa, T. K.; Winkler, J. D.; Crews, C. M. Targeted protein degradation by PROTACs. *Pharmacol. Ther.* **2017**, 174, 138−144. (d) Luh, L. M.; Scheib, U.; Juenemann, K.; Wortmann, L.; Brands, M.; Cromm, P. M. Prey for the Proteasome: Targeted Protein Degradation—A Medicinal Chemist's Perspective. *Angew. Chem., Int. Ed.* **2020**, 59, 15448−15466.
2. Garber, K**.** The PROTAC gold rush. *Nat. Biotechnol.* **2022**, 40, 12-16.
3. Békés, M.; Langley, D. R.; Crews, C. M. PROTAC targeted protein degraders: the past is prologue. *Nat. Rev. Drug Discov.* **2022**, 21, 181–200.
4. (a) Bondeson, D. P. et al. Lessons in PROTAC design from selective degradation with a promiscuous warhead. *Cell Chem. Biol.* **2018**, 25, 78–87.

5. (a) Ward, C. C.; Kleinman, J. I.; Brittain, S. M.; Lee, P. S.; Chung, C. Y. S.; Kim, K.; Petri, Y.; Thomas, J. R.; Tallarico, J. A.; McKenna, J. M.; Schirle, M.; Nomura, D. K. Covalent Ligand Screening Uncovers a RNF4 E3 Ligase Recruiter for Targeted Protein Degradation Applications. *ACS Chem. Biol.* **2019**, 14 (11), Article. (b) Zhang, X.; Crowley, V. M.; Wucherpfennig, T. G.; Dix, M. M.; Cravatt, B. F. Electrophilic PROTACs that degrade nuclear proteins by engaging DCAF16. *Nat. Chem. Biol.* **2019**, 15 (7), 737-746. (c) Zhang, X.; Luukkonen, L. M.; Eissler, C. L.; Crowley, V. M.; Yamashita, Y.; Schafroth, M. A.; Kikuchi, S.; Weinstein, D. S.; Symons, K. T.; Nordin, B. E.; Rodriguez, J. L.; Wucherpfennig, T. G.; Bauer, L. G.; Dix, M. M.; Stamos, D.; Kinsella, T. M.; Simon, G. M.; Baltgalvis, K. A.; Cravatt, B. F. DCAF11 Supports Targeted Protein Degradation by Electrophilic Proteolysis-Targeting Chimeras. *J. Am. Chem. Soc.* **2021**, 143,5141-5149. (d) Henning, N. J.; Manford, A. G.; Spradlin, J. N.; Brittain, S. M.; Zhang, E.; McKenna, J. M.; Tallarico, J. A.; Schirle, M.; Rape, M.; Nomura, D. K. Discovery of a Covalent FEM1B Recruiter for Targeted Protein Degradation Applications. *J. Am. Chem. Soc.* **2022**, 144,701-708.

6. (a) Roberts, B. L.; Ma, Z.-X.; Gao, A.; Leisten, E. D.; Yin, D.; Xu, W.; Tang, W. Two-stage strategy for development of proteolysis targeting chimeras and its application for estrogen receptor degraders. *ACS Chem. Biol*. **2020**, 15, 1487-1496. . (b) Li, J.; Li, C.; Zhang, Z.; Zhang, Z.; Wu, Z.; Liao, J.; Wang, Z.; McReynolds, M.; Xie, H.; Guo, L.; Fan, Q.; Peng, J.; Tang, W. A platform for the rapid synthesis of molecular glues (Rapid-Glue) under miniaturized conditions for direct biological screening. *Eur. J. Med. Chem.* **2023**, 258, 115567. (c) Guo, L.; Zhou, Y.; Nie, X.; Zhang, Z.; Zhang, Z.; Li, C.; Wang, T.; Tang,

W. A Platform for the Rapid Synthesis of Proteolysis Targeting Chimeras (Rapid-TAC) under Miniaturized Conditions. *Eur. J. Med. Chem.* **2022**, 236, 114317.

7. (a) Blackman, M. L.; Royzen, M.; Fox, J. M. Tetrazine Ligation: Fast Bioconjugation Based on Inverse-Electron-Demand Diels−Alder Reactivity. *J. Am. Chem. Soc.* **2008**, 130, 13518−13519. (b) Selvaraj, R.; Fox, J. M. trans-Cyclooctene - a stable, voracious dienophile for bioorthogonal labeling. *Curr. Opin. Chem. Biol.* **2013**, 17, 753−760. (c) Sai, Y.-H.; Essig, S.; James, J. R.; Lang, K.; Chin, J. W. Selective, rapid and optically switchable regulation of protein function in live mammalian cells. *Nat. Chem.* **2015**, 7, 554−561. (d) Reiner, T.; Earley, S.; Turetsky, A.; Weissleder, R. Bioorthogonal Small-Molecule Ligands for PARP1 Imaging in Living Cells. *ChemBioChem* **2010**, 11, 2374−2377.
8. Lebraud, H.; Wright, D. J.; Johnson, C. N.; Heightman, T. D. Protein Degradation by In-Cell Self-Assembly of Proteolysis-Targeting Chimeras. *ACS Cent. Sci.* **2016**, 2, 927−934.
9. (a) Backus, K. M.; Correia, B. E.; Lum, K. M.; Forli, S.; Horning, B. D.; González-Páez, G. E.; Chatterjee, S.; Lanning, B. R.; Teijaro, J. R.; Olson, A. J.; Wolan, D. W.; Cravatt, B. F. Proteome-wide covalent ligand discovery in native biological systems. *Nature* **2016**, 570–574. (b) Kuljanin, M.; Mitchell, D. C.; Schweppe, D. K.; Gikandi, A. S.; Nusinow, D. P.; Bulloch, N. J.; Vinogradova, E. V.; Wilson, D. L.; Kool, E. T.; Mancias, J. D.; Cravatt, B. F.; Gygi, S. P. Reimagining high-throughput profiling of reactive cysteines for cell-based screening of large electrophile libraries. *Nat. Biotechnol.* **2021**, 39, 630–641.

Chapter 2

Design and Synthesis of Phenyl Dihydrouracil as the Novel Achiral Cereblon Ligands for Targeted Protein Degradation

2.1. Introduction

Targeted protein degradation (TPD) has emerged as a promising therapeutic strategy for addressing a wide range of medical needs. Among the various approaches, proteolysis-targeting chimeras (PROTACs) have gained significant attention[1]. PROTACs are bifunctional molecules composed of an E3 ubiquitin ligase binding motif, a linker, and a protein of interest (POI) binding motif. By serving as molecular bridges, PROTACs facilitate the interaction between the POI and the E3 ligase, leading to the polyubiquitination and subsequent proteasomal degradation of the POI. Despite the presence of over 600 E3 ubiquitin ligase complexes in the human proteome[2], only a few have been harnessed for PROTAC development. Among these, Cereblon (CRBN) is the most extensively utilized E3 ligase, largely due to the favorable properties of its glutarimide ligands, including thalidomide, pomalidomide, and lenalidomide[3] (**Scheme 2.1)**. These glutarimide ligands were initially employed in PROTAC design to recruit CRBN for targeted protein degradation.

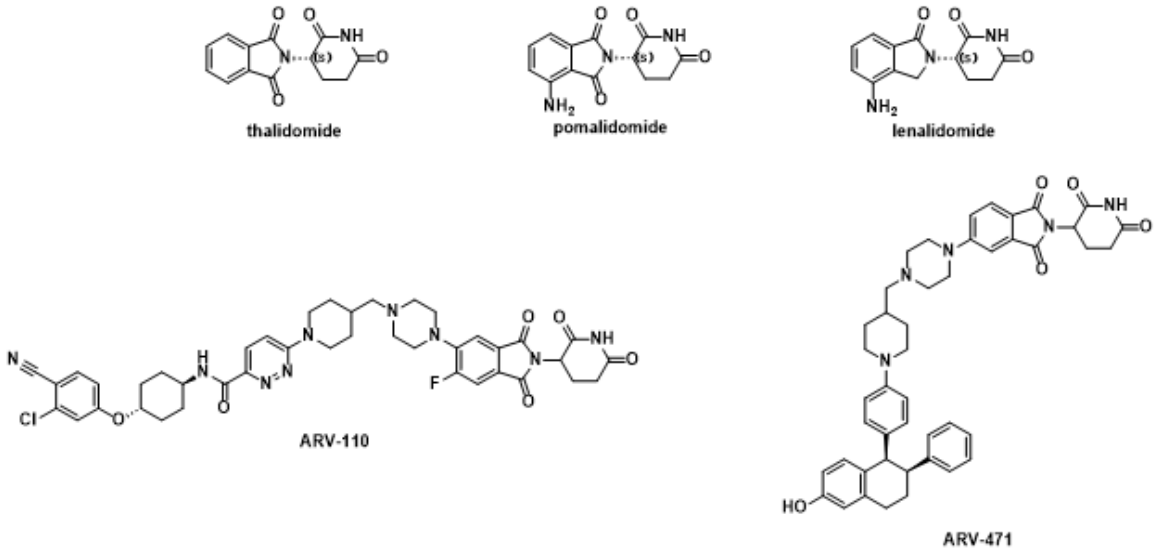

Scheme 2.1. Traditional CRBN ligands and PROTACs based on them.

However, one of the major challenges with glutarimide-based CRBN ligands is their rapid racemization both in vitro and in vivo[4], leading to a mixture of enantiomers (**Scheme 2.2)**. The (S)-enantiomer is primarily responsible for binding to CRBN, while the (R)-enantiomer exhibits significantly lower activity[5]. The presence of the inactive (R)-enantiomer complicates the drug development process by reducing the overall efficacy of the PROTACs and increasing the complexity of pharmacological characterization required by regulatory agencies.

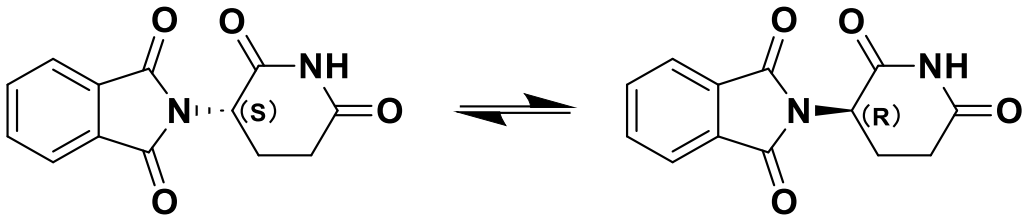

Scheme 2.2. Racemization of thalidomide.

To address the issue of racemization in CRBN ligands, several strategies have been employed (**Scheme 2.3)**. One approach is the substitution of hydrogen with deuterium at specific positions within the ligand, which slows racemization due to the stronger bonds formed by deuterium[6]. Another method involves creating quaternary carbon centers at the stereocenter, preventing racemization by stabilizing the configuration, though this can sometimes reduce binding affinity[6]. Furthermore, there has been a growing interest in developing non-racemic or achiral CRBN ligands[7]. Achiral ligands eliminate the issues related to enantiomeric mixtures, providing a more straightforward and potentially more effective approach to targeted protein degradation.

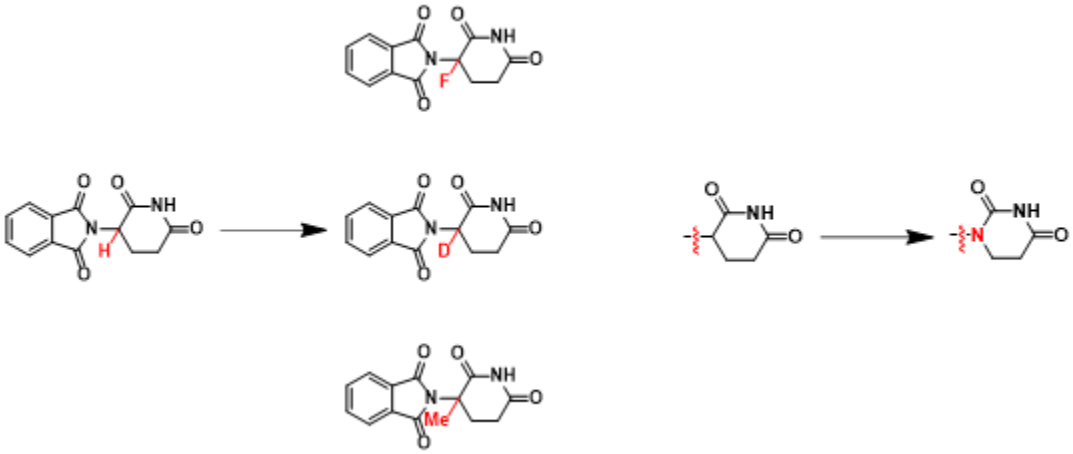

Scheme 2.3. Previous strategies to address the racemization issue of thalidomide.

Compared to the glutarimide motif, phenyl dihydrouracil is much flatter, resulting in worse binding affinity with the CRBN protein complex. To improve the binding affinity of achiral phenyl dihydrouracil, our group previously developed a series of substituted achiral phenyl dihydrouracil (PDHU) that can be used as a novel class of CRBN ligands for the development of PROTACs[8] (**Scheme 2.4)**. Additionally, we have used these ligands to develop several BRD4 degraders. Unlike traditional CRBN ligands, which can induce the degradation of neo-substrates such as IKZF1, IKZF3, and GSPT1, our achiral ligand-based BRD4 degrader does not induce the degradation of these well-known neo-substrates and demonstrates good hydrolysis resistance. Although we successfully developed BRD4 degraders with the achiral ligands, we still aim to develop more potent achiral ligands to improve the degradation efficiency of PROTAC degraders. In addition, the achiral ligand in Scheme 2.4 has two hydrogen bond donors, which are not desired for oral bioavailability.

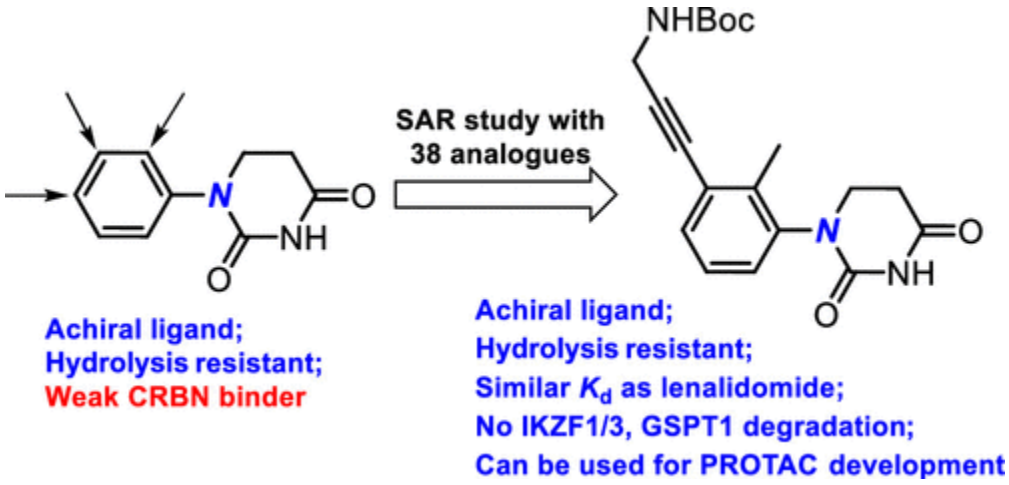

Scheme 2.4. Achiral CRBN ligands previously reported by our group[8].

2.2. Development of Achiral Ligands for CRBN

Recognizing the need for further improving the binding affinity and reducing the number of hydrogen bond donors, we embarked on a project aimed at exploring various substituents on the phenyl group of the dihydrouracil motif. Dr. Haibo Xie identified HX 4280 as a potent lead for achiral CRBN ligands (**Scheme 2.5)**. However, HX 4280 exhibited slightly lower binding affinity compared to lenalidomide, a well-established ligand in the field. We decided to perform extensive SAR studies around the structure of HX 4280. As an initial step in this endeavor, I focused on understanding the impact of the methyl group present in the HX 4280 molecule. To this end, I designed and synthesized a series of analogues with and without a methyl group at different positions (2a-2c), in addition to the original HX 4280 compound. These analogues showed slightly lower binding affinities compared to the parent compound. These results suggest that the ortho-position methyl group may induce dihydrouracil to adopt a more twisted configuration, enhancing the binding of PDHU with the CRBN protein complex.

To understand the role of the aldehyde group, I synthesized analogue 2d by removing the aldehyde group from the parent structure. This modification led to a reduction in binding affinity to 62%, indicating that the aldehyde group contributes positively to the interaction with the CRBN-DDB1 complex.

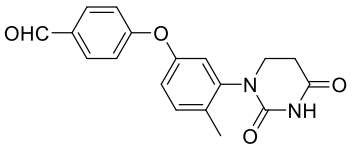

HX4280

70

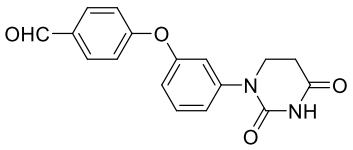

2a

33

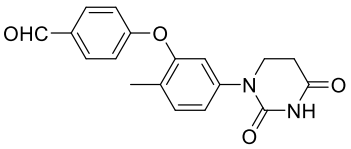

2b

57

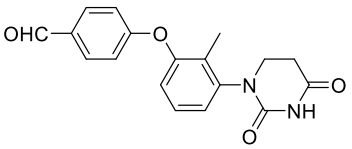

2c

21

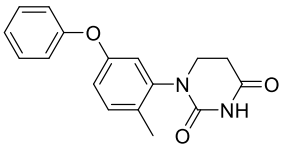

2d

62

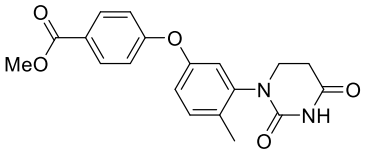

2e

74

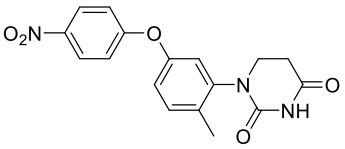

2f

83

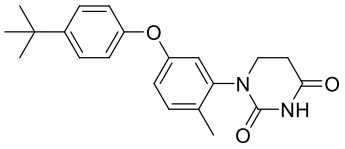

2g

63

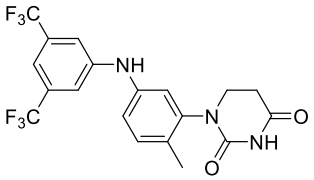

2h

33

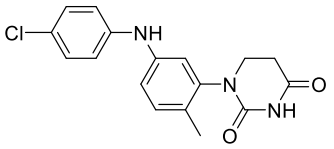

2i

64

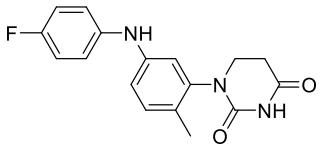

2j

77

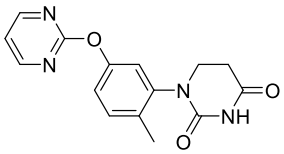

2k

85

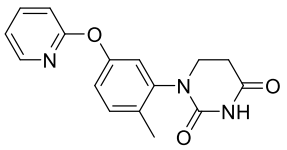

2l

74

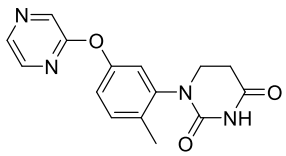

2m

60

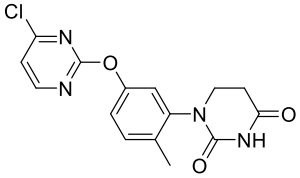

2n

78

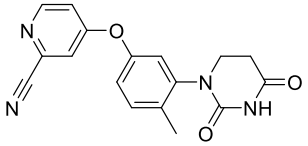

2o

34

Scheme 2.5. Development of achiral ligands for CRBN.

Further exploration involved the replacement of the benzaldehyde moiety with different phenyl rings bearing various substituents. Analogue 2e, featuring an ester group, showed a slightly improved binding affinity of 74%, while analogue 2f, with a nitro group, significantly enhanced binding to 83%. This result suggests that the nitro group's electron-withdrawing nature may facilitate stronger interactions with CRBN. Conversely, the introduction of a tert-butyl group in analogue 2g resulted in a 63% binding affinity, which is slightly lower than the parent compound, indicating that steric bulk may decrease the binding affinity.

In another series of modifications, I replaced the oxygen linker in the parent compound with an NH linker in analogues 2h-j. However, these NH linker analogues demonstrated reduced binding affinities, likely due to poor solubility or less favorable electronic interactions, which suggests that the oxygen linker plays a critical role in maintaining optimal binding.

In addition to the modifications that I previously explored, I also incorporated different electron-deficient heteroaromatic rings, such as pyrimidine, pyridine, and pyrazine, to replace the substituted benzyl ring in a new series of analogues (2k-i). The results were promising: analogue 2k demonstrated an improved binding affinity of 85%, while analogue 2l showed a binding affinity of 74%. However, analogue 2m, which incorporated a different positioning of the nitrogen atom, surprisingly exhibited only a 60% binding affinity. This suggests that the position of the nitrogen atom in these heteroaromatic rings can significantly influence the interaction with the CRBN complex.

I also tested various electron-withdrawing groups on these heteroaromatic rings in analogues 2n-p, but these modifications did not result in any improvement in binding affinity. Based on these findings, I selected analogue 2k, which exhibited the highest binding affinity, for further study. This choice is informed by its superior performance and potential for further optimization in developing high-affinity CRBN ligands.

In the next phase of my research, I focused on the development of PROTACs by installing linkers on the analogue 2k. Based on the structural analysis of 2k, I hypothesized that the installation of a linker could be effectively achieved either on the phenyl group or the pyrimidine group of the molecule. To test this hypothesis, I synthesized several analogues with linkers attached to these positions and evaluated their binding affinities.

2.3. Achiral Ligands with Different Linkers.

As shown in **Scheme 2.6**, I found that the analogue 3a, which featured an alkyne linker attached to the phenyl group, significantly improved binding affinity, reaching a level of 87%. This result suggests that the phenyl group is a suitable site for linker attachment in this context. However, most of the analogues that had linkers attached to the pyrimidine ring did not exhibit enhanced binding affinities.

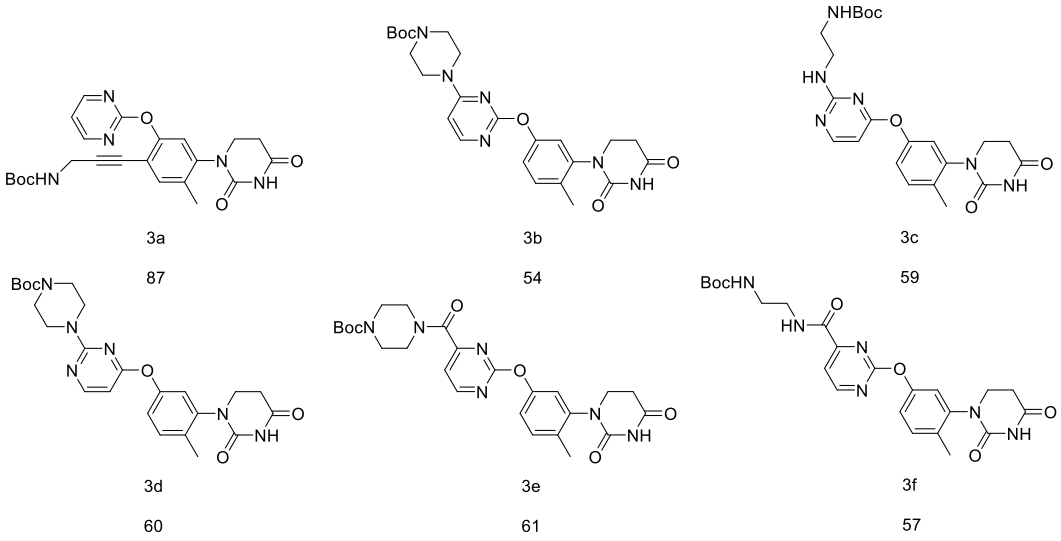

Scheme 2.6. Achiral Ligands with different linkers.

2.4. Achiral Ligands Based BTK PROTACs.

With the newly identified achiral ligand 3a for CRBN in hand, I proceeded to investigate whether ligand 3a could serve as a foundation for developing novel PROTACs targeting Bruton's tyrosine kinase (BTK). To achieve this, I conjugated ibrutinib, a well-established BTK ligand, to the achiral ligand 3a. This process allowed me to prepare a series of potential BTK degraders (compounds 4, 5a-c, 6a-b, 7), each incorporating different linkers, as illustrated in **Scheme 2.7**.

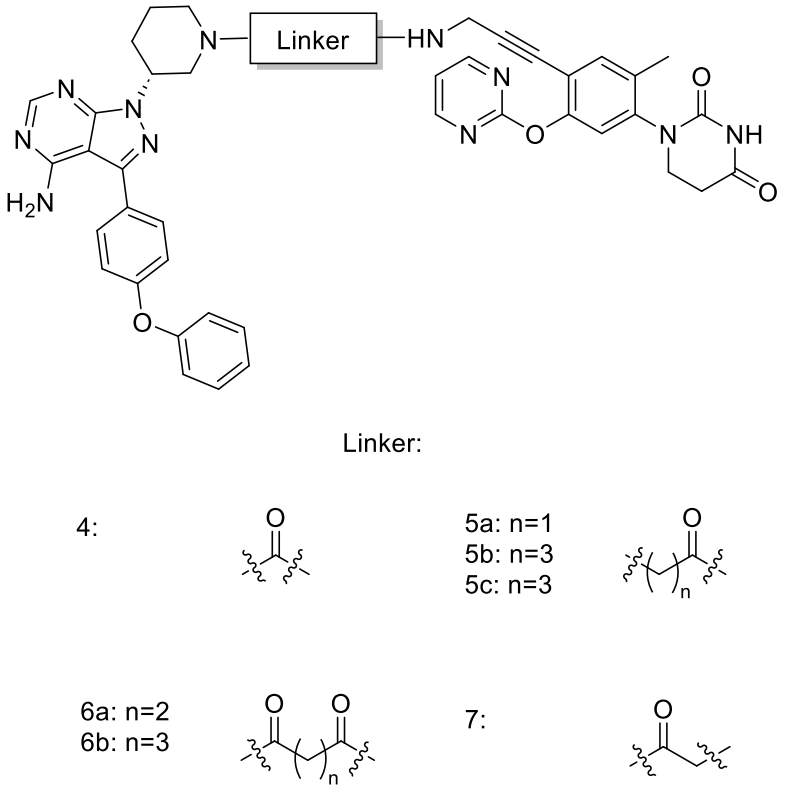

Scheme 2.7. BTK degraders with achiral CRBN ligands.

2.5. Biological Activities of BTK Degraders

To evaluate the efficacy of this new series of degraders, Ira Tandon, a graduate student in our group, employed the HiBiT assay developed by Promega (**Scheme 2.8)**. Ira treated BTK-HiBiT cells with concentrations of 10 μM and 1 μM of each compound for 8 h. This approach enabled us to assess the potential of these degraders in inducing BTK degradation effectively.

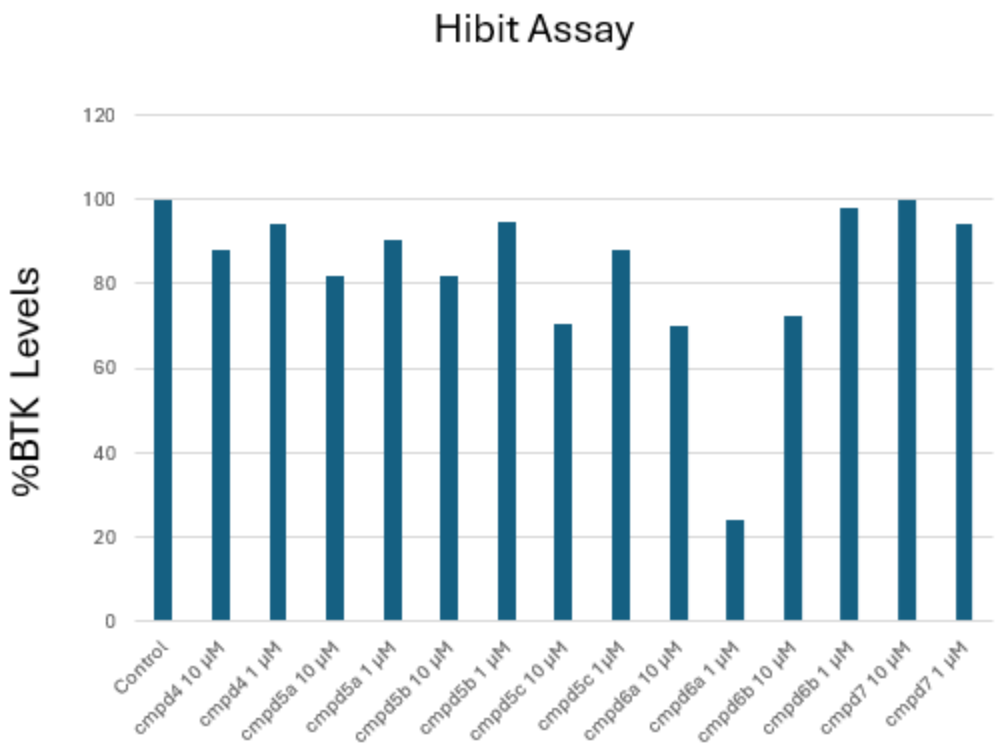

Scheme 2.8. Pre-screening of BTK degraders.

Among members of the PROTAC library, compound 6a showed the highest degradation activity at 1 μM. To evaluate the potency of degrader 6a, we performed a full dose response experiment with compound 6a concentrations ranging from 0.1 nM to 10 μM in TMD8 and OCI-Ly10 cells. In addition, we also evaluated the downstream effect of degrading BTK and observed that degrader 3a inhibited Stat3 and MAPK phosphorylation in Ramos cells in a dose-dependent manner (**Scheme 2.9**).

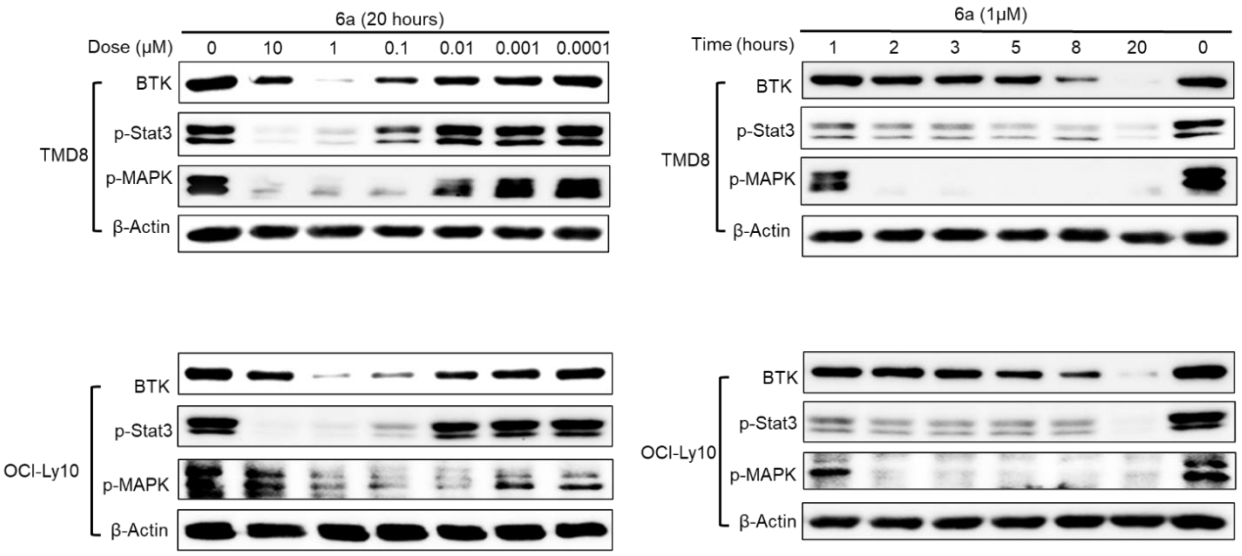

Scheme 2.9. Dose response of 6a at a concentration from 0.1nM to 10μM

To probe the efficiency of compound 6a, we treated TMD8 and OCI-Ly10 with 1 μM 6a and monitored the change of BTK protein level by time (Figure 4C). The BTK degradation started around 5 h and reached maximal degradation effect at 20 h. Subsequently, we treated TMD8 and OCl-Ly10 cells with 6a (1 μM) for 20 h (**Scheme 2.10**).

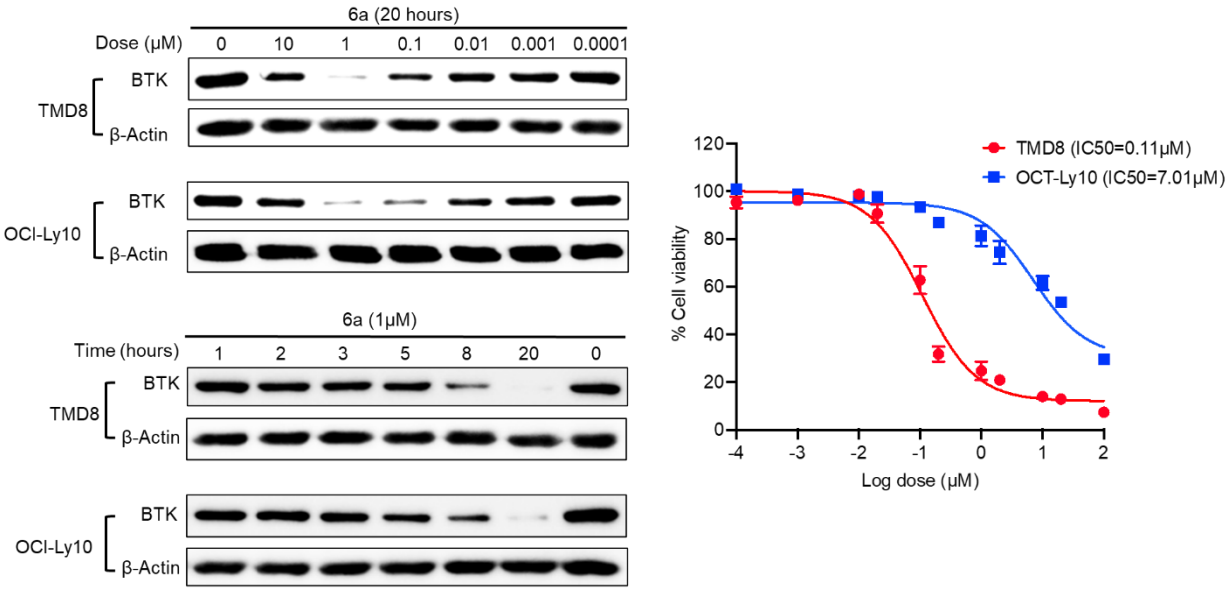

Scheme 2.10. Time-course change of proteins level under treatment of 6a at 1 μM.

To demonstrate the degradation of BTK via the hijacking of the ubiquitin-proteasome system, we co-treated the cells with the degrader 6a and binding competitors ibrutinib or thalidomide. Both compounds attenuated the degradation of BTK, indicating that the binding of the degrader to both BTK and CRBN E3 ligase is required for the induced protein's degradation. The loss of BTK was also attenuated by proteasome and NEDDylation inhibitors, consistent with a proteasome- and Cullin E3 ligase-dependent mechanism of BTK degradation (**Scheme 2.11)**.

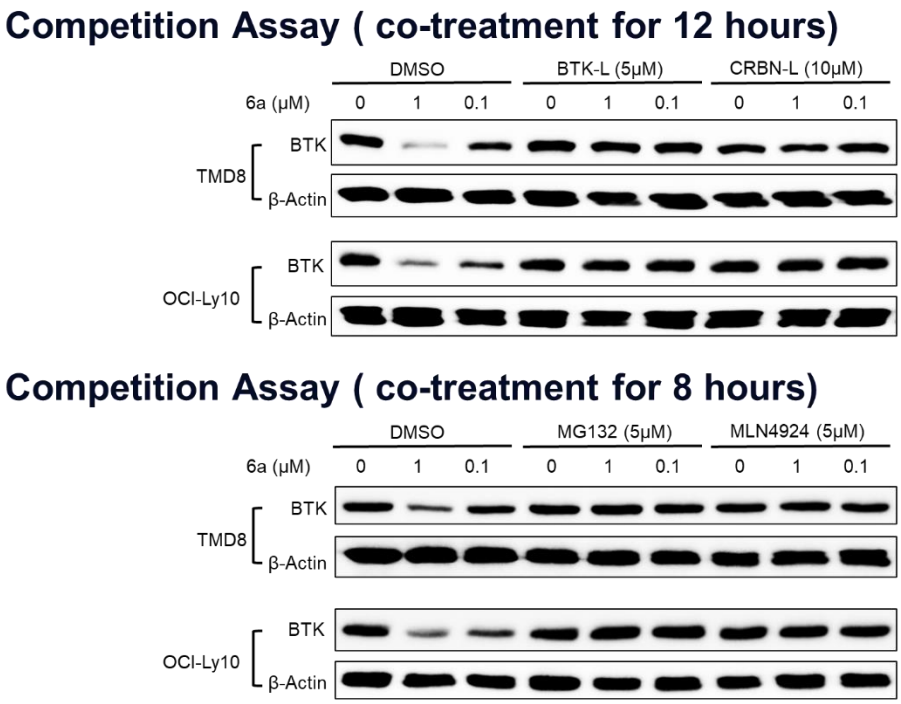

Scheme 2.11. Mechanistic studies of compound 6a.

2.6. Discussion and Perspectives

Traditional glutarimide-based CRBN ligands used in PROTAC development face significant challenges due to rapid racemization and low stability, which complicate the drug development process. To overcome these issues, we successfully designed and synthesized phenyl dihydrouracil compounds as novel achiral CRBN ligands for targeted protein degradation. Our comprehensive evaluation identified analogue 2k, incorporating an electron-deficient pyrimidine ring, as the most promising ligand due to its high binding affinity and stability. We further developed BTK degraders by linking ibrutinib to the achiral ligand 3a, resulting in significant BTK degradation and inhibition of downstream signaling pathways in TMD8 and OCI-Ly10 cells. These results underscore the potential of phenyl dihydrouracil-based ligands in creating effective PROTACs with improved stability and efficiency. This study paves the way for further optimization and

development of more potent and stable achiral ligands, offering promising therapeutic applications in drug discovery and development.

2.7. Experimental Sections

General Information

Unless otherwise stated, all commercial reagents were used as received. Reactions were conducted in dry glassware using anhydrous solvents (pass through activated alumina columns). Unless stated otherwise, reactions were performed at room temperature (rt). Thin-layer chromatography (TLC) was conducted on plates (EMD Chemical Inc. 60, F254) and visualized using a combination of UV, sulfuric acid, and ceric ammonium molybdate staining. Flash column chromatography was performed with silica gel (Silicycle, 40-63 μm). Infrared spectra (IR) were obtained on a Bruker Equinox 55 Spectrophotometer. Optical rotations were recorded on Perkin-Elmer 241 polarimeter. ^{1}H and ^{13}C nuclear magnetic resonance spectra (NMR) were obtained on a Brooker 400 MHz. Chemical shifts were reported in parts per million (ppm), and the residual solvent peak was used as an internal reference: proton (chloroform δ 7.26), carbon (chloroform δ 77.16) or tetramethylsilane (TMS δ 0.00) was used as a reference. Multiplicity was indicated as follows: s (singlet), d (doublet), t (triplet), m (multiplet), dd (doublet of doublet), td (triplet of doublet), bs (broad singlet). Coupling constants (*J*) were reported in Hertz (Hz). All high-resolution mass spectra were performed by Analytical Instrument Center at the School of Pharmacy (UW-Madison) on an Electron Spray Injection (ESI) mass spectrometer.

Experimental Procedures

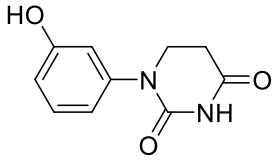

To a solution of 4-hydroxyaniline (4.37 g, 40.0 mmol) in toluene (50 mL, 0.8 M) was added acrylic acid (3.57 mL, 52.0 mmol). The reaction mixture was stirred at 110 °C until the starting material disappeared as indicated by TLC, and then the toluene was removed using a rotavapor. Acetic acid (60 mL) and urea (7.20 g, 120.0 mmol) were then added to the flask and heated to 120 °C for 16 h. Most of the acetic acid was removed by the rotavapor. The residue was then dissolved in water (100 mL) and extracted with ethyl acetate (3 × 100 mL). The organic layers were combined, dried over Na_2SO_4, and concentrated under reduced pressure. The solid residue was suspended in ethyl acetate (10 mL) and stirred for 2 h. The slurry was filtered, and the solid was washed with ethyl acetate (2 × 5 mL). The residue was directly used in the next step.

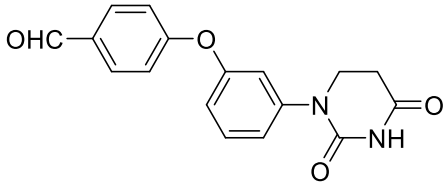

To a solution of 1-(3-hydroxyphenyl)dihydropyrimidine-2,4(1H,3H)-dione (206 mg, 1 mmol) in anhydrous DMF was added 4-fluorobenzaldehyde (146 mg, 1.2 mmol, 1.2 eq) and cesium carbonate (323 mg, 1 mmol, 1.0 eq). The mixture was then stirred at 90 °C for 4 h. Upon completion of the reaction, 10 mL of water was slowly added, followed by extraction with ethyl acetate (3 × 20 mL). The combined organic layers were concentrated in vacuo. The residue was purified by flash column chromatography on silica gel to afford the desired product. ^{1}H NMR (400 MHz, $CDCl_3$) δ 9.93 (s, 1H), 8.19 (s, 1H), 7.87 (d, *J* = 8.3 Hz, 2H), 7.43 (t, *J* = 8.1 Hz, 1H), 7.19

– 7.04 (m, 4H), 6.99 (dd, *J* = 8.2, 2.4 Hz, 1H), 3.88 (t, *J* = 6.6 Hz, 2H), 2.83 (t, *J* = 6.6 Hz, 2H). ^{13}C NMR (101 MHz, $CDCl_3$) δ 190.8, 169.4, 162.4, 155.7, 151.8, 142.7, 132.1, 131.7, 130.5, 120.9, 118.3, 118.0, 117.0, 45.0, 31.3.

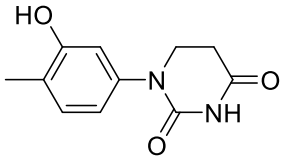

To a solution of 5-amino-2-methylphenol (1.23 g, 10.0 mmol) in toluene (12.5 mL, 0.8 M) was added acrylic acid (0.9 mL, 13.0 mmol). The reaction mixture was stirred at 110 °C until the starting material disappeared as indicated by TLC, and then the toluene was removed using a rotavapor. Acetic acid (20 mL) and urea (1.8 g, 30.0 mmol) were then added to the flask and heated to 120 °C for 16 h. Most of the acetic acid was removed by the rotavapor. The residue was then dissolved in water (25 mL) and extracted with ethyl acetate (3 × 25 mL). The organic layers were combined, dried over Na_2SO_4, and concentrated under reduced pressure. The solid residue was suspended in ethyl acetate (2.5 mL) and stirred for 2 h. The slurry was filtered, and the solid was washed with ethyl acetate (2 × 2 mL). The residue was directly used in the next step.

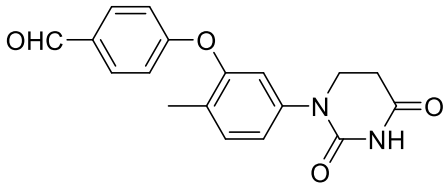

To a solution of 1-(3-hydroxy-4-methylphenyl)dihydropyrimidine-2,4(1H,3H)-dione (220 mg, 1 mmol) in anhydrous DMF was added 4-fluorobenzaldehyde (146 mg, 1.2 mmol, 1.2 eq) and cesium carbonate (323 mg, 1 mmol, 1.0 eq). The mixture was then stirred at 90 °C for 4 h. Upon completion of the reaction, 10 mL of water was slowly added, followed by extraction with ethyl acetate (3 × 20 mL). The combined organic layers were concentrated in vacuo. The residue was

purified by flash column chromatography on silica gel to afford the desired product. ^{1}H NMR (400 MHz, $CDCl_3$) δ 9.90 (s, 1H), 8.37 (s, 1H), 8.00 – 7.74 (m, 2H), 7.32 (d, *J* = 8.2 Hz, 1H), 7.11 (dd, *J* = 8.1, 2.3 Hz, 1H), 7.05 – 6.92 (m, 3H), 3.83 (t, *J* = 6.7 Hz, 2H), 2.80 (t, *J* = 6.7 Hz, 2H), 2.19 (s, 3H). ^{13}C NMR (101 MHz, $CDCl_3$) δ 190.8, 169.6, 162.7, 152.8, 151.9, 140.2, 132.1, 132.0, 131.2, 129.1, 121.6, 117.7, 116.7, 45.1, 31.2, 15.7.

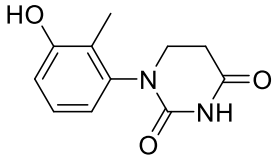

To a solution of 3-amino-2-methylphenol (1.23 g, 10.0 mmol) in toluene (12.5 mL, 0.8 M) was added acrylic acid (0.9 mL, 13.0 mmol). The reaction mixture was stirred at 110 °C until the starting material disappeared as indicated by TLC, and then the toluene was removed using a rotavapor. Acetic acid (20 mL) and urea (1.8 g, 30.0 mmol) were then added to the flask and heated to 120 °C for 16 h. Most of the acetic acid was removed by the rotavapor. The residue was then dissolved in water (25 mL) and extracted with ethyl acetate (3 × 25 mL). The organic layers were combined, dried over Na_2SO_4, and concentrated under reduced pressure. The solid residue was suspended in ethyl acetate (2.5 mL) and stirred for 2 h. The slurry was filtered, and the solid was washed with ethyl acetate (2 × 2 mL). The residue was directly used in the next step.

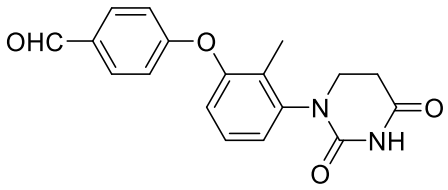

To a solution of 1-(3-hydroxy-2-methylphenyl)dihydropyrimidine-2,4(1H,3H)-dione (220 mg, 1 mmol) in anhydrous DMF was added 4-fluorobenzaldehyde (146 mg, 1.2 mmol, 1.2 eq) and cesium carbonate (323 mg, 1 mmol, 1.0 eq). The mixture was then stirred at 90 °C for 4 h. Upon

completion of the reaction, 10 mL of water was slowly added, followed by extraction with ethyl acetate (3 × 20 mL). The combined organic layers were concentrated in vacuo. The residue was purified by flash column chromatography on silica gel to afford the desired product. ^{1}H NMR (400 MHz, MeOD) δ 9.87 (s, 1H), 7.97 (s, 1H), 7.88 (d, *J* = 8.7 Hz, 2H), 7.35 (t, *J* = 8.1 Hz, 1H), 7.24 (dd, *J* = 8.1, 1.3 Hz, 1H), 7.09 – 7.02 (m, 3H), 3.97 – 3.85 (m, 1H), 3.68 (dt, *J* = 12.4, 6.1 Hz, 1H), 2.84 (d, *J* = 9.3 Hz, 2H), 2.09 (s, 3H). ^{13}C NMR (101 MHz, MeOD) δ 191.3, 171.5, 163.1, 153.5, 152.8, 142.2, 131.8, 131.3, 129.2, 127.6, 124.0, 120.5, 116.3, 45.0, 30.7, 10.1.

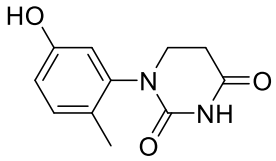

To a solution of 3-amino-4-methylphenol (1.23 g, 10.0 mmol) in toluene (12.5 mL, 0.8 M) was added acrylic acid (0.9 mL, 13.0 mmol). The reaction mixture was stirred at 110 °C until the starting material disappeared as indicated by TLC, and then the toluene was removed using a rotavapor. Acetic acid (20 mL) and urea (1.8 g, 30.0 mmol) were then added to the flask and heated to 120 °C for 16 h. Most of the acetic acid was removed by the rotavapor. The residue was then dissolved in water (25 mL) and extracted with ethyl acetate (3 × 25 mL). The organic layers were combined, dried over Na_2SO_4, and concentrated under reduced pressure. The solid residue was suspended in ethyl acetate (2.5 mL) and stirred for 2 h. The slurry was filtered, and the solid was washed with ethyl acetate (2 × 2 mL). The residue was directly used in the next step.

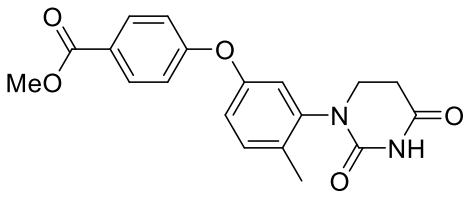

To a solution of 1-(5-hydroxy-2-methylphenyl)dihydropyrimidine-2,4(1H,3H)-dione (220 mg, 1 mmol) in anhydrous DMF was added methyl 4-fluorobenzoate (185 mg, 1.2 mmol, 1.2 eq) and cesium carbonate (323 mg, 1 mmol, 1.0 eq). The mixture was then stirred at 90 °C for 4 h. Upon completion of the reaction, 10 mL of water was slowly added, followed by extraction with ethyl acetate (3 × 20 mL). The combined organic layers were concentrated in vacuo. The residue was purified by flash column chromatography on silica gel to afford the desired product. ^{1}H NMR (400 MHz, $CDCl_3$) δ 8.01 (d, *J* = 8.9 Hz, 2H), 7.44 (s, 1H), 7.30 (d, *J* = 8.4 Hz, 1H), 7.05 – 6.95 (m, 3H), 6.91 (d, *J* = 2.5 Hz, 1H), 3.90 (s, 3H), 3.85 – 3.60 (m, 1H), 2.94 – 2.71 (m, 1H), 2.83 (m, 2H), 2.27 (s, 3H).; ^{13}C NMR (101 MHz, $CDCl_3$) δ 169.2, 166.5, 161.3, 154.6, 151.0, 140.8, 132.5, 131.8, 131.6, 124.9, 119.8, 118.3, 117.5, 52.1, 45.1, 31.5, 17.4.

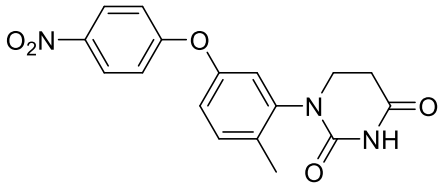

To a solution of 1-(5-hydroxy-2-methylphenyl)dihydropyrimidine-2,4(1H,3H)-dione (220 mg, 1 mmol) in anhydrous DMF was added methyl 1-fluoro-4-nitrobenzene (169 mg, 1.2 mmol, 1.2 eq) and cesium carbonate (323 mg, 1 mmol, 1.0 eq). The mixture was then stirred at 90 °C for 4 h. Upon completion of the reaction, 10 mL of water was slowly added, followed by extraction with ethyl acetate (3 × 20 mL). The combined organic layers were concentrated in vacuo. The residue was purified by flash column chromatography on silica gel to afford the desired product. ^{1}H NMR (400 MHz, $CDCl_3$) δ 8.29 – 8.08 (m, 2H), 7.65 (s, 1H), 7.35 (d, *J* = 8.4 Hz, 1H), 7.12 – 6.99 (m, 3H), 6.96 (d, *J* = 2.5 Hz, 1H), 3.87 – 3.77 (m, 1H), 3.67 (m, 1H), 2.85 (q, *J* = 7.0 Hz, 2H), 2.29 (s, 3H). ^{13}C NMR (101 MHz, $CDCl_3$) δ 169.2, 162.9, 153.5, 151.1, 142.9, 141.0, 132.8, 132.7, 126.0, 120.3, 119.0, 117.3, 45.1, 31.5, 17.5.

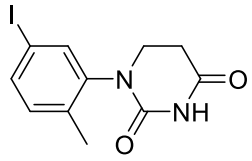

To a solution of 5-iodo-2-methylaniline (9.28 g, 40.0 mmol) in toluene (50 mL, 0.8 M) was added acrylic acid (3.57 mL, 52.0 mmol). The reaction mixture was stirred at 110 °C until the starting material disappeared as indicated by TLC, and then the toluene was removed using a rotavapor. Acetic acid (60 mL) and urea (7.20 g, 120.0 mmol) were then added to the flask and heated to 120 °C for 16 h. Most of the acetic acid was removed by the rotavapor. The residue was then dissolved in water (100 mL) and extracted with ethyl acetate (3 × 100 mL). The organic layers were combined, dried over Na_2SO_4, and concentrated under reduced pressure. The solid residue was suspended in ethyl acetate (10 mL) and stirred for 2 h. The slurry was filtered, and the solid was washed with ethyl acetate (2 × 5 mL). The residue was directly used in the next step.

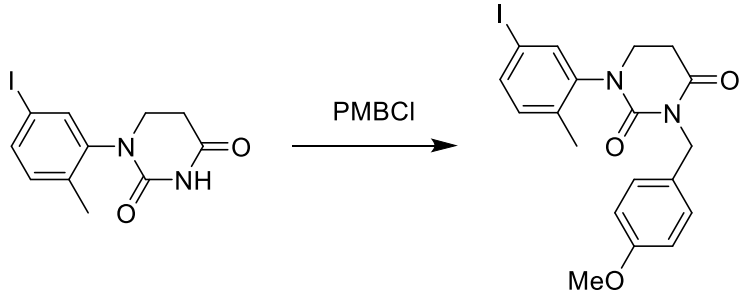

To a solution of 1-(5-iodo-2-methylphenyl)dihydropyrimidine-2,4(1H,3H)-dione (0.5 g, 1.58 mmol) in DMF was added PMBCl (0.22 mL, 1.58 mmol, 1.0 eq.) and cesium carbonate (1.03 g, 3.16 mmol, 2.0 eq). The mixture was then stirred at room temperature for 6 h. Upon completion of the reaction, 8 mL of water was slowly added, followed by extraction with ethyl acetate (3 × 16 mL). The combined organic layers were concentrated in vacuo. The residue was purified by flash column chromatography on silica gel to afford the desired product.

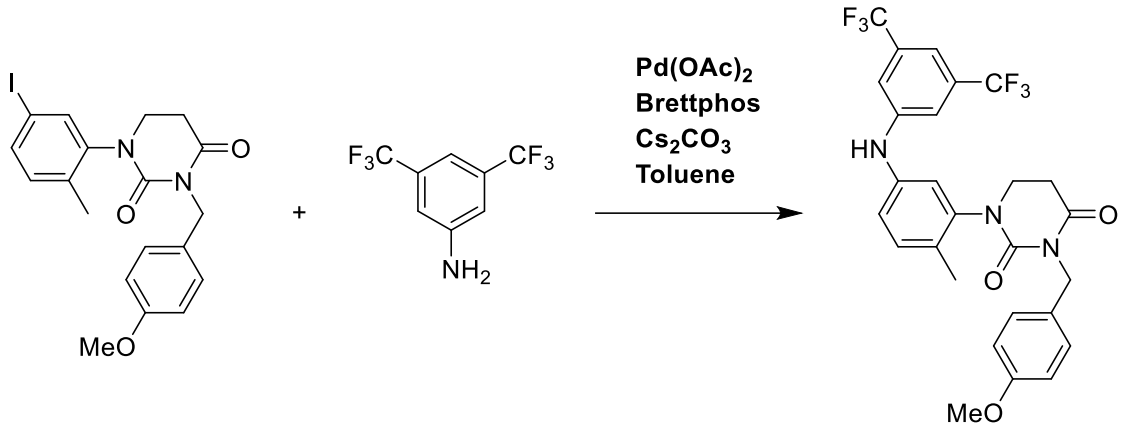

To a solution of intermediate (45 mg, 0.1 mmol) in dioxane was added $Pd(OAc)_2$ (2mg, 0.01 mmol, 0.1 eq.), Brettphos (10 mg, 0.02 mmol, 0.2 eq.), cesium carbonate (64 mg, 0.2 mmol, 2.0 eq.) and 3,5-bis(trifluoromethyl)aniline (28 mg, 0.12 mmol, 1.2 eq.). The reaction mixture was stirred at 80 °C for 6h. Upon completion of the reaction, 4 mL of water was slowly added, followed by extraction with ethyl acetate (3 × 8 mL). The combined organic layers were concentrated in vacuo. The residue was purified by flash column chromatography on silica gel to afford the desired product.

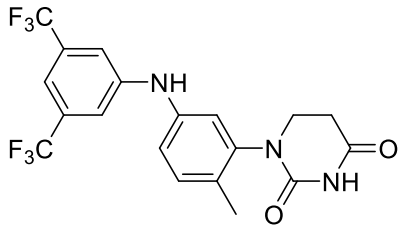

To a solution of intermediate (20 mg) in toluene was added MsOH (10 μL, 0.2 mmol). The reaction mixture was stirred at 100 °C for 6h. Upon completion of the reaction, 4 mL of water was slowly added, followed by extraction with ethyl acetate (3 × 8 mL). The combined organic layers were concentrated in vacuo. The residue was purified by flash column chromatography on silica gel to afford the desired product. ^{1}H NMR (400 MHz, $CDCl_3$) δ 7.48 (s, 1H), 7.30 (m, 4H), 7.07 (dd, *J* = 8.2, 2.4 Hz, 1H), 6.94 (d, *J* = 2.3 Hz, 1H), 6.07 (s, 1H), 3.95 – 3.75 (m, 1H), 3.68 (q, *J* = 6.3 Hz,

1H), 2.91 – 2.78 (m, 2H), 2.26 (s, 3H). ^{13}C NMR (101 MHz, DMSO) δ 171.2, 152.3, 146.9, 142.1, 139.5, 132.1, 131.8(q, *J* = 32.5), 130.5, 125.2, 122.5, 119.9, 114.2, 110.9, 44.9, 31.6, 17.4.

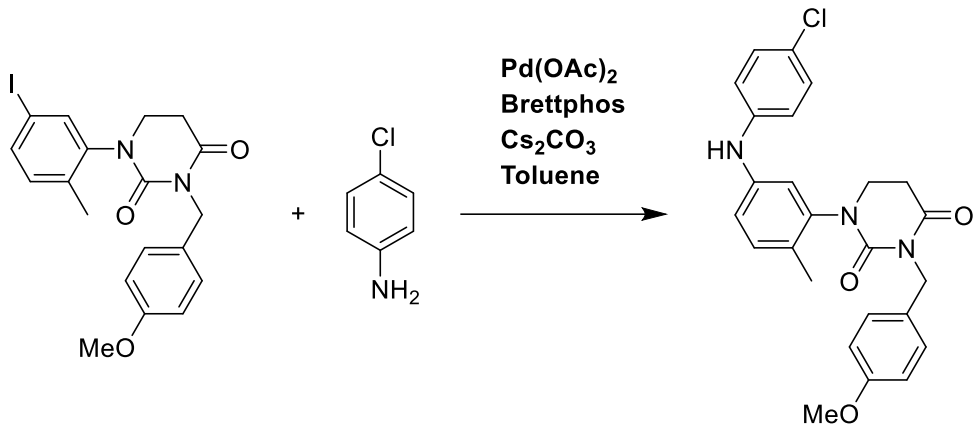

To a solution of intermediate (45 mg, 0.1 mmol) in dioxane was added $Pd(OAc)_2$ (2mg, 0.01 mmol, 0.1 eq.), Brettphos (10 mg, 0.02 mmol, 0.2 eq.), cesium carbonate (64 mg, 0.2 mmol, 2.0 eq.) and 4-chloroaniline (15 mg, 0.12 mmol, 1.2 eq.). The reaction mixture was stirred at 80 °C for 6h. Upon completion of the reaction, 4 mL of water was slowly added, followed by extraction with ethyl acetate (3 × 8 mL). The combined organic layers were concentrated in vacuo. The residue was purified by flash column chromatography on silica gel to afford the desired product.

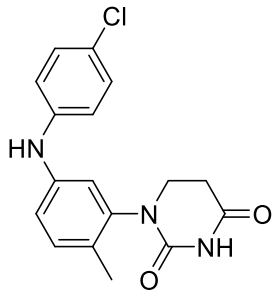

To a solution of intermediate (24 mg) in toluene was added MsOH (10 μL, 0.2 mmol). The reaction mixture was stirred at 100 °C for 6h. Upon completion of the reaction, 4 mL of water was slowly added, followed by extraction with ethyl acetate (3 × 8 mL). The combined organic layers were concentrated in vacuo. The residue was purified by flash column chromatography on silica gel to

afford the desired product. ^{1}H NMR (400 MHz, $CDCl_3$) δ 7.42 (s, 1H), 7.24 – 7.15 (m, 3H), 6.99 – 6.93 (m, 3H), 6.87 (d, *J* = 2.4 Hz, 1H), 5.65 (s, 1H), 3.77 (m, 1H), 3.65 (m, 1H), 2.83 (q, *J* = 6.5 Hz, 2H), 2.21 (s, 3H). ^{13}C NMR (101 MHz, DMSO) δ 171.2, 152.2, 143.2, 141.9, 141.9, 131.6, 129.4, 127.5, 122.9, 117.9, 117.4, 116.8, 44.9, 31.6, 17.2.

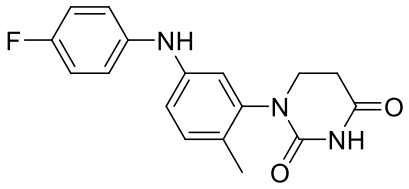

To a solution of intermediate (24 mg) in toluene was added MsOH (10 μL, 0.2 mmol). The reaction mixture was stirred at 100 °C for 6h. Upon completion of the reaction, 4 mL of water was slowly added, followed by extraction with ethyl acetate (3 × 8 mL). The combined organic layers were concentrated in vacuo. The residue was purified by flash column chromatography on silica gel to afford the desired product. ^{1}H NMR (400 MHz, $CDCl_3$) δ 7.43 (s, 1H), 7.15 (d, *J* = 8.3 Hz, 1H), 7.08 – 6.93 (m, 4H), 6.88 (dd, *J* = 8.3, 2.5 Hz, 1H), 6.79 (d, *J* = 2.4 Hz, 1H), 5.56 (s, 1H), 3.77 (m, 1H), 3.65 (m, 1H), 2.90 – 2.73 (m, 2H), 2.19 (s, 3H). ^{13}C NMR (101 MHz, $CDCl_3$) δ 169.5, 158.2 (d, *J* = 240.6 Hz), 151.3, 143.3, 140.3, 138.5 (d, *J* = 2.5 Hz), 132.0, 126.9, 120.7 (d, *J* = 8.0 Hz), 116.9, 116.1 (d, *J* = 22.6 Hz), 115.0, 45.1, 31.5, 17.1.

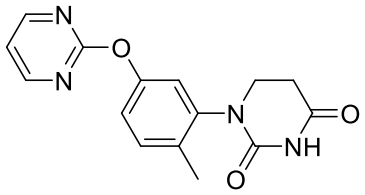

To a solution of 1-(5-hydroxy-2-methylphenyl)dihydropyrimidine-2,4(1H,3H)-dione (220 mg, 1 mmol) in anhydrous DMF was added 2-chloropyrimidine (137 mg, 1.2 mmol, 1.2 eq) and cesium carbonate (323 mg, 1 mmol, 1.0 eq). The mixture was then stirred at 90 °C for 4 h. Upon

completion of the reaction, 10 mL of water was slowly added, followed by extraction with ethyl acetate (3 × 20 mL). The combined organic layers were concentrated in vacuo. The residue was purified by flash column chromatography on silica gel to afford the desired product. ^{1}H NMR (400 MHz, $CDCl_3$) δ 8.55 (d, *J* = 4.8 Hz, 2H), 7.53 (s, 1H), 7.35 (d, *J* = 8.4 Hz, 1H), 7.15 (dd, *J* = 8.3, 2.4 Hz, 1H), 7.08 (d, *J* = 2.4 Hz, 1H), 7.05 (t, *J* = 4.8 Hz, 1H), 3.90 – 3.79 (m, 1H), 3.74 – 3.65 (m, 1H), 2.88 – 2.78 (m, 2H), 2.29 (s, 3H);. ^{13}C NMR (101 MHz, $CDCl_3$) δ 169.4, 165.2, 159.8, 151.5, 151.0, 140.3, 132.7, 132.0, 121.8, 120.19, 116.4, 45.2, 31.5, 17.5.

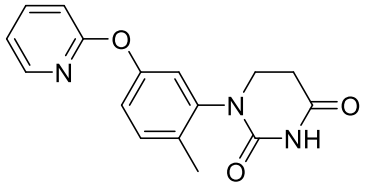

To a solution of 1-(5-hydroxy-2-methylphenyl)dihydropyrimidine-2,4(1H,3H)-dione (220 mg, 1 mmol) in anhydrous DMF was added 2-chloropyridine (136 mg, 1.2 mmol, 1.2 eq) and cesium carbonate (323 mg, 1 mmol, 1.0 eq). The mixture was then stirred at 90 °C for 4 h. Upon completion of the reaction, 10 mL of water was slowly added, followed by extraction with ethyl acetate (3 × 20 mL). The combined organic layers were concentrated in vacuo. The residue was purified by flash column chromatography on silica gel to afford the desired product. ^{1}H NMR (400 MHz, $CDCl_3$) δ 8.18 (ddd, *J* = 5.0, 2.0, 0.8 Hz, 1H), 7.69 (ddd, *J* = 8.3, 7.2, 2.0 Hz, 1H), 7.57 (s, 1H), 7.31 (d, *J* = 8.4 Hz, 1H), 7.09 – 7.04 (m, 1H), 7.03 – 6.97 (m, 2H), 6.92 (d, *J* = 8.3 Hz, 1H), 3.87 – 3.75 (m, 1H), 3.68 (q, *J* = 6.2 Hz, 1H), 2.82 (dd, *J* = 6.9, 4.9 Hz, 2H), 2.26 (s, 3H). ^{13}C NMR (101 MHz, $CDCl_3$) δ 169.4, 163.4, 152.8, 151.1, 147.7, 140.3, 139.6, 132.1, 131.7, 121.2, 119.6, 118.8, 111.7, 45.1, 31.5, 17.4.

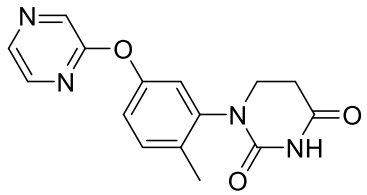

To a solution of 1-(5-hydroxy-2-methylphenyl)dihydropyrimidine-2,4(1H,3H)-dione (220 mg, 1 mmol) in anhydrous DMF was added 2-chloropyrazine (136 mg, 1.2 mmol, 1.2 eq) and cesium carbonate (323 mg, 1 mmol, 1.0 eq). The mixture was then stirred at 90 °C for 4 h. Upon completion of the reaction, 10 mL of water was slowly added, followed by extraction with ethyl acetate (3 × 20 mL). The combined organic layers were concentrated in vacuo. The residue was purified by flash column chromatography on silica gel to afford the desired product. ^{1}H NMR (400 MHz, $CDCl_3$) δ 8.44 (d, *J* = 1.4 Hz, 1H), 8.28 (d, *J* = 2.7 Hz, 1H), 8.09 (dd, *J* = 2.7, 1.4 Hz, 1H), 7.73 (s, 1H), 7.34 (d, *J* = 8.4 Hz, 1H), 7.10 (dd, *J* = 8.4, 2.5 Hz, 1H), 7.05 (d, *J* = 2.5 Hz, 1H), 3.94 – 3.77 (m, 1H), 3.68 (m, 1H), 2.92 – 2.76 (m, 2H), 2.28 (s, 3H). ^{13}C NMR (101 MHz, $CDCl_3$) δ 169.4, 159.9, 151.6, 151.1, 141.0, 140.5, 138.8, 135.9, 132.7, 132.2, 121.3, 119.8, 45.1, 31.5, 17.5.

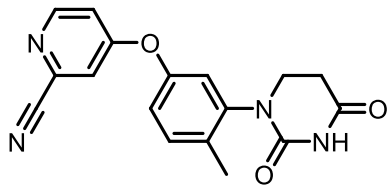

To a solution of 1-(5-hydroxy-2-methylphenyl)dihydropyrimidine-2,4(1H,3H)-dione (220 mg, 1 mmol) in anhydrous DMF was added 4-chloropicolinonitrile (166 mg, 1.2 mmol, 1.2 eq) and cesium carbonate (323 mg, 1 mmol, 1.0 eq). The mixture was then stirred at 90 °C for 4 h. Upon completion of the reaction, 10 mL of water was slowly added, followed by extraction with ethyl acetate (3 × 20 mL). The combined organic layers were concentrated in vacuo. The residue was purified by flash column chromatography on silica gel to afford the desired product. ^{1}H NMR (400 MHz, $CDCl_3$) δ 8.54 (d, *J* = 5.8 Hz, 1H), 7.62 (s, 1H), 7.40 (d, *J* = 8.4 Hz, 1H), 7.24 (d, *J* = 2.5

Hz, 1H), 7.07 – 7.01 (m, 2H), 6.98 (d, *J* = 2.5 Hz, 1H), 3.87 – 3.76 (m, 1H), 3.69 (m, 1H), 2.86 (q, *J* = 6.9 Hz, 2H), 2.32 (s, 3H). ^{13}C NMR (101 MHz, $CDCl_3$) δ 169.1, 165.0, 152.8, 151.6, 151.1, 141.3, 135.4, 134.0, 133.1, 120.6, 119.53, 117.0, 116.8, 114.7, 45.1, 31.4, 17.6.

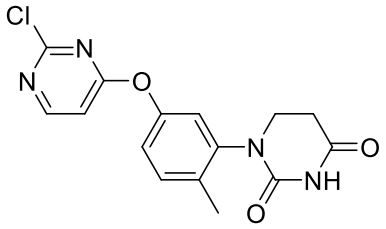

To a solution of 1-(5-hydroxy-2-methylphenyl)dihydropyrimidine-2,4(1H,3H)-dione (220 mg, 1 mmol) in anhydrous DMF was added 2,4-dichloropyrimidine (178 mg, 1.2 mmol, 1.2 eq) and cesium carbonate (323 mg, 1 mmol, 1.0 eq). The mixture was then stirred at 90 °C for 4 h. Upon completion of the reaction, 10 mL of water was slowly added, followed by extraction with ethyl acetate (3 × 20 mL). The combined organic layers were concentrated in vacuo. The residue was purified by flash column chromatography on silica gel to afford the desired product.

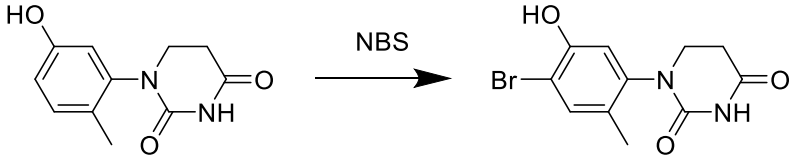

To a solution of 1-(5-hydroxy-2-methylphenyl)dihydropyrimidine-2,4(1H,3H)-dione (1.1 g, 5 mmol) in anhydrous DMF was added NBS (1.06 g, 6mmol, 1.2 eq.). The mixture was then stirred at room temperature for 4 h. Upon completion of the reaction, 20 mL of water was slowly added, followed by extraction with ethyl acetate (3 × 40 mL). The combined organic layers were concentrated in vacuo. The residue was purified by flash column chromatography on silica gel to afford the desired product.

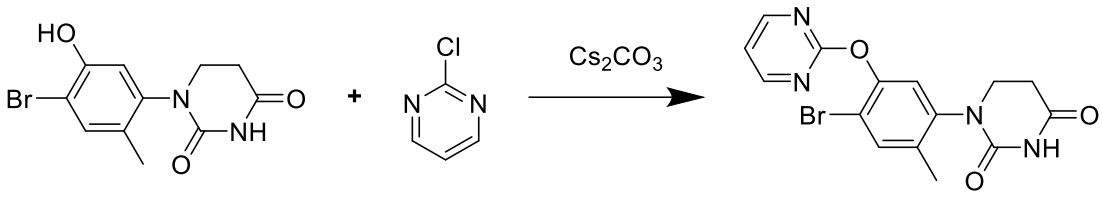

To a solution of 1-(4-bromo-5-hydroxy-2-methylphenyl)dihydropyrimidine-2,4(1H,3H)-dione (298 mg, 1 mmol) in anhydrous DMF was added 2-chloropyrimidine (136 mg, 1.2 mmol, 1.2 eq) and cesium carbonate (323 mg, 1 mmol, 1.0 eq). The mixture was then stirred at 90 °C for 4 h. Upon completion of the reaction, 10 mL of water was slowly added, followed by extraction with ethyl acetate (3 × 20 mL). The combined organic layers were concentrated in vacuo. The residue was purified by flash column chromatography on silica gel to afford the desired product.

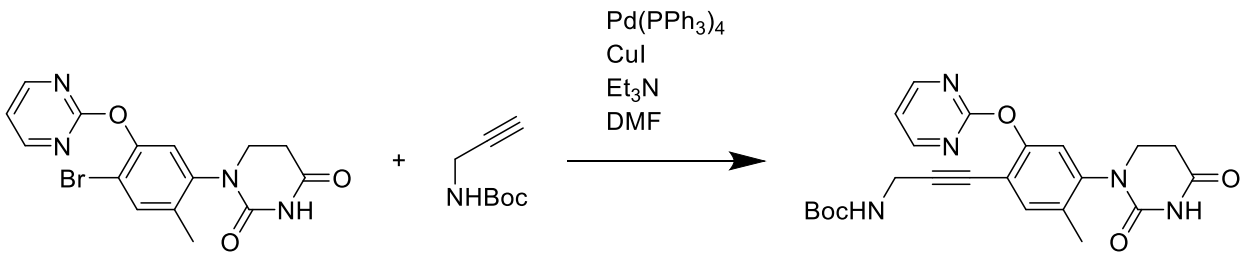

To a solution of 1-(4-bromo-2-methyl-5-(pyrimidin-2-yloxy)phenyl)dihydropyrimidine-2,4(1H,3H)-dione (376 mg, 1 mmol) in anhydrous DMF was added $Pd(PPh_3)_4$ (58 mg, 0.05 mmol), CuI (19 mg, 0.1 mmol), Et_3N (121 mg, 1.2 mmol, 1.2 eq.) and N-Boc-propargylamine (155 mg, 1mmol, 1.0 eq.). The mixture was then stirred at 100 °C for 6 h. Upon completion of the reaction, 10 mL of water was slowly added, followed by extraction with ethyl acetate (3 × 20 mL). The combined organic layers were concentrated in vacuo. The residue was purified by flash column chromatography on silica gel to afford the desired product. ^{1}H NMR (400 MHz, $CDCl_3$) δ 8.56 (d, *J* = 4.8 Hz, 2H), 7.86 (s, 1H), 7.40 (s, 1H), 7.09 – 7.04 (m, 2H), 3.91 (d, *J* = 5.4 Hz, 2H), 3.85 (m,

1H), 3.69 (m, 1H), 2.90 – 2.74 (m, 2H), 2.25 (s, 3H), 1.44 (s, 9H). ^{13}C NMR (101 MHz, $CDCl_3$) δ 169.38, 164.97, 159.86, 159.73, 152.43, 151.09, 140.39, 135.44, 135.10, 133.00, 122.21, 120.65, 116.88, 116.64, 116.42, 91.61, 45.12, 31.45, 28.37, 17.46.

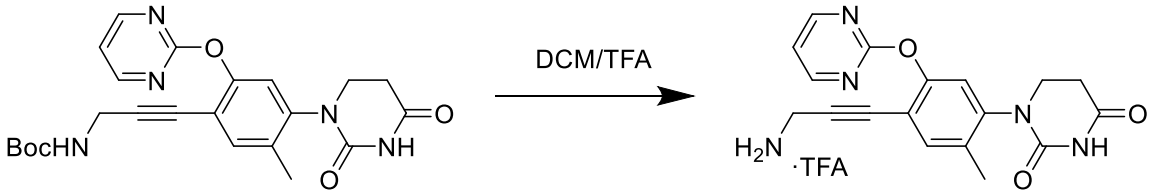

To a solution of tert-butyl (3-(4-(2,4-dioxotetrahydropyrimidin-1(2H)-yl)-5-methyl-2-(pyrimidin-2-yloxy)phenyl)prop-2-yn-1-yl)carbamate in anhydrous DCM (2 mL) was added TFA (1 mL) slowly. The mixture was stirred at room temperature for 2 h. The solvent was then removed in vacuo, and the residue was directly used in the next step.

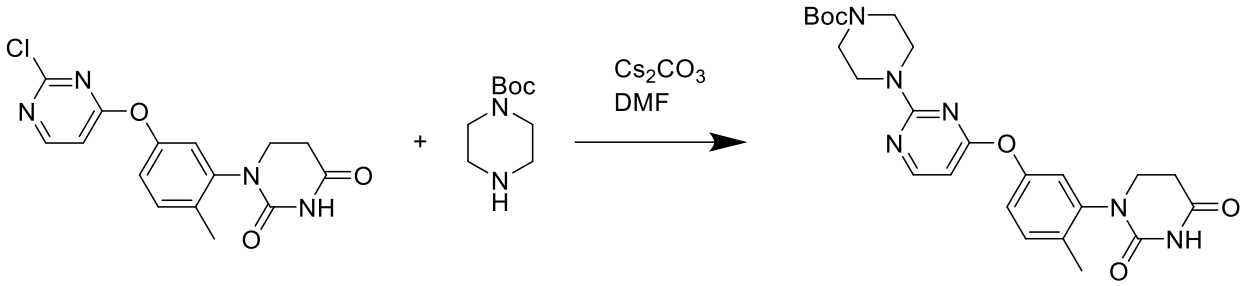

To a solution of 1-(5-hydroxy-2-methylphenyl)dihydropyrimidine-2,4(1H,3H)-dione (220 mg, 1 mmol) in anhydrous DMF was added N-Boc-piperazine (223 mg, 1.2 mmol, 1.2 eq) and cesium carbonate (323 mg, 1 mmol, 1.0 eq). The mixture was then stirred at 100 °C for 6 h. Upon completion of the reaction, 10 mL of water was slowly added, followed by extraction with ethyl acetate (3 × 20 mL). The combined organic layers were concentrated in vacuo. The residue was purified by flash column chromatography on silica gel to afford the desired product. ^{1}H NMR (400 MHz, DMSO) δ 10.37 (s, 1H), 8.26 (d, *J* = 5.6 Hz, 1H), 7.34 (d, *J* = 8.4 Hz, 1H), 7.21 (d, *J* = 2.5 Hz, 1H), 7.10 (dd, *J* = 8.3, 2.5 Hz, 1H), 6.19 (d, *J* = 5.5 Hz, 1H), 3.83 – 3.72 (m, 1H), 3.64 – 3.49

(m, 5H), 3.39 – 3.28 (m, 4H), 2.82 – 2.62 (m, 2H), 2.20 (s, 3H), 1.41 (s, 9H). ^{13}C NMR (101 MHz, DMSO) δ 171.2, 169.5, 161.5, 160.5, 154.4, 152.1, 150.8, 141.9, 132.9, 131.6, 121.1, 120.7, 96.55, 79.5, 44.9, 43.6, 31.6, 28.5, 17.5.

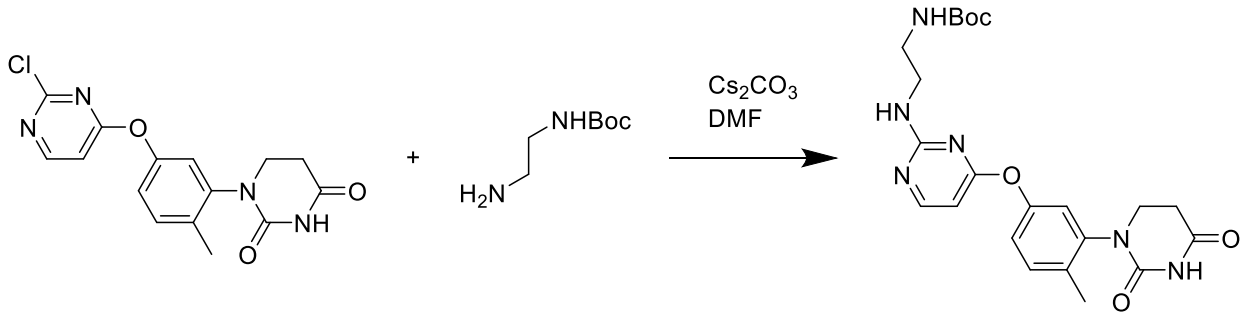

To a solution of 1-(5-hydroxy-2-methylphenyl)dihydropyrimidine-2,4(1H,3H)-dione (220 mg, 1 mmol) in anhydrous DMF was added N-Boc-ethylenediamine (192 mg, 1.2 mmol, 1.2 eq) and cesium carbonate (323 mg, 1 mmol, 1.0 eq). The mixture was then stirred at 100 °C for 6 h. Upon completion of the reaction, 10 mL of water was slowly added, followed by extraction with ethyl acetate (3 × 20 mL). The combined organic layers were concentrated in vacuo. The residue was purified by flash column chromatography on silica gel to afford the desired product. ^{1}H NMR (400 MHz, DMSO) δ 10.36 (s, 1H), 8.15 (d, *J* = 5.6 Hz, 1H), 7.31 (d, *J* = 8.4 Hz, 1H), 7.16 (s, 1H), 7.06 (d, *J* = 8.6 Hz, 1H), 6.75 (s, 1H), 6.14 (s, 1H), 3.82 – 3.73 (m, 1H), 3.57 – 3.49 (m, 1H), 3.23 (s, 2H), 3.01 (s, 2H), 2.71 (m, 2H), 2.18 (s, 3H), 1.35 (s, 8H).

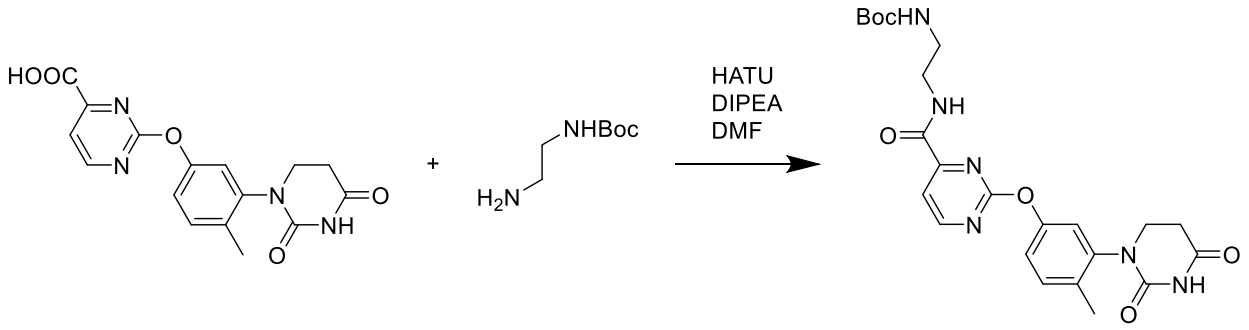

To a solution of 2-(3-(2,4-dioxotetrahydropyrimidin-1(2H)-yl)-4-methylphenoxy)pyrimidine-4-carboxylic acid (34 mg, 0.1 mmol) in DMF was added HATU (40 mg, 0.12 mmol), N-Boc-ethylenediamine (19 mg, 0.12 mmol), and DIPEA (21 mg, 0.2 mmol). The reaction mixture was stirred at room temperature overnight. The mixture was then extracted and concentrated in vacuo. The residue was purified by flash column chromatography on silica gel to afford the desired product. ^{1}H NMR (400 MHz, DMSO) δ 10.37 (s, 1H), 8.83 (d, *J* = 4.9 Hz, 1H), 8.77 (t, *J* = 6.0 Hz, 1H), 7.74 (d, *J* = 4.9 Hz, 1H), 7.37 – 7.34 (m, 1H), 7.28 (d, *J* = 2.5 Hz, 1H), 7.14 (dd, *J* = 8.3, 2.5 Hz, 1H), 6.91 (t, *J* = 5.7 Hz, 1H), 3.84 – 3.74 (m, 1H), 3.61 – 3.53 (m, 2H), 3.16 – 3.06 (m, 2H), 2.84 – 2.62 (m, 2H), 2.21 (s, 3H), 1.36 (s, 9H).

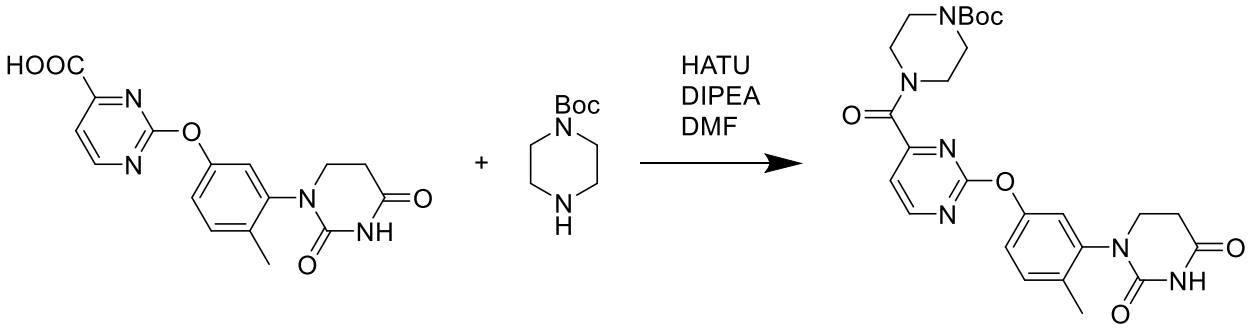

To a solution of 2-(3-(2,4-dioxotetrahydropyrimidin-1(2H)-yl)-4-methylphenoxy)pyrimidine-4-carboxylic acid (34 mg, 0.1 mmol) in DMF was added HATU (40 mg, 0.12 mmol), N-Boc-piperazine (22 mg, 0.12 mmol), and DIPEA (21 mg, 0.2 mmol). The reaction mixture was stirred at room temperature overnight. The mixture was then extracted and concentrated in vacuo. The residue was purified by flash column chromatography on silica gel to afford the desired product.

^{1}H NMR (400 MHz, DMSO) δ 10.36 (s, 1H), 8.80 (d, *J* = 4.9 Hz, 1H), 7.41 (d, *J* = 4.9 Hz, 1H), 7.34 (d, *J* = 8.4 Hz, 1H), 7.24 (d, *J* = 2.5 Hz, 1H), 7.15 (dd, *J* = 8.3, 2.5 Hz, 1H), 3.80 – 3.73 (m, 1H), 3.59 – 3.55 (m, 1H), 3.55 – 3.51 (m, 2H), 3.43 – 3.36 (m, 2H), 3.32 – 3.26 (m, 2H), 3.24 –

3.08 (m, 2H), 2.20 (s, 3H), 1.40 (s, 9H). ^{13}C NMR (101 MHz, DMSO) δ 171.2, 164.6, 164.4, 163.6, 162.4, 154.2, 152.1, 151.5, 142.1, 133.2, 131.7, 121.2, 120.8, 115.4, 79.7, 46.5, 45.0, 41.9, 31.6, 28.5, 17.5.

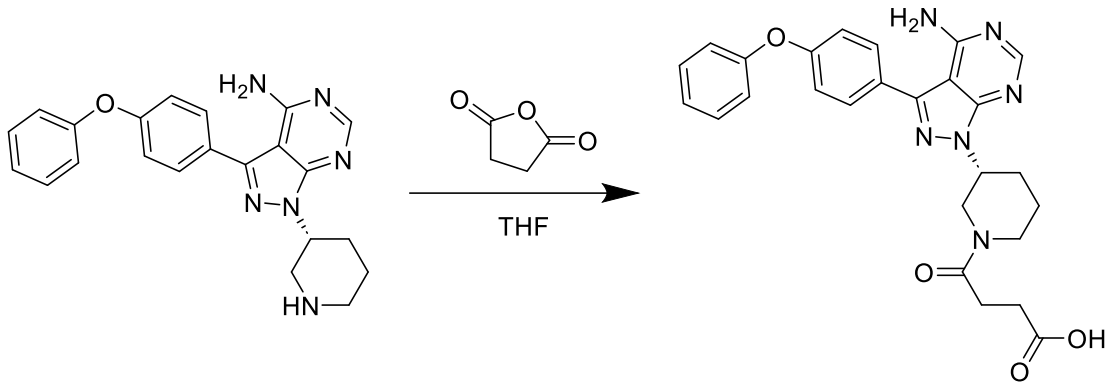

To a solution of the BTK ligand (386 mg) in anhydrous THF (10 mL) was added succinic anhydride (112 mg, 1.1 equivalents) and Et_3N (200 mg, 2.0 equivalents). The mixture was heated at 60 °C. After completion, the solvent was removed under reduced pressure, and the residue was directly used in the next step.

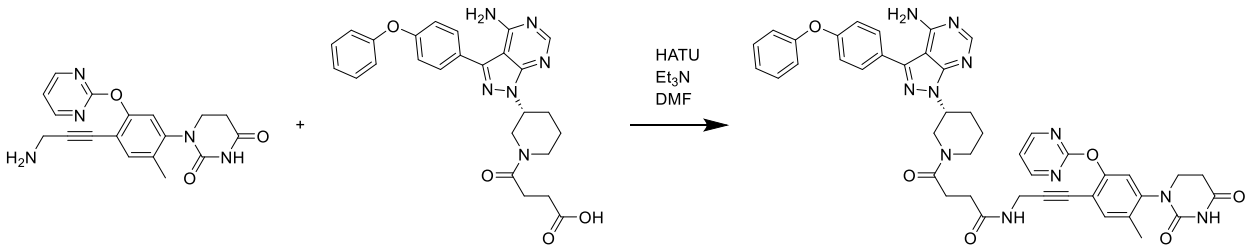

To a solution of BTK ligand (10 mg, 0.02 mmol) in DMF was added HATU (9 mg, 0.024 mmol, 1.2 eq.), achiral ligand (8 mg, 0.024 mmol), and DIPEA (21 mg, 0.2 mmol). The reaction mixture was stirred at room temperature overnight. The mixture was then extracted and concentrated in vacuo. The residue was purified by flash column chromatography on silica gel to afford the desired product. ^{1}H NMR (400 MHz, DMSO) δ 10.41 (s, 1H), 8.63 (d, *J* = 4.7 Hz, 1H), 8.27 (s, 2H), 7.67 (d, *J* = 8.6 Hz, 2H), 7.50 – 7.37 (m, 3H), 7.32 – 7.21 (m, 2H), 7.19 – 7.11 (m, 4H), 6.94 (t, *J* = 5.5

Hz, 1H), 4.63 (dq, *J* = 10.7, 5.2 Hz, 1H), 4.14 (d, *J* = 13.2 Hz, 1H), 3.92 (d, *J* = 13.3 Hz, 1H), 3.84 (m, 3H), 3.53 (m, 2H), 3.18 (t, *J* = 11.8 Hz, 1H), 2.78 (t, *J* = 12.4 Hz, 2H), 2.68 (s, 1H), 2.51 (d, *J* = 1.9 Hz, 1H), 2.18 (m, 5H), 1.81 (d, *J* = 13.2 Hz, 1H), 1.53 (d, *J* = 13.0 Hz, 1H).

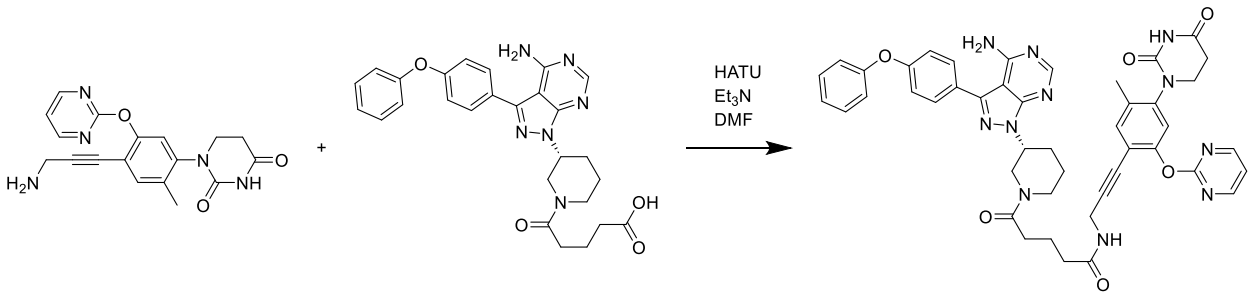

To a solution of BTK ligand (10 mg, 0.02 mmol) in DMF was added HATU (9 mg, 0.024 mmol, 1.2 eq.), achiral ligand (8 mg, 0.024 mmol), and DIPEA (21 mg, 0.2 mmol). The reaction mixture was stirred at room temperature overnight. The mixture was then extracted and concentrated in vacuo. The residue was purified by flash column chromatography on silica gel to afford the desired product. ^{1}H NMR (400 MHz, DMSO) δ 10.45 (s, 1H), 8.67 (d, *J* = 4.7 Hz, 1H), 8.23 (s, 2H), 7.69 (d, *J* = 8.6 Hz, 2H), 7.54 – 7.39 (m, 3H), 7.36 – 7.27 (m, 2H), 7.18– 7.18 (m, 4H), 6.97 (t, *J* = 5.5 Hz, 1H), 4.67 (dq, *J* = 10.7, 5.2 Hz, 1H), 4.17(d, *J* = 13.2 Hz, 1H), 3.99 (d, *J* = 13.3 Hz, 1H), 3.84 (m, 3H), 3.54 (m, 2H), 3.17 (t, *J* = 11.8 Hz, 1H), 2.78 (t, *J* = 12.4 Hz, 2H), 2.56 (m, 2H), 2.66 (s, 1H), 2.41 (d, *J* = 1.9 Hz, 1H), 2.17 (m, 5H), 1.81 (d, *J* = 13.2 Hz, 1H), 1.58 (d, *J* = 13.0 Hz, 1H).

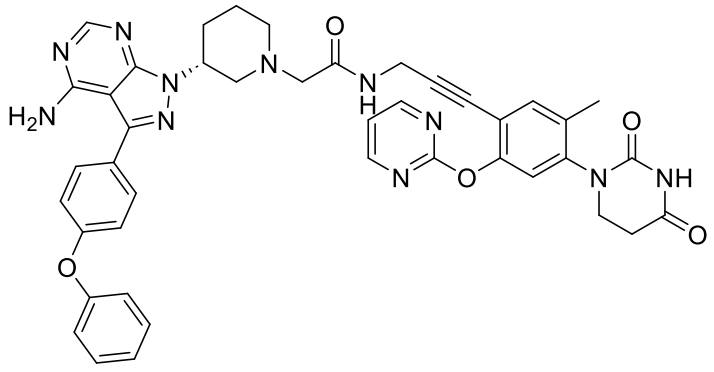

To a solution of BTK ligand (10 mg, 0.02 mmol) in DMF was added HATU (9 mg, 0.024 mmol, 1.2 eq.), achiral ligand (8 mg, 0.024 mmol), and DIPEA (21 mg, 0.2 mmol). The reaction mixture was stirred at room temperature overnight. The mixture was then extracted and concentrated in vacuo. The residue was purified by flash column chromatography on silica gel to afford the desired product.

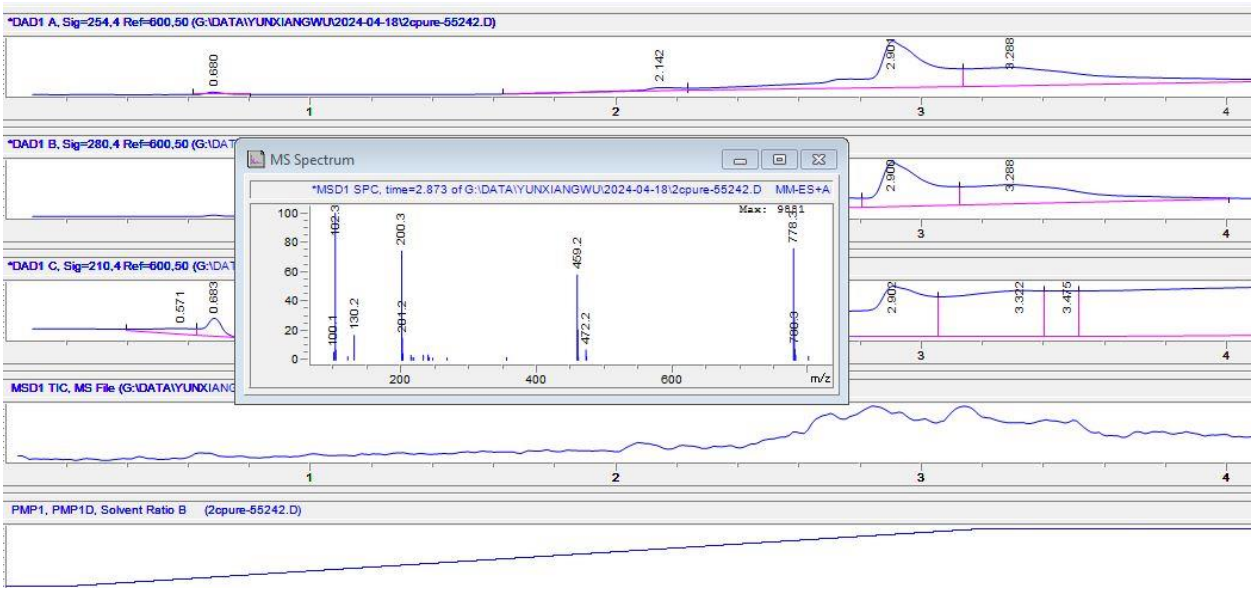

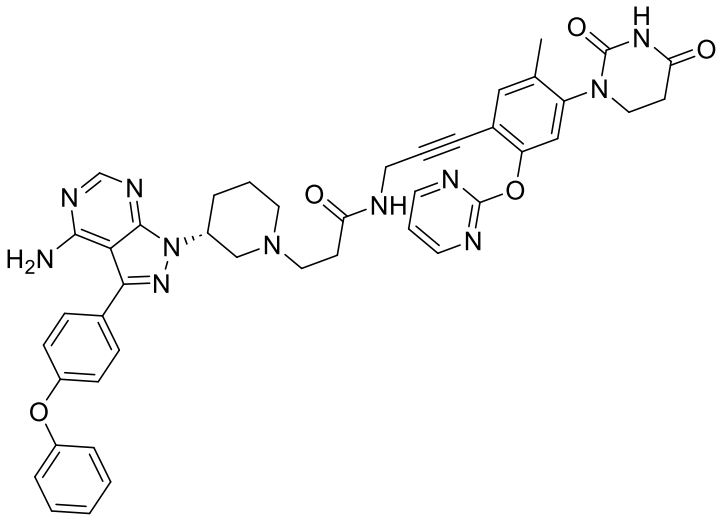

To a solution of BTK ligand (10 mg, 0.02 mmol) in DMF was added HATU (9 mg, 0.024 mmol, 1.2 eq.), achiral ligand (8 mg, 0.024 mmol), and DIPEA (21 mg, 0.2 mmol). The reaction mixture was stirred at room temperature overnight. The mixture was then extracted and concentrated in vacuo. The residue was purified by flash column chromatography on silica gel to afford the desired product.

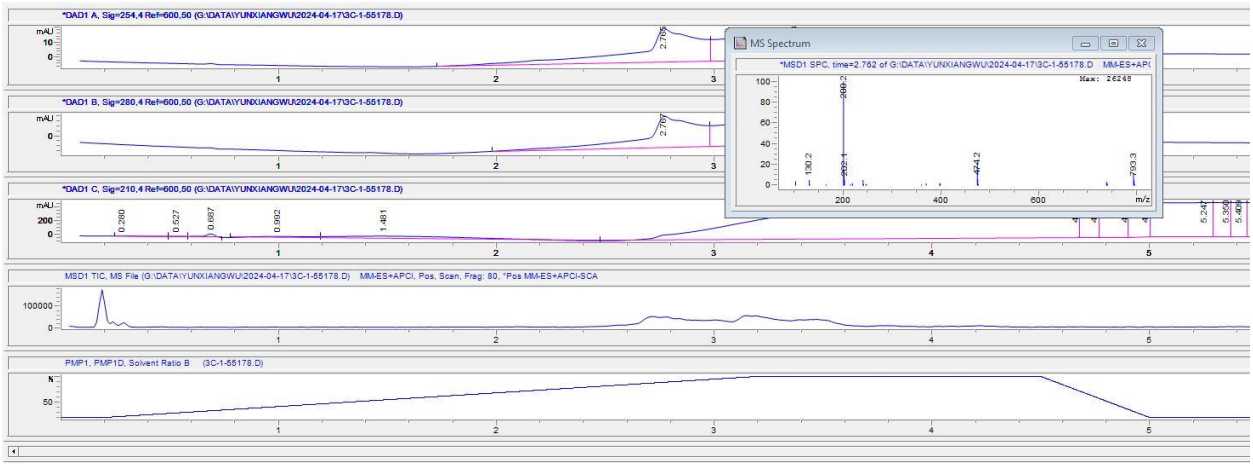

2.8. References

1. (a) Lai, A. C.; Crews, C. M. Induced protein degradation: an emerging drug discovery paradigm. *Nat. Rev. Drug Discov.* **2017**, 16, 101-114. (b) Salami, J.; Crews, C. M. Waste disposal-An attractive strategy for cancer therapy. *Science* **2017**, 355, 1163-1167. (c) Cromm, P. M.; Crews, C. M. Targeted Protein Degradation: from Chemical Biology to Drug Discovery. *Cell Chem. Biol.* **2017**, 24, 1181-1190. (d) Ottis, P.; Crews, C. M. Proteolysis-Targeting Chimeras: Induced Protein Degradation as a Therapeutic Strategy. *ACS Chem. Biol.* **2017**, 12, 892-898.
2. Schapira, M.; Calabrese, M. F.; Bullock, A. N.; Crews, C. M. Targeted Protein Degradation: Expanding the Toolbox. *Nat. Rev. Drug Discov.* **2019**, 18, 949−963.

3. (a) Békés, M.; Langley, D. R.; Crews, C. M. PROTAC Targeted Protein Degraders: The Past Is Prologue. *Nat. Rev. Drug Discov.* **2022**, 21, 181−200. (b) Leeson, P. D.; Springthorpe, B. The Influence of Drug-like Concepts on Decision-Making in Medicinal Chemistry. *Nat. Rev. Drug Discov.* **2007**, 6, 881−890. (c) Wang, C.; Zhang, Y.; Wu, Y.; Xing, D. Developments of CRBN-Based PROTACs as Potential Therapeutic Agents. *Eur. J. Med. Chem.* **2021**, 225, 113749.
4. Eriksson, T.; Björkman, S.; Roth, B.; Fyge, Å.; Höglund, P. Stereospecific Determination, Chiral Inversion in Vitro and Pharmacokinetics in Humans of the Enantiomers of Thalidomide. *Chirality* **1995**, 7, 44−52.
5. (a) Chamberlain, P. P.; Lopez-Girona, A.; Miller, K.; Carmel, G.; Pagarigan, B.; Chie-Leon, B.; Rychak, E.; Corral, L. G.; Ren, Y. J.; Wang, M.; Riley, M.; Delker, S. L.; Ito, T.; Ando, H.; Mori, T.; Hirano, Y.; Handa, H.; Hakoshima, T.; Daniel, T. O.; Cathers, B. E. Structure of the Human Cereblon−DDB1−Lenalidomide Complex Reveals Basis for Responsiveness to Thalidomide Analogs. *Nat. Struct. Mol. Biol.* **2014**, 21, 803−809. (b) Mori, T.; Ito, T.; Liu, S.; Ando, H.; Sakamoto, S.; Yamaguchi, Y.; Tokunaga, E.; Shibata, N.; Handa, H.; Hakoshima, T. Structural Basis of Thalidomide Enantiomer Binding to Cereblon. *Sci. Rep.* **2018**, 8, 1294.
6. (a) Yamamoto, T.; Tokunaga, E.; Nakamura, S.; Shibata, N.; Toru, T. Synthesis and Configurational Stability of (S)- and (R) Deuteriothalidomides. *Chem. Pharm. Bull.* **2010**, 58, 110−112. (b) Hansen, J. D.; Correa, M.; Nagy, M. A.; Alexander, M.; Plantevin, V.; Grant, V.; Whitefield, B.; Huang, D.; Kercher, T.; Harris, R.; Narla, R. K.; Leisten, J.; Tang, Y.; Moghaddam, M.; Ebinger, K.; Piccotti, J.; Havens, C. G.; Cathers, B.; Carmichael, J.; Daniel, T.; Vessey, R.; Hamann, L. G.; Leftheris, K.; Mendy, D.; Baculi, F.; LeBrun, L.

A.; Khambatta, G.; Lopez-Girona, A. Discovery of CRBN E3 Ligase Modulator CC-92480 for the Treatment of Relapsed and Refractory Multiple Myeloma. *J. Med. Chem.* **2020**, 63, 6648−6676. (c) Nishimura, K.; Hashimoto, Y.; Iwasaki, S. (S)-Form of α-Methyl-N(α)-Phthalimidoglutarimide, But not Its (R)-Form, Enhanced Phorbol Ester-Induced Tumor Necrosis Factor-α Production by Human Leukemia Cell HL-60: Importance of Optical Resolution of Thalidomidal Effects. *Chem. Pharm. Bull.* **1994**, 42, 1157−1159.

7. Min, J.; Mayasundari, A.; Keramatnia, F.; Jonchere, B.; Yang, S. W.; Jarusiewicz, J.; Actis, M.; Das, S.; Young, B.; Slavish, J.; Yang, L.; Li, Y.; Fu, X.; Garrett, S. H.; Yun, M.-K.; Li, Z.; Nithianantham, S.; Chai, S.; Chen, T.; Shelat, A.; Lee, R. E.; Nishiguchi, G.; White, S. W.; Roussel, M. F.; Potts, P. R.; Fischer, M.; Rankovic, Z. Phenyl Glutarimides: Alternative Cereblon Binders for the Design of PROTACs. *Angew. Chem., Int. Ed.* **2021**, 60, 26663−26670.
8. Xie, H.; Li, C.; Tang, H.; Tandon, I.; Liao, J.; Roberts, B. L.; Zhao, Y.; Tang, W. Development of Substituted Phenyl Dihydrouracil as the Novel Achiral Cereblon Ligands for Targeted Protein Degradation. *J. Med. Chem.* **2023**, 66, 2904−2917.

Chapter 3

Two-Stage Strategy for Development of Proteolysis Targeting Chimeras Targeting RIPK

3.1. Introduction

Receptor-interacting protein kinase 3 (RIPK3) is a pivotal regulator of necroptosis, a programmed form of necrosis that plays a key role in inflammation and cell death[1](**Figure 3.1**). Dysregulated necroptosis is linked to various pathological conditions, such as neurodegenerative diseases, inflammatory disorders, and ischemic injuries. Therefore, targeting RIPK3 holds potential as a therapeutic strategy to mitigate these diseases. Numerous RIPK3 inhibitors have been developed and are being evaluated in clinical research. Although these inhibitors show promise in reducing necroptosis and its pathological outcomes, their cellular toxicity is a significant concern[2]. Prolonged use of RIPK3 inhibitors has been associated with off-target effects that compromise cell viability and function. Interestingly, knockout of the RIPK3 protein does not produce similar side effects[1,3]. Based on previous studies, we are exploring whether PROTACs can be employed to mimic the effects of RIPK3 knockout, thereby inhibiting its functions while minimizing the toxicity associated with RIPK3 inhibitors.

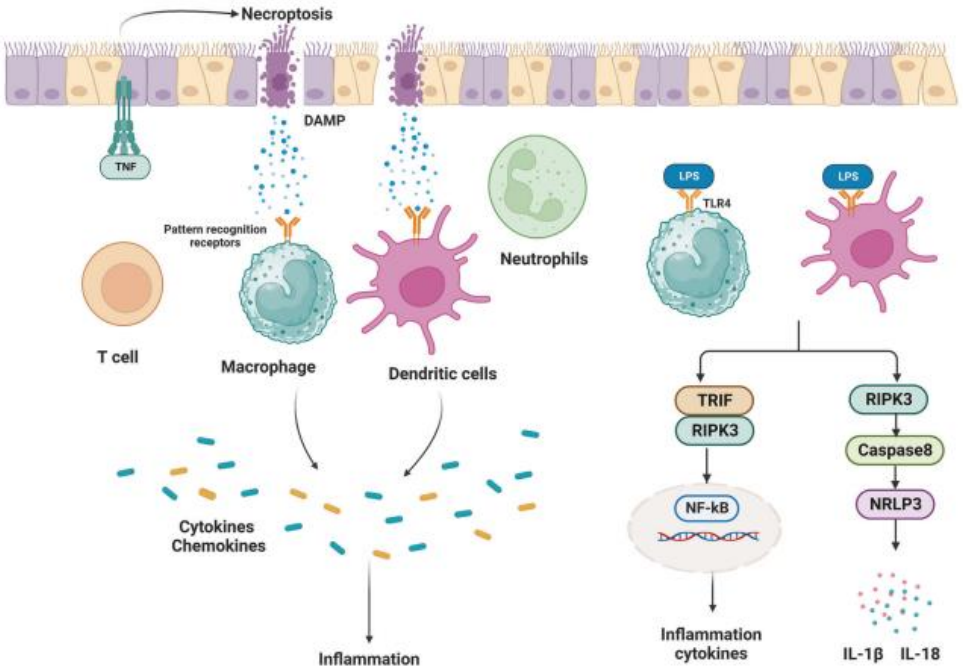

Figure 3.1. RIPK3 signaling-mediated necroptosis[4]

Proteolysis-targeting chimeras (PROTACs) signify a revolutionary targeted protein degradation method in drug discovery[5]. These bifunctional molecules comprise two specific ligands joined by a linker: one ligand targets the protein of interest, while the other attracts an E3 ubiquitin ligase **(Figure 3.2)**. This interaction leads to the formation of a ternary complex, ubiquitination and subsequent proteasomal degradation of the target protein. In contrast to conventional inhibitors that only inhibit protein activity, PROTACs completely remove the protein, providing sustained and more effective suppression of its function.

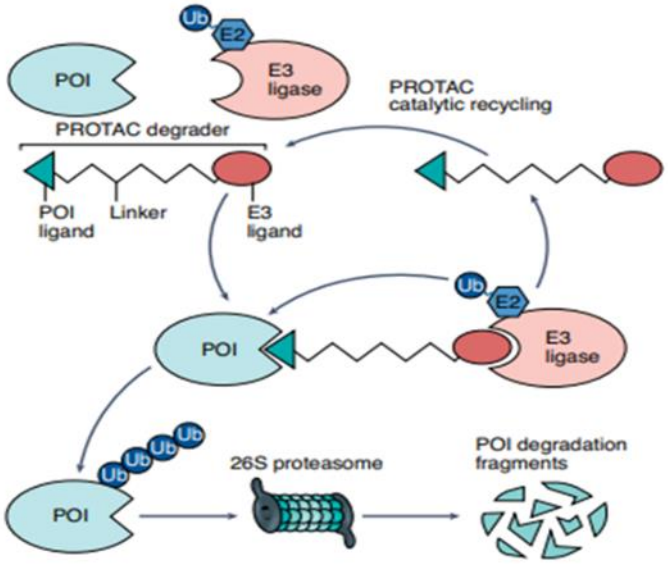

Figure 3.2. The mechanism of PROTAC[6]

Selecting the most suitable E3 ligase ligand and linker for PROTAC development can be challenging[7]. To address this, our group developed a platform called "Rapid-TAC." This platform splits a complete PROTAC into two components: one part consists of the E3 ligase ligand, various linkers, and a reactive group A, while the other part includes the target protein ligand, and a reactive group B. Groups A and B can spontaneously react to form a complete PROTAC (as illustrated in **Figure 3.3**). The Rapid-TAC platform can significantly accelerate the development

of PROTACs, particularly its high-throughput screening capabilities, which allow for the rapid evaluation of numerous E3 ligase ligands. Its automated and miniaturized processes streamline the synthesis and testing phases, significantly reducing time and resource expenditure. In this chapter, we want to use this “rapid-Tac” strategy to develop a series of RIPK3 PROTACs.

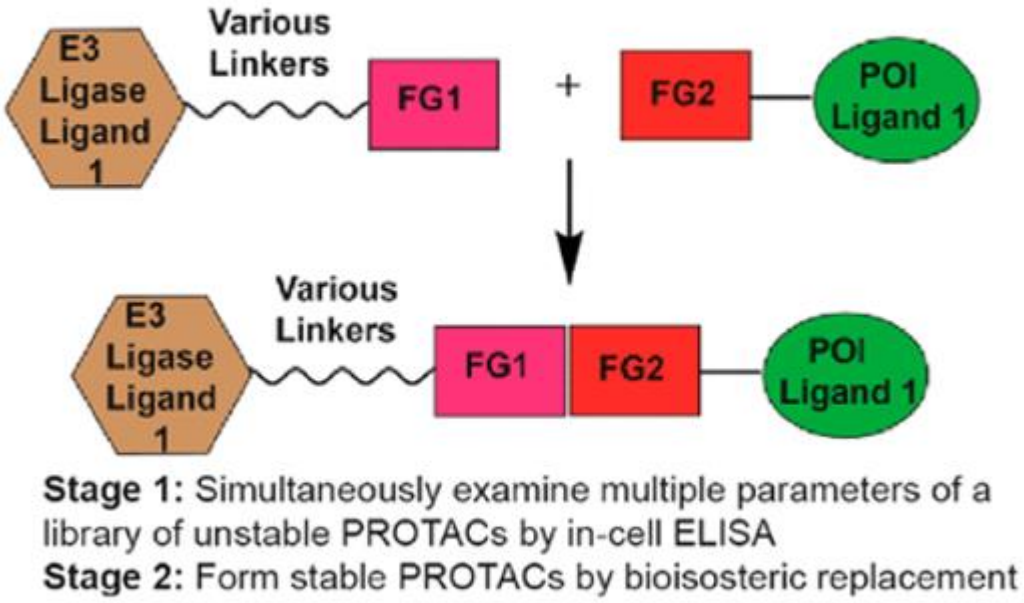

Figure 3.3. Graphical abstract of Rapid-TAC[7]

3.2. Preliminary Studies

We screened small chemical libraries (Selleck, GSK (2014) set 1, and GSK (2014) set 2) containing 1,141 kinase inhibitors available at the Small Molecule Screening Facility at UW-Madison. Through this screening[8], we identified a group of compounds, including C9 (GSK2593074A, shown in **Figure 3.4 (A)**, R = Me), which effectively protected cells from necrosis. In biochemical assays, C9 was found to bind and inhibit the kinase activity of human recombinant RIP3 as well as its partner, RIP1. When tested across various cell types, including human cells, C9 demonstrated protective effects against multiple necroptotic triggers, with an IC_{50} of less than 10 nM. Additionally, the related compound C7 (**Figure 3.4 (A)**, R = H) exhibited a similar dose-dependent inhibition of necroptosis. Based on prior studies, we selected C7 as the ligand for developing RIPK3-targeting PROTACs. Leveraging molecular docking of GSK'074 with the kinase domain of human RIPK3 (**Figure 3.4 (B)**), we identified the pyrazole ring as a solvent-exposed site, making it an ideal position for attaching a linker.

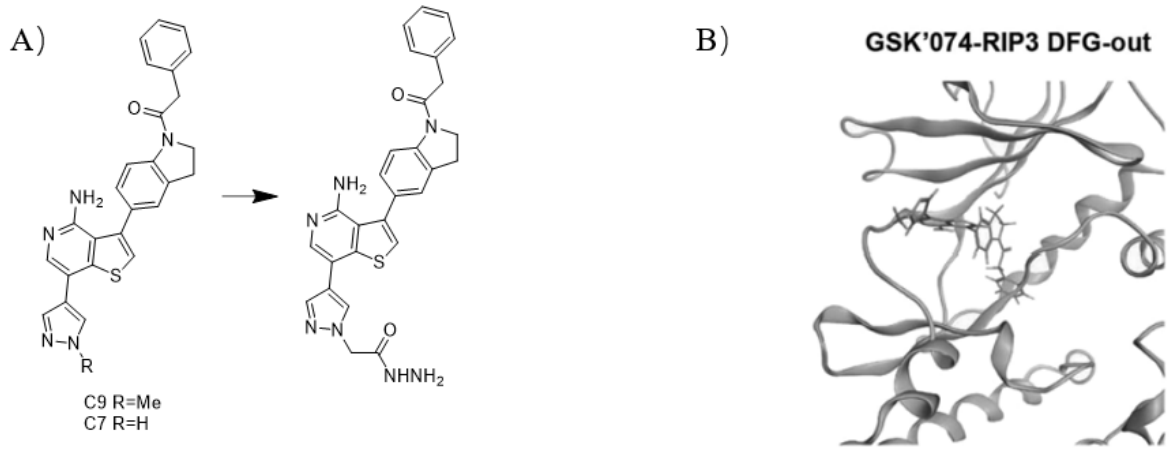

Figure 3.4. (A) Structures of RIP3 inhibitors; **(B)** Molecular docking of GSK'074 and kinase domain of human RIP3[8]

3.3. Synthesis of RIPK3 PROTACs

Dan Yin synthesized and conjugated RIPK3 ligand to thalidomide/VHL ligand with a flexible linker (**Figure 3.5**) and varied the lengths and properties of the linker (hydrophilic or hydrophobic) to improve the efficiency of the degradation and other pharmacological properties of the degraders (solubility and metabolic stability).

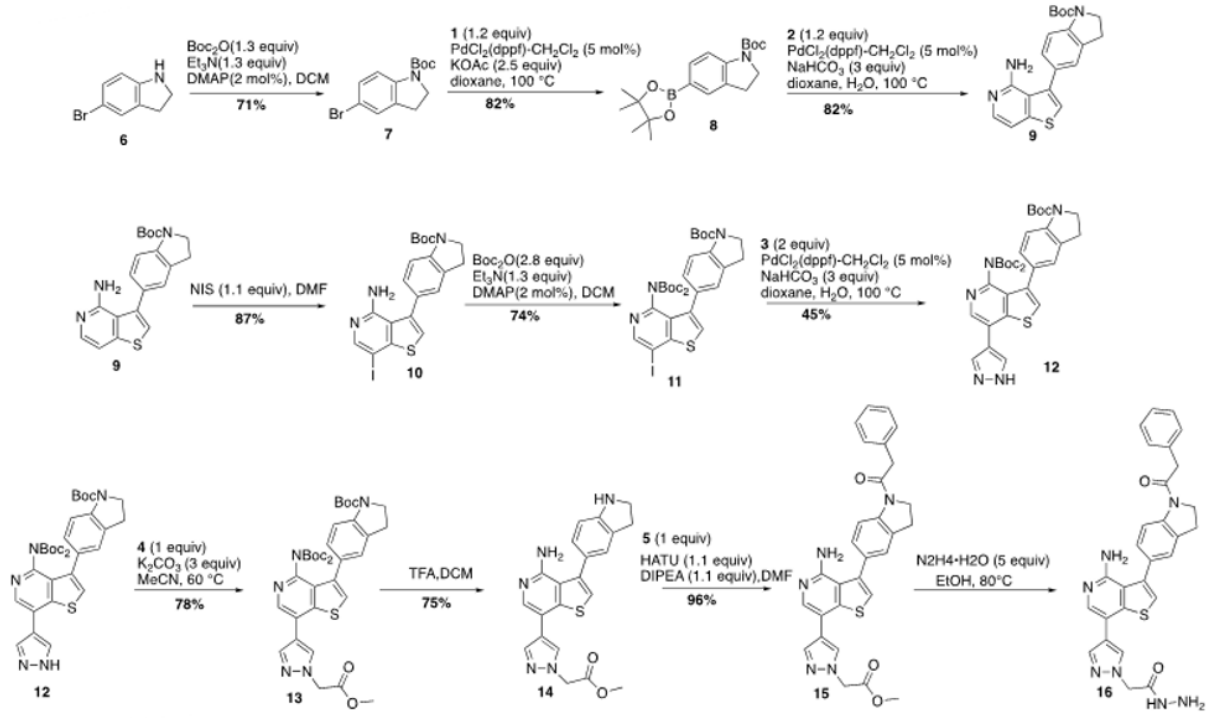

Dan Yin's work

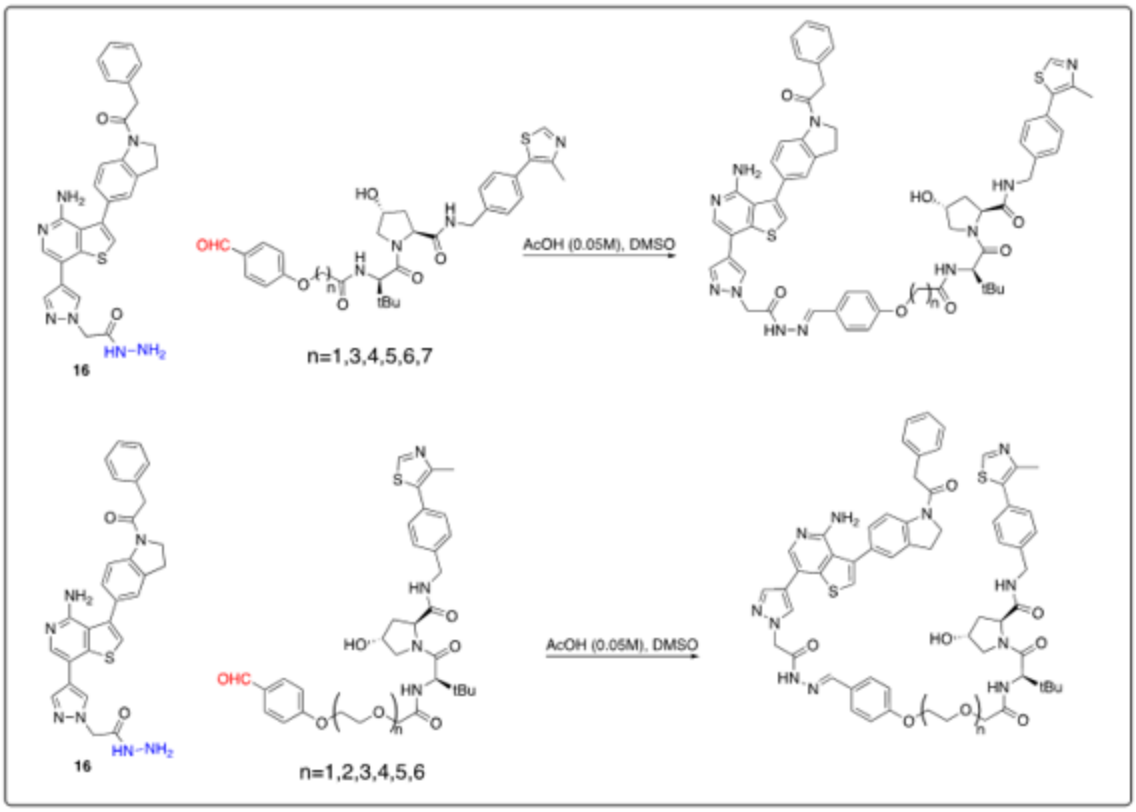
16
n=1,3,4,5,6,7
AcOH (0.05M), DMSO
16
n=1,2,3,4,5,6
AcOH (0.05M), DMSO

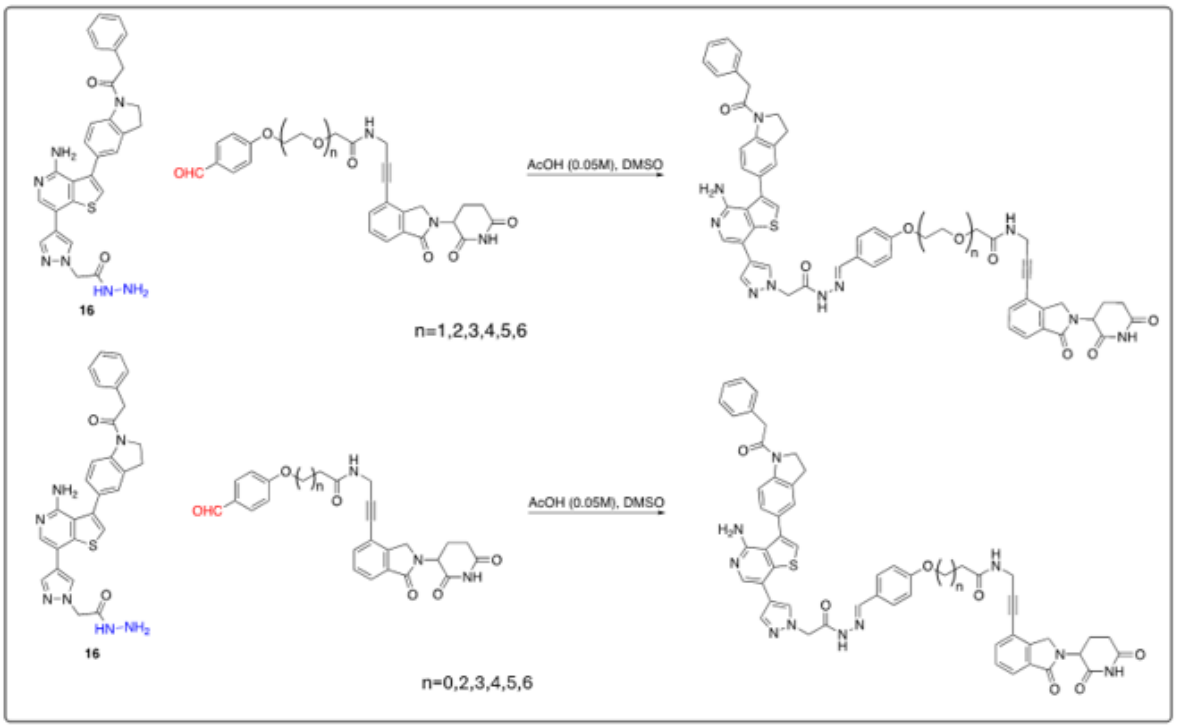

Figure 3.5. Library of RIP PROTACs

3.4. Biological Study of RIPK PROTACs

The degraders were tested across several cell lines (NOVAS, THP-1, HT-29, and NOMO-1) to assess their effect on RIP kinase degradation. Among them, the human acute myeloid leukemia (AML) cell line NOMO-1 exhibited the highest sensitivity, showing a significant down-regulation of RIP expression when treated with the degraders. Our group member Binkai Liu then conducted Western blot assays on cells treated with compounds DY-1 to DY-24. NOMO-1 cells were exposed to 0.1 and 1 μM concentrations of these compounds. After 6 h of treatment, the cells were lysed for SDS-PAGE and immunoblotting (**Figure 3.6**). Based on the results of the Western blot analysis, DY-15 demonstrated strongest degradation efficiency for both RIPK1 and RIPK2, while

DY-2 showed effective degradation specifically for RIPK1. However, we didn't observe any degradation of RIPK3.

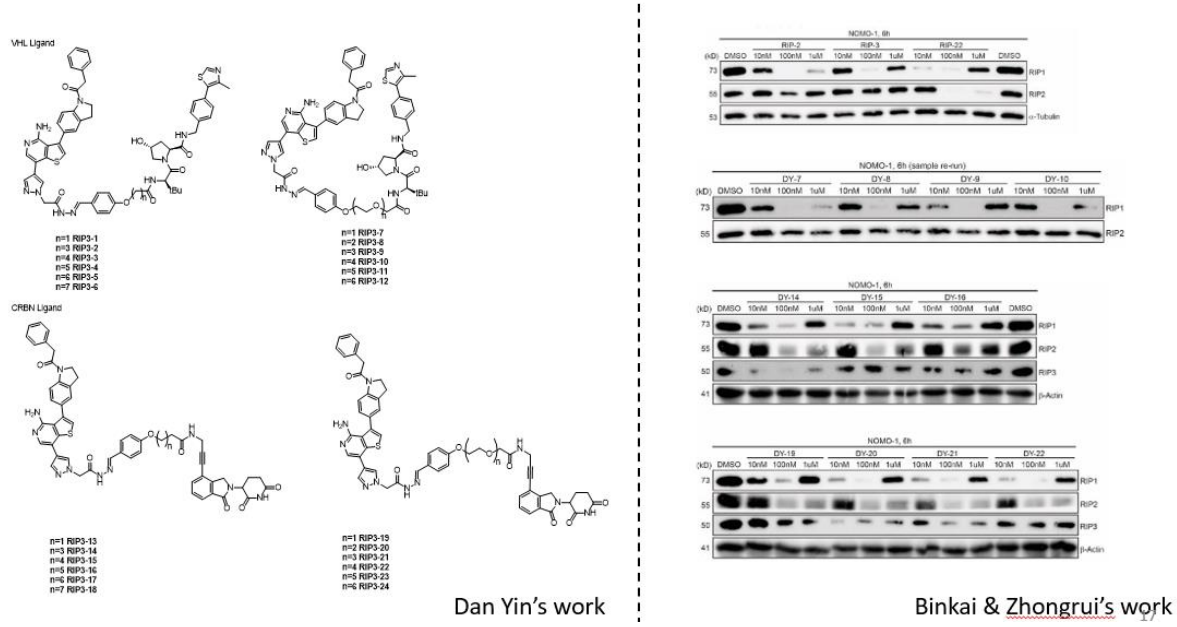

Figure 3.6. Previous experimental results about RIP PROTACs

3.5. Synthesis of stable RIPK1 PROTACs

Through the creation and screening of our library, formed by coupling aldehydes and hydrazides, we quickly identified DY-2 as an effective RIPK1 degrader and DY-15 as a dual RIK1/RIPK2 degrader. This was accomplished by fine-tuning various factors, such as linker length, linker type, and the attachment point to the POI ligand. It is widely recognized that acyl hydrazones can be hydrolyzed at moderately acidic pH, reverting to their original hydrazide and aldehyde components. To solve this problem, I synthesized the stable version of DY-2 by replacing the C-N double bond with a C-C single bond AM-DY-2, which has a more stable amide functional group instead of the hydrolytic labile acylhydrazone motif (**Figure 3.7**).

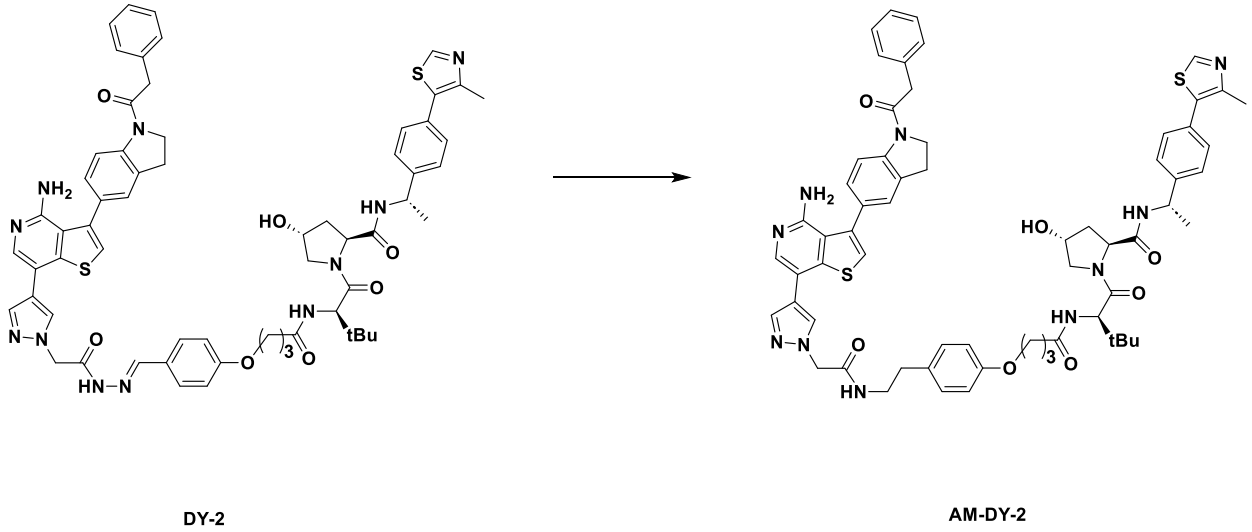

Figure 3.7. Structure of AM-DY-2

By adapting the synthetic route previously used by Yin Dan, we conducted the nine-step synthesis of RIPK1 ligand, which involves several protection and de-protection steps. We also realize that the product can be prepared more efficiently by reducing the protection/de-protection steps. For example, if we perform the acylation reaction first, we wouldn't need to protect the nitrogen atom on the indoline. Similarly, if we carry out the alkylation reaction on the pyrroline in advance, we wouldn't need to protect the aniline group. Finally, I completed the five-step sequence to prepare the RIPK1 ligand (**Figure 3.8**).

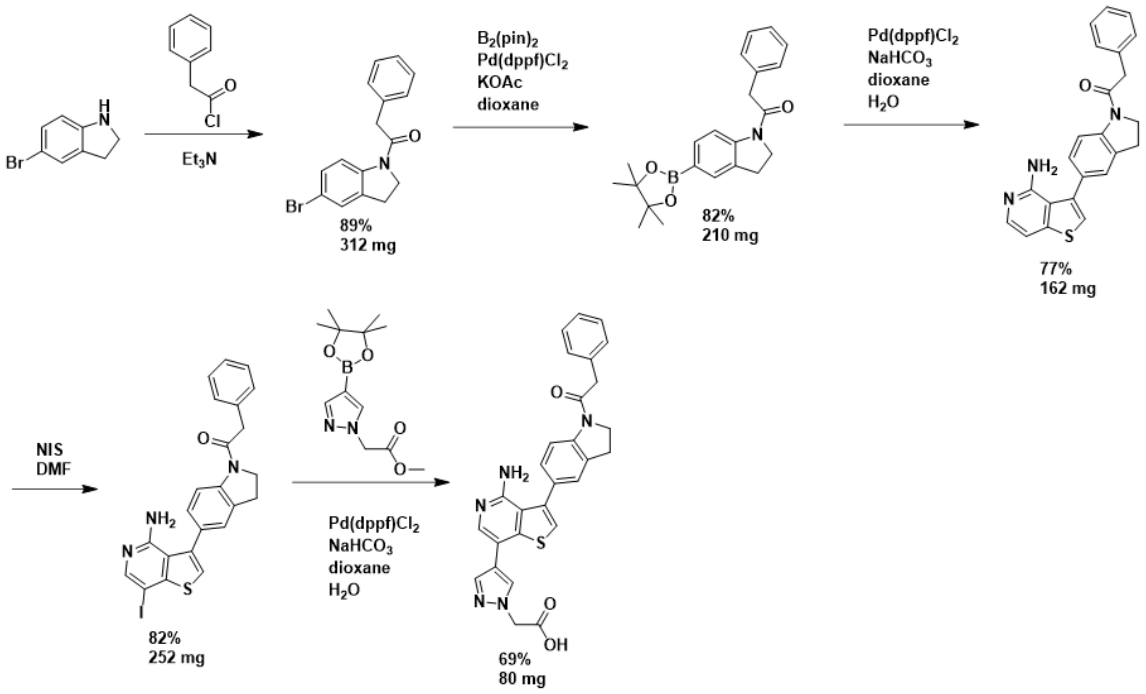

Figure 3.8. An efficient synthetic route of RIPK1 ligand

Subsequently, I synthesized the VHL ligand and successfully conjugated it with the RIPK1 ligand, resulting in our stable RIP1 PROTACs.

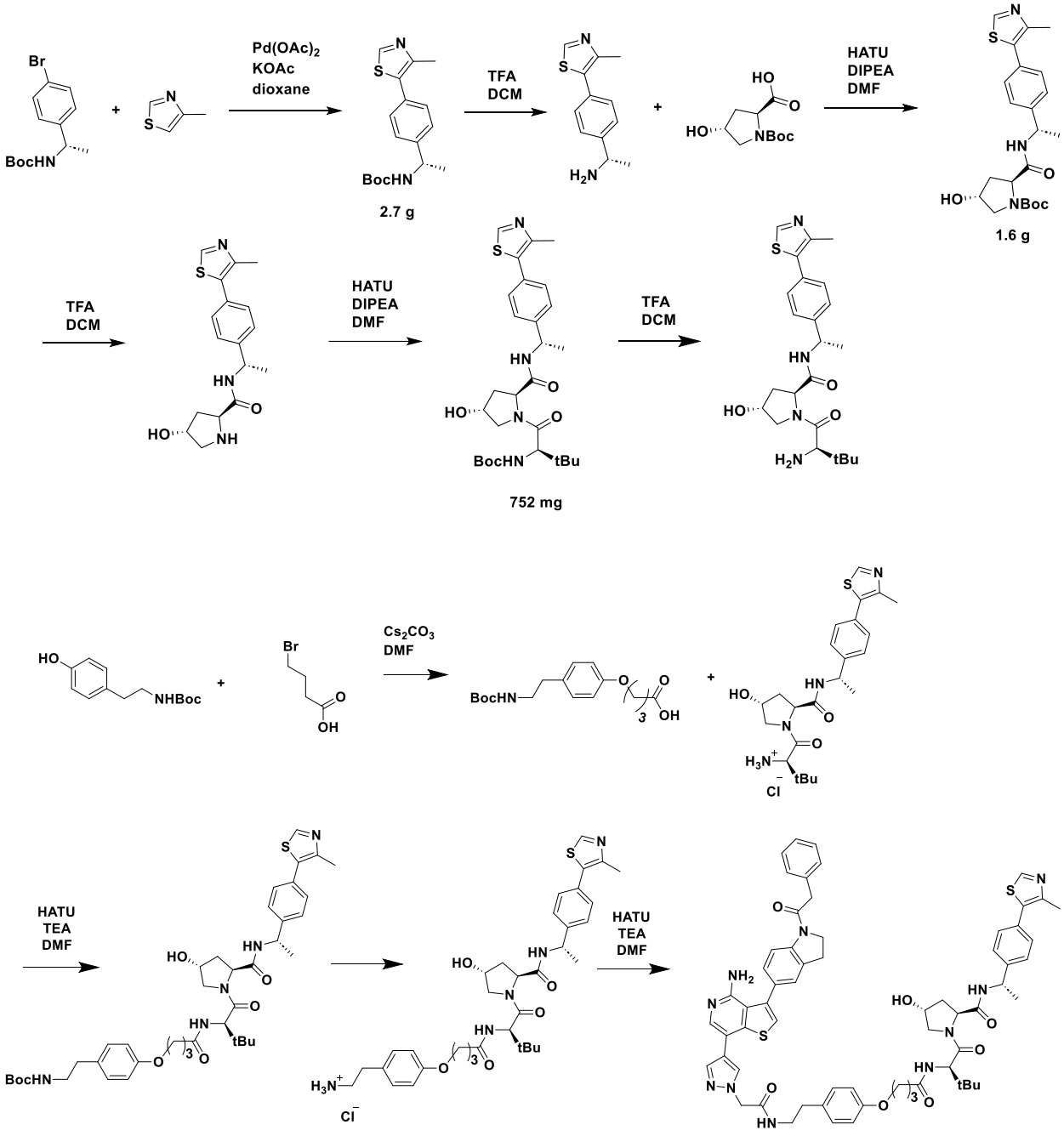

Figure 3.9. Synthetic route of a stable RIPK1 PROTAC

3.6. Biological Study of Stable RIPK1 PROTACs

To determine the activity of AM-DY2, our group member Dr. Zhongrui Zhang performed in vitro experiments where cells were treated with AM-DY2 at various concentrations, spanning from 1 nM to 10 μM (**Figure 3.10 (A)**). The immunoblot analysis indicates that incorporating an amide bond preserved the degradation efficiency observed with DY2. Importantly, even at the highest tested concentration, AM-DY2 did not display any notable hook effect, indicating its stability and efficacy across a broad concentration range. Our results also revealed that AM-DY2 has a half-maximal degradation concentration (DC_{50}) of 14.5 nM, indicating strong efficacy at relatively low concentrations. Furthermore, AM-DY2 achieved a maximum degradation percentage (Dmax) of 96% (**Figure 3.10 (B)**).

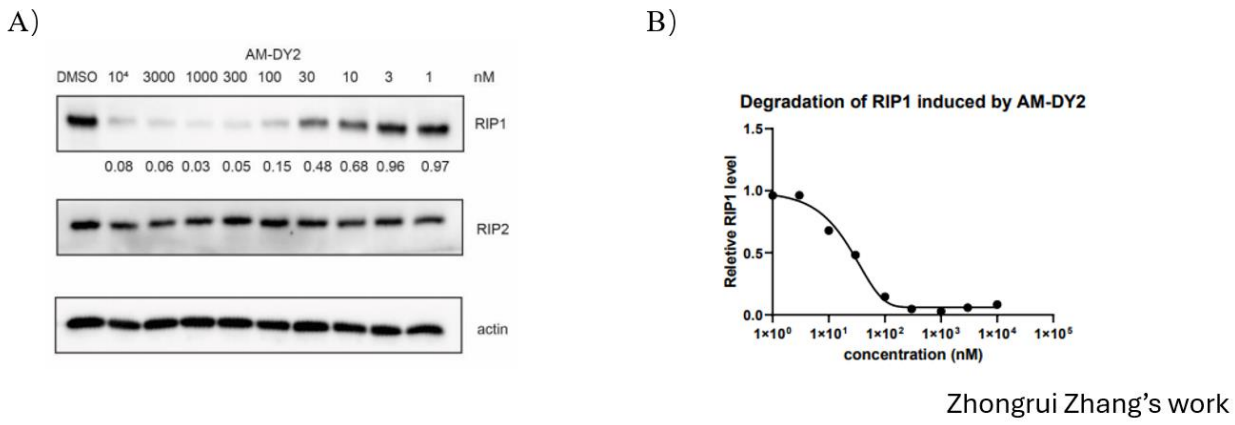

Figure 3.10. Western blot analysis of AM-DY2 degrading RIP1.

To elucidate the mechanism of action of our PROTAC AM-DY2, we conducted time-course experiments in NOMO-1 cells. Immunoblot results indicated that at a concentration of 100 nM, AM-DY2 initiated the degradation of RIPK1 after approximately 2 h (**Figure 3.11**).

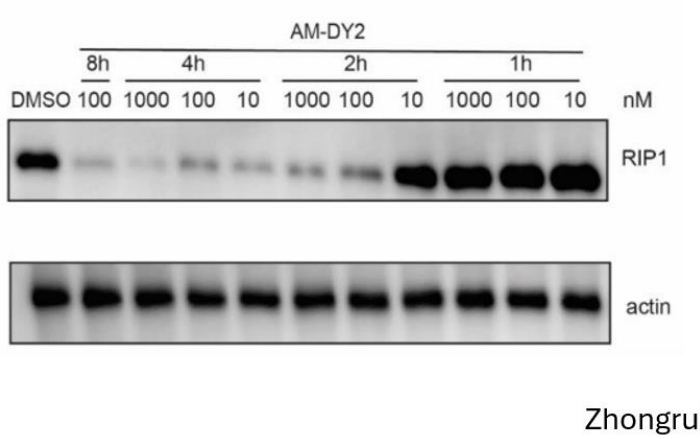

Figure 3.11. Time-course study of AM-DY2 in NOMO1 cells.

To confirm that RIPK1 degradation is mediated through hijacking the ubiquitin-proteasome system, we co-treated cells with the degrader and the pathway competitors, such as RIPK1 ligand C9 (GSK074) and VHL ligand (**Figure 3.12**). Both compounds reduced the degradation of RIPK1, indicating that the degrader's binding to both RIPK1 and the VHL E3 ligase is essential for inducing RIPK1 degradation. Additionally, the degradation of RIPK1 was attenuated by proteasome and NEDDylation inhibitors, further supporting that the RIPK1 degradation is dependent on the proteasome and E3 ligase activity.

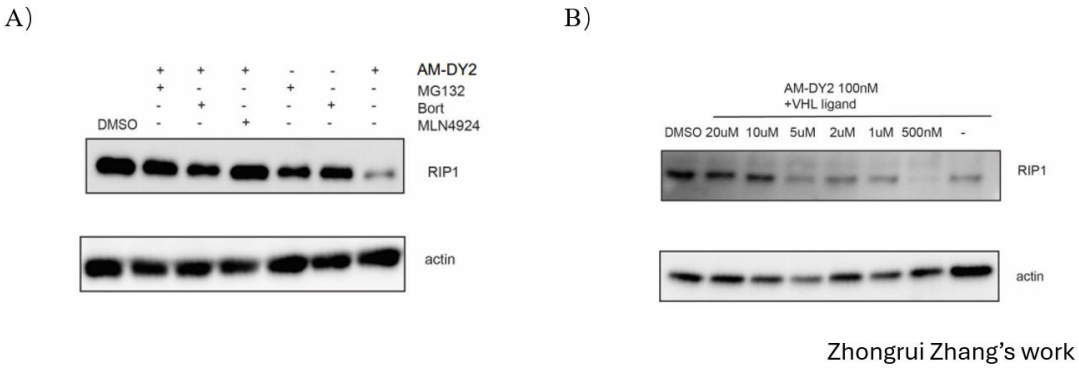

Figure 3.12. Mechanistic study of AM-DY2.

3.7. Design and Synthesis of the New Library of RIPK PROTACs

Since our original goal was to develop degraders for RIP3, we chose GSK 843 as a new warhead for RIP3. GSK 843 was reported as a highly selective inhibitor for RIP3. Based on our modeling studies, the five-membered pyrazole ring is solvent-exposed. To exploit this feature, we introduced a hydrazide group to the nitrogen of the pyrazole ring. This modification was intended to enhance the compound's potential for forming further conjugates with other moieties.

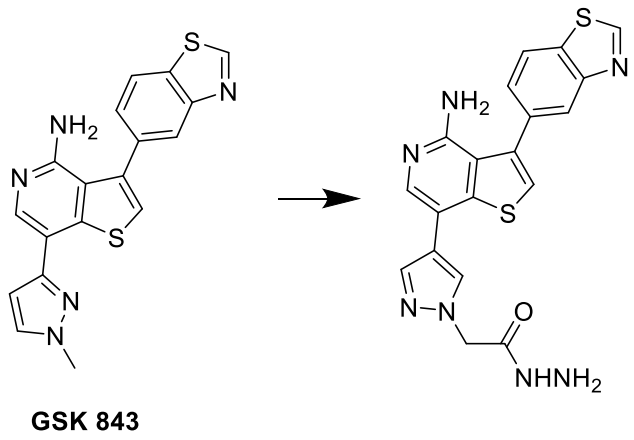

GSK 843

Figure 3.13. Selective ligands for RIPK3.

I synthesized a RIPK3 ligand (**Figure 3.14**) and subsequently linked it with conventional E3 ligands of VHL and CRBN to create a small library of 24 compounds (**Figure 3.15**). These compounds featured variable-length alkyl or PEG linkers, designed to optimize the spatial arrangement and enhance the efficacy of the resulting degraders.

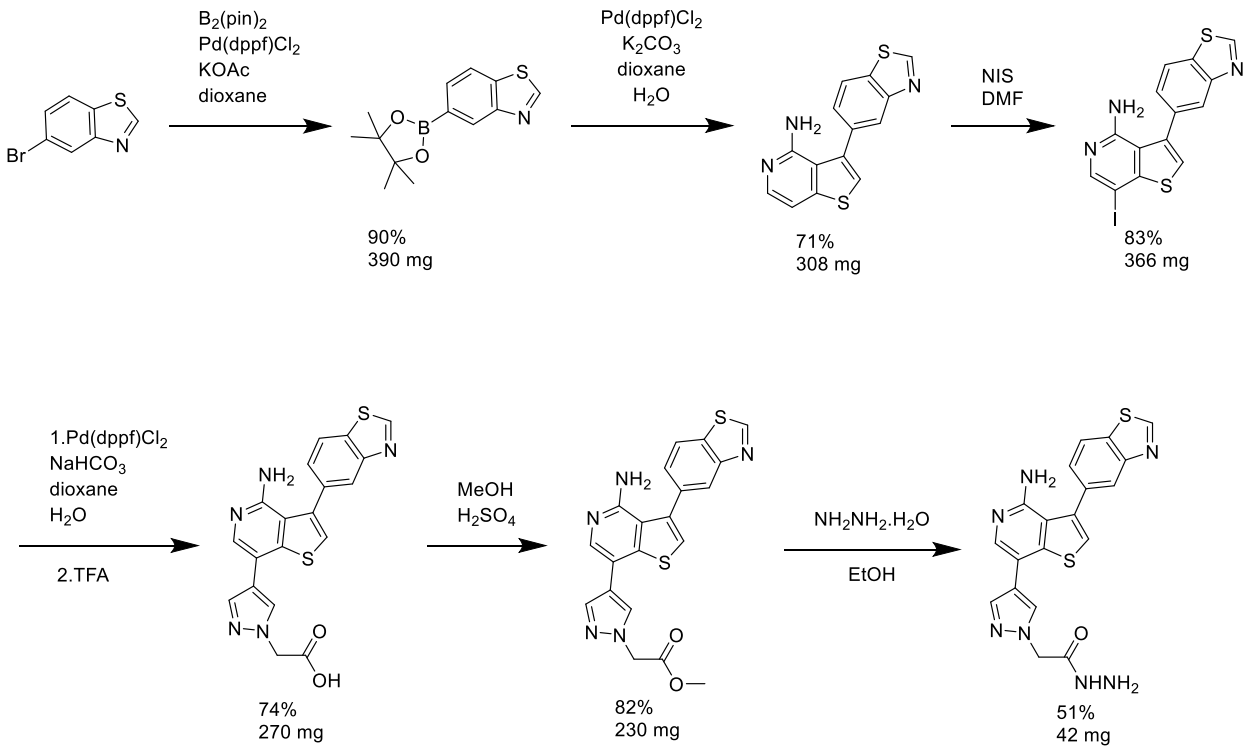

Figure 3.14. Synthetic route for ligand of RIP3.

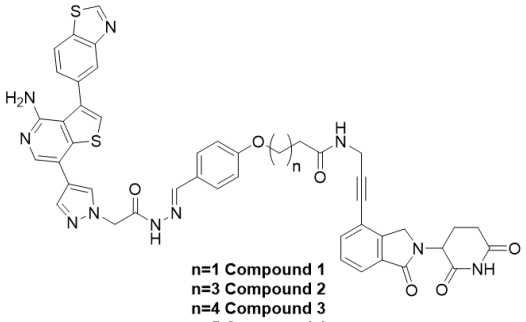

n=1 Compound 1
n=3 Compound 2
n=4 Compound 3
n=5 Compound 4
n=6 Compound 5
n=7 Compound 6

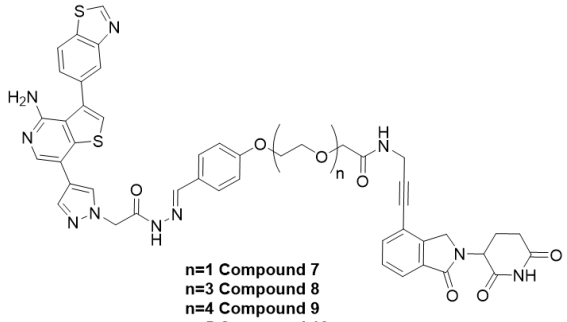

n=1 Compound 7
n=3 Compound 8
n=4 Compound 9
n=5 Compound 10
n=6 Compound 11
n=7 Compound 12

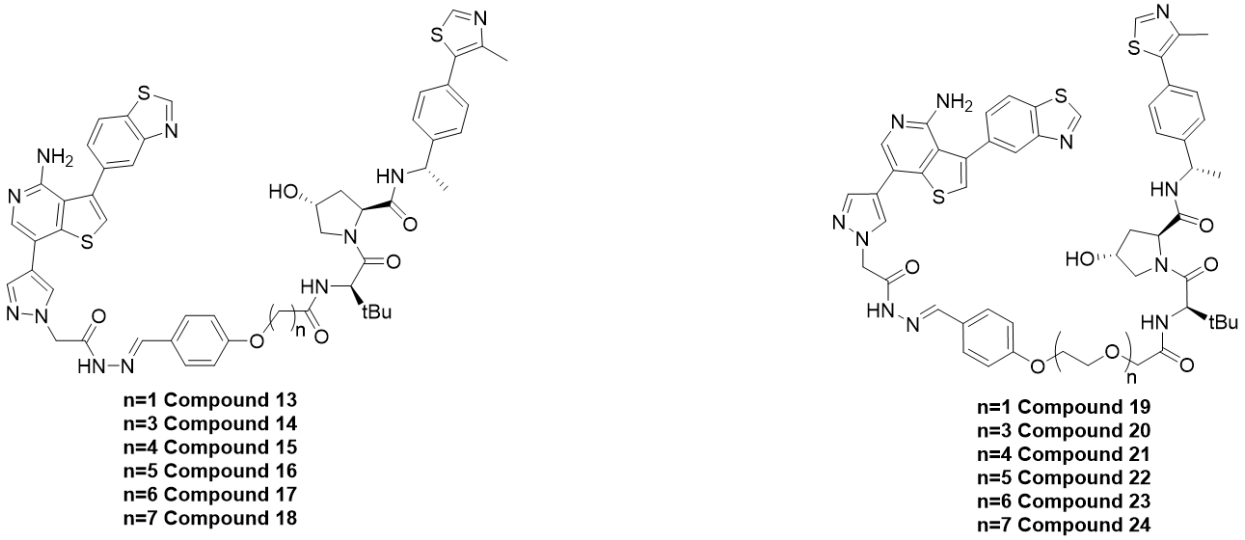

Figure 3.15. Library of RIP3 PROTACs.

3.8. Biological Study of the Library of RIPK3 PROTACs

Next, we conducted Western blot assays on cells treated with the synthesized compounds. We treated the NOMO-1 cells with 0.1 and 1 µM of compounds 1 to 24 (**Figure 3.16**). After 4 hours, cells were lysed for SDS-PAGE and immunoblot. Unfortunately, we didn't observe any degradation of RIPK3 and RIPK1.

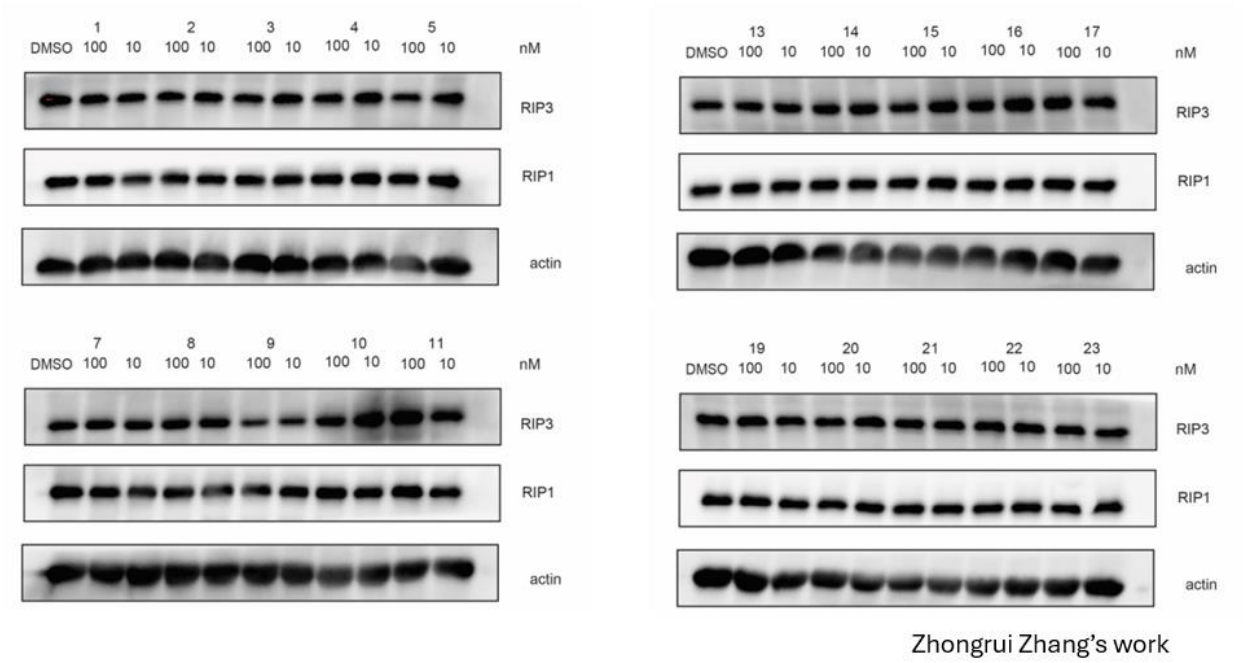

Figure 3.16. Biological study of RIP3 PROTACs

3.9. Discussion and Perspectives

Building upon our Rapid-TAC methodology, we have successfully developed a novel PROTAC molecule targeting RIP1 kinase. This was accomplished by linking a VHL ligand to the RIPK1/RIPK3 inhibitor GSK-074. Initial structure-activity relationship (SAR) explorations led to the identification of a potent degrader, DY-2, in the first stage. In the subsequent stage, we synthesized a more stable analogue, AM-DY2, and confirmed its biological activity.

We also demonstrate that it is possible to selectively degrade RIP1 without affecting RIP2 levels, underscoring its specificity. Mechanistic studies revealed that AM-DY2 induces the proteasomal degradation of RIP1, with the degradation effect initiating as early as two hours post-treatment. This rapid action, compared to siRNA-mediated knockdown, establishes our PROTAC as a powerful tool for probing RIP1 function.

Our PROTAC molecule presents an alternative strategy for temporarily knocking down/out RIP1, with RIP1 levels gradually recovering upon removal of the PROTAC. The rapid degradation may not allow cells sufficient time to compensate for RIP1 loss, potentially offering new opportunities for RIP1-related research and therapeutic applications.

3.10. Experimental Sections

General Information

Unless otherwise stated, all commercial reagents were used as received. Reactions were conducted in dry glassware using anhydrous solvents (pass through activated alumina columns). Unless stated otherwise, reactions were performed at room temperature (rt). Thin-layer chromatography (TLC) was conducted on plates (EMD Chemical Inc. 60, F254) and visualized using a combination of UV, sulfuric acid, and ceric ammonium molybdate staining. Flash column chromatography was performed with silica gel (Silicycle, 40-63 μm). Infrared spectra (IR) were obtained on a Bruker Equinox 55 Spectrophotometer. Optical rotations were recorded on Perkin-Elmer 241 polarimeter. ^{1}H and ^{13}C nuclear magnetic resonance spectra (NMR) were obtained on a Brooker 400 MHz. Chemical shifts were reported in parts per million (ppm), and the residual solvent peak was used as an internal reference: proton (chloroform δ 7.26), carbon (chloroform δ 77.16) or tetramethylsilane (TMS δ 0.00) was used as a reference. Multiplicity was indicated as follows: s (singlet), d (doublet), t (triplet), m (multiplet), dd (doublet of doublet), td (triplet of doublet), bs (broad singlet). Coupling constants (*J*) were reported in Hertz (Hz). All high-resolution mass spectra were performed by Analytical Instrument Center at the School of Pharmacy (UW-Madison) on an Electron Spray Injection (ESI) mass spectrometer.

Experimental Procedures

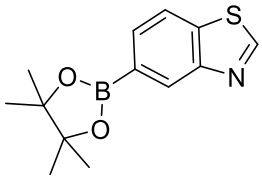

5-bromobenzo[b]thiophene (330 mg, 1.5 mmol, 1.00 equiv.), $B_2(pin)_2$ (589 mg, 2.25 mmol, 1.50 eq.), Pd(dppf)Cl_2 (56 mg, 5 mol%) and KOAc (442 mg, 4.50 mmol, 3.00 eq.) were dissolved in 5 mL dioxane. The resulting mixture was stirred at 95 ℃ under inert atmosphere for 2 h. Then the solvent was removed under reduced pressure. The mixture was further purified with Hexane/EA (7:1) to afford the desired product. (354 mg, 88%) ^{1}H NMR (400 MHz, $CDCl_3$) δ 8.96 (d, J = 1.9 Hz, 1H), 8.58 (s, 1H), 7.94 (dd, J = 8.1, 1.8 Hz, 1H), 7.83 (dd, J = 8.0, 2.1 Hz, 1H), 1.35 (s, 12H). ^{13}C NMR (100 MHz, $CDCl_3$) δ 153.61, 152.97, 136.76, 131.13, 130.34, 121.29, 84.06, 83.48, 25.03.

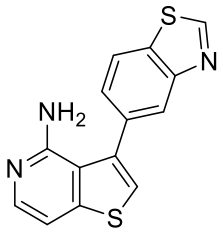

5-(4,4,5,5-tetramethyl-1,3,2-dioxaborolan-2-yl)benzo[d]thiazole (104 mg, 0.398 mmol, 1.00 equiv.), 3-bromothieno[3,2-c]pyridin-4-amine (91 mg, 0.398 mmol, 1.00 eq.), Pd(dppf) Cl_2 (14 mg, 5 mol%), K_2CO_3 (192 mg, 3.5 eq.) were dissolved in 1.5 mL dioxane and 0.75 mL H_2O. The resulting mixture was stirred at 95 ℃ under nitrogen for 2 h, then cooled to room temperature. The reaction mixture was poured into ice water (10 mL), and then extracted with EA (10 mL) three

times. The combined extracts were washed successively saturated aqueous sodium chloride, dried over Na_2SO_4, and evaporated on a rotary evaporator. The mixture was further purified with Hexane/EA (4:1) to afford the desired product. (90 mg, 81%)

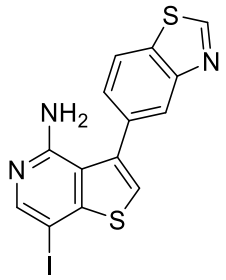

To a solution of 3-(benzo[d]thiazol-5-yl)thieno[3,2-c]pyridin-4-amine (115 mg, 0.4 mmol) in DMF (4 mL) was added NIS (110 mg, 0.5 mmol, 1.2 eq.). The resulting mixture was stirred at room temperature overnight. The reaction mixture was poured into ice water. The precipitate was filtered and washed with water 3 times. The precipitate was used directly in the next step without further purification. (152 mg, 92%)

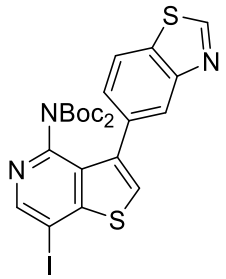

3-(benzo[d]thiazol-5-yl)-7-iodothieno[3,2-c]pyridin-4-amine (100 mg, 0.254 mmol, 1.00 eq.), Boc_2O (144 mg, 0.15 mL, 2.70 eq.), Et_3N (74 mg, 0.1 mL), DMAP (3 mg, 0.1 eq.) were dissolved in 1.5 mL DCM. The resulting mixture was stirred at room temperature overnight. Then the solvent was removed under reduced pressure. The mixture was further purified with Hexane/EA (10:1) to afford the desired product. ^{1}H NMR (400 MHz, $CDCl_3$) δ 9.06 (s, 1H), 8.65 (s, 1H), 8.19 (d, *J* = 1.6 Hz, 1H), 7.96 (d, *J* = 8.3 Hz, 1H), 7.54 (dd, *J* = 8.3, 1.7 Hz, 1H), 7.51 (s, 1H), 1.23 (s, 18H).

^{13}C NMR (101 MHz, $CDCl_3$) δ 171.10, 156.46, 154.51, 153.25, 150.87, 148.47, 146.91, 137.97, 133.99, 133.51, 130.65, 127.06, 126.84, 124.25, 121.31, 86.76, 83.13, 60.38, 27.80.

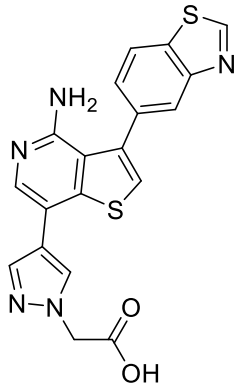

A mixture of 3-(benzo[d]thiazol-5-yl)-7-iodothieno[3,2-c]pyridin-4-amine (120 mg, 0.2 mmol, 1.0 eq.), methyl 2-(4-(4,4,5,5-tetramethyl-1,3,2-dioxaborolan-2-yl)-1H-pyrazol-1-yl)acetate (44 mg, 0.22 mmol, 1.1 eq.), $Pd(dppf)Cl_2$ (20 mg, 5 mol%), and $NaHCO_3$ (48 mg, 0.6 mmol, 3.0 equiv.) was dissolved in 3 mL of dioxane and 1.5 mL of H_2O. The resulting mixture was stirred at 95 °C under a nitrogen atmosphere for 12 hours, then allowed to cool to room temperature. The reaction mixture was then acidified by the addition of TFA, and the solvent was removed under reduced pressure. The crude product was further purified using a DCM/Methanol/TFA (100:5:1) solvent system to afford the desired product.

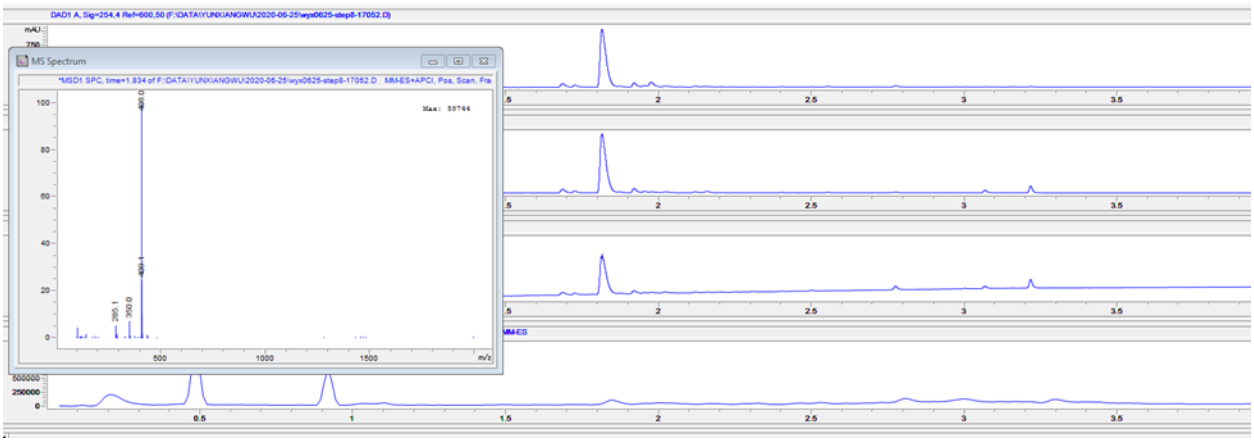

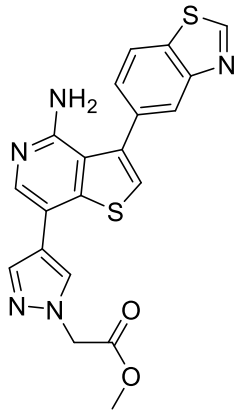

To a solution of 2-(4-(4-amino-3-(benzo[d]thiazol-5-yl)thieno[3,2-c]pyridin-7-yl)-1H-pyrazol-1-yl)acetic acid (42 mg, 0.1 mmol, 1.0 eq.) in MeOH was added H_2SO_4 (20 μL). The resulting mixture was stirred at 65 ℃ for 2 h. Then the mixture was quenched by Et_3N. The solvent was removed under reduced pressure. The mixture was further purified with DCM/Methanol (20:1) to afford desired product. (35 mg, 70%) ^{1}H NMR (400 MHz, $CDCl_3$) δ 9.06 (s, 1H), 8.56 (s, 1H), 8.22 (d, *J* = 1.6 Hz, 1H), 8.09 (s, 1H), 8.04 (s, 1H), 7.97 (d, *J* = 8.3 Hz, 1H), 7.59 (dd, *J* = 8.3, 1.7 Hz, 1H), 7.47 (s, 1H), 5.08 (s, 2H), 3.85 (s, 3H).

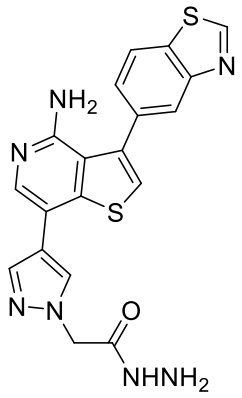

Methyl 2-(4-(4-amino-3-(benzo[d]thiazol-5-yl)thieno[3,2-c]pyridin-7-yl)-1H-pyrazol-1-yl)acetate (21 mg, 0.05 mmol, 1.0 eq.) and $NH_2NH_2 \cdot H_2O$ (10 mg, 20.0 eq.) were dissolved in 3 mL EtOH. The resulting mixture was stirred at 65 ℃ overnight. Then the solvent was removed under reduced pressure. The mixture was further purified with DCM/Methanol (10:1) to afford desired product. (8 mg) ^{1}H NMR (400 MHz, $CDCl_3$) δ 9.13 (d, *J* = 2.6 Hz, 1H), 8.28 (s, 1H), 8.10 (dd, *J* = 8.2, 3.1 Hz, 1H), 8.08 – 7.98 (m, 2H), 7.93 (d, *J* = 9.2 Hz, 1H), 7.59 (d, *J* = 8.3 Hz, 1H), 7.29 (d, *J* = 1.8 Hz, 1H), 5.03 (s, 2H).

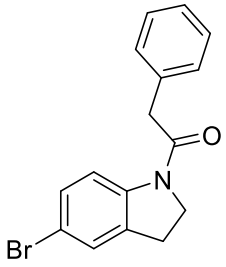

5-bromoindoline (540 mg, 2.72 mmol, 1.0 eq.), Et_3N (409 mg, 4 mmol, 1.5 eq.) and DMAP (40 mg, 0.13 mmol, 0.05 eq.) were dissolved in 5 mL DCM. Then 2-phenylacetyl chloride (0.42 mL, 1.1 eq.) was added to the mixture. The resulting mixture was stirred at room temperature for 2 h. Then the solvent was removed under reduced pressure. The mixture was further purified with Hexane/EA (7:1) to afford the desired product. (772 mg, 89%)

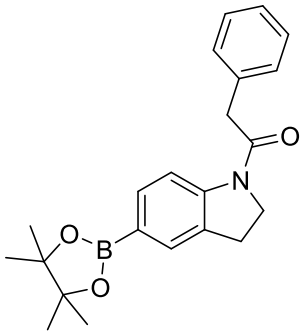

1-(5-bromoindolin-1-yl)-2-phenylethan-1-one (312 mg, 0.7 mmol, 1.00 eq.), $B_2(pin)_2$ (290 mg, 1.1 mmol, 1.5 eq.), Pd(dppf)Cl_2 (56 mg, 5 mol%) and KOAc (221 mg, 2.5 mmol, 3.0 eq.) were dissolved in 5 mL dioxane. The resulting mixture was stirred at 95 ℃ under inert atmosphere for 2 h. Then the solvent was removed under reduced pressure. The mixture was further purified with Hexane/EA (7:1) to afford the desired product. (210 mg, 82%)

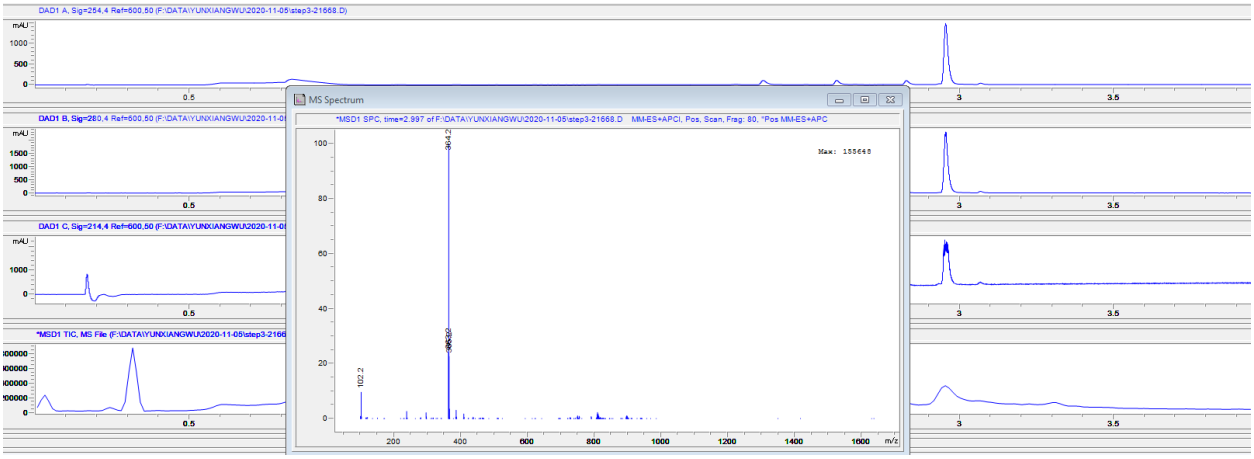

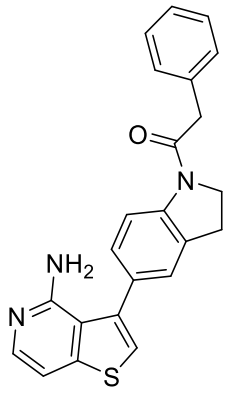

2-phenyl-1-(5-(4,4,5,5-tetramethyl-1,3,2-dioxaborolan-2-yl)indolin-1-yl)ethan-1-one (88 mg, 0.398 mmol, 1.0 eq.), 3-bromothieno[3,2-c]pyridin-4-amine (91 mg, 0.398 mmol, 1.0 eq.), Pd(dppf)Cl_2 (14 mg, 5 mol%) and K_2CO_3 (192 mg, 3.5 eq.) were dissolved in 1.5 mL dioxane and 0.75 mL H_2O. The resulting mixture was stirred at 95 ℃ under nitrogen for 2 h, then cooled to room temperature. The reaction mixture was poured into ice water (10 mL), and then extracted

with EA (10 mL) three times. The combined extracts were washed successively saturated aqueous sodium chloride, dried over Na_2SO_4, and evaporated on a rotary evaporator. The mixture was further purified with Hexane/EA (4:1) to afford the desired product. (66 mg, 82%)

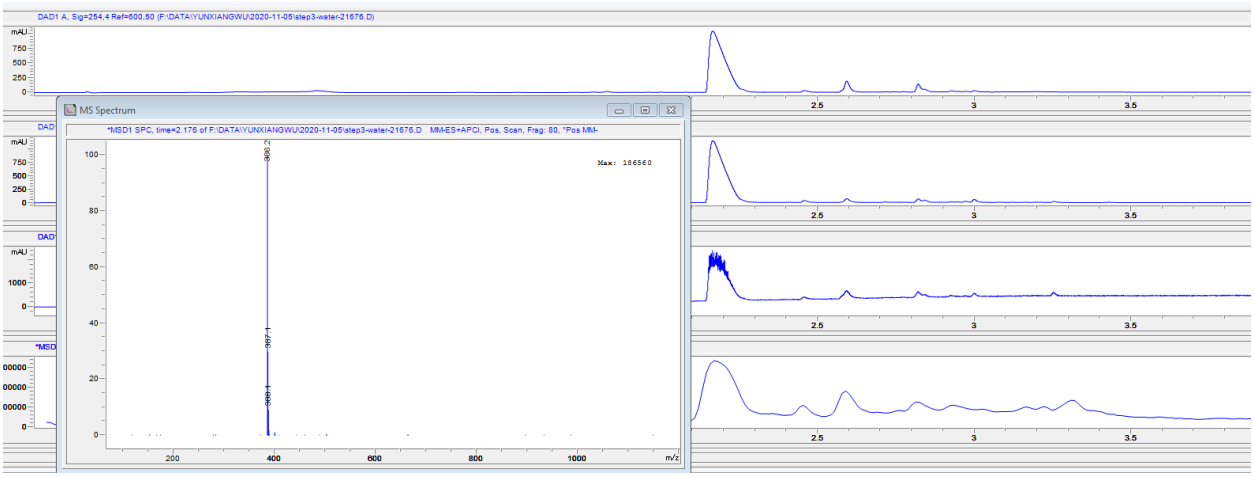

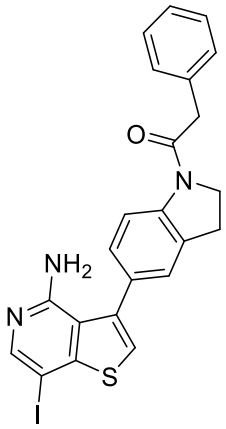

To a solution of 1-(5-(4-aminothieno[3,2-c]pyridin-3-yl)indolin-1-yl)-2-phenylethan-1-one (154 mg, 0.4 mmol) in DMF (4 mL) was added NIS (110 mg, 0.5 mmol, 1.2 eq.). The resulting mixture was stirred at room temperature overnight. The reaction mixture was poured into ice water. The precipitate was filtered and washed with water 3 times. The precipitate was used directly in the next step without further purification. (152 mg, 92%)

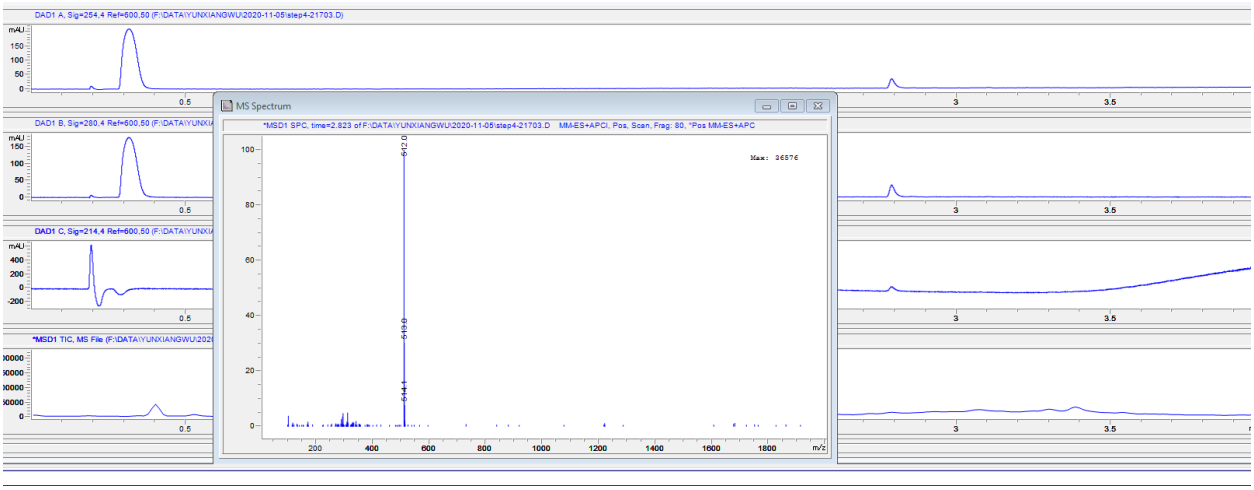

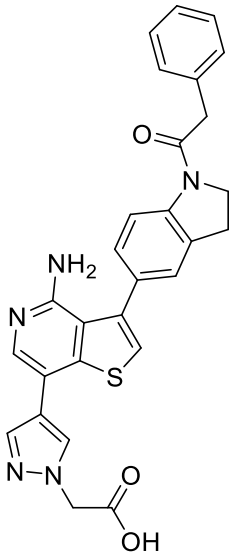

A mixture of 1-(5-(4-amino-7-iodothieno[3,2-c]pyridin-3-yl)indolin-1-yl)-2-phenylethan-1-one (115 mg, 0.23 mmol, 1.0 eq.), methyl 2-(4-(4,4,5,5-tetramethyl-1,3,2-dioxaborolan-2-yl)-1H-pyrazol-1-yl)acetate (44 mg, 0.22 mmol, 1.1 eq.), Pd(dppf)Cl_2 (20 mg, 5 mol%), and $NaHCO_3$ (48 mg, 0.6 mmol, 3.0 equiv.) was dissolved in 3 mL of dioxane and 1.5 mL of H_2O. The resulting mixture was stirred at 95 °C under a nitrogen atmosphere for 12 h, then allowed to cool to room temperature. The reaction mixture was then acidified by the addition of TFA, and the solvent was removed under reduced pressure. The crude product was further purified using a DCM/Methanol/TFA (100:5:1) solvent system to afford the desired product. (80 mg, 64%)

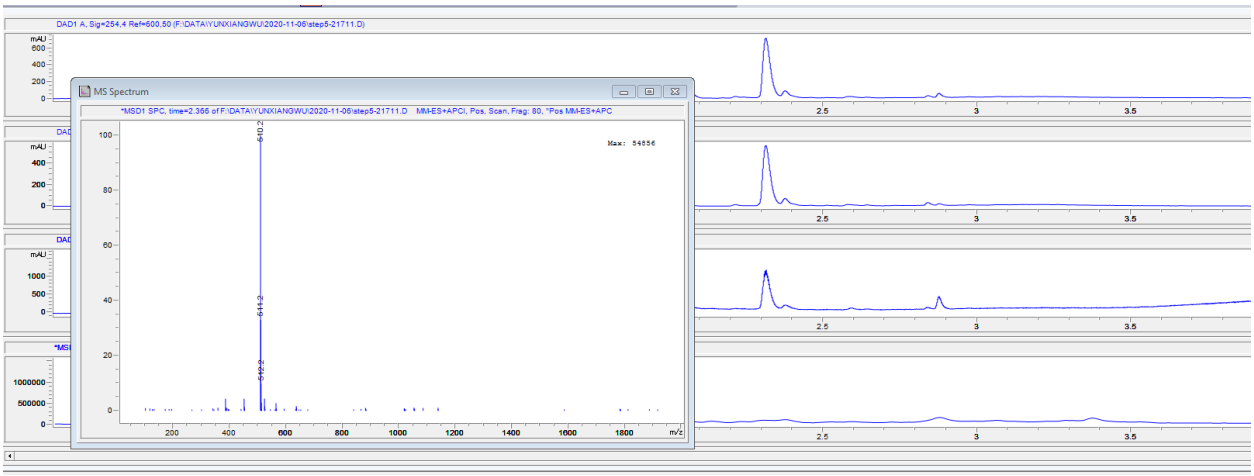

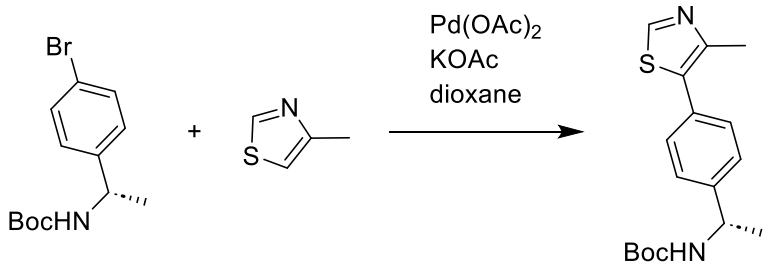

A mixture of crude tert-butyl (S)-(1-(4-bromophenyl)ethyl)carbamate (6.2 g, 18 mmol), 4-methylthiazole (5.4 g, 42 mmol), and KOAc (4.1 g, 42 mmol) in DMAc (42 mL) was degassed with nitrogen for 20 min. To this solution was added $Pd(OAc)_2$ (0.1 g, 0.5mmol). The mixture was degassed with nitrogen for another 10 min and then heated to 130 °C. The mixture was stirred at 130 °C for 4 h. The reaction mixture was concentrated. EA (80 mL) and water (30 mL) were added to the residue and filtered through a pad of diatomite. The diatomite pad was rinsed with EA (20 mL). The filtrate was separated, and the EA phase was washed with water (20 mL) twice and brine (20 mL) twice. The EA phase was concentrated. DCM (20 mL) was added to the residue and concentrated (repeat once). The resulting residue was used directly for the next step.

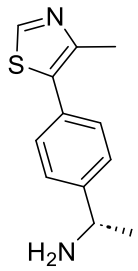

To the solution, HCl (16 mL, 4 M in dioxane) was added dropwise at room temperature for over 30 min. A solid precipitated out during addition. The slurry was stirred at room temperature overnight. The mixture was filtered and dried under vacuum to get a 8.3 g dark yellow solid.

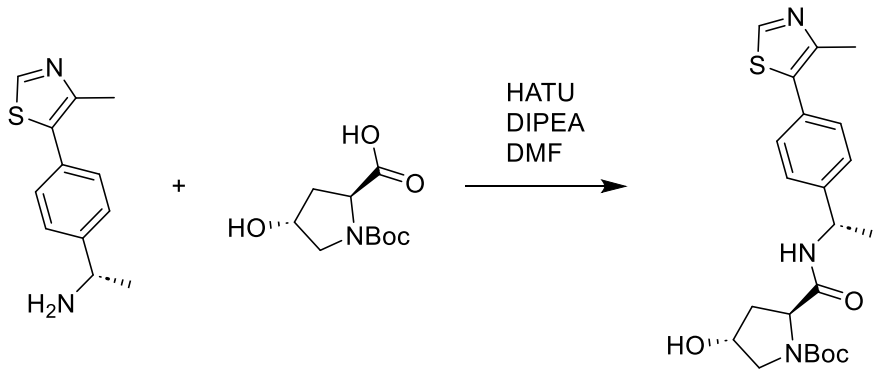

(2S,4R)-1-(tert-butoxycarbonyl)-4-hydroxypyrrolidine-2-carboxylic acid (6.7 g, 26 mmol) was dissolved in DMF (30 mL) and DCM (30 mL). The solution was cooled to 0 °C, and TEA (10 mL, 72 mmol) was added. Then, (S)-1-(4-(4-methylthiazol-5-yl)phenyl)ethan-1-amine (6.1 g, 2.6 mmol) and HATU (11.9 g, 31.2 mmol) were added. The mixture was stirred at 0 °C for 1 h and then stirred at room temperature overnight. Most of the solvent was removed under vacuum. To the residue was added saturated $NaHCO_3$ solution (0.1 L) and then extracted with EA (80 mL) once and (40 mL) twice. The organic phase was combined and washed with $NaHCO_3$ solution (4.5 mL) once and brine (45 mL) twice. The organic phase was dried over sodium sulfate, filtered, and concentrated under vacuum to give a 12.7 g crude product

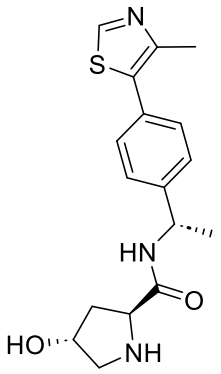

Bocprotected intermediate (125 g, 300 mmol) was dissolved in dioxane (40 mL) and EA (10 mL). Then, HCl (55 mL, 4 M in dioxane) was added dropwise at room temperature over 1 h. The mixture was stirred at room temperature overnight. The yellow solid was filtered, washed with EA, and dried under vacuum to give a 10.5 g crude product.

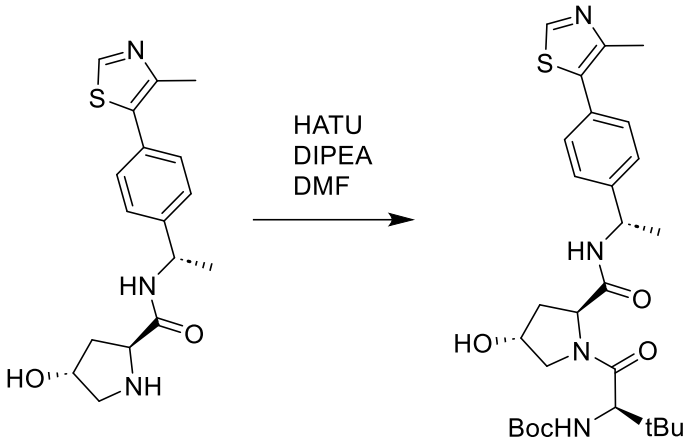

Carboxylic acid (4.6 g, 20 mmol) was dissolved in DCM (53 ml). The solution was cooled to 0 °C, and DIPEA (8.7 mL, 50 mmol) was added, followed by HATU (8.9 g, 23.4 mmol). The mixture was stirred at room temperature for 2 h, then cooled to 0 °C, and amine (5.3 g, 12.3 mmol) was added slowly. The reaction mixture was allowed to warm to room temperature and stirred overnight. DCM (53 mL) was added to the reaction mixture. Then, the reaction mixture was transferred to a separation funnel and washed with 10% citric acid (30 mL) twice, saturated

$NaHCO_3$ (30 mL) twice, water (30 mL) twice, and brine (30 mL) once. The organic phase was concentrated under vacuum to about 600 mL and used for the next step directly.

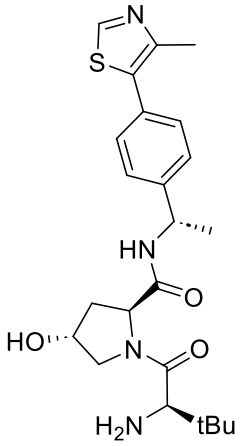

DCM was added to the above residue to reach a final volume of 40 mL. To the solution was added HCl (16 mL, 4 M in dioxane) dropwise at room temperature for over 30 min. A solid precipitated out during addition. The slurry was stirred at room temperature overnight. The mixture was filtered and dried under vacuum to get a 4.2 g dark yellow solid

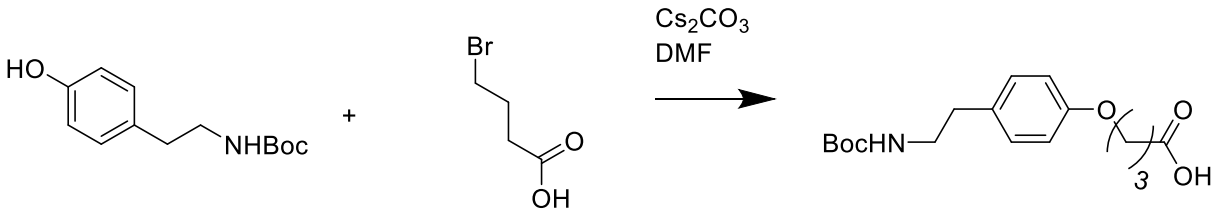

To a solution of tert-butyl (4-hydroxyphenethyl)carbamate (224 mg, 1mmol) in anhydrous DMF were added 4-bromobutanoic acid (167 mg, 1.2 mmol, 1.2 equiv), cesium carbonate (646 mg, 2 mmol, 2.0equiv). Then the mixture was stirred for 4 h at 55 °C. When the reaction was completed, 10 ml water was slowly added to the mixture and acidified by HCl (6 mL, 4 M in dioxane). The resulting solution was then extracted with ethyl acetate (20 mL*3). The mixture was concentrated

in vacuo. The residue was purified by flash column chromatography on silica gel to afford the desired product.

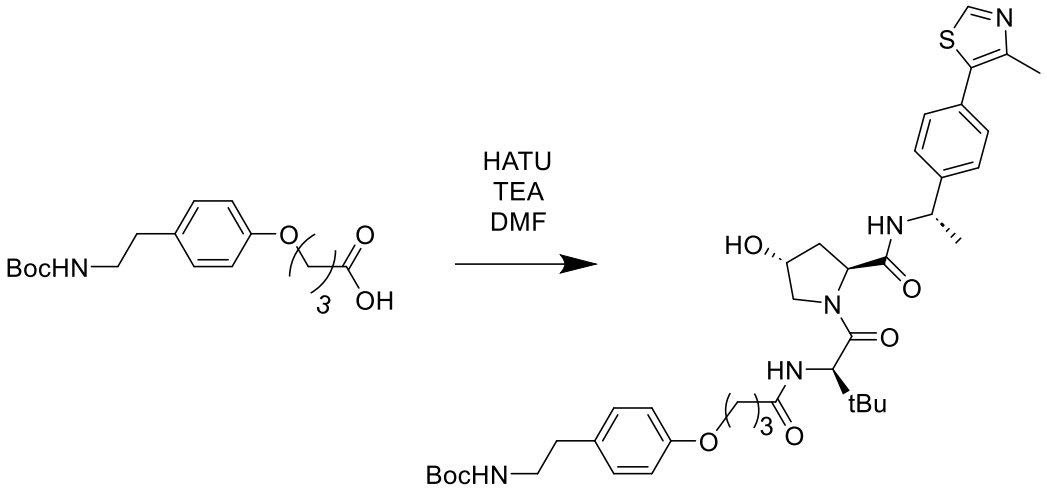

To a solution of VHL ligand (444 mg, 1 mmol), acetic acid (309 mg, 1 mmol) in DMF (1.8 mL) was added DIPEA (0.28 mL, 2 mmol) and HATU (456 mg, 1.2 mmol) successively. The reaction was then stirred at rt overnight and then concentrated under reduced pressure to afford a crude mixture which was purified with DCM/EtOAC to afford the desired product. (311 mg, 42%)

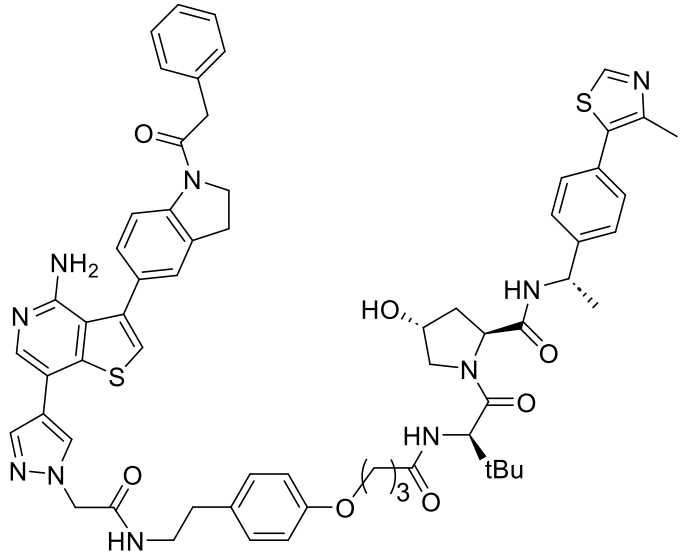

To a solution of VHL ligand (6 mg, 0.01 mmol), 2-(4-(4-amino-3-(1-(2-phenylacetyl) indolin-5-yl) thieno[3,2-c] pyridin-7-yl)-1H-pyrazol-1-yl) acetic acid (6 mg, 0.01 mmol) in DMF (1.8 mL) was added DIPEA(10 μL, 0.02 mmol) and HATU (6 mg, 0.012 mmol) successively. The reaction was then stirred at rt overnight and then concentrated under reduced pressure to afford a crude mixture which was purified with DCM/EtOAC to afford the desired product. (21 mg, 42%)

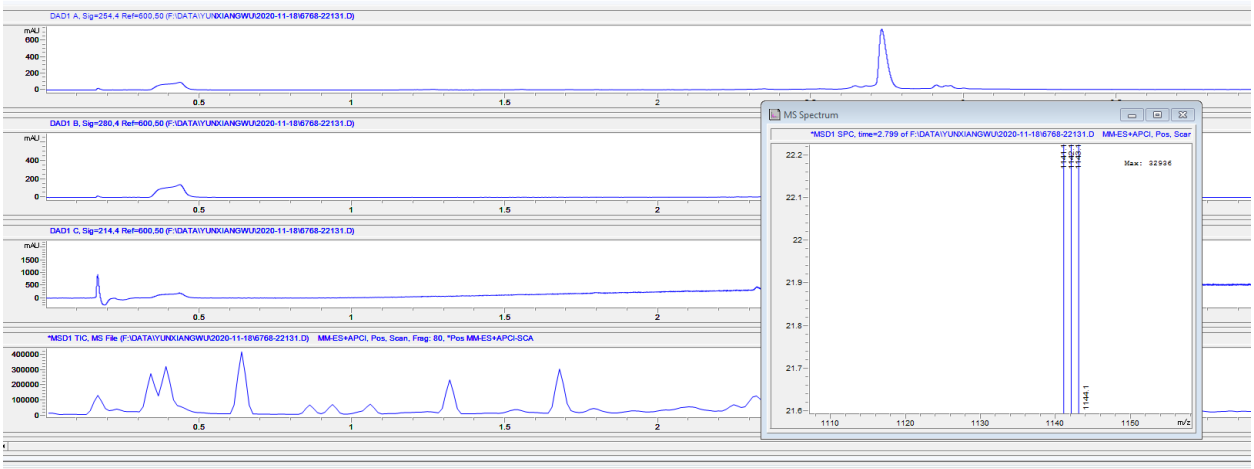

3.11. References

1. (a) Zhang, T.; Zhang, Y.; Cui, M.; Jin, L.; Wang, Y.; Lv, F.; Liu, Y.; Zheng, W.; Shang, H.; Zhang, J.; Zhang, M.; Wu, H.; Guo, J.; Zhang, X.; Hu, X.; Cao, C.-M.; Xiao, R.-P. Camkii is a rip3 substrate mediating ischemia- and oxidative stress-induced myocardial necroptosis. *Nat. Med.* **2016**, 22, 175-182. (b) Newton, K.; Dugger, D. L.; Maltzman, A.; Greve, J. M.; Hedehus, M.; Martin-McNulty, B.; Carano, R. A. D.; Cao, T. C.; van Bruggen, N.; Bernstein, L.; Lee, W. P.; Wu, X.; DeVoss, J.; Zhang, J.; Jeet, S.; Peng, I.; McKenzie, B. S.; Roose-Girma, M.; Caplazi, P.; Diehl, L.; Webster, J. D.; Vucic, D. Ripk3 deficiency or catalytically inactive ripk1 provides greater benefit than mlkl deficiency in mouse models of inflammation and tissue injury. *Cell Death Differ.* **2016**. (c) Lin, J.; Li, H.; Yang, M.; Ren, J.; Huang, Z.; Han, F.; Huang, J.; Ma, J.; Zhang, D.; Zhang, Z.; Wu, J.; Huang, D.; Qiao, M.; Jin, G.; Wu, Q.; Huang, Y.; Du, J.; Han, J. A role of rip3-mediated macrophage necrosis in atherosclerosis development. *Cell Reports* **2013**, 3, 200-210. (d) Wang, Q.; Liu, Z.; Ren, J.; Morgan, S.; Assa, C.; Liu, B**.** Receptor-interacting protein kinase 3 contributes to abdominal aortic aneurysms via smooth muscle cell necrosis and inflammation. *Circ. Res.* **2015**.
2. Mandal, P.; Berger, S. B.; Pillay, S.; Moriwaki, K.; Huang, C.; Guo, H.; Lich, J. D.; Finger, J.; Kasparcova, V.; Votta, B.; Ouellette, M.; King, B. W.; Wisnoski, D.; Lakdawala, A. S.; DeMartino, M. P.; Casillas, L. N.; Haile, P. A.; Sehon, C. A.; Marquis, R. W.; Upton, J.; Daley-Bauer, L. P.; Roback, L.; Ramia, N.; Dovey, C. M.; Carette, J. E.; Chan, F. K.-M.; Bertin, J.; Gough, P. J.; Mocarski, E. S.; Kaiser, W. J. Rip3 induces apoptosis independent of pronecrotic kinase activity. *Mol. Cell* **2014**, 56, 481-495.
3. Luedde, M.; Lutz, M.; Carter, N.; Sosna, J.; Jacoby, C.; Vucur, M.; Gautheron, J.; Roderburg, C.; Borg, N.; Reisinger, F.; Hippe, H.-J.; Linkermann, A.; Wolf, M. J.; Rose-

John, S.; Lüllmann-Rauch, R.; Adam, D.; Flögel, U.; Heikenwalder, M.; Luedde, T.; Frey, **N.** Rip3, a kinase promoting necroptotic cell death, mediates adverse remodelling after myocardial infarction. *Cardiovasc. Res.* 2**014**, 103, 206-216.

4. Zhou, Y.; Xiang, Y.; Liu, S.; Li, C.; Dong, J.; Kong, X.; Ji, X.; Cheng, X.; Zhang, L. RIPK3 signaling and its role in regulated cell death and diseases. *Cell Death Discov.* **2024**, 10, 200.
5. (a) Lai, A. C.; Crews, C. M. Induced protein degradation: an emerging drug discovery paradigm. *Nat. Rev. Drug Discov.* **2017**, 16, 101-114. (b) Salami, J.; Crews, C. M. Waste disposal-An attractive strategy for cancer therapy. *Science* **2017**, 355, 1163-1167. (c) Cromm, P. M.; Crews, C. M. Targeted Protein Degradation: from Chemical Biology to Drug Discovery. *Cell Chem. Biol.* **2017**, 24, 1181-1190. (d) Ottis, P.; Crews, C. M. Proteolysis-Targeting Chimeras: Induced Protein Degradation as a Therapeutic Strategy. *ACS Chem. Biol.* **2017**, 12, 892-898.
6. Garber, K**.** The PROTAC gold rush. *Nat. Biotechnol.* **2022**, 40, 12-16.
7. (a) Roberts, B. L.; Ma, Z.-X.; Gao, A.; Leisten, E. D.; Yin, D.; Xu, W.; Tang, W. Two-stage strategy for development of proteolysis targeting chimeras and its application for estrogen receptor degraders. *ACS Chem. Biol*. **2020**, 15, 1487-1496. (b) Li, J.; Li, C.; Zhang, Z.; Zhang, Z.; Wu, Z.; Liao, J.; Wang, Z.; McReynolds, M.; Xie, H.; Guo, L.; Fan, Q.; Peng, J.; Tang, W. A platform for the rapid synthesis of molecular glues (Rapid-Glue) under miniaturized conditions for direct biological screening. *Eur. J. Med. Chem.* **2023**, 258, 115567. (c) Guo, L.; Zhou, Y.; Nie, X.; Zhang, Z.; Zhang, Z.; Li, C.; Wang, T.; Tang, W. A Platform for the Rapid Synthesis of Proteolysis Targeting Chimeras (Rapid-TAC) under Miniaturized Conditions. *Eur. J. Med. Chem.* **2022**, 236, 114317.

8. Zhou, T.; Wang, Q.; Phan, N.; Ren, J.; Yang, H.; Feldman, C. C.; Feltenberger, J. B.; Ye, Z.; Wildman, S. A.; Tang, W.; Liu, B. Identification of a novel class of RIP1/RIP3 dual inhibitors that impede cell death and inflammation in mouse abdominal aortic aneurysm models. *Cell Death Dis.* **2019**, 10, 226.

Chapter 4

Design and Synthesis of Novel MDM2 PROTACs with Covalent Ligands

4.1. Introduction

Murine Double Minute 2 (MDM2) is a pivotal negative regulator of the tumor suppressor protein p53[1], which plays a critical role in safeguarding cellular integrity by initiating cell cycle arrest and apoptosis in response to stress signals like DNA damage. MDM2 exerts its influence by binding to p53, inhibiting its transcriptional activity, and promoting its ubiquitination and subsequent degradation through the proteasome pathway[2] (**Figure 4.1**). The overexpression of MDM2, frequently observed in various cancers, leads to the suppression of p53 activity, allowing cancer cells to evade apoptosis and proliferate uncontrollably[3]. Given its central role in p53 regulation, MDM2 has become a prominent target in anti-cancer drug development.

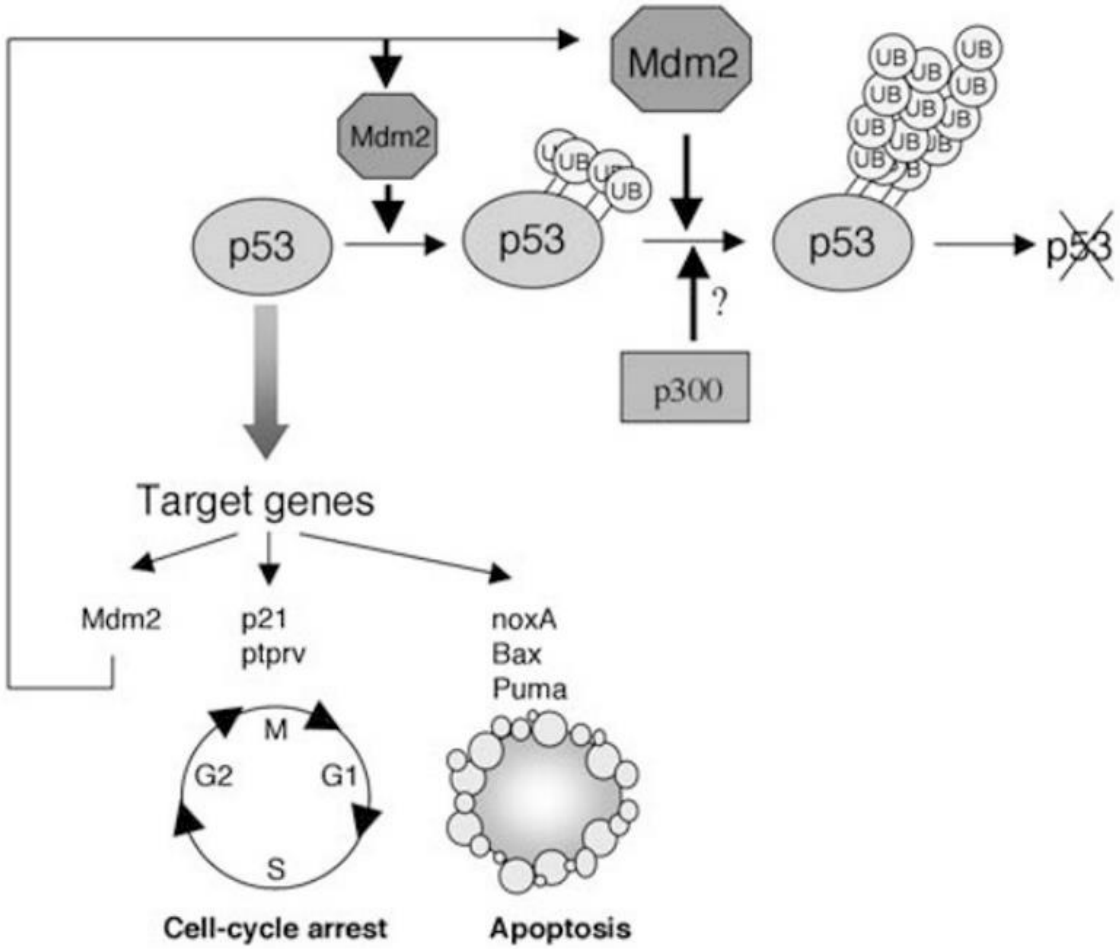

Figure 4.1. MDM2-p53 pathway[4]

Traditional approaches to targeting MDM2 have focused on small molecule inhibitors that disrupt the MDM2-p53 interaction[5] (**Figure 4.2**), thereby stabilizing p53 and reactivating its tumor suppressor functions. However, these inhibitors have several limitations, including the transient nature of inhibition and upregulation of MDM2 level by feedback loop, potentially reducing therapeutic efficacy. Moreover, the accumulation of MDM2 protein in cells may continue to present oncogenic risks, even when its interaction with p53 is inhibited[5d].

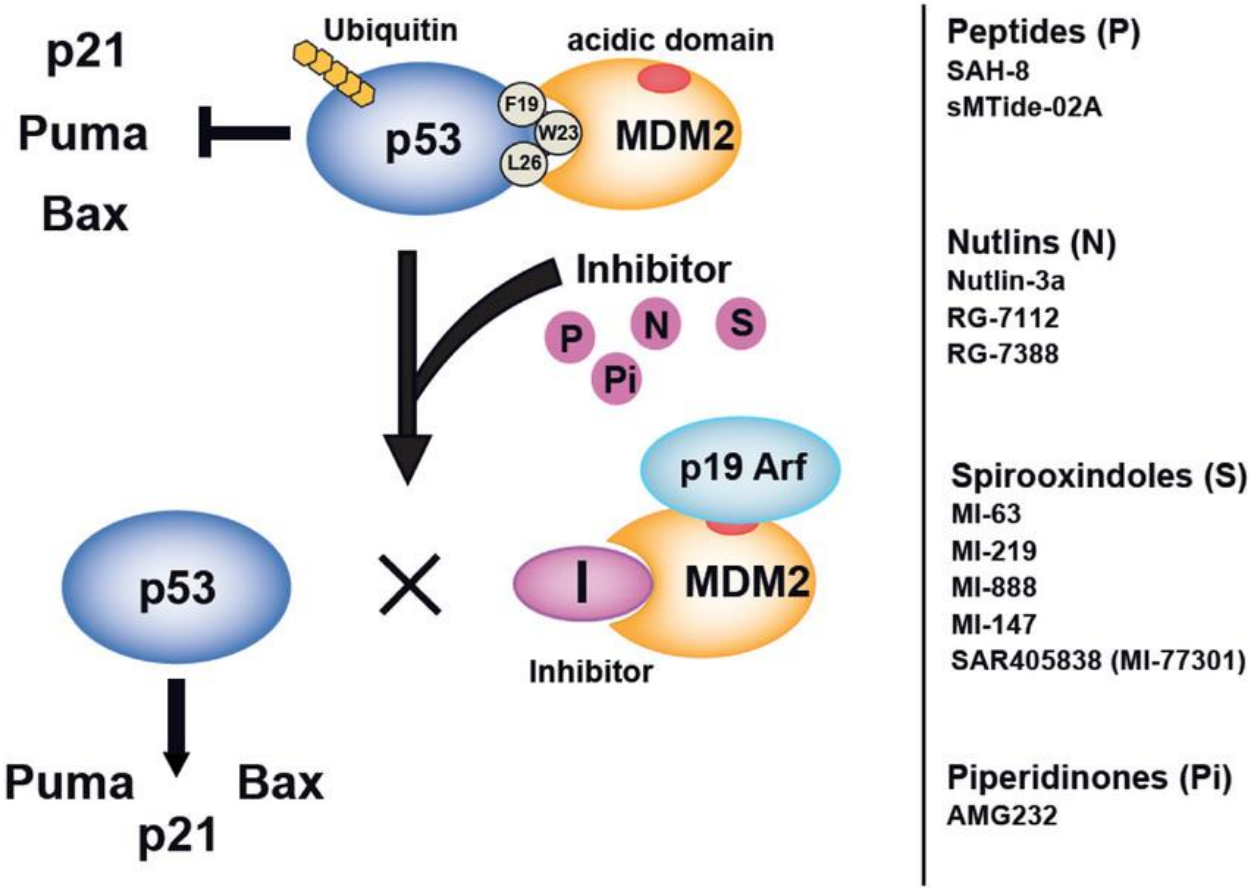

Figure 4.2. The mechanism of most MDM2 inhibitors[6].

Proteolysis Targeting Chimeras (PROTACs) offer a novel and promising alternative to traditional inhibitors by leveraging the cell's ubiquitin-proteasome system to selectively degrade target proteins[7], including MDM2. Unlike conventional inhibitors, PROTACs do not merely block the function of the target protein; instead, they induce its degradation, leading to a more sustained reduction in protein levels. This approach not only prevents the upregulation of MDM2 observed with inhibitors but also provides a potential solution to the issue of protein accumulation.

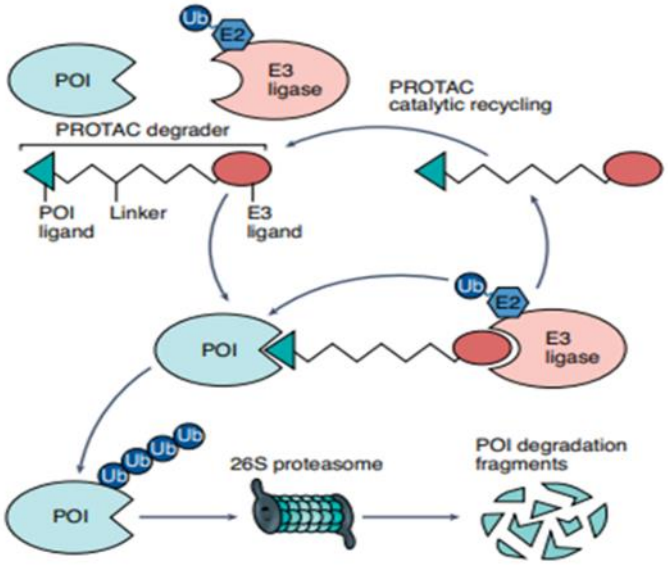

Figure 4.3. PROTAC strategy mechanism[8]

Recent studies have revealed that MDM2 PROTACs using different E3 ligase ligands may exhibit varying anti-proliferative effects (**Figure 4.3**). For instance, some VHL-recruiting MDM2 PROTACs have shown activity in p53 mutant cancer cell lines, whereas CRBN-recruiting MDM2 PROTACs do not show such activity[9]. Furthermore, the development of new MDM2 PROTAC based on E3 ubiquitin ligase beyond CRBN and VHL can bring us more options for the treatment of MDM2 dependent cancers and is expected to overcome drug resistance of current MDM2 PROTACs to some extent.

RNF126 is a RING-type E3 ubiquitin ligase involved in the degradation of misfolded proteins and is implicated in the development of breast and lung cancers, as well as playing a crucial role in DNA damage repair mechanisms. Recently, the Nomura group discovered a novel covalent ligand for RNF126[10]. These covalent RNF126 ligands can be directly attached to ligands targeting specific proteins, leading to the formation of linker-free PROTACs (**Figure 4.4**). This innovative design approach has the potential to produce compounds with enhanced drug-like properties, such as lower molecular weight and greater structural rigidity. In this study, we designed and synthesized several MDM2 PROTACs utilizing the covalent ligands of RNF126.

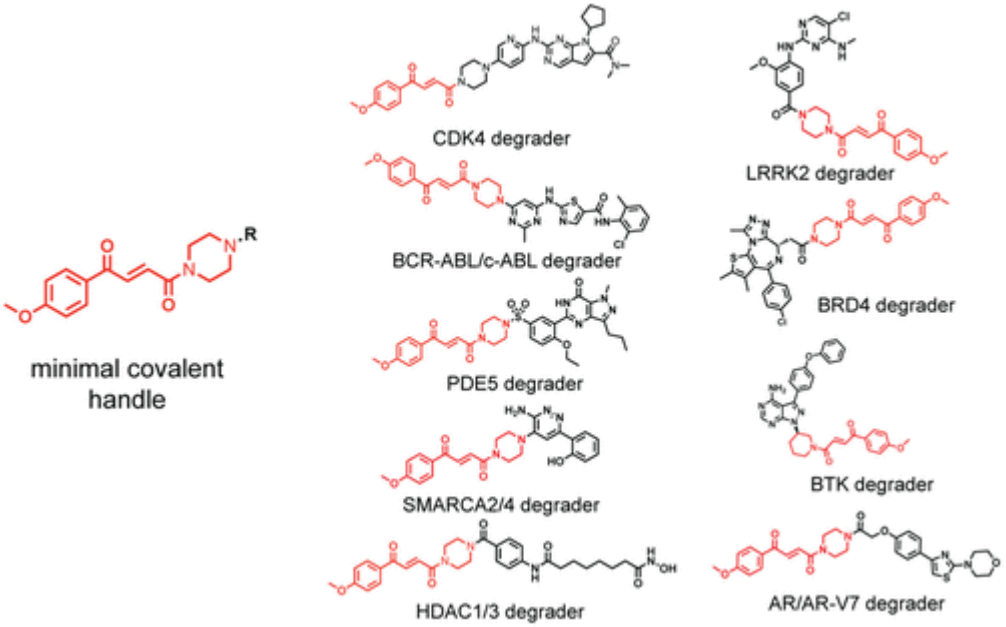

Figure 4.4. RNF 126 based PROTACs[6]

4.2. Design of Novel MDM2 PROTACs with Covalent Ligands

Recently, MI-1061 and nutlin 3 were reported as inhibitors of the MDM2. These inhibitors have been successfully utilized to develop MDM2 PROTACs. By analyzing the structures of MD 224 and WB156, we identified the solvent exposure site of each PROTACs (red circle). Additionally,

by analyzing the structures of JP-2-224, we identified the solvent-exposed sites of RNF 126-recruiting PROTACs. Most RNF126-recruiting PROTACs reported so far are linker-free, suggesting that a long linker may not be necessary for this type of PROTACs. Building on previous research, we designed several MDM2 PROTACs incorporating different MDM2 ligands (**Figure 4.5**).

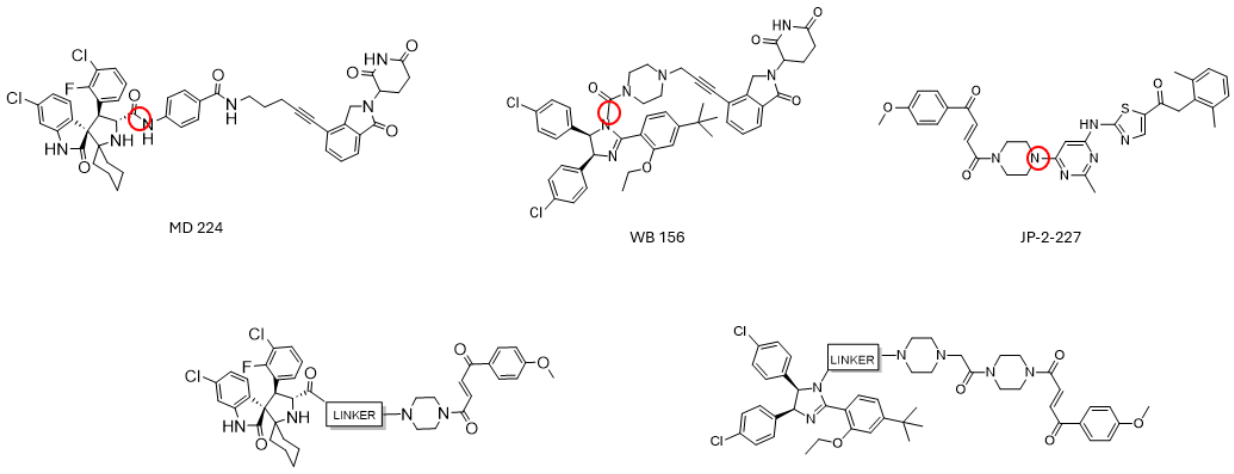

Figure 4.5. Design of RNF 126-recruiting PROTACs

4.3. Synthesis of Novel MDM2 PROTACs with Covalent Ligands

The synthetic route for compounds YX-1 to YX-4 is depicted in **Scheme 1**. The ligands for MDM2 are provided by Dr. Qiuhua Fan. With 1 step coupling, I synthesized four RNF 126-recruiting MDM2 degraders.

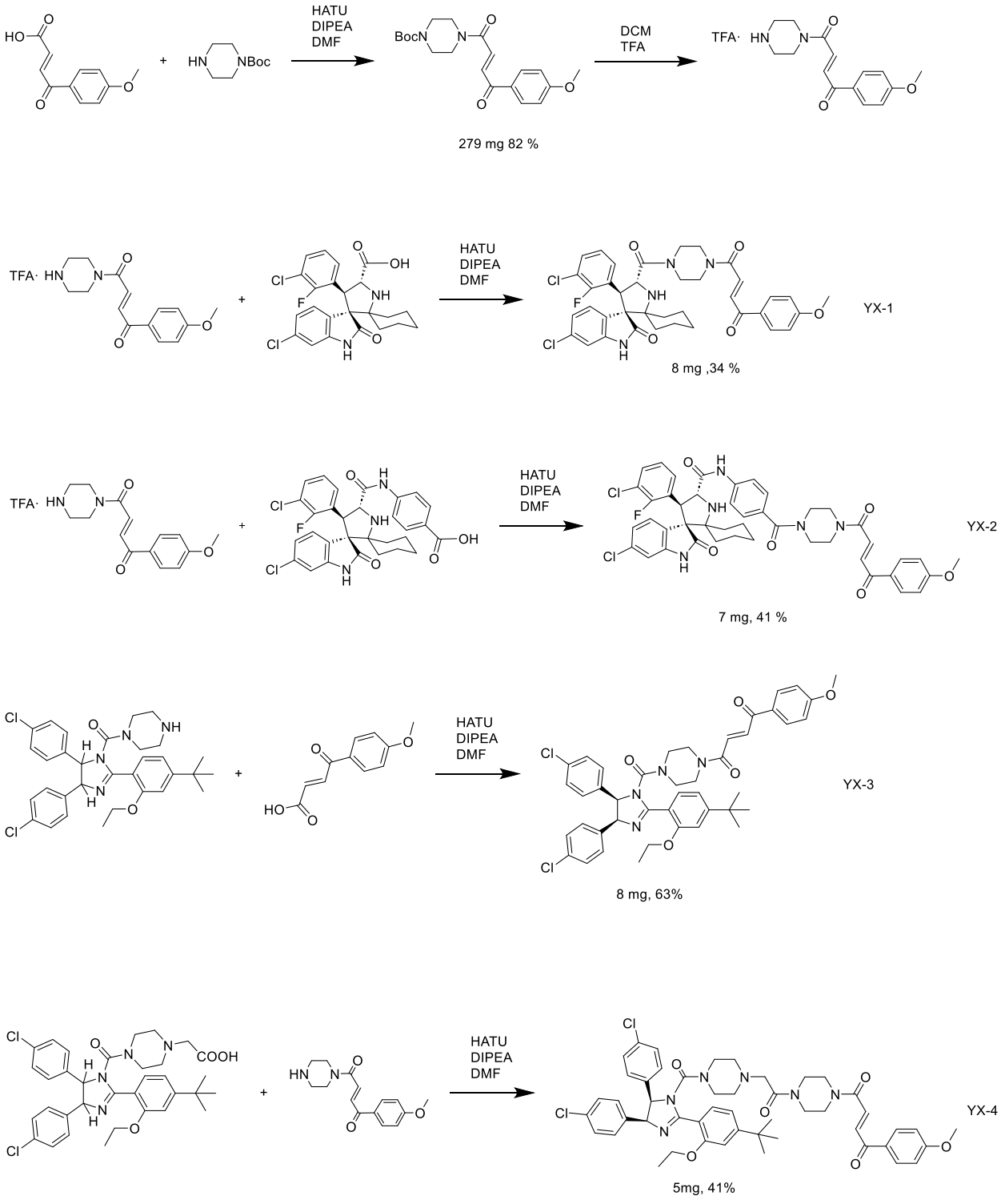

Scheme 4.1. Synthesis of RNF 126-recruiting PROTACs

4.4. Biological Study of MDM2 PROTACs with Covalent Ligands

To assess the activity of YX 1-4, our group member Ira Tandon treated cells with 1 µM and 10 µM concentrations of YX-1, YX-2, YX-3, and YX-4 for 6 h, using WB 156 as a positive control. Notably, only YX-1 and YX-3, which are linker less PROTACs, induced the degradation of MDM2 (**Figure 4.6**).

Figure 4.6. Biological study of RNF 126 based MDM2 PROTACs

To further evaluate the impact of these novel degraders and ligands on MDM2 and p53 protein levels in MOLT-4 and RS4;11 cell lines, we treated the cells with varying concentrations of YX-1, YX-3, and an RNF ligand for 3 and 6 h. Western blot analysis was performed to measure the expression levels of MDM2, p53, and GSPT1, using β-Actin as the loading control (**Figure 4.7**). Our results demonstrated that treatment with YX-1, YX-3, and the RNF ligand led to a significant reduction in MDM2 protein levels across all tested concentrations and time points. Unexpectedly,

we also observed a decrease in p53 levels, which typically would be expected to increase following MDM2 degradation. This simultaneous degradation of MDM2 and p53 suggests that these compounds may have broader, non-specific effects or could be influencing additional regulatory mechanisms involved in p53 stability. Additionally, we observed the degradation of GSPT1. However, further investigations are necessary to determine if the degradation of GSPT1 is induced by our small molecule PROTAC directly or indirectly.

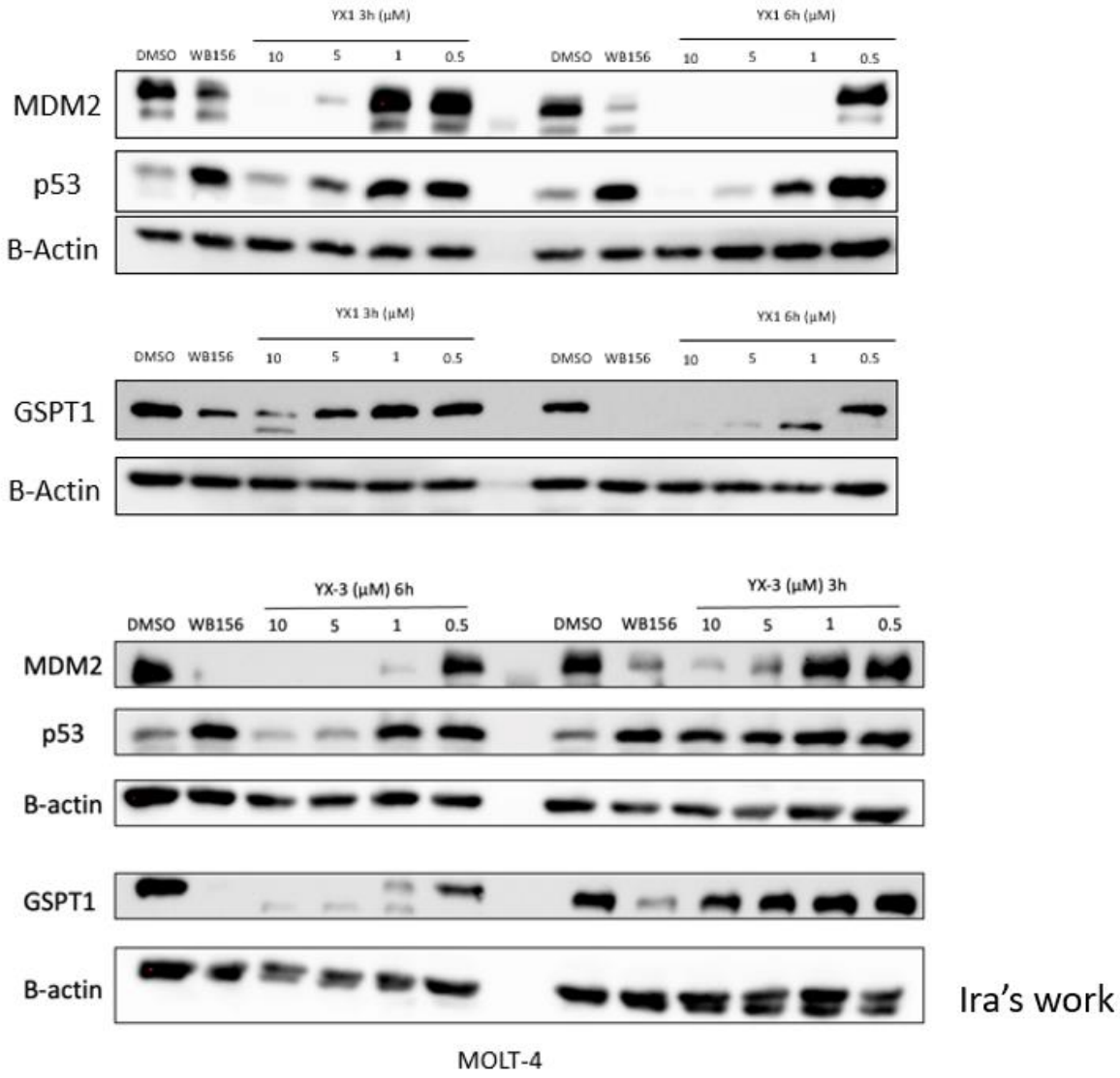

Figure 4.7. Biological study of RNF 126-recruiting MDM2 PROTACs

YX-1, YX-3, and the RNF126 ligand also exhibited significant antiproliferative activity in the MOLT-4 and RS4;11 cell lines. The antiproliferative effects of YX-1 were nearly identical to those of YX-3, while the RNF126 ligand alone was slightly less potent than the RNF126-recruiting MDM2 PROTACs (**Figure 4.8**).

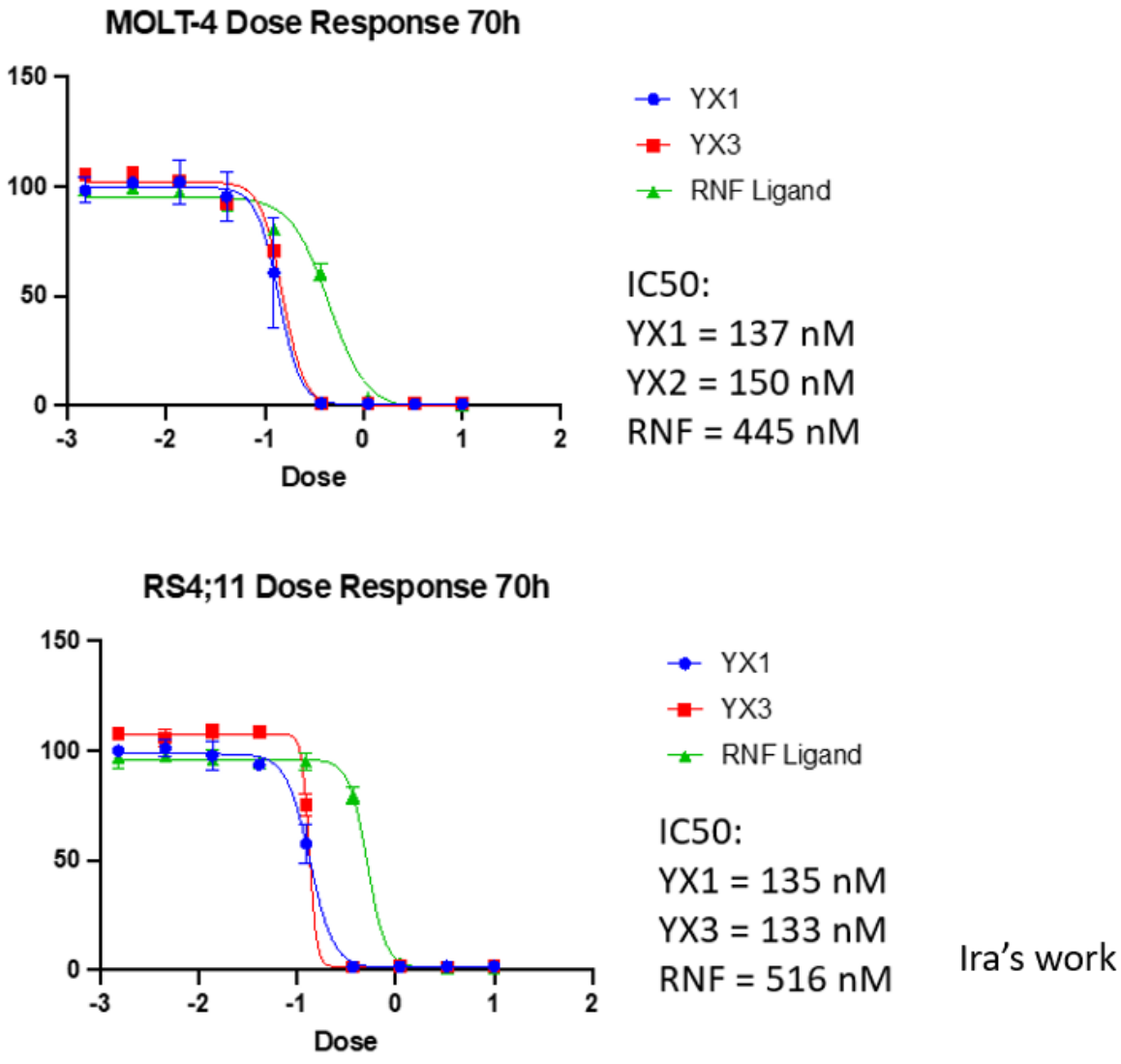

Figure 4.8. The anti-proliferative activity of MDM2 PROTACs

4.5. Discussion and Perspectives

The development of novel MDM2 PROTACs based on RNF126 ligands has opened new avenues in targeted protein degradation, offering a promising alternative to traditional MDM2 inhibitors. Our study demonstrates that linker-free RNF126-recruiting PROTACs, such as YX-1 and YX-3, effectively induce the degradation of MDM2 and exhibit significant antiproliferative activity in cancer cell lines like MOLT-4 and RS4;11.

Unexpectedly, our data revealed that the degradation of MDM2 by YX-1 and YX-3 was accompanied by a simultaneous reduction in p53 protein levels. This outcome was counterintuitive, given that p53 levels are typically expected to increase following MDM2 degradation. The concurrent degradation of both MDM2 and p53 suggests that these RNF126-recruiting PROTACs may have broader, non-specific effects or may influence additional regulatory pathways that govern p53 stability. This observation raises important questions about the specificity of these PROTACs and highlights the need for further investigation of their off-target effects.

4.6. Experimental Sections

General Information

Unless otherwise stated, all commercial reagents were used as received. Reactions were conducted in dry glassware using anhydrous solvents (pass through activated alumina columns). Unless stated otherwise, reactions were performed at room temperature (rt). Thin-layer chromatography (TLC) was conducted on plates (EMD Chemical Inc. 60, F254) and visualized using a combination of UV, sulfuric acid, and ceric ammonium molybdate staining. Flash column chromatography was performed with silica gel (Silicycle, 40-63 μm). Infrared spectra (IR) were obtained on a Bruker Equinox 55 Spectrophotometer. Optical rotations were recorded on Perkin-Elmer 241 polarimeter. ^{1}H and ^{13}C nuclear magnetic resonance spectra (NMR) were obtained on a Brooker 400 MHz.

Chemical shifts were reported in parts per million (ppm), and the residual solvent peak was used as an internal reference: proton (chloroform δ 7.26), carbon (chloroform δ 77.16) or tetramethylsilane (TMS δ 0.00) was used as a reference. Multiplicity was indicated as follows: s (singlet), d (doublet), t (triplet), m (multiplet), dd (doublet of doublet), td (triplet of doublet), bs (broad singlet). Coupling constants (*J*) were reported in Hertz (Hz). All high-resolution mass spectra were performed by Analytical Instrument Center at the School of Pharmacy (UW-Madison) on an Electron Spray Injection (ESI) mass spectrometer.

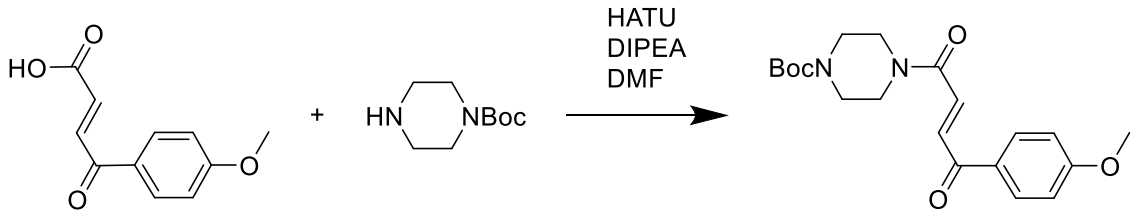

To a solution of (E)-4-(4-methoxyphenyl)-4-oxobut-2-enoic acid (412 mg, 2 mmol) in DMF was added HATU (800 mg, 2.4 mmol), N-Boc-piperazine (372 mg, 2 mmol), and DIPEA (0.5 mL, 4 mmol). The reaction mixture was stirred at room temperature overnight. The mixture was then extracted and concentrated in vacuo. The residue was purified by flash column chromatography on silica gel to afford the desired product.

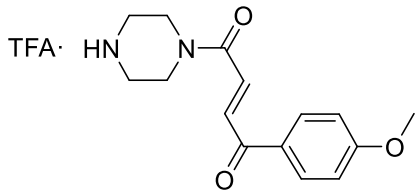

To a solution of t-butyl protected intermediate in anhydrous DCM (2 mL) was slowly added TFA (1 mL). The mixture was stirred at room temperature for 2 h. The solvent was then removed in vacuo, and the residue was directly used in the next step.

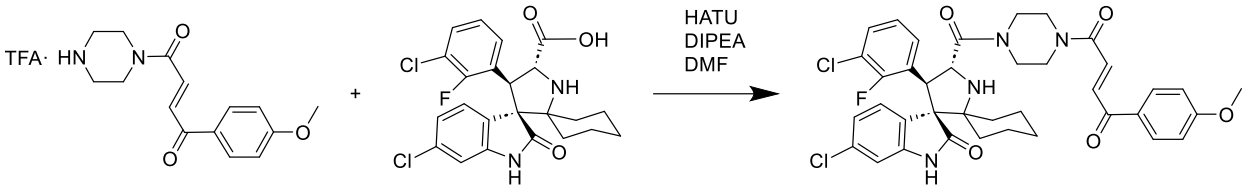

To a solution of MDM2 ligand (46 mg, 0.1 mmol) in DMF was added HATU (40 mg, 0.12 mmol), RNF 126 ligand (28 mg, 0.1 mmol), and DIPEA (21 mg, 0.2 mmol). The reaction mixture was stirred at room temperature overnight. The mixture was then extracted and concentrated in vacuo. The residue was purified by flash column chromatography on silica gel to afford the desired product. ^{1}H NMR (400 MHz, MeOD) δ 8.06 (dd, *J* = 8.0, 4.3 Hz, 2H), 7.98 (s, 1H), 7.90 (dd, *J* = 15.1, 6.7 Hz, 1H), 7.55 – 7.40 (m, 2H), 7.20 (ddd, *J* = 8.4, 7.0, 1.6 Hz, 1H), 7.05 (td, *J* = 8.0, 2.0 Hz, 4H), 6.74 (d, *J* = 1.9 Hz, 1H), 5.45 – 5.34 (m, 1H), 4.79 (d, *J* = 9.1 Hz, 1H), 4.07 (dd, *J* = 17.9, 10.8 Hz, 1H), 3.90 (m, 4H), 3.87 – 3.67 (m, 2H), 3.69 – 3.53 (m, 2H), 3.49 – 3.38 (m, 2H), 2.17 (d, *J* = 12.5 Hz, 1H), 1.85 – 1.40 (m, 7H), 1.10 – 0.85 (m, 2H). ^{13}C NMR (101 MHz, MeOD) δ 188.1, 178.9, 172.0, 164.6, 163.4, 143.5, 134.3, 133.6, 131.5, 131.0, 129.6, 129.0, 128.2, 127.4, 125.2, 124.1, 120.9, 113.9, 109.4, 69.7, 69.0, 60.2, 54.7, 44.6, 35.5, 32.8, 32.1, 30.2, 25.6, 22.5, 21.6.

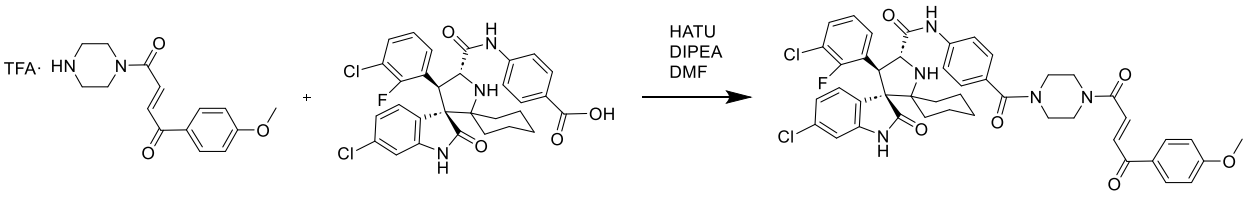

To a solution of MDM2 ligand (46 mg, 0.1 mmol) in DMF was added HATU (40 mg, 0.12 mmol), RNF 126 ligand (28 mg, 0.1 mmol), and DIPEA (21 mg, 0.2 mmol). The reaction mixture was stirred at room temperature overnight. The mixture was then extracted and concentrated in vacuo. The residue was purified by flash column chromatography on silica gel to afford the desired product. ^{1}H NMR (400 MHz, MeOD) δ 8.05 (d, *J* = 8.9 Hz, 2H), 7.97 (s, 1H), 7.90 (d, *J* = 15.2 Hz, 1H), 7.73 (d, *J* = 8.6 Hz, 2H), 7.67 (ddd, *J* = 8.1, 6.4, 1.6 Hz, 1H), 7.48 – 7.44 (m, 3H), 7.22 (t, *J* = 1.3 Hz, 1H), 7.08 – 7.00 (m, 4H), 6.73 (d, *J* = 1.9 Hz, 1H), 4.81 (d, *J* = 9.4 Hz, 1H), 4.71 (d, *J* = 9.2 Hz, 1H), 4.16 – 4.00 (m, 1H), 3.89 (s, 3H), 3.65 (d, *J* = 91.9 Hz, 6H), 2.08 (d, *J* = 12.8 Hz, 1H), 1.97 (m, 2H), 1.75 (dd, *J* = 26.8, 12.9 Hz, 3H), 1.64 – 1.53 (m, 2H), 1.43 (dd, *J* = 7.9, 6.6 Hz, 1H), 1.41 – 1.32 (m, 1H), 1.32 – 1.18 (m, 1H), 1.16 – 1.02 (m, 1H), 0.98 – 0.83 (m, 1H). ^{13}C NMR (101 MHz, MeOD) δ 188.0, 178.4, 173.6, 171.0, 165.2, 164.6, 163.5, 143.5, 139.6, 134.4, 133.9, 131.4, 131.0, 130.3, 129.6, 128.9, 127.6, 128.1, 124.5, 124.1, 121.0, 119.1, 113.9, 109.4, 70.1, 68.6, 63.1, 54.7, 46.3, 35.5, 32.3, 32.0, 30.2, 25.5, 22.5, 22.1, 13.1.

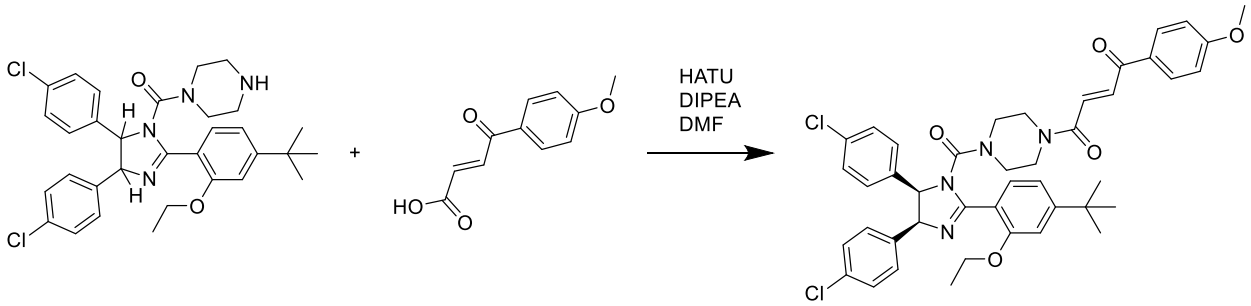

To a solution of MDM2 ligand (58 mg, 0.1 mmol) in DMF was added HATU (40 mg, 0.12 mmol), RNF 126 ligand (21 mg, 0.1 mmol), and DIPEA (21 mg, 0.2 mmol). The reaction mixture was stirred at room temperature overnight. The mixture was then extracted and concentrated in vacuo.

The residue was purified by flash column chromatography on silica gel to afford the desired product. ^{1}H NMR (400 MHz, $CDCl_3$) δ 7.93 (d, *J* = 8.9 Hz, 1H), 7.86 – 7.77 (m, 1H), 7.48 (dd, *J* = 10.2, 8.0 Hz, 1H), 7.27 – 7.17 (m, 1H), 7.03 (d, *J* = 8.5 Hz, 3H), 6.98 – 6.94 (m, 2H), 6.94 – 6.85 (m, 5H), 6.80 (dd, *J* = 8.5, 3.2 Hz, 2H), 6.32 (d, *J* = 11.9 Hz, 1H), 5.58 (d, *J* = 9.8 Hz, 1H), 5.42 (dd, *J* = 9.8, 4.8 Hz, 1H), 4.21 – 3.96 (m, 2H), 3.81 (s, 3H), 3.06 (m, 8H), 1.42 – 1.34 (m, 2H), 1.27 (s, 9H). ^{13}C NMR (101 MHz, $CDCl_3$) δ 188.0, 166.3, 164.2, 163.9, 163.9, 160.4, 160.1, 156.9, 156.8, 156.6, 155.7, 136.1, 135.1, 133.1, 132.9, 131.3, 130.6, 130.3, 138.6,128.3, 118.2 109.6, 72.4, 69.2, 64.1, 55.5, 35.3, 31.2, 14.8.

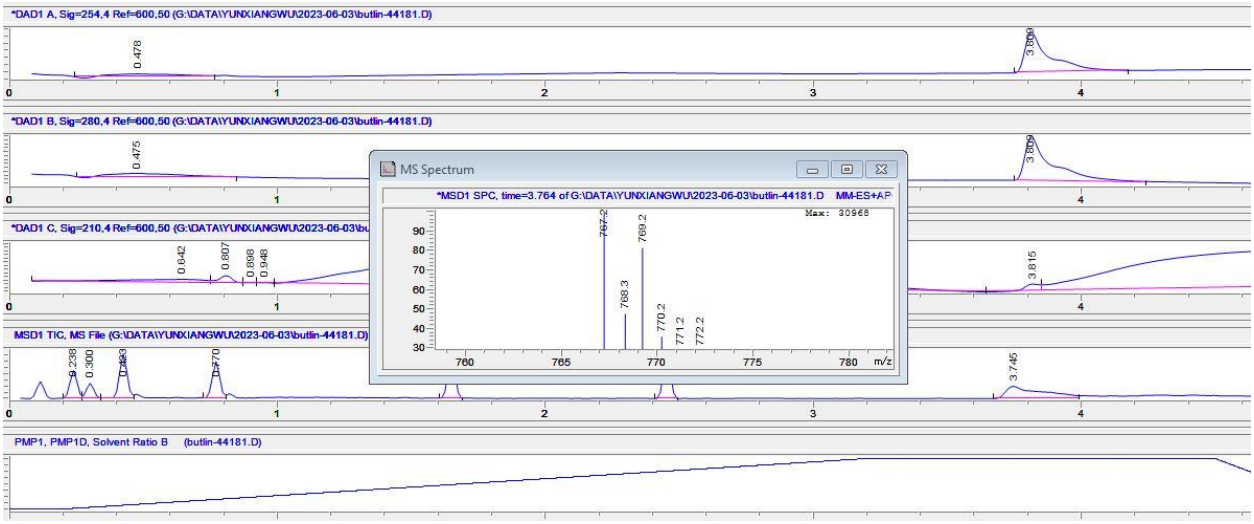

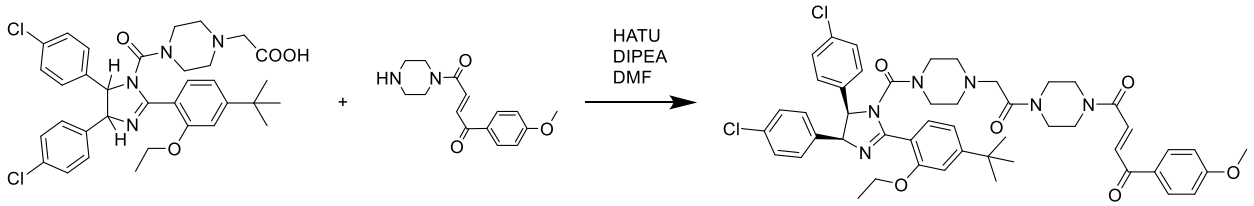

To a solution of MDM2 ligand (64 mg, 0.1 mmol) in DMF was added HATU (40 mg, 0.12 mmol), RNF 126 ligand (28 mg, 0.1 mmol), and DIPEA (21 mg, 0.2 mmol). The reaction mixture was stirred at room temperature overnight. The mixture was then extracted and concentrated in vacuo.

The residue was purified by flash column chromatography on silica gel to afford the desired product.

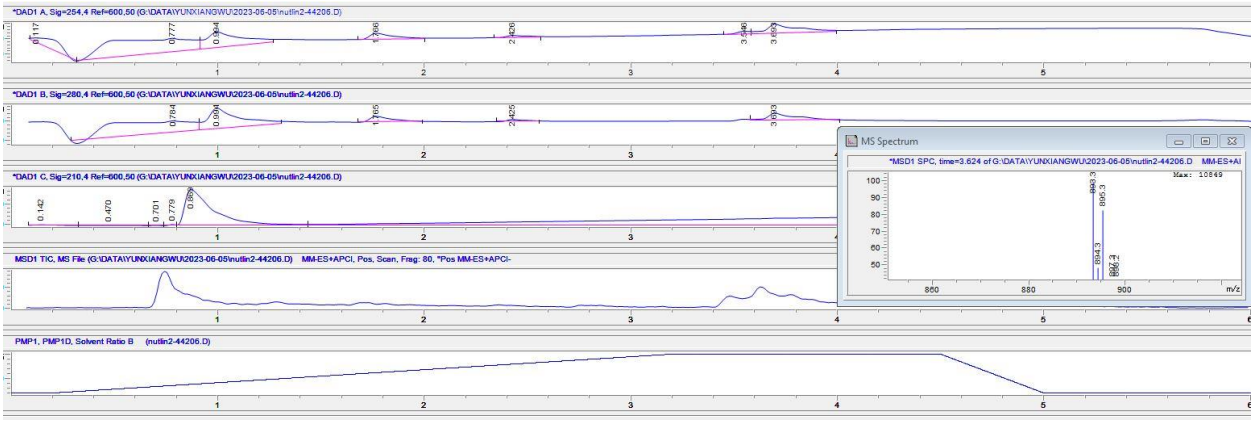

4.7. References

1. (a) Wade, M.; Li, Y.-C.; Wahl, G. M. MDM2, MDMX and p53 in oncogenesis and cancer therapy. *Nat. Rev. Cancer* **2013**, 13, 83−96. (b) Brown, C. J.; Lain, S.; Verma, C. S.; Fersht, A. R.; Lane, D. P. Awakening guardian angels: drugging the p53 pathway. *Nat. Rev. Cancer* **2009**, 9, 862−873. (c) Stiewe, T. The p53 family in differentiation and tumorigenesis. *Nat. Rev. Cancer* **2007**, 7, 165−167. (d) Juven-Gershon, T.; Oren, M. Mdm2: the ups and downs. *Mol. Med.* **1999**, 5, 71−83.
2. (a) Freedman, D. A.; Wu, L.; Levine, A. J. Functions of the MDM2 oncoprotein. *Cell. Mol. Life Sci.* **1999**, 55, 96−107. (b) Wu, X.; Bayle, J. H.; Olson, D.; Levine, A. J. The p53-mdm-2 autoregulatory feedback loop. Genes Dev. 1993, 7, 1126−1132.
3. Momand, J.; Zambetti, G. P.; Olson, D. C.; George, D.; Levine, A. J. The mdm-2 oncogene product forms a complex with the p53 protein and inhibits p53-mediated transactivation. *Cell* **1992**, 69, 1237−1245.

4. Marine, J.-C.; Lozano, G. Mdm2-mediated ubiquitylation: p53 and beyond. *Cell Death Differ*. **2010**, 17, 93–102.
5. (a) Ding, Q.; Zhang, Z.; Liu, J.-J.; Jiang, N.; Zhang, J.; Ross, T. M.; Chu, X.-J.; Bartkovitz, D.; Podlaski, F.; Janson, C.; Tovar, C.; Filipovic, Z. M.; Higgins, B.; Glenn, K.; Packman, K.; Vassilev, L. T.; Graves, B. Discovery of RG7388, a potent and selective p53-MDM2 inhibitor in clinical development. *J. Med. Chem.* **2013**, 56, 5979−5983. (b) Holzer, P.; Masuya, K.; Furet, P.; Kallen, J.; Valat-Stachyra, T.; Ferretti, S.; Berghausen, J.; Bouisset-Leonard, M.; Buschmann, N.; Pissot-Soldermann, C.;Rynn,C.;Ruetz,S.;Stutz, S.;Chene,P.; Jeay,S.; Gessier, F. Discovery of a dihydroisoquinolinone derivative (NVP CGM097): Ahighly potent and selective MDM2 inhibitor undergoing Phase 1 clinical trials in p53wt tumors. *J. Med. Chem*. **2015**, 58, 6348− 6358. (c) Vu, B.; Wovkulich, P.; Pizzolato, G.; Lovey, A.; Ding, Q.; Jiang, N.; Liu, J.-J.; Zhao, C.; Glenn, K.; Wen, Y.; Tovar, C.; Packman, K.; Vassilev, L.; Graves, B. Discovery of RG7112: A small-molecule MDM2 inhibitor in clinical development. *ACS Med. Chem. Lett.* **2013**, 4, 466−469. (d) Wang, S.; Sun, W.; Zhao, Y.; McEachern, D.; Meaux, I.; Barriere, C.; Stuckey, J. A.; Meagher, J. L.; Bai, L.; Liu, L.; Hoffman-Luca, C. G.; Lu, J.; Shangary, S.; Yu, S.; Bernard, D.; Aguilar, A.; Dos-Santos, O.; Besret, L.; Guerif, S.; Pannier, P.; Gorge-Bernat, D.; Debussche, L. SAR405838: An optimized inhibitor of MDM2-p53 interaction that induces complete and durable tumor regression. *Cancer Res.* **2014**, 74, 5855−5865.
6. Merkel, O., Taylor, N., Prutsch, N., Staber, P., Moriggl, R., Turner, S., & Kenner, L. (2017). When the guardian sleeps: Reactivation of the p53 pathway in cancer. https://doi.org/10.17863/CAM.10629

7. (a) Lai, A. C.; Crews, C. M. Induced protein degradation: an emerging drug discovery paradigm. *Nat. Rev. Drug Discov.* **2017**, 16, 101−114. (b) Crews, C. M.; Georg, G.; Wang, S. Inducing protein degradation as a therapeutic strategy. *J. Med. Chem.* **2016**, 59, 5129−5130. (c) Neklesa, T. K.; Winkler, J. D.; Crews, C. M. Targeted protein degradation by PROTACs. *Pharmacol. Ther.* **2017**, 174, 138−144.
8. Garber, K**.** The PROTAC gold rush. *Nat. Biotechnol.* **2022**, 40, 12-16.
9. Adams, C. M.; Mitra, R.; Xiao, Y.; Michener, P.; Palazzo, J.; Chao, A.; Gour, J.; Cassel, J.; Salvino, J. M.; Eischen, C. M. Targeted MDM2 Degradation Reveals a New Vulnerability for p53-Inactivated Triple-Negative Breast Cancer. *Cancer Discov.* **2023**, 13 (5), 1210-1229.
10. Toriki, E. S.; Papatzimas, J. W.; Nishikawa, K.; Dovala, D.; Frank, A. O.; Hesse, M. J.; Dankova, D.; Song, J.-G.; Bruce-Smythe, M.; Struble, H.; Garcia, F. J.; Brittain, S. M.; Kile, A. C.; McGregor, L. M.; McKenna, J. M.; Tallarico, J. A.; Schirle, M.; Nomura, D. K. Rational Chemical Design of Molecular Glue Degraders. *ACS Cent. Sci.* **2023**, 9, 915−926.

Appendix

NMR Spectrums

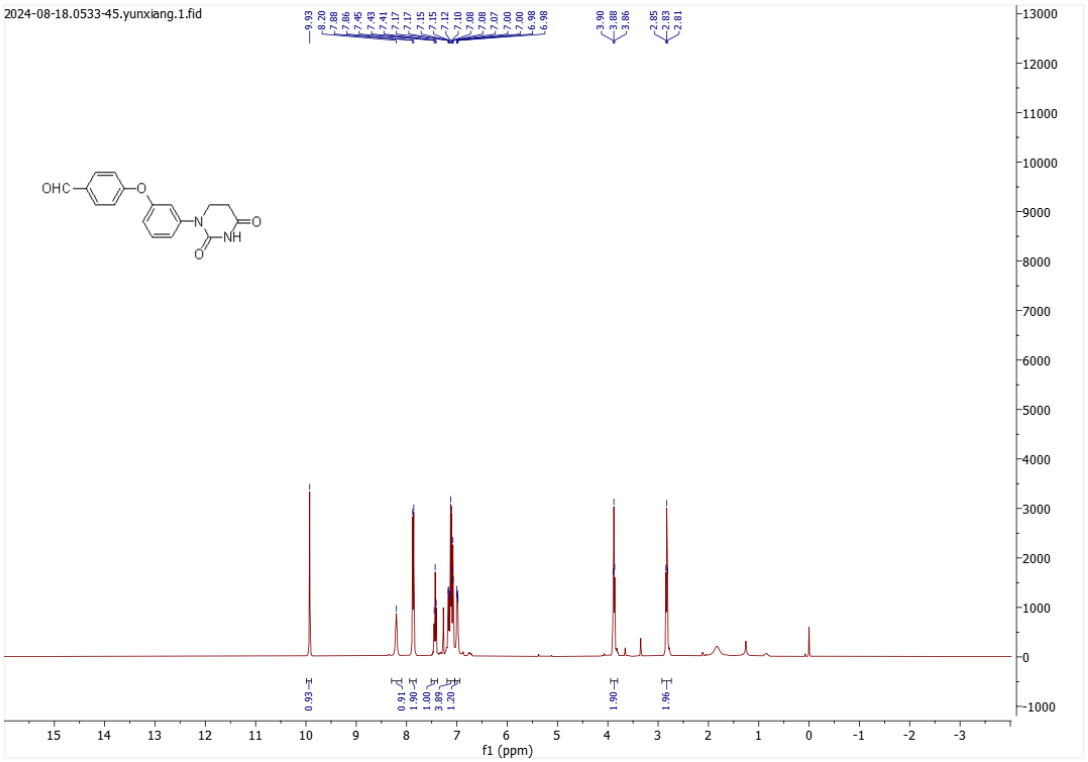
2024-08-18.0533-45.yunxiang.1.fid
9.93
8.70
7.88
7.86
7.45
7.43
7.41
7.17
7.17
7.15
7.15
7.12
7.10
7.08
7.08
7.07
7.00
7.00
6.98
6.98
3.90
3.88
3.86
2.85
2.83
2.81
OHC
O
N
O
NH
O
0.93
0.91
1.90
1.00
3.89
1.20
1.90
1.96
f1 (ppm)

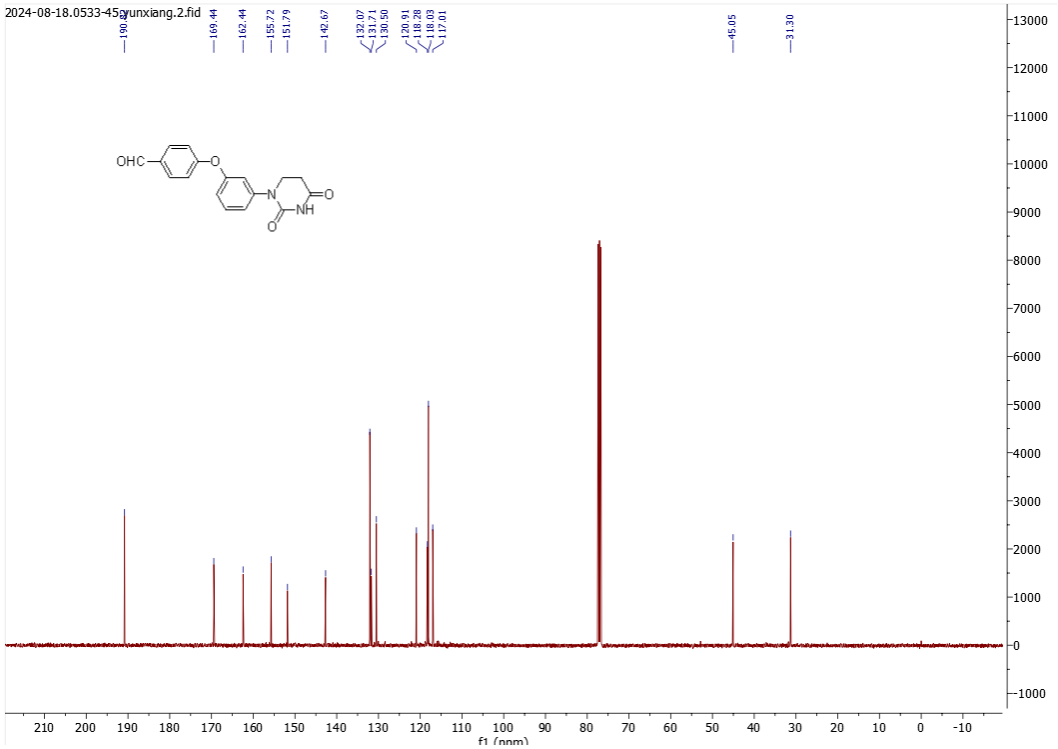
2024-08-18.0533-45.yunxiang.2.fid
190.82
169.44
162.44
155.72
151.79
142.67
132.07
131.71
130.50
120.91
118.28
118.03
117.01
45.05
31.30
OHC
O
N
O
NH
O
f1 (ppm)

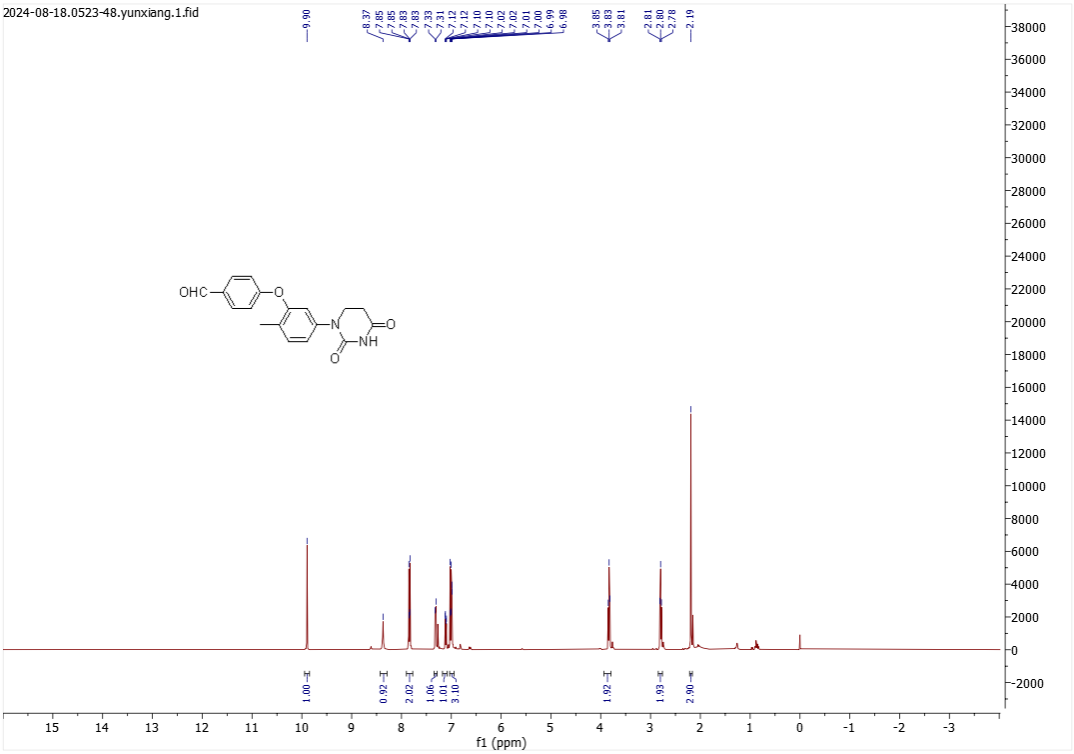
2024-08-18.0523-48.yunxiang.1.fid
9.90
8.37
7.85
7.85
7.83
7.83
7.33
7.31
7.12
7.12
7.10
7.02
7.02
7.01
7.00
6.99
6.98
3.85
3.83
3.81
2.81
2.80
2.78
2.19
OHC
O
N
O
NH
O
1.00
0.92
2.02
1.06
1.01
3.10
1.92
1.93
2.90
f1 (ppm)

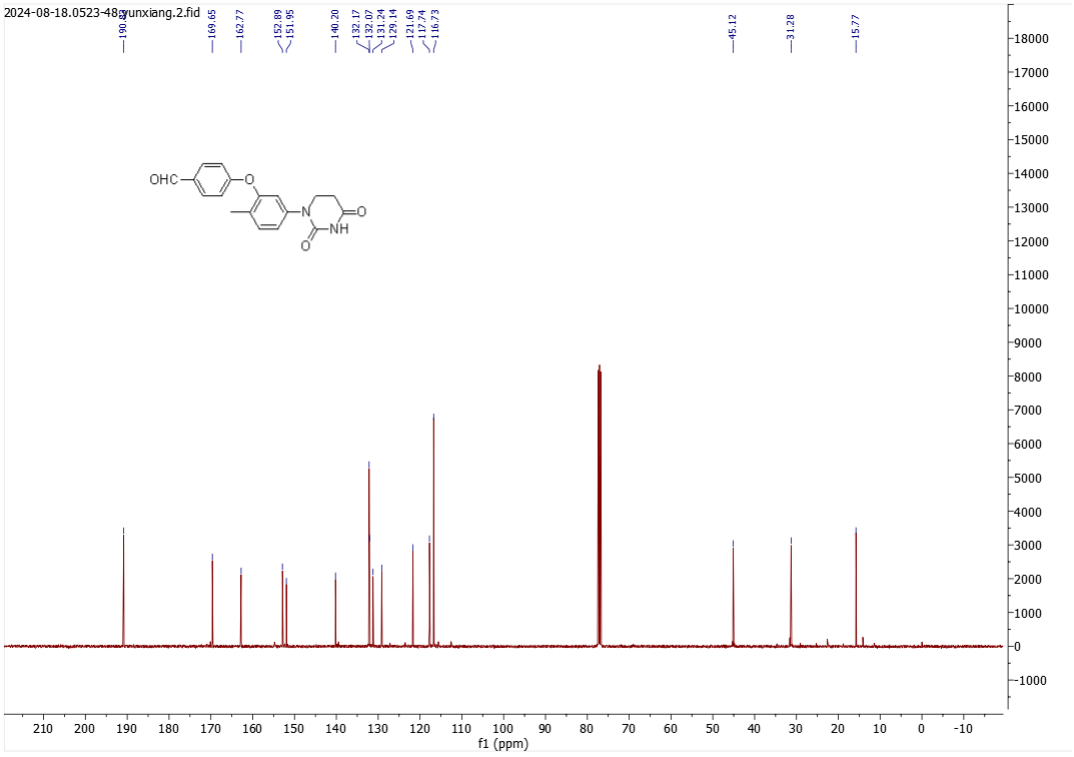
2024-08-18.0523-48.yunxiang.2.fid
190.47
169.65
162.77
152.89
151.95
140.20
132.17
132.07
131.24
129.14
121.69
117.74
116.73
45.12
31.28
15.77
OHC
O
N
O
NH
O
f1 (ppm)

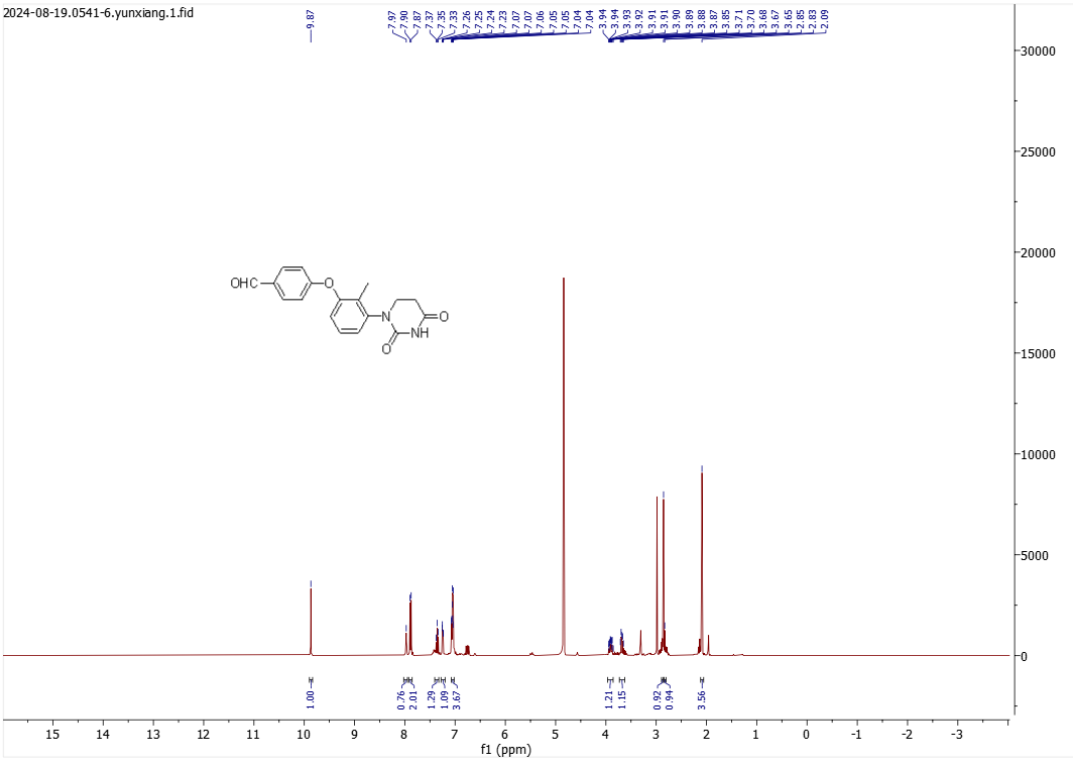
2024-08-19.0541-6.yunxiang.1.fid
OHC
O
N
NH
O
f1 (ppm)

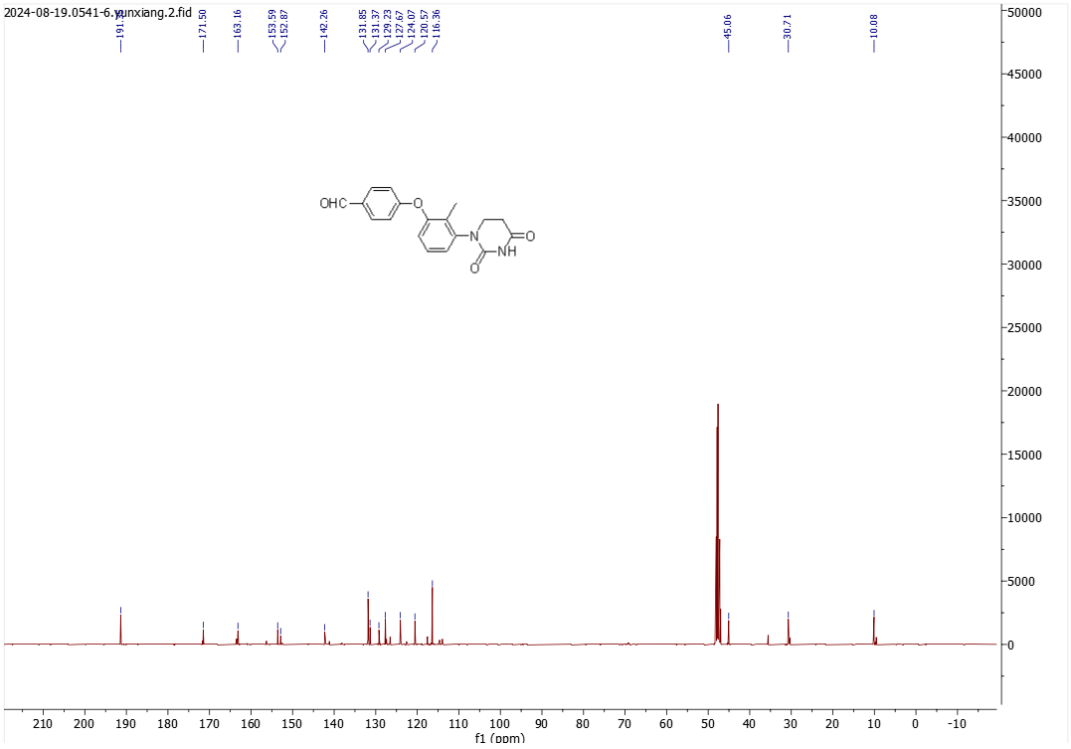
2024-08-19.0541-6.yunxiang.2.fid
OHC
O
N
NH
O
f1 (ppm)

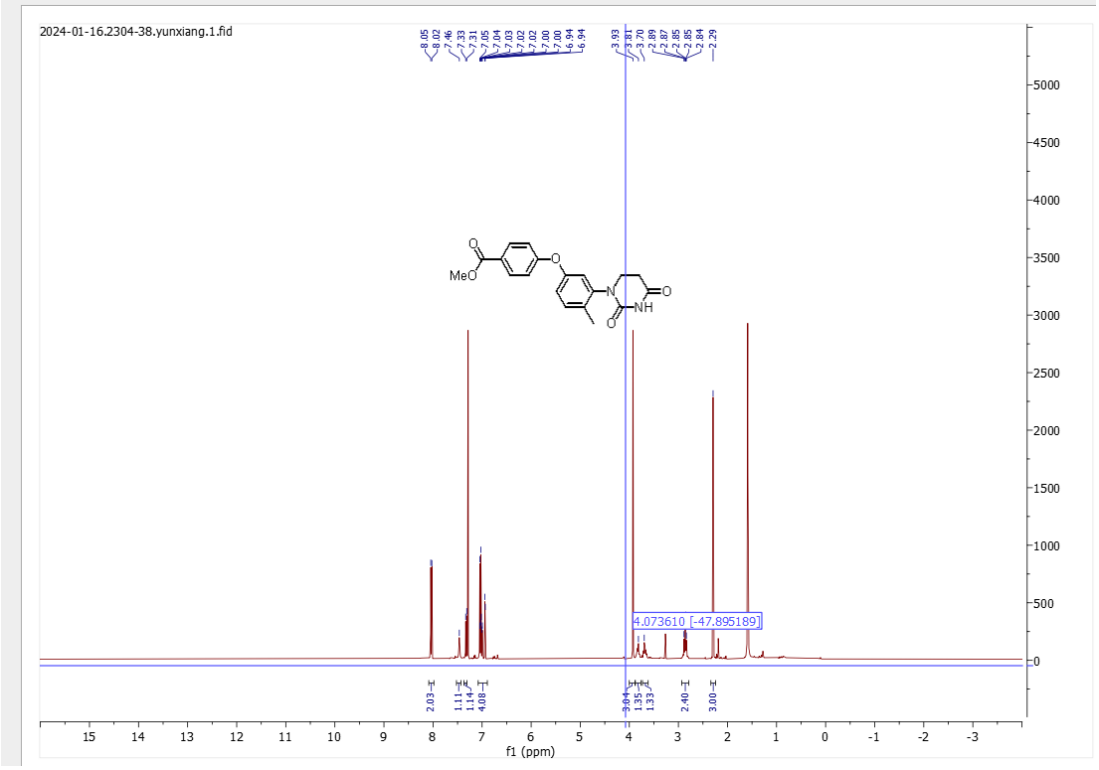
2024-01-16.2304-38.yunxiang.1.fid
8.05
8.02
7.96
7.33
7.31
7.05
7.04
7.03
7.02
7.02
7.00
7.00
6.94
6.94
3.93
3.91
3.70
2.89
2.87
2.85
2.85
2.84
2.29
MeO
O
O
N
O
NH
O
4.073610 [-47.895189]
2.03
1.11
1.14
4.08
3.04
1.35
1.33
2.40
3.00
f1 (ppm)

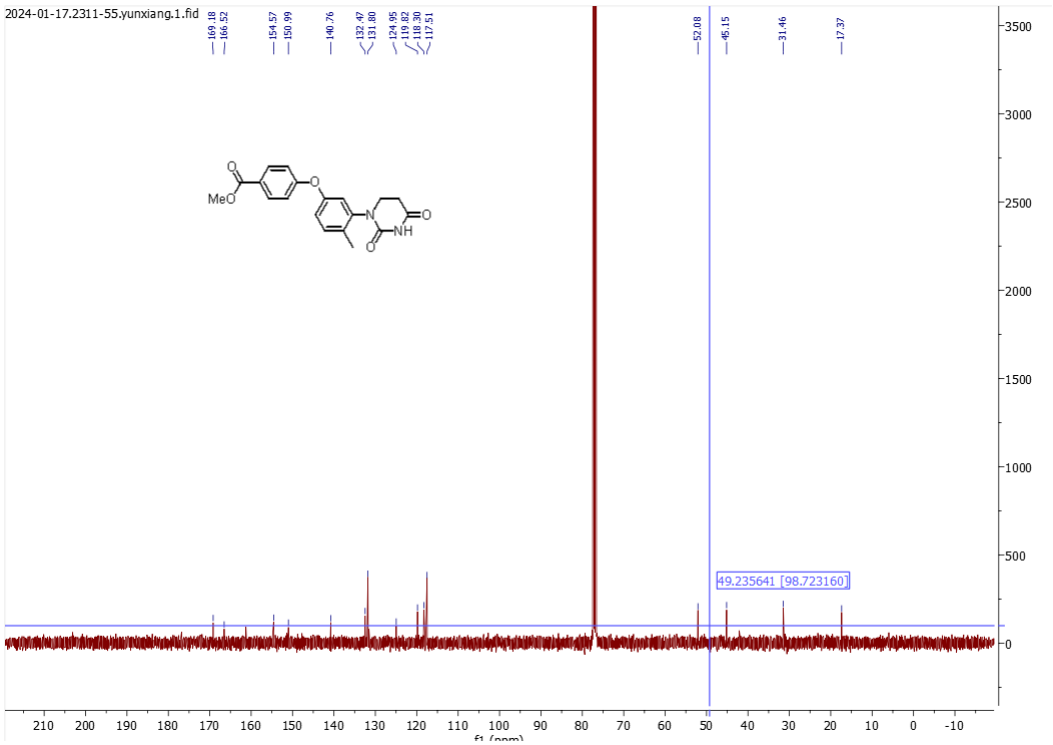
2024-01-17.2311-55.yunxiang.1.fid
169.18
166.52
154.57
150.99
140.76
132.47
131.80
124.95
119.82
118.30
117.51
52.08
46.15
31.46
17.37
MeO
O
O
N
O
NH
O
49.235641 [98.723160]
f1 (ppm)

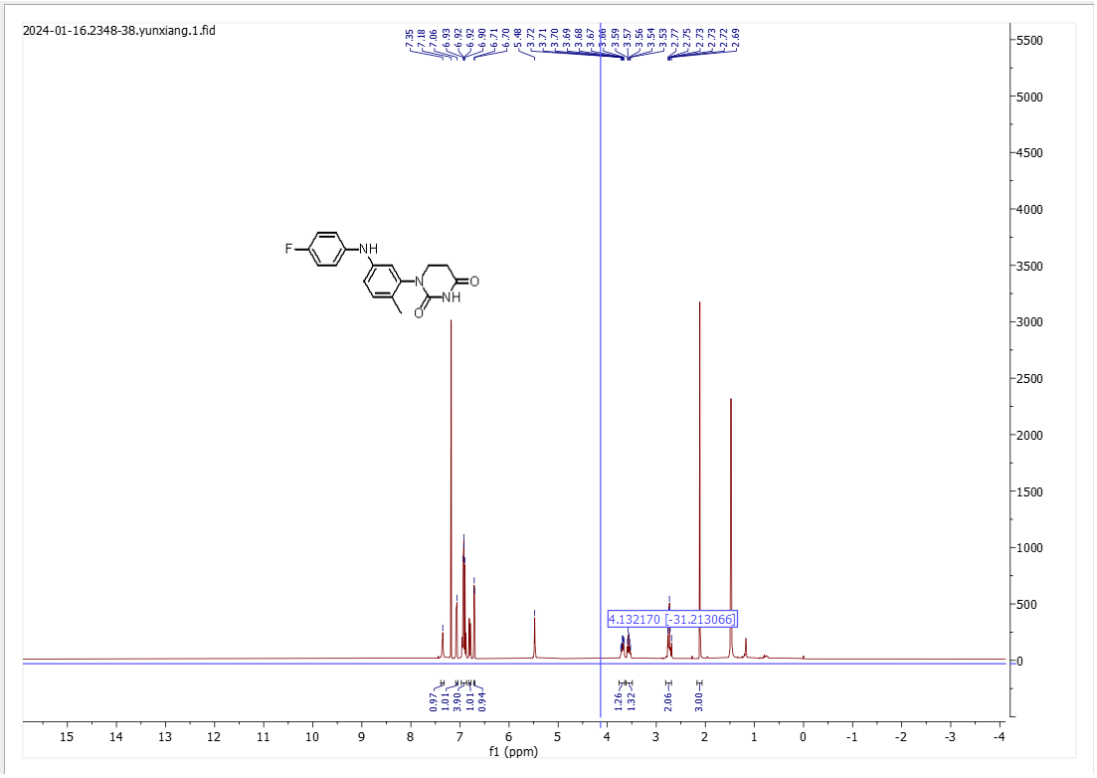
2024-01-16.2348-38.yunxiang.1.fid
F
NH
N
O
NH
O
4.132170 [-31.213066]
f1 (ppm)

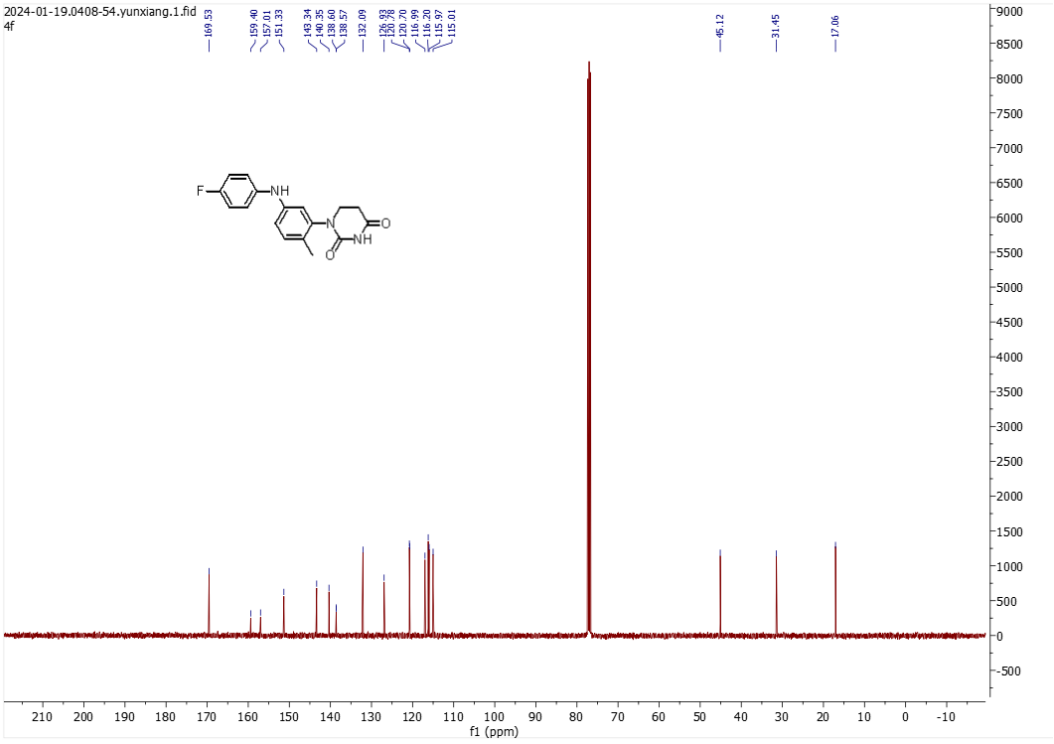
2024-01-19.0408-54.yunxiang.1.fid
4f
F
NH
N
O
NH
O
f1 (ppm)

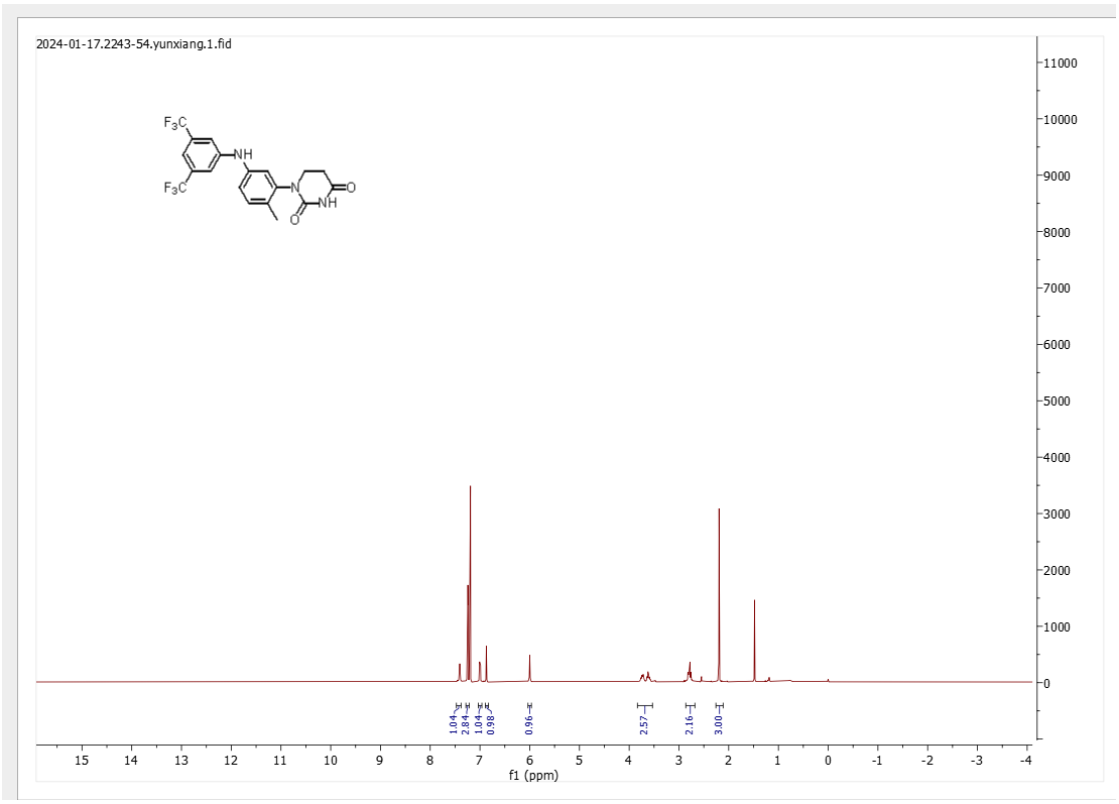
2024-01-17.2243-54.yunxiang.1.fid
F3C
NH
F3C
N
O
NH
O
11000
10000
9000
8000
7000
6000
5000
4000
3000
2000
1000
0
1.04
2.84
1.04
0.98
0.96
2.57
2.16
3.00
15 14 13 12 11 10 9 8 7 6 5 4 3 2 1 0 -1 -2 -3 -4
f1 (ppm)

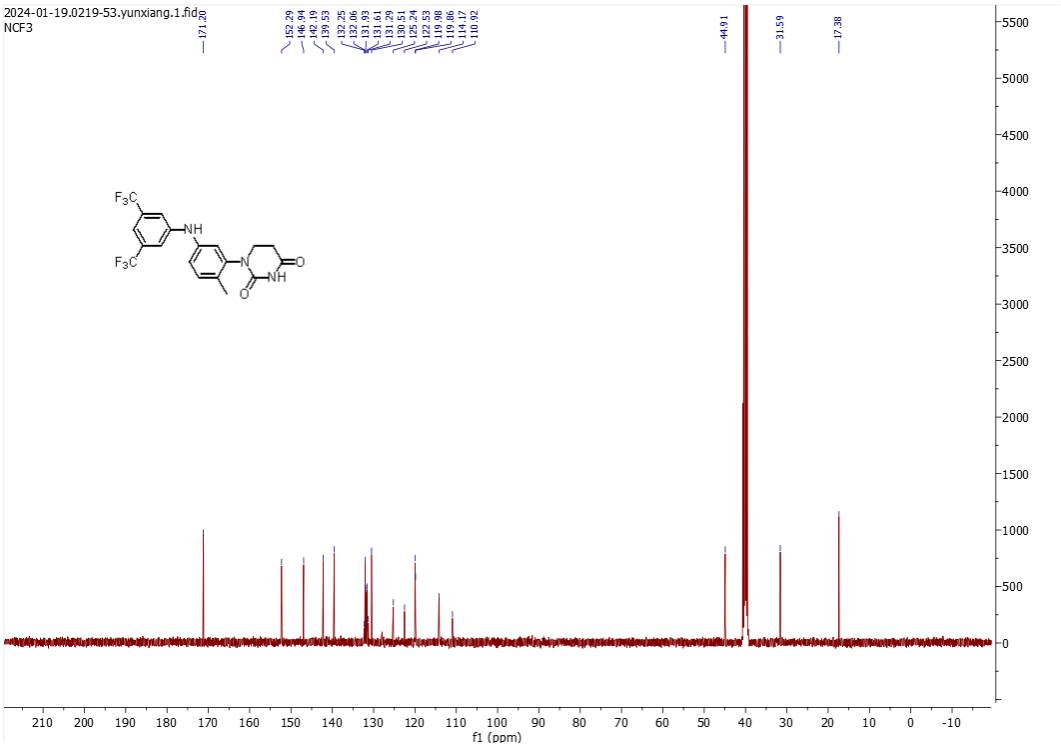
2024-01-19.0219-53.yunxiang.1.fid
NCF3
171.20
152.29
146.94
142.19
139.53
132.25
132.06
131.93
131.61
131.29
130.51
126.24
122.53
119.98
119.86
114.17
110.92
44.91
31.59
17.38
F3C
NH
F3C
N
O
NH
O
5500
5000
4500
4000
3500
3000
2500
2000
1500
1000
500
0
210 200 190 180 170 160 150 140 130 120 110 100 90 80 70 60 50 40 30 20 10 0 -10
f1 (ppm)

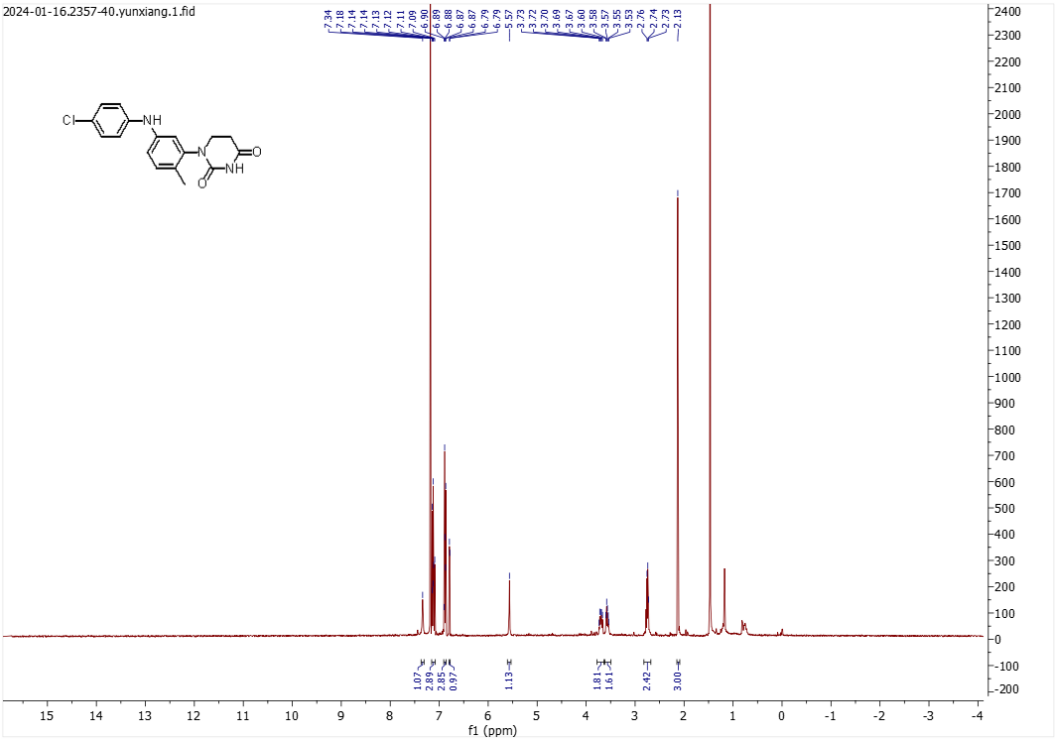
2024-01-16.2357-40.yunxiang.1.fid
f1 (ppm)

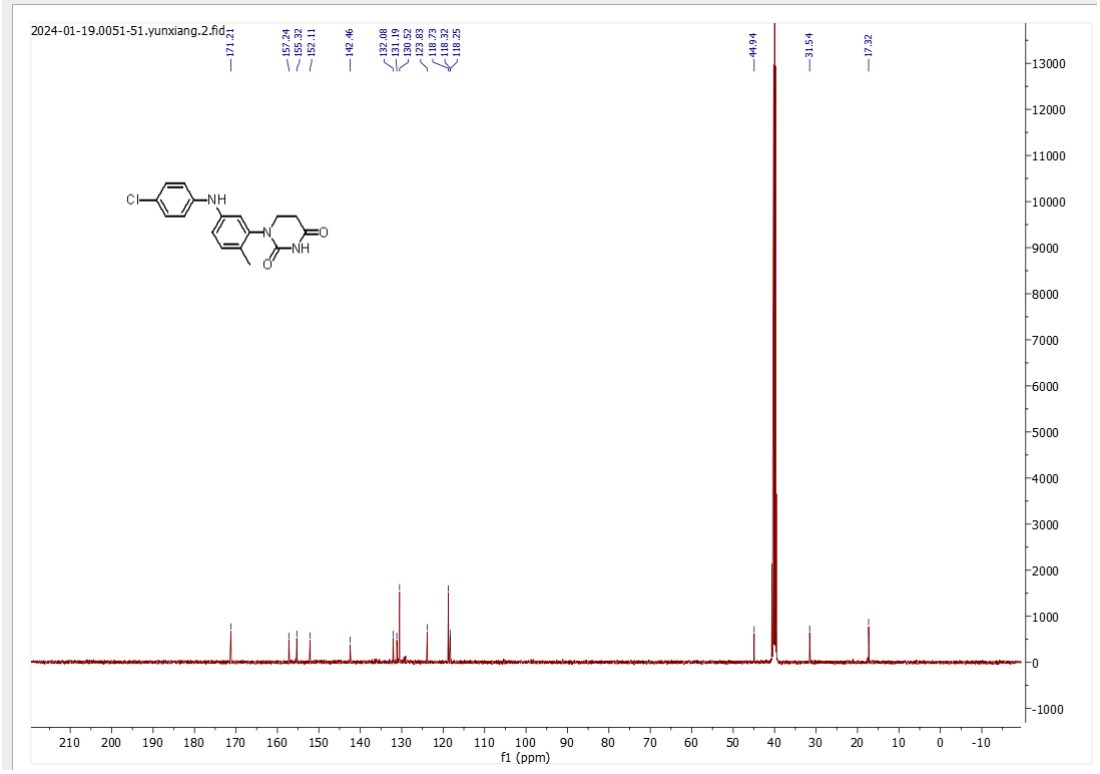
2024-01-19.0051-51.yunxiang.2.fid
f1 (ppm)

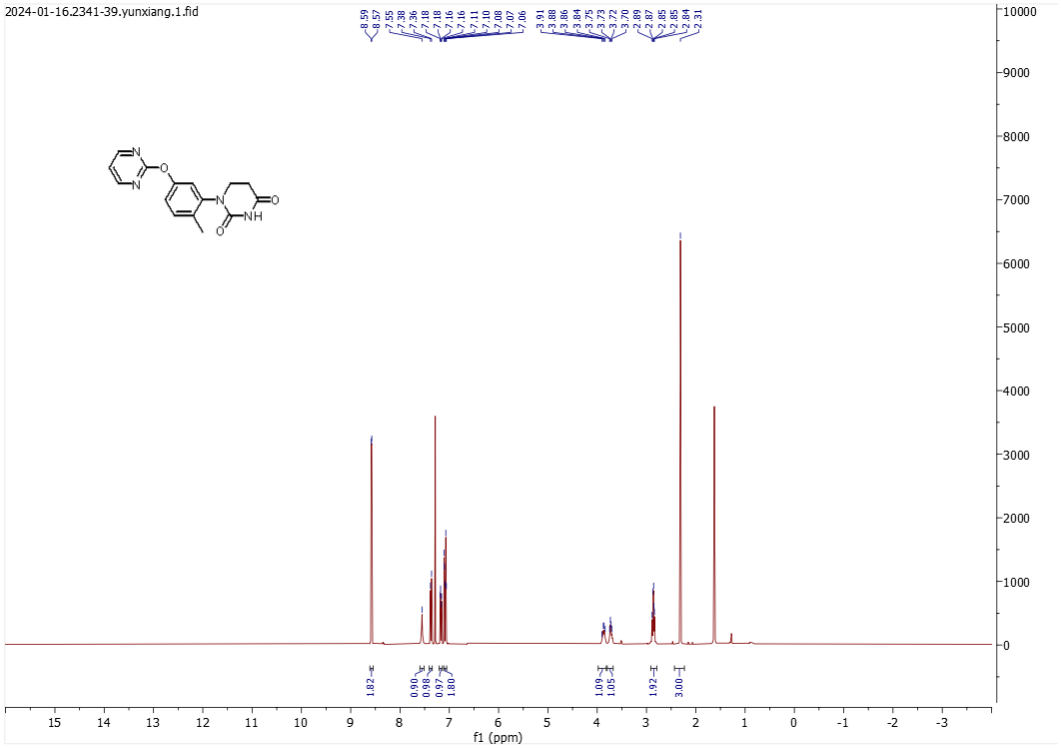
2024-01-16.2341-39.yunxiang.1.fid
f1 (ppm)

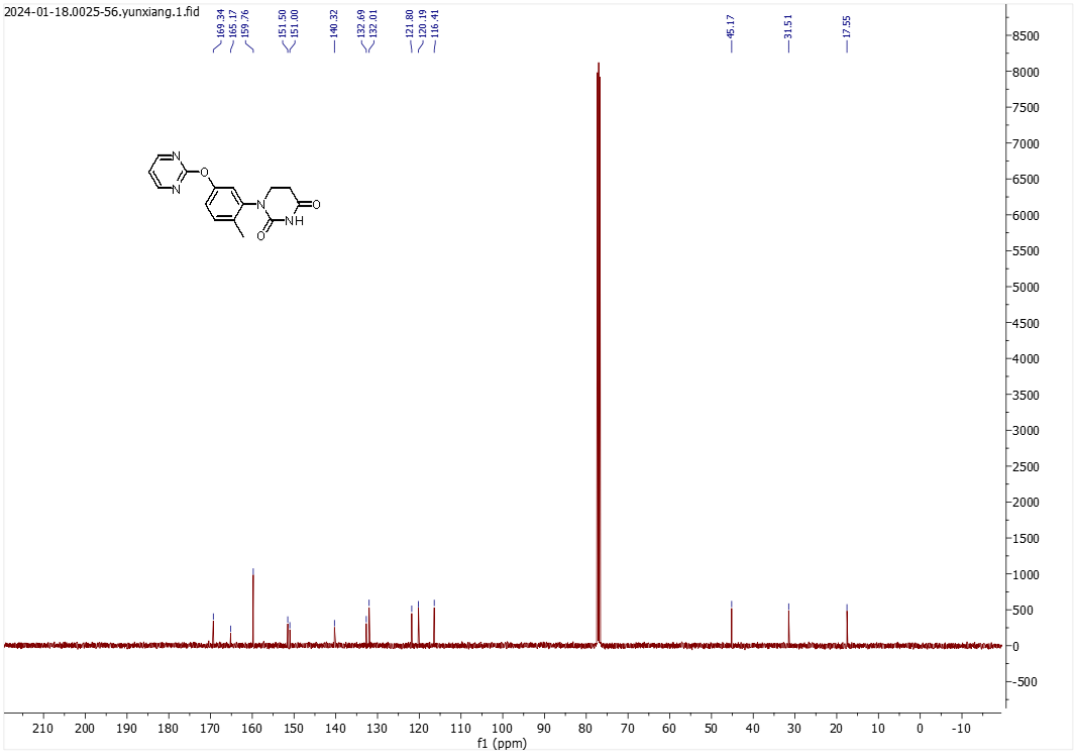
2024-01-18.0025-56.yunxiang.1.fid
f1 (ppm)

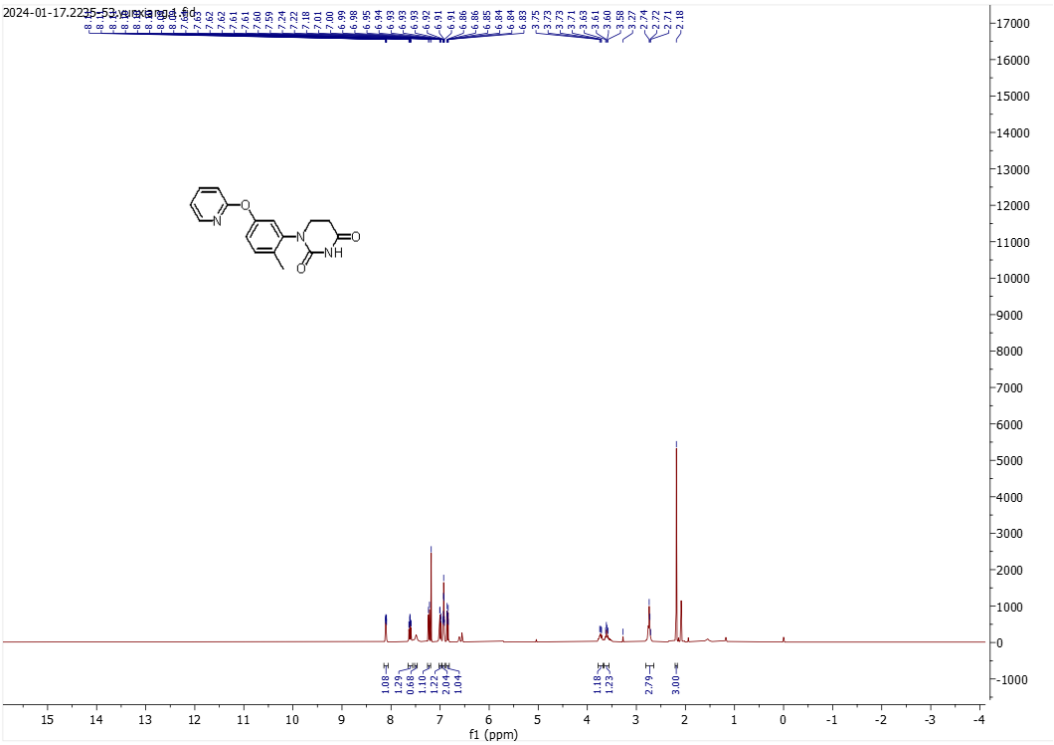
2024-01-17.2235-52.yuxiang-1-6d
f1 (ppm)

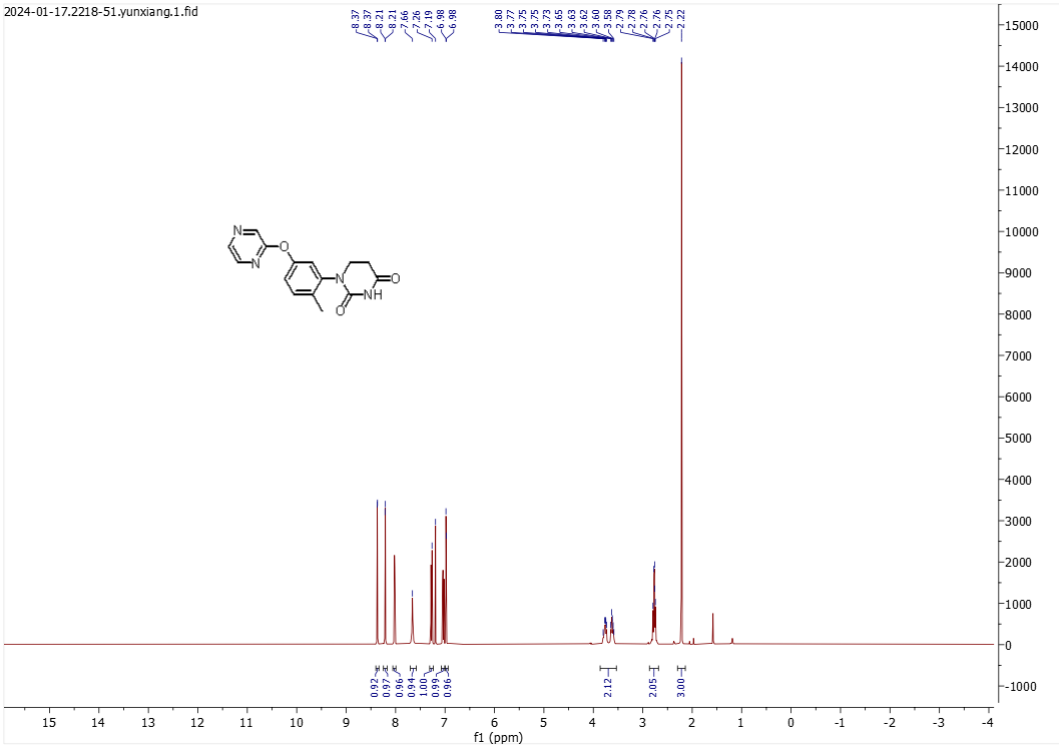
2024-01-17.2218-51.yunxiang.1.fid
f1 (ppm)

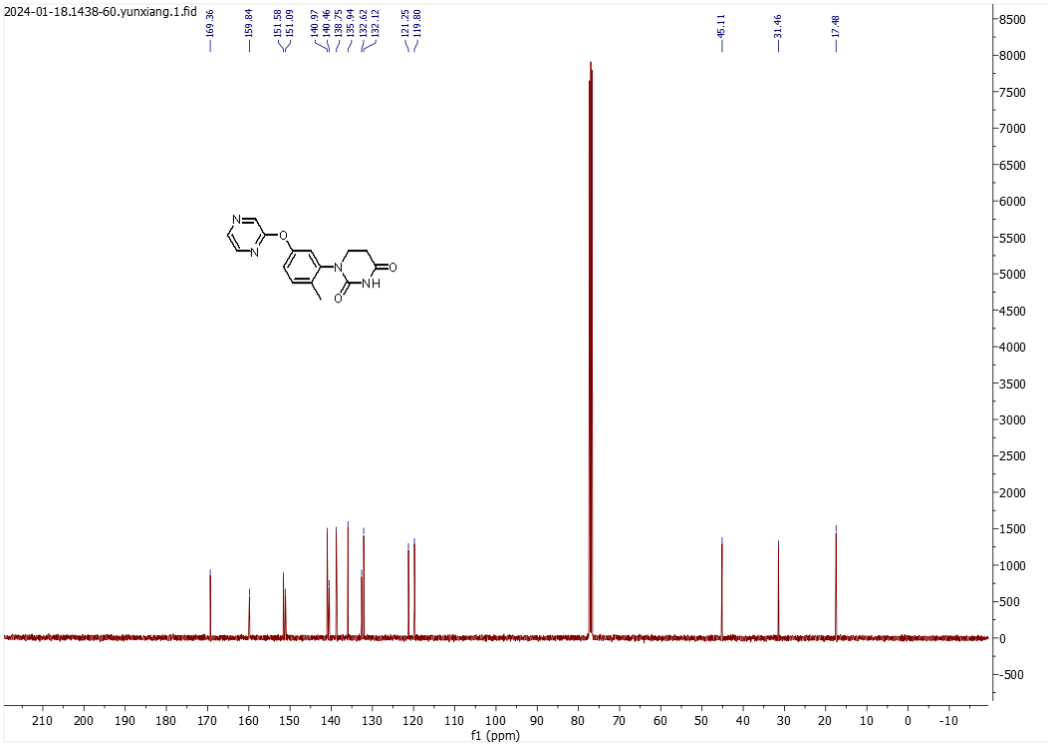
2024-01-18.1438-60.yunxiang.1.fid
f1 (ppm)

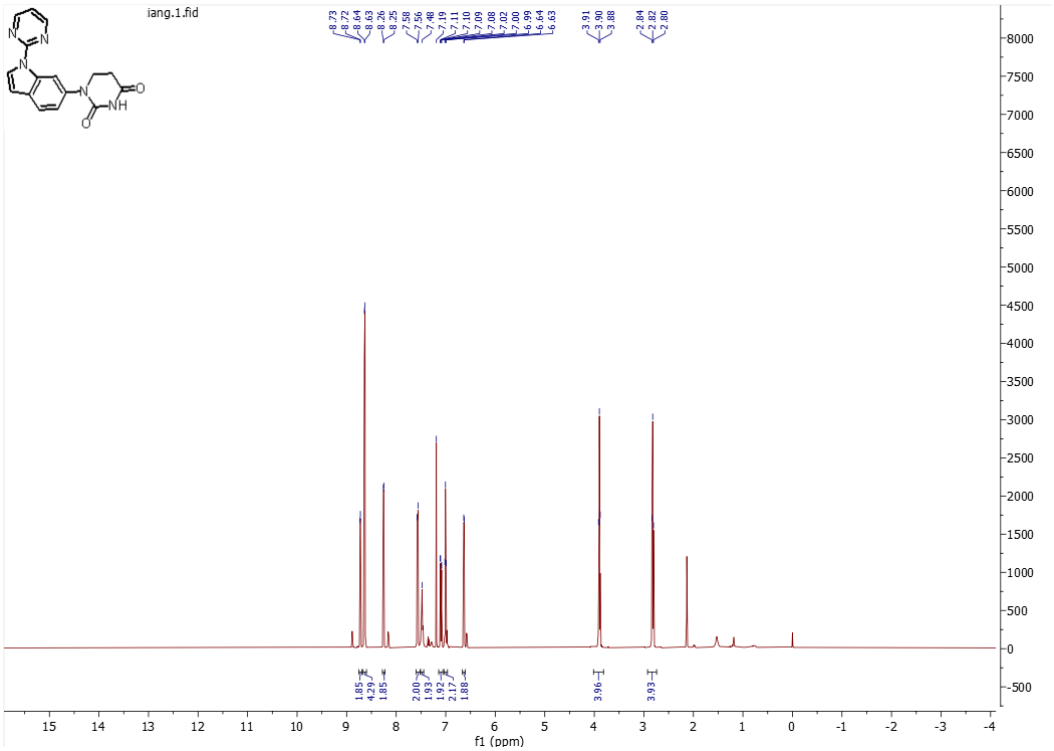
iang.1.fid
8.73
8.72
8.64
8.63
8.26
8.25
7.58
7.56
7.48
7.19
7.11
7.10
7.09
7.08
7.02
7.00
6.99
6.64
6.63
3.91
3.90
3.88
2.84
2.82
2.80
1.85
4.29
1.85
2.00
1.93
1.92
2.17
1.88
3.96
3.93
f1 (ppm)

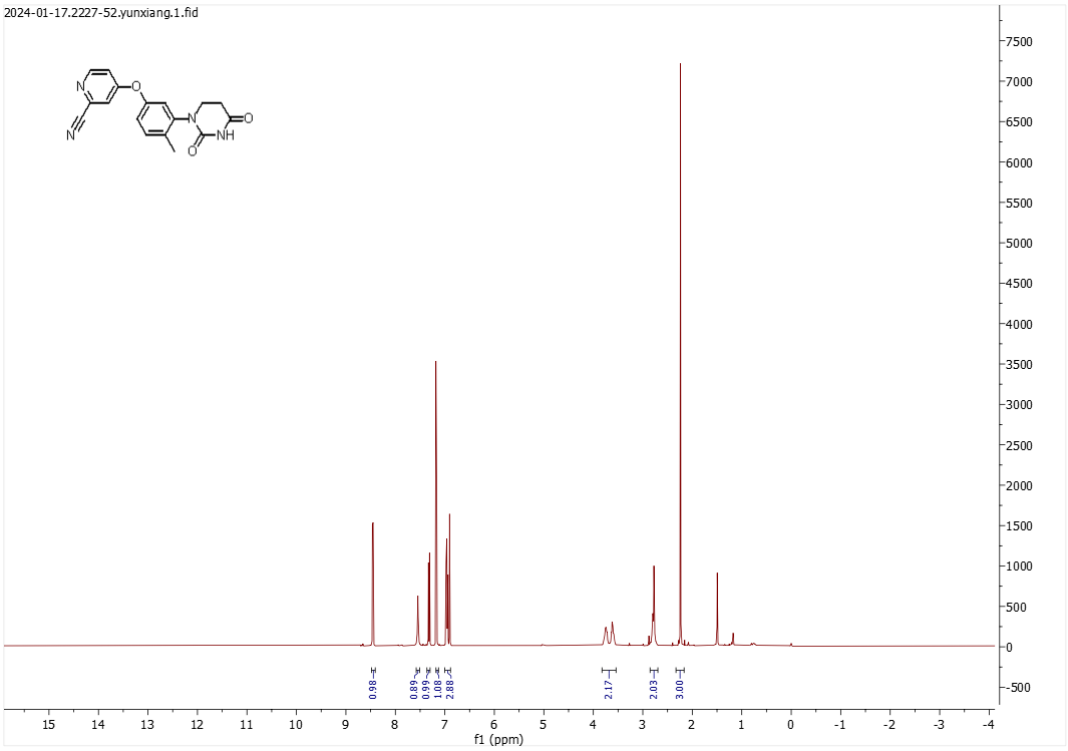
2024-01-17.2227-52.yunxiang.1.fid
0.98
0.89
0.99
1.08
2.88
2.17
2.03
3.00
f1 (ppm)

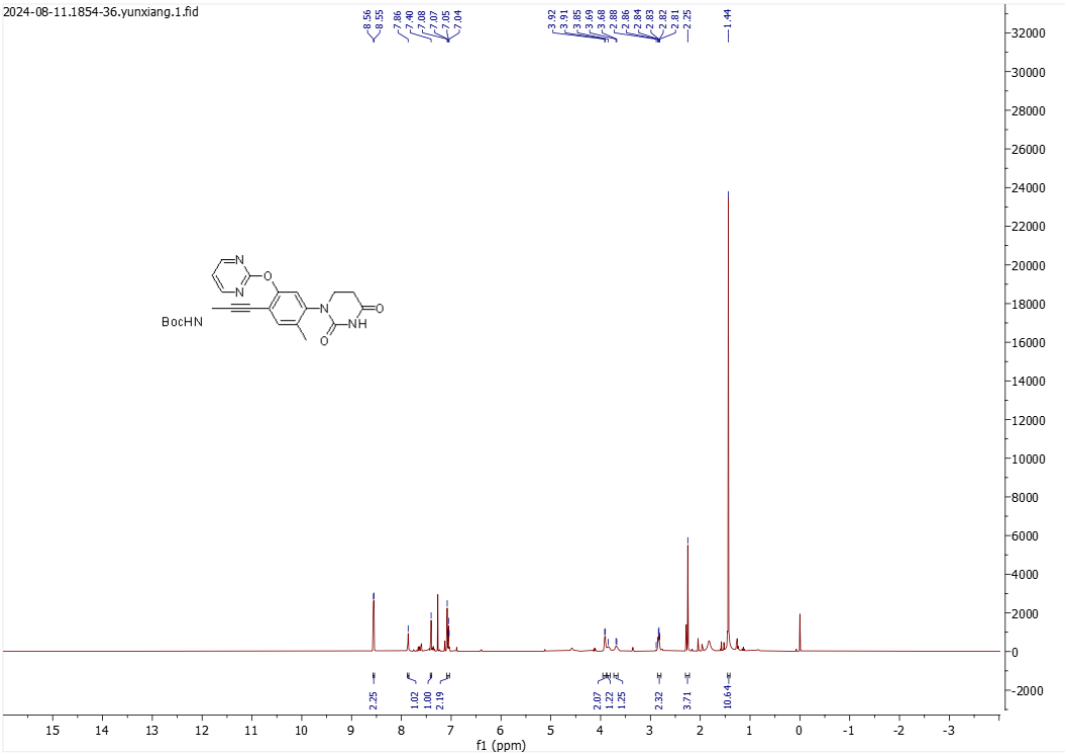
2024-08-11.1854-36.yunxiang.1.fid
BocHN
f1 (ppm)

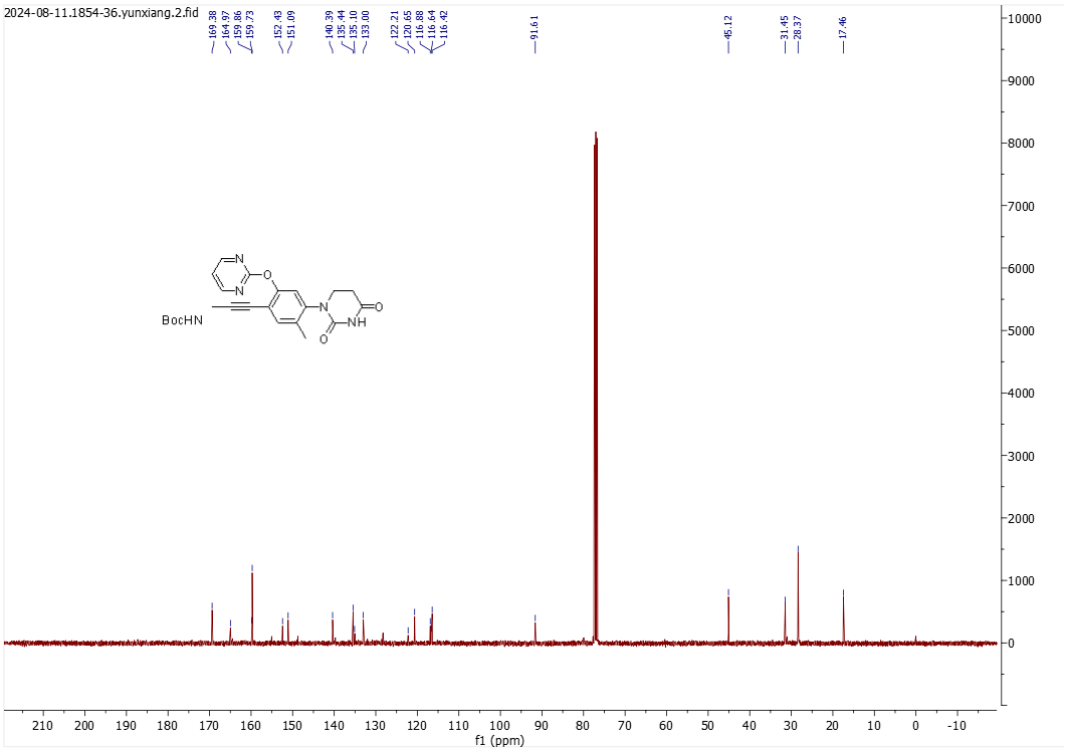
2024-08-11.1854-36.yunxiang.2.fid
BocHN
f1 (ppm)

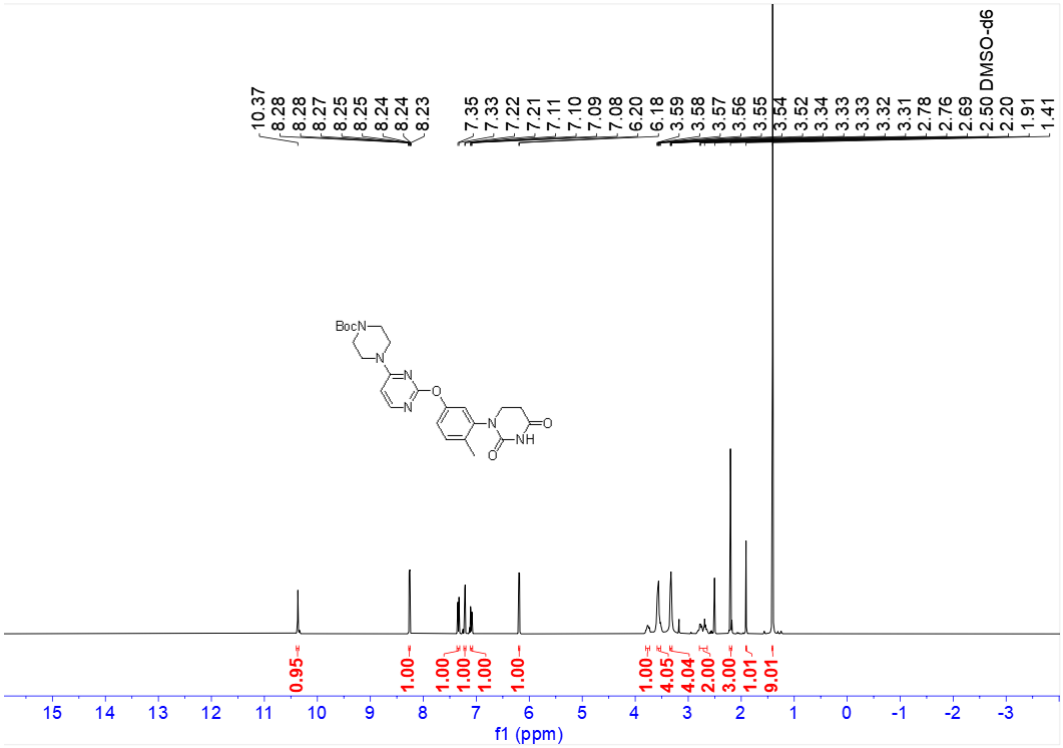
10.37
8.28
8.28
8.27
8.25
8.25
8.24
8.24
8.23
7.35
7.33
7.22
7.21
7.11
7.10
7.09
7.08
6.20
6.18
3.59
3.58
3.57
3.56
3.55
3.54
3.52
3.34
3.33
3.33
3.32
3.31
2.78
2.76
2.69
2.50 DMSO-d6
2.20
1.91
1.41
BocN
N
N
N
O
N
O
NH
O
0.95
1.00
1.00
1.00
1.00
1.00
1.00
4.05
4.04
2.00
3.00
1.01
9.01
15 14 13 12 11 10 9 8 7 6 5 4 3 2 1 0 -1 -2 -3
f1 (ppm)

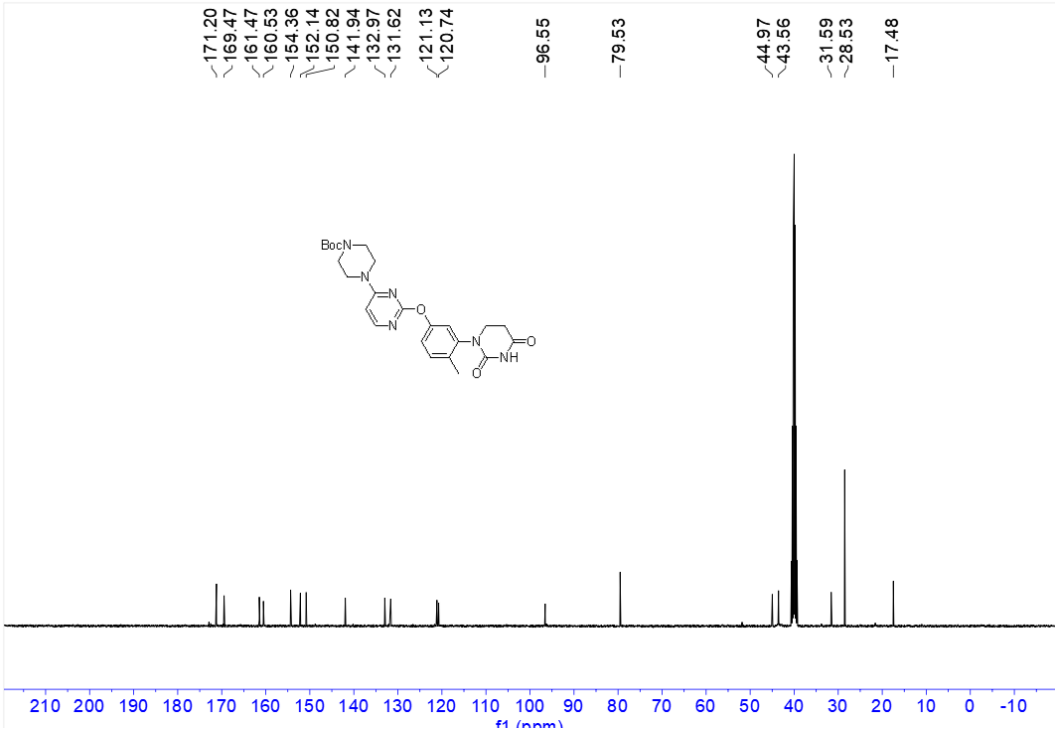
171.20
169.47
161.47
160.53
154.36
152.14
150.82
141.94
132.97
131.62
121.13
120.74
96.55
79.53
44.97
43.56
31.59
28.53
17.48
BocN
N
N
N
O
N
O
NH
O
210 200 190 180 170 160 150 140 130 120 110 100 90 80 70 60 50 40 30 20 10 0 -10

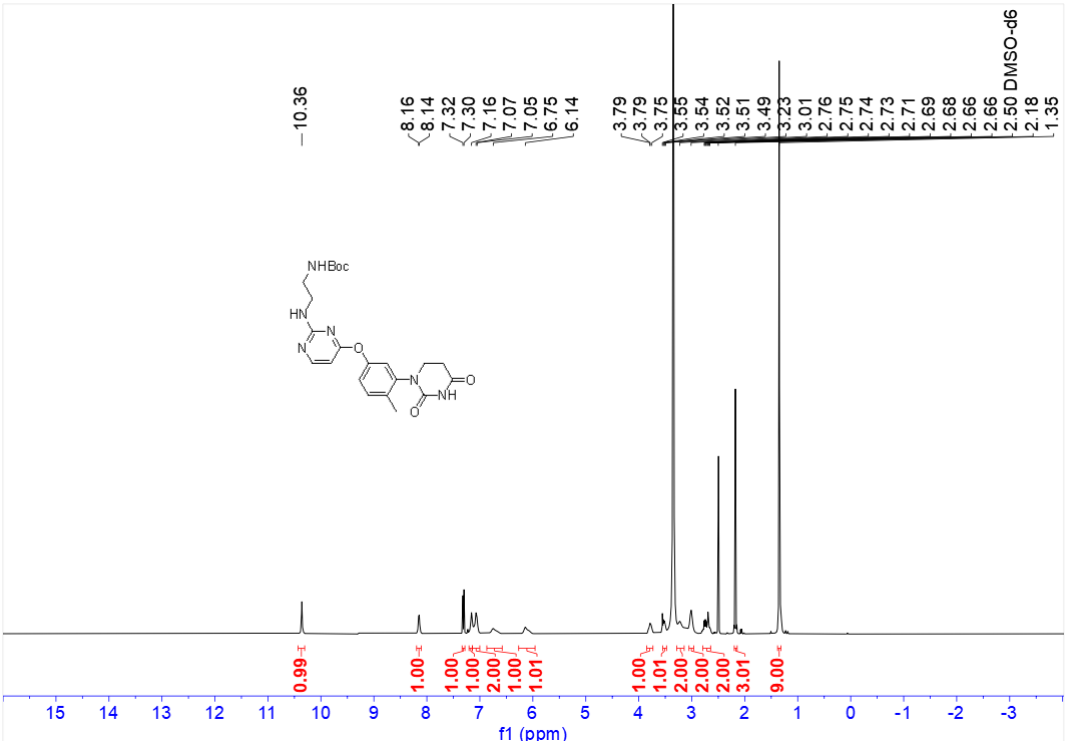
10.36
8.16
8.14
7.32
7.30
7.16
7.07
7.05
6.75
6.14
3.79
3.79
3.75
3.55
3.54
3.52
3.51
3.49
3.23
3.01
2.76
2.75
2.74
2.73
2.71
2.69
2.68
2.66
2.50 DMSO-d6
2.18
1.35
NHBoc
HN
N
N
O
N
O
NH
O
0.99
1.00
1.00
1.00
2.00
1.00
1.01
1.00
1.01
2.00
2.00
3.01
9.00
15 14 13 12 11 10 9 8 7 6 5 4 3 2 1 0 -1 -2 -3
f1 (ppm)

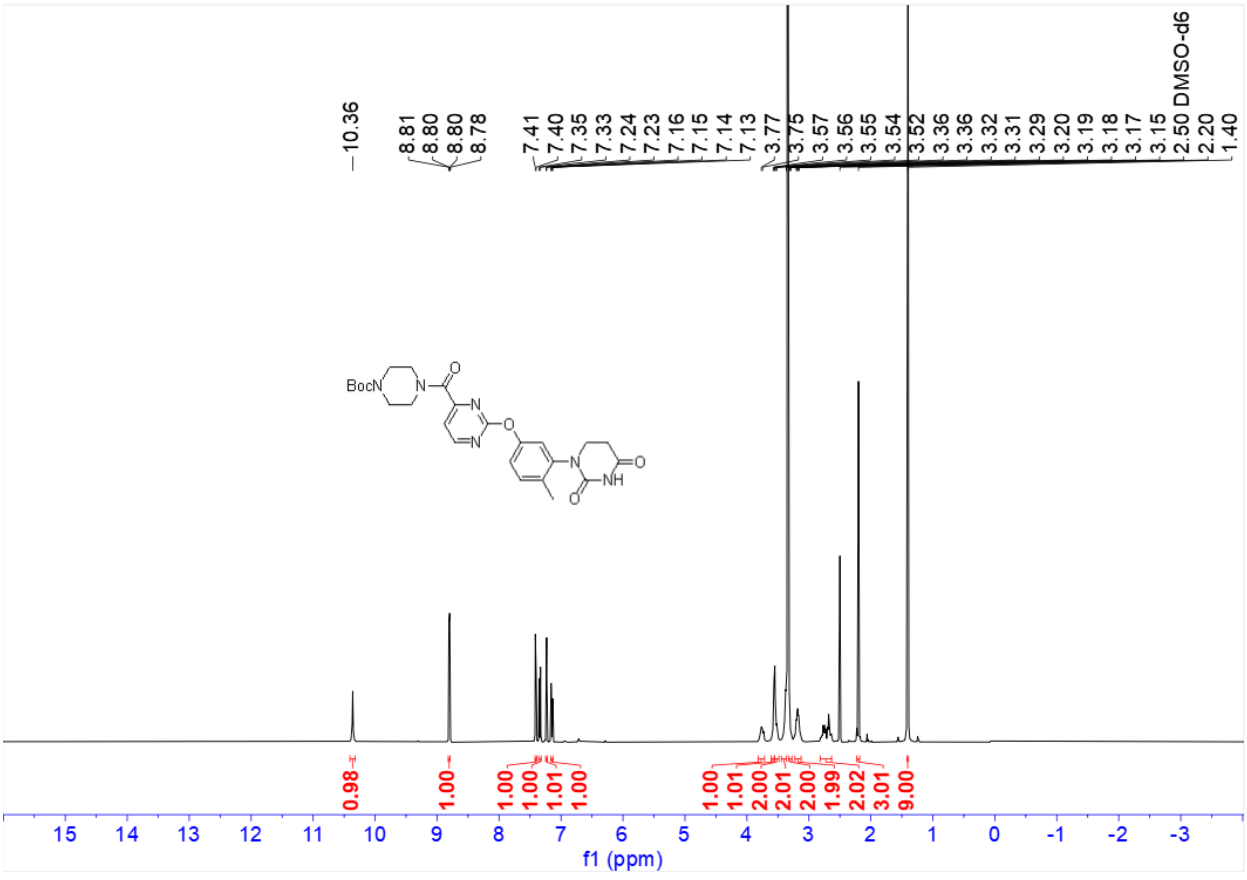
10.36
8.81
8.80
8.80
8.78
7.41
7.40
7.35
7.33
7.24
7.23
7.16
7.15
7.14
7.13
3.77
3.75
3.57
3.56
3.55
3.54
3.52
3.36
3.36
3.32
3.31
3.29
3.20
3.19
3.18
3.17
3.15
2.50 DMSO-d6
2.20
1.40
BocN
N
O
N
N
O
N
O
NH
O
0.98
1.00
1.00
1.00
1.01
1.00
1.00
1.01
2.00
2.01
2.00
1.99
2.02
3.01
9.00
15 14 13 12 11 10 9 8 7 6 5 4 3 2 1 0 -1 -2 -3
f1 (ppm)

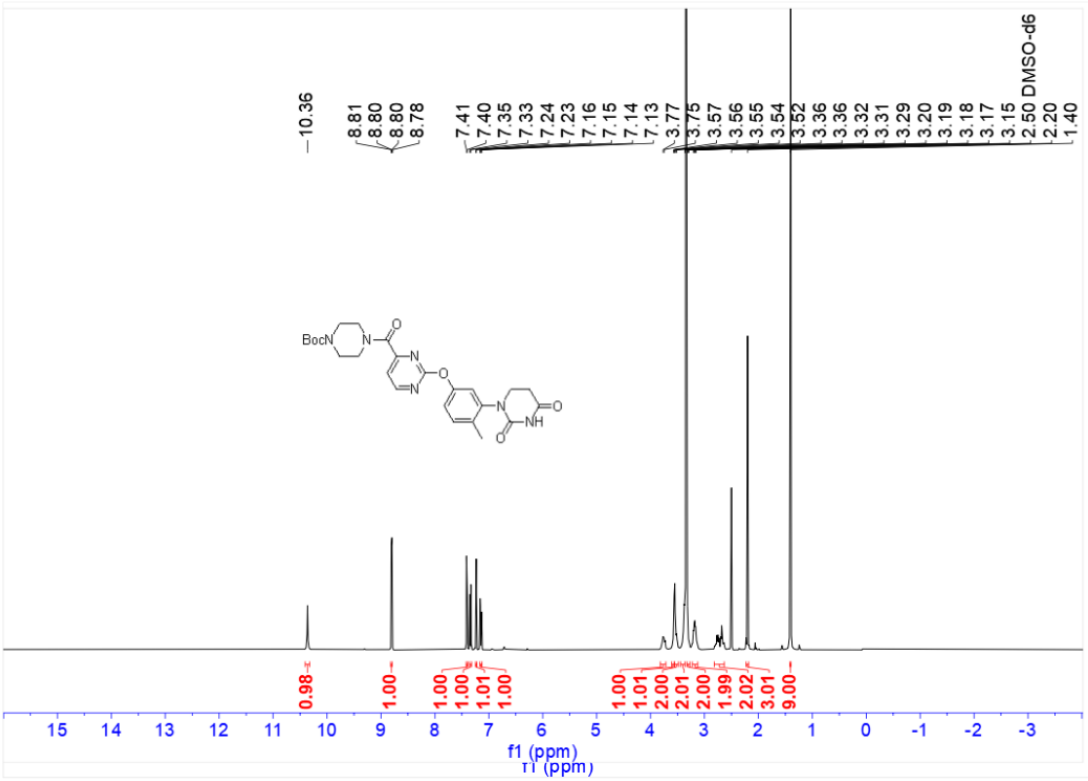
10.36
8.81
8.80
8.80
8.78
7.41
7.40
7.35
7.33
7.24
7.23
7.16
7.15
7.14
7.13
3.77
3.75
3.57
3.56
3.55
3.54
3.52
3.36
3.32
3.31
3.29
3.20
3.19
3.18
3.17
3.15
2.50 DMSO-d6
2.20
1.40
BocN
O
N
N
O
N
O
NH
O
0.98
1.00
1.00
1.00
1.01
1.00
1.00
1.01
2.00
2.01
2.00
1.99
2.02
3.01
9.00
15 14 13 12 11 10 9 8 7 6 5 4 3 2 1 0 -1 -2 -3
f1 (ppm)

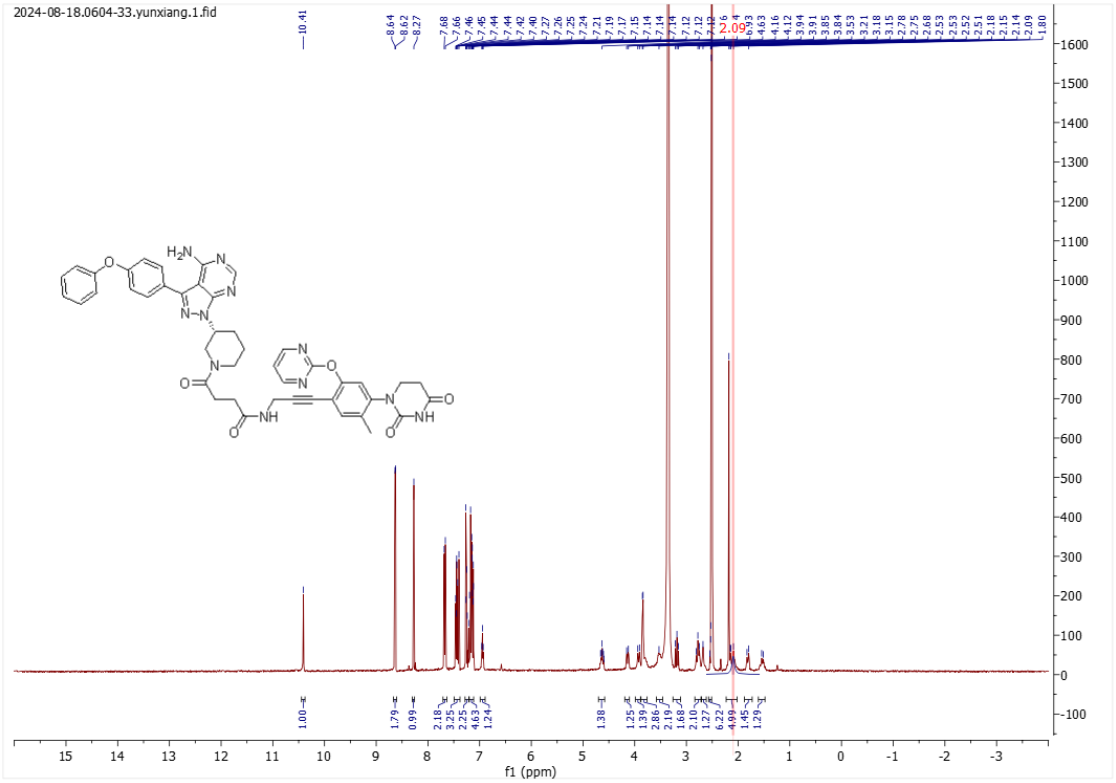
2024-08-18.0604-33.yunxiang.1.fid
10.41
8.64
8.62
8.27
2.09
H2N
N
O
N
N
N
O
N
O
NH
O
NH
O
1.00
1.79
0.99
2.18
3.25
2.25
4.63
1.24
1.38
1.25
1.39
2.86
2.19
2.10
1.27
6.22
4.09
1.45
1.29
15 14 13 12 11 10 9 8 7 6 5 4 3 2 1 0 -1 -2 -3
f1 (ppm)
1600 1500 1400 1300 1200 1100 1000 900 800 700 600 500 400 300 200 100 0 -100

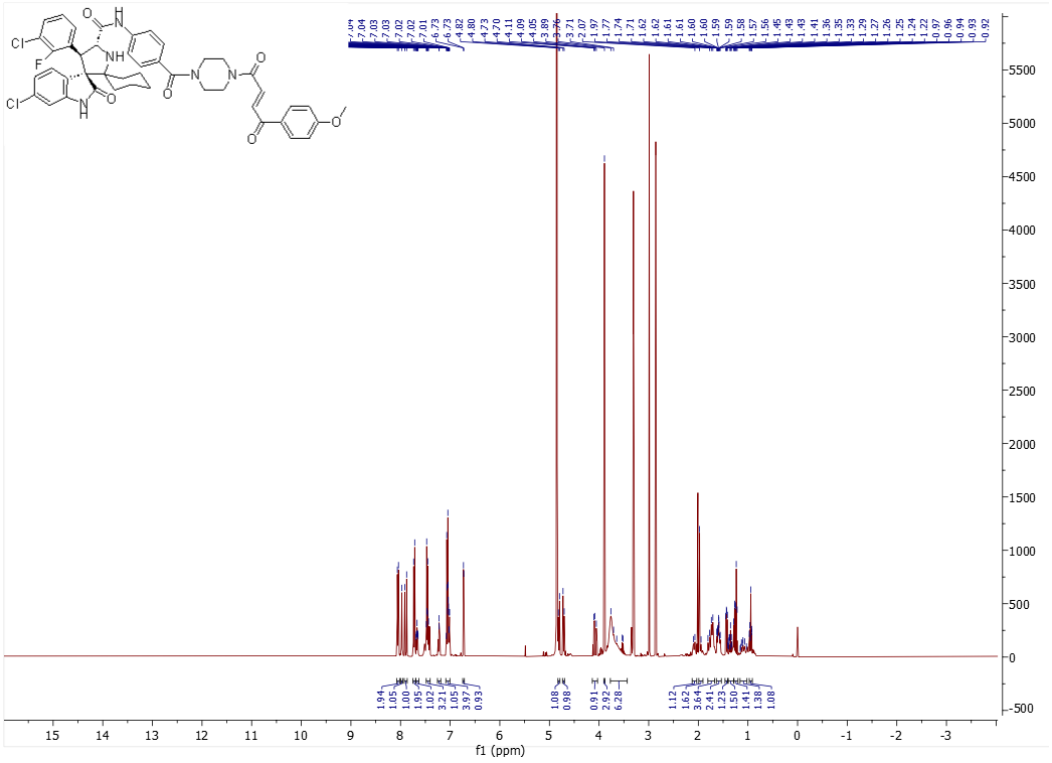
f1 (ppm)

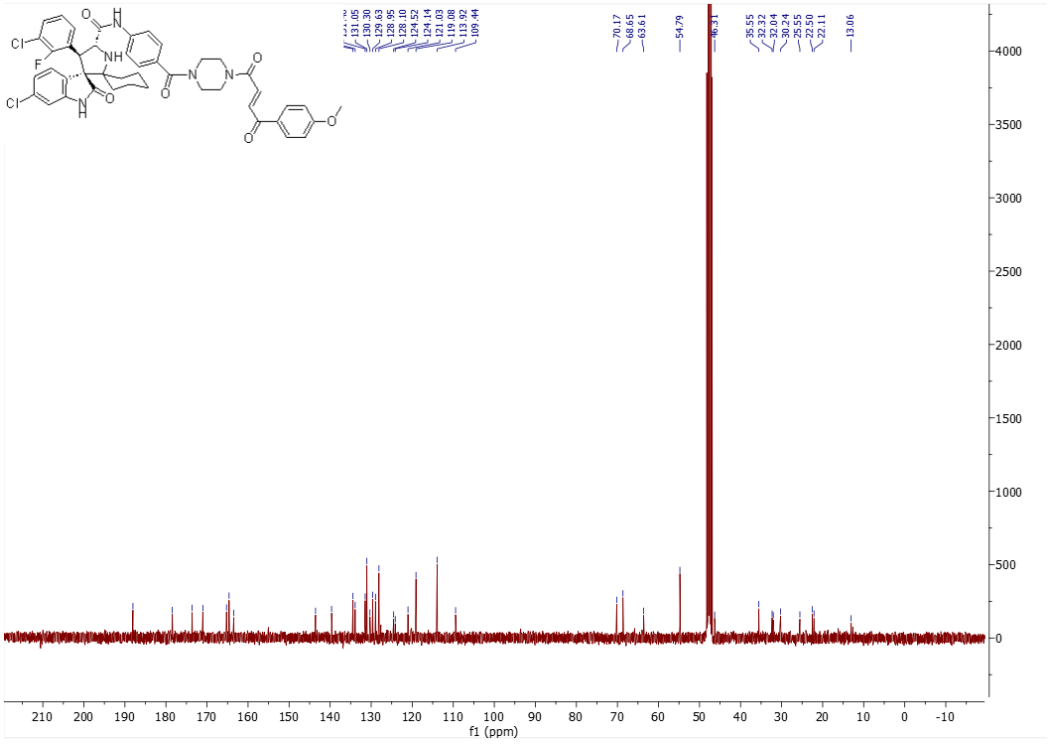
f1 (ppm)

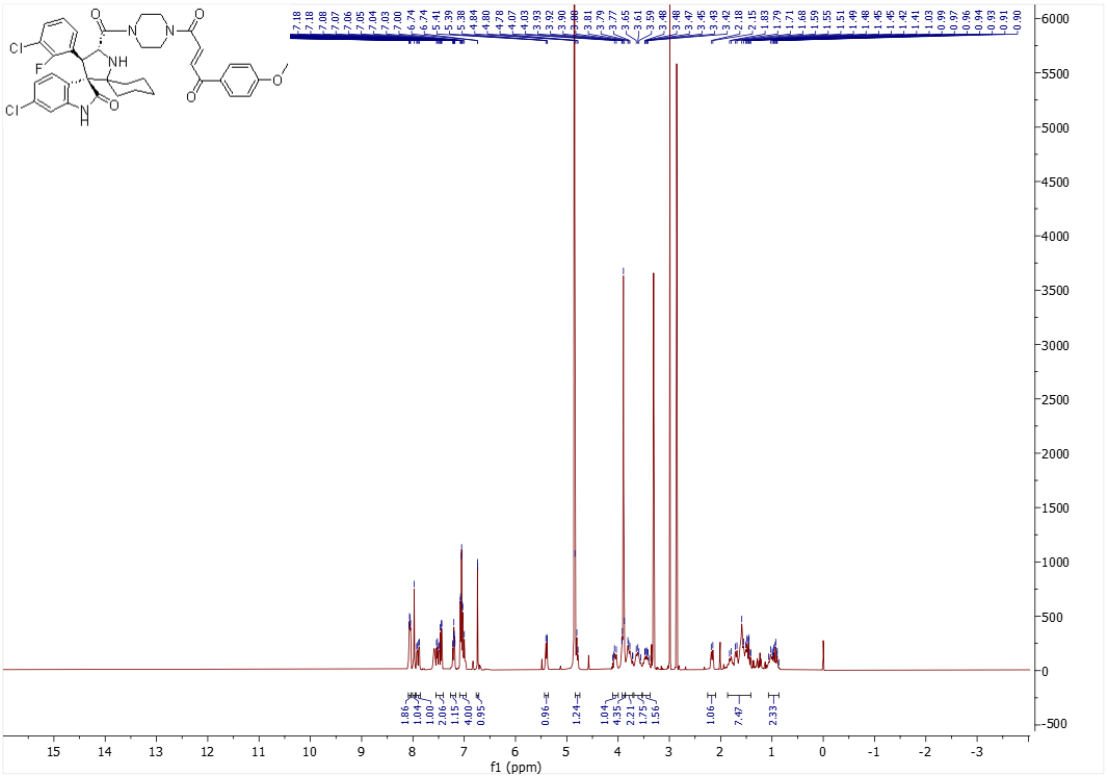
f1 (ppm)

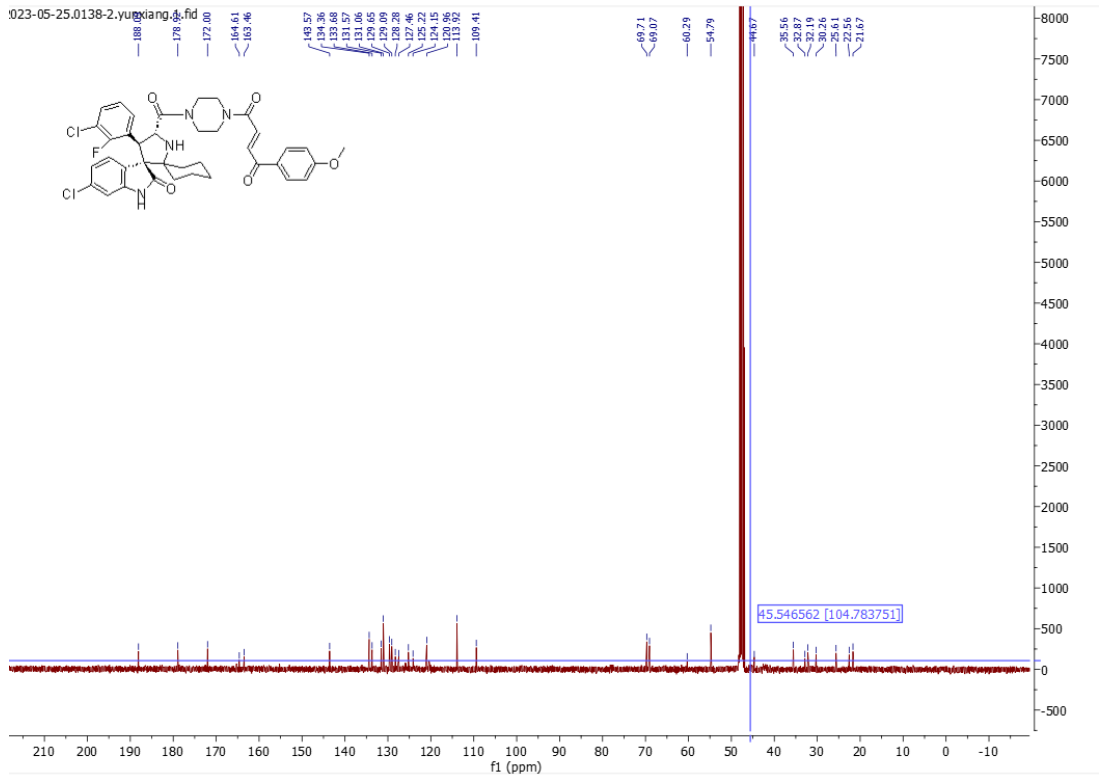
45.546562 [104.783751]
f1 (ppm)